

NI 43-101 Report

LITHIUM RESOURCES UPDATE
PASTOS GRANDES PROJECT
SALTA PROVINCE, ARGENTINA

PREPARED FOR

LithiumAmericas

PREPARED BY

Frederik Reidel, CPG

Effective Date: April 30, 2023

DATE AND SIGNATURE PAGE

This report titled “Lithium Resources Update Pastos Grandes Project, Salta Province, Argentina” has an effective date of April 30, 2023. This report was prepared by Frederik Reidel, CPG.

(Signed & Sealed) “*Frederik Reidel*”

Signed at Santiago, Chile, on June 16, 2023

Frederik Reidel, CPG

TABLE OF CONTENTS

1 SUMMARY	1
1.1 Terms of reference.....	1
1.2 Property description and ownership	1
1.3 Physiography and climate	2
1.4 Geology and mineralization	2
1.5 Drilling and testing	3
1.6 Current project status	4
1.7 Mineral resources	4
1.8 Conclusion and Recommendations	6
2 INTRODUCTION	8
2.1 Terms of reference.....	8
2.2 Sources of information	8
3 RELIANCE ON OTHER EXPERTS	10
4 PROPERTY DESCRIPTION AND LOCATION	11
4.1 Property location	11
4.2 Mining license	11
4.3 Ownership and title	13
4.4 Royalties.....	17
4.5 Environmental liabilities	18
4.6 Other significant factors and risks	18
5 ACCESSIBILITY, CLIMATE, LOCAL RESOURCES, INFRASTRUCTURE AND PHYSIOGRAPHY	19
5.1 Accessibility.....	19
5.2 Physiography.....	19
5.3 Climate	22
5.3.1 Temperature.....	22
5.3.2 Rainfall	22
5.3.3 Solar radiation	25
5.3.4 Wind	25
5.3.5 Evaporation	26
5.3.6 Summary of meteorological parameters.....	27
5.4 Local Infrastructure.....	27
5.4.1 Railroad.....	27
5.4.2 Natural gas.....	28
5.4.3 Water	28
5.4.4 Surface area.....	28
5.5 Vegetation.....	28
6 HISTORY	29
7 GEOLOGICAL SETTING AND MINERALIZATION	31
7.1 Regional geology	31
7.1.1 Tectonic context	31
7.1.2 Stratigraphy	31
7.1.3 Structures	39
7.2 Local geology.....	42
7.2.1 Borehole information	42

7.2.2 Geophysical surveys	44
7.3 Local geology description.....	44
7.3.1 Fluvial/Alluvial Unit.....	45
7.3.2 Upper clay unit (Blanca Lila Formation)	45
7.3.3 Saline/Lacustrine unit.....	45
7.3.4 Central clastic unit	45
7.3.5 Base Breccia/Gravels unit.....	46
7.4 Mineralization	55
8 DEPOSIT TYPE	56
8.1 General.....	56
8.2 Hydrogeology	57
8.3 Water balance.....	58
8.4 Drainable porosity.....	58
8.5 Permeability	60
9 EXPLORATION	61
9.1 Surface brine sampling.....	61
9.2 Geophysical studies	62
9.2.1 Eramet (2011-2013).....	62
9.2.2 Millennial exploration (2017 – 2019)	62
9.3 LSC exploration (2017 – 2018)	64
9.3.1 VES survey (2017b)	64
9.3.2 Seismic survey (2018)	64
9.4 Centaur/AMSA exploration (2018 – 2022)	64
9.4.1 TEM survey (2018).....	64
9.4.2 Passive seismic survey (2019).....	65
9.4.3 TEM survey (2022a).....	65
9.5 LAC exploration (2022)	65
9.5.1 ERT survey (2022b).....	65
10 DRILLING	66
10.1 Overview	66
10.2 Exploration drilling.....	70
10.3 Production well drilling	70
10.4 Freshwater Exploration Drilling	71
10.5 Hydraulic testing	71
10.5.1 Brine Well Pumping Tests.....	71
10.5.2 Pumping tests conducted in freshwater wells	75
11 SAMPLE PREPARATION, ANALYSIS, AND SECURITY.....	86
11.1 Sampling Methods and Assays.....	86
11.1.1 Millennial drainable porosity analysis (2016-2019)	86
11.1.2 AMSA drainable porosity samples (2021-2022)	87
11.1.3 Brine samples	89
11.2 Drainable porosity QA/QC	91
11.3 Brine QA/QC.....	95
11.3.1 Millennial duplicate brine samples.....	95
11.3.2 AMSA duplicate brine samples.....	108
11.3.3 Centaur duplicate brine samples.....	115

12 DATA VERIFICATION	121
13 MINERAL PROCESSING AND METALLURGICAL TESTING	122
14 BRINE RESOURCE ESTIMATES.....	123
14.1 Overview	123
14.2 Resource model domain and aquifer geometry	123
14.3 Specific Yield	123
14.4 Brine Concentrations	124
14.5 Resource category	124
14.6 Resource model methodology and construction	129
14.6.1 Univariate statistical description	130
14.6.2 Variography	132
14.7 Grade estimate	137
14.8 Resource estimate	141
15 MINERAL RESERVE ESTIMATES.....	143
16 MINING METHODS	144
17 RECOVERY METHODS	145
18 PROJECT INFRASTRUCTURE	146
19 MARKET STUDIES AND CONTRACTS	147
20 ENVIRONMENTAL STUDIES, PERMITTING AND SOCIAL OR COMMUNITY IMPACT	148
20.1 Environmental studies	148
20.2 Permits.....	148
20.3 Social and community.....	148
21 CAPITAL AND OPERATING COSTS	149
22 ECONOMIC ANALYSIS	150
23 ADJACENT PROPERTIES	151
24 ADDITIONAL INFORMATION.....	154
25 INTERPRETATION AND CONCLUSIONS	155
26 RECOMMENDATIONS	157
27 REFERENCES.....	159

LIST OF FIGURES

Figure 4.1 Location map of the Pastos Grandes Project	12
Figure 4.2 Location map of LAC mining concessions.....	15
Figure 5.1 Hydrological subdivisions of the Pastos Grandes Basin	20
Figure 5.2 Surface water features within Pastos Grandes basin.....	21

Figure 5.3 Isohyet map for Salar de Pastos Grandes.....	23
Figure 5.4 Correlation between observed and predicted annual precipitation (M&A,2018).....	24
Figure 5.5 Predicted annual precipitation for the Salar de Pastos Grandes (M&A,2018)	24
Figure 5.6 Solar radiation measured at Salar de Pastos Grandes (M&A,2018).....	25
Figure 5.7 Wind speed measured at Salar de Pastos Grandes (M&A,2018).....	26
Figure 7.1 Stratigraphic chart (modified from Blasco et al., 1996)	32
Figure 7.2 Regional geological Scheme (modified from Blasco et al., 1996)	33
Figure 7.3 Geological cross section, Pastos Grandes Depression (modified from Alonso, 1992).....	34
Figure 7.4 Structural setting of the Puna	41
Figure 7.5 Generalized evolution of the structures of the Puna (Houston, 2010).....	42
Figure 7.6 Plan view of the interpreted geological units.....	46
Figure 7.7 N-S section, through the geological model looking from the NW)	47
Figure 7.8 Spatial distribution Fluvial/Alluvial Unit	48
Figure 7.9 Spatial distribution Upper Clay Unit (Blanca Lila Formation).....	49
Figure 7.10 Spatial distribution Saline-Lacustrine Unit	50
Figure 7.11 Spatial distribution Central Clastic Unit.....	51
Figure 7.12 Spatial distribution Base Breccia/Gravel Unit	52
Figure 7.13 Cross sections AA' and BB' through the of the Pastos Grandes basin	53
Figure 7.14 Cross section CC' and DD' through the Pastos Grandes basin	54
Figure 8.1 Conceptual model for mature and immature (Houston et al., 2011)	56
Figure 8.2 Hydrogeological cross section	59
Figure 9.1 Historical surface brine samples in Salar de Pastos Grandes	61
Figure 9.2 Geophysical surveys conducted in Salar de Pastos Grandes.....	63
Figure 10.1 Borehole locations in Salar de Pastos Grandes	67
Figure 10.2 Location map of the pumping tests conducted in Salar de Pastos Grandes	72
Figure 10.3 Location, setup and results of pumping test well PGPW16-01 (2017).....	77
Figure 10.4 Location, setup and results of pumping test PGPW17-04.....	78
Figure 10.5 Location, setup and results of pumping test PGPW18-15.....	79
Figure 10.6 Location, setup and results of pumping test PGPW18-17.....	80
Figure 10.7 Location, setup and results of pumping test PGPW16-01 (2019)	81
Figure 10.8 Location, setup and results of pumping test PGWW19-02	82
Figure 10.9 Location, setup and results of pumping test PGWW19-03	83
Figure 11.1 Pt comparison for check samples DBSA - GSA.....	93
Figure 11.2 Sy comparison for check samples DBSA - GSA	94
Figure 11.3 Sy and RBR comparison for check samples DBSA - GSA.....	94
Figure 11.4 Max-min plot for lithium in duplicates - ASANOA.....	97
Figure 11.5 Max-min plot for potassium in duplicates - ASANOA.....	98
Figure 11.6 Max-min plot for lithium in duplicates - SGS.....	98
Figure 11.7 Max-min plot for potassium in duplicates - SGS	99
Figure 11.8 Max-min plot for lithium in check samples: ASANOA - SGS.....	100
Figure 11.9 Max-min plot for potassium in check samples: ASANOA - SGS.....	101
Figure 11.10 Blank vs previous samples for lithium - ASANOA	102
Figure 11.11 Blank vs previous samples for potassium - ASANOA.....	102
Figure 11.12 Blank vs previous samples for lithium - SGS.....	103
Figure 11.13 Blank vs previous samples for potassium - SGS	103
Figure 11.14 Graphical analysis of lithium within 'RR' Standards assayed by ASANOA.....	105

Figure 11.15 Graphical analysis of potassium within 'RR' Standards assayed by ASANOA.	105
Figure 11.16 Graphical analysis of lithium within 'RR' Standards assayed by SGS.	106
Figure 11.17 Graphical analysis of potassium within 'RR' Standards assayed by SGS.	107
Figure 11.18 Graphical analysis of lithium within 'INBEMI' Standards assayed by SGS.	107
Figure 11.19 Graphical analysis of potassium within 'INBEMI' Standards assayed by SGS.	108
Figure 11.20 Max-min plot for lithium in duplicates - SGS.	109
Figure 11.21 Max-min plot for potassium in duplicates - SGS.	110
Figure 11.22 Blank vs previous samples for lithium - SGS.	111
Figure 11.23 Blank vs previous samples for potassium - SGS.	111
Figure 11.24 Graphical analysis of lithium within 'STD-1' Standards assayed by SGS.	113
Figure 11.25 Graphical analysis of potassium within 'STD-1' Standards assayed by SGS.	113
Figure 11.26 Graphical analysis of lithium within 'STD-2' Standards assayed by SGS.	114
Figure 11.27 Graphical analysis of potassium within 'STD-2' Standards assayed by SGS.	114
Figure 11.28 Max-min plot for lithium in duplicates - ASANOA.	116
Figure 11.29 Max-min plot for potassium in duplicates - ASANOA.	116
Figure 11.30 Blank vs previous samples for lithium - ASANOA.	117
Figure 11.31 Blank vs previous samples for potassium - ASANOA.	118
Figure 11.32 Graphical analysis of lithium within 'STD-A' Standards assayed by ASANOA.	119
Figure 11.33 Graphical analysis of potassium within 'STD-A' Standards assayed by ASANOA.	119
Figure 14.1 Schematic section illustrating resource categories based on data density for different zones.	127
Figure 14.2 Spatial distribution of resource classification by depth.	128
Figure 14.3 lithium and potassium histograms and cumulative distributions.	131
Figure 14.4 Lithium and potassium histograms and cumulative distributions for region I.	132
Figure 14.5 Experimental variogram and variogram model for the indicator variable.	135
Figure 14.6 Experimental variogram and variogram model for potassium and lithium in region I.	136
Figure 14.7 N-S section through the resource model showing the lithium grade distribution.	138
Figure 14.8 W-E section through the resource model showing the lithium grade distribution.	139
Figure 14.9 SW-NE section through the resource model showing the lithium grade distribution.	140
Figure 23.1 Location map of adjacent properties.	153

LIST OF TABLES

Table 1.1 Maximum, average and minimum elemental concentrations of the Pastos Grandes brine.	3
Table 1.2 Average values (mg/L) of key components and ratios for the Pastos Grandes brine.	3
Table 1.3 Results of drainable porosity analyses.	5
Table 1.4 Mineral Resources of the Pastos Grandes Project – Dated April 30, 2023.	5
Table 4.1 Mining tenement of the Pastos Grandes Project.	13
Table 5.1 Principal meteorological parameters of Salar de Pastos Grandes.	27
Table 7.1 Boreholes incorporated in the geological model.	43
Table 7.2 Maximum, average and minimum elemental concentrations of the Pastos Grandes brine.	55
Table 7.3 Average values (mg/L) of key components and ratios for the Pastos Grandes brine.	55
Table 8.1 Water Balance for Salar de Pastos Grandes.	58
Table 8.2 Results of drainable porosity analyses.	60

Table 8.3 Summary of permeability values	60
Table 10.1 Summary of 2016-2022 boreholes	68
Table 10.2 Summary of pumping test PGPW16-01 (2017)	73
Table 10.3 Summary of pumping test PGPW17-04	73
Table 10.4 Summary of pumping test PGPW18-15	74
Table 10.5 Summary of pumping test PGPW18-17	74
Table 10.6 Summary of pumping test PGPW16-01 (2019)	75
Table 10.7 Summary of pumping test PGWW18-01	75
Table 10.8 Summary of pumping test PGWW19-02	75
Table 10.9 Summary of pumping test PGWW19-03	76
Table 10.10 Summary of brine well tests	84
Table 10.11 Summary of freshwater pumping tests	85
Table 11.1 Summary of laboratory tests conducted by GSA	88
Table 11.2 Analytical methods used by ASANOVA and SGS for brine assays	91
Table 11.3 Total porosity results for paired samples using GSA lithologic classification	92
Table 11.4 Specific yield results for paired samples using GSA lithologic classification	93
Table 11.5 Summary of QAQC insertion rates for each campaign	95
Table 11.6 Statistical analysis of duplicate samples – ASANOVA	96
Table 11.7 Statistical analysis of duplicate samples – SGS	96
Table 11.8 Statistical analysis of check samples – ASANOVA & SGS	99
Table 11.9 Element concentrations (best values) for Standard RR – Millennial	104
Table 11.10 Element concentrations for Standard INBEMI - Millennial	104
Table 11.11 Statistical analysis of duplicate samples – SGS	108
Table 11.12 Element concentrations (best values) for Standards 1 & 2 - AMSA	112
Table 11.13 Statistical analysis of duplicate samples – ASANOVA	115
Table 11.14 Element concentrations (best values) for Standards A & B - Centaur	118
Table 14.1 Summary statistics of drainable porosity for geological units	124
Table 14.2 Summary of brine chemistry composition	124
Table 14.3 Summary of univariate statistics of Li and K	130
Table 14.4 Parameters for the calculation of the experimental variograms of the indicator variable	133
Table 14.5 Parameters for the calculation of the experimental variograms of the K and Li concentrations	133
Table 14.6 Mineral Resources of the Pastos Grandes Project – Dated April 30, 2023	141
Table 14.7 Pastos Grandes Project resources expressed as LCE and KCl	141
Table 23.1 Mining properties in the vicinity of the Pastos Grandes Project	151
Table 25.1 Summary of the average brine composition (g/L) and ratios	155
Table 25.2 Mineral Resources of the Pastos Grandes Project - Dated April 30, 2023	156
Table 25.3 Pastos Grandes Project resources expressed as LCE and KCl	156

1 SUMMARY

1.1 Terms of reference

Lithium Americas Corp. (“LAC” or the “Company”) acquired the Pastos Grandes project (the “Pastos Grandes Project” or the “Project”) from Millennial Lithium Corp (“Millennial”) in January 2022. LAC subsequently acquired additional mining concessions (LAC Norte and Sur) during 2022. LAC retained Atacama Water to prepare this Technical Report for the Pastos Grandes Project with the objective of updating the mineral resource estimate for lithium contained in brine for the LAC properties in the Pastos Grandes basin based on the consolidation and integration of available information.

LAC completed the acquisition of all the shares of Arena Minerals Inc.’s (“AMSA”) in April 2023. AMSA owns 65% of the Sal de la Puna project (“the Sal de la Puna Project”) through a joint venture interest in Sal de la Puna Holdings Ltd., the 100% owner of the Argentine subsidiary, Puna Argentina S.A.U. (“PASAU”), the owner of the claims forming part of the Sal de la Puna Project. The remaining 35% of Sal de la Puna Holdings Ltd. is owned by joint venture partner Ganfeng New Energy Technology Development (Suzhou) Co., Ltd. The mineral resource estimate presented herein does not include any resources on the Sal de la Puna properties. LAC anticipates conducting additional work to evaluate consolidating the Pastos Grandes basin to include potential upside from the Sal de la Puna Project.

This report has been prepared in conformance with the requirements of National Instrument 43-101 – Standards of Disclosure for Mineral Projects (“NI 43-101”) and the associated Companion Policy 43-101CP and Form 43-101F1 of the Canadian Securities Administrators and the associated Best Practice Guidelines for Industrial Minerals and Mineral Processing as issued by the Canadian Institute of Mining and Metallurgy. The Report also includes technical judgement of appropriate additional technical parameters to accommodate certain specific characteristics of minerals hosted in liquid brine as outlined in CIM Best Practice Guidelines for Resource and Reserve Estimation for Lithium Brines and as discussed by Houston (Houston et al, 2011).

1.2 Property description and ownership

The Pastos Grandes Project is situated within the Department of Los Andes approximately 10 km south of the village of Santa Rosa de Los Pastos Grandes and 130 km west of the city of Salta, the capital of the Salta Province in Argentina. The property's location is defined by its center point, which is at approximately 3,428,966 mE, 7,283,194 mN (POSGAR 04 / Argentina zone 3). The Project encompasses a surface area of more than 24,000 ha in Salar de Pastos Grandes at an elevation of roughly 3,785 masl.

The Project site is near Highway 129 which connects 40 km north with Highway 51. Highway 51 traverses from Salta to the international border with Chile at the Sico Pass and connects further west to the major mining center of Calama, as well as the ports of Antofagasta and Mejillones in northern Chile. Both ports are major transportation hubs for the importation of mining equipment and the exportation of mineral commodities.

Through its 100% percent ownership of Pastos Grandes S.A. (“PGSA”), LAC controls the mining concessions of the Pastos Grandes Project. These concessions include El Milagro, Neptali II, Norte Argentino, Juan Eduardo, Aguamarga 15, Taba PG, Papadopoulos LXXIV, Ignacio, Ignacio IV, Daniel Ramon, Aguamarga 10, Nueva Sijesyta 01, Papadopoulos XXXII and cover an area of 12,729 ha. In addition, PGSA controls several other mining concessions and easements to further facilitate project development which are under application and cover some additional 11,000 ha. A legal opinion provided by Mr. Rafael Argañaraz Olivero indicates that all claims are in good standing and all payments are current.

1.3 Physiography and climate

The hydrographic basin of the Salar de Pastos Grandes (“Salar de Pastos Grandes” or the “Salar”) covers 16,901 km² in the Altiplano of northwestern Argentina. The average elevation of the basin is 4,301 masl. The Pastos Grandes Basin had been divided into two subbasins according to topographic criteria, the Río Sijes subbasin at the east and Pastos Grandes subbasin at the west. The active saline crust of the Salar is in the western section of the hydrographic basin and covers nearly 31.4 km². The Salar nucleus sits at an approximate elevation of 3,767 masl. Unlike other salars of the region, the topography of the nucleus of Salar the Pastos Grandes is irregular.

Surface runoff is mainly restricted to the rainy season during summer. Three intermittent to ephemeral rivers enter the Salar, Río Sijes from the east, Río Pastos Grandes from the north, and Río Corral Colorado from the northeast. Three semi-permanent lagoons occur near the discharge areas of the three above-mentioned rivers into the nucleus of the Salar. Springs and wetlands occur towards the north of the Salar over the interface between the alluvium and evaporitic crust in the lower parts of the Río Pastos Grandes and Río Corral Colorado.

The climate in the Project area is severe and can be described as a typical continental, cold, high-altitude desert, with resultant scarce vegetation. Daily temperature variations may exceed 25°C. Solar radiation is intense, especially during the months of October through March, leading to high evaporation rates. The rainy season occurs between the months of December and March when occasional flooding can develop in the Salar and may limit certain activities.

1.4 Geology and mineralization

Based on the lithological descriptions of drill core and cuttings together with the interpretation of the available geophysical information and field observations, five major geological units were defined and correlated.

- A Fluvial/Alluvial Unit is characterized by a heterogeneous sequence of alluvial and fluvial sediments of variable texture, dominated by clastic sediments formed by gravel and sand that surround the Salar. These fractions may present low proportions of fine sediments (sands or clays) which develop mainly along the northern and southern edges of Salar de Pastos Grandes, prograding in depth towards the center to interdigitate with finer silt sediments (clay and sandy clays) from the Central Clastics Unit.
- An Upper Clay Unit (Blanca Lila Fm) occurs in the center-south of the basin as well as in the western margins where it occurs in outcrop. This clay-dominated unit intercalates with layers of evaporites, halites, and borates.
- A Saline/Lacustrine Unit occurs immediately below the Blanca Lila Fm and in the north-central part of the Salar at surface. This Unit is characterized by a massive and compact halite body with the presence of interstitial clastic material and occasional intercalations of finer levels of clay. The average thickness of this Unit ranges between 200 m and 300 m, reaching maximum thicknesses of 700 m in the central-eastern sector of the basin which is interpreted as an ancient depocenter.
- A Central Clastic Unit consists of clay and clayey sands and occurs within the central sector of the basin underneath the halite deposits and seems to represent a distal sector of an alluvial fan and its interaction with marginal lacustrine deposits of the Salar.

- A Base Breccia/Gravels Unit is a sedimentary breccia unit of coarse fragments of silicified conglomerate and ignimbrites. It contains intermixed levels of sand and gravel with a thickness of 200 m on the western edge of the basin and deepening towards the north-central limit of the resource area where due to limited information its thickness becomes uncertain.

The brines from Pastos Grandes are solutions saturated in sodium chloride with an average concentration of total dissolved solids (TDS) of 302 g/L and an average density of 1.19 g/cm³. The other components present in the Pastos Grandes brine are K, Li, Mg, SO₄, Cl and B with relatively low Ca. The brine can be classified as a sulphate-chloride type with anomalous lithium. Lithium concentrations in Salar de Pastos Grandes have an average value of 392 mg/L, with some samples reaching up to 700 mg/L.

Table 1.1 shows a breakdown of the principal chemical constituents in the Pastos Grandes brine including maximum, average, and minimum values, based on 501 primary brine samples collected between 2017 and 2022.

Table 1.1 Maximum, average and minimum elemental concentrations of the Pastos Grandes brine

	B	Ca	Cl	Li	Mg	K	Na	SO ₄	Density
Units	mg/L	mg/L	mg/L	mg/L	mg/L	mg/L	mg/L	mg/L	g/cm ³
Maximum	938.00	1,707	196,869	701.0	5,130	6,660	130,032	13,998	1,22
Average	557.62	821	169,838	391.8	2,257	3,733	102,381	7,547	1,19
Minimum	20.2	11.00	116.00	8.75	23.20	18.00	196.00	12.00	1,00

Brine quality is evaluated through the relationship of the elements of commercial interest, such as lithium and potassium with those components that constitute impurities, such as Mg, Ca and SO₄. The calculated ratios for the averaged chemical composition are presented in Table 1.2.

Table 1.2 Average values (mg/L) of key components and ratios for the Pastos Grandes brine

K	Li	Mg	Ca	SO ₄	B	Mg/Li	K/Li
3,733	392	2,257	821	7,547	558	5.76	9.53

1.5 Drilling and testing

Three drilling campaigns have been carried out for the Project since 2011. Eramet SA (“Eramet”) conducted the first exploration program in 2011 including 11 shallow exploration boreholes (“SW” series), two diamond drill holes (DW01PGDDH and DW02PGDDH), four shallow exploration holes completed with 6-inch diameter casing (“PMP” series), and three exploration wells of varying depths completed with 6-inch diameter casing (DW03PG, DW04PG, DW05PG).

The second and third campaigns conducted by Millennial included 32 brine exploration boreholes (PGMW16-01 through PGMW19-22), 6 freshwater exploration wells (PGWW18-01 to PGWW19-06) and 4 brine production wells (PGPW16-01 to PGPW18-17) with drilling depths of up to 640 m. Most of the monitoring wells were

completed as piezometers with 2-inch diameter PVC slotted casing, while production wells were constructed with 6 to 8-inch diameter screened casing.

AMSA carried out a drilling program on the Sal de la Puna Project immediately south and adjacent to the LAC properties in Salar de Pastos Grandes during 2021/2. This program consisted of two diamond core holes (DD-01 and DD-02), three combination core /rotary holes (RR-01 through RR-03), a production well (PW-1), and several piezometer installations.

The exploration drilling during these campaigns allowed for the collection of continuous cores to prepare “undisturbed” samples from specified depth intervals for laboratory porosity analyses and the collection of depth-representative brine samples at specified intervals. A total of 76 drainable porosity analyses were carried out and 501 primary brine chemistry analyses have been received from certified laboratories.

Eight pumping tests had been completed in Salar de Pastos Grandes. These tests included three one-day tests on freshwater wells PGWW18-02, PGWW19-02 and PGWW19-03, three three-day tests on brine wells PGPW16-01, PGPW18-15 and PGPW18-17; and two long-term pumping tests on brine wells PGPW16-01 and PGPW17-04.

1.6 Current project status

A positive NI 43-101 Feasibility Study (“FS”) was completed (Worley 2019) for Millennial for a 24 KTPY battery lithium carbonate production plant with a 40-year mine-life using conventional lithium processing technology. LAC is currently carrying out additional works, engineering, and other optimization studies with the view of publishing an updated technical report supporting the economic and other parameters for the Project and arrive to a construction decision by the end of 2023. LAC further anticipates conducting work to evaluate consolidating the Pastos Grandes basin to include potential upside from the Sal de la Puna Project.

1.7 Mineral resources

The brine resource estimate was determined by defining the aquifer geometry, the drainable porosity or specific yield (“Sy”) of the hydrogeological units in the Salar, and the concentration of the elements of economic interest, mainly lithium and potassium. Brine resources were defined as the product of the first three parameters. The model resource estimate is limited to the LAC mining concessions in Salar de Pastos Grandes and do not include the AMSA properties. The resource model domain is constrained by the following factors:

- The upper boundary of the model is determined by the highest elevation samples within the dataset and, or the phreatic brine level.
- The lateral extent of the resource model covers an area of 56 km², confined within the boundaries of the LAC mining claims in the Salar. Additionally, the extent is restricted by the contact between the Quaternary basin and the underlying basement rock.
- The lower boundary of the model domain is set to coincide with the basement from the geological model or the total depth of 635 m when the basement is not present.

The specific yield values used to develop the resources are based on results of the logging and hydrogeological interpretation of chip samples and recovered core from the drilling programs, results of drainable porosity analyses carried out on 76 undisturbed core samples by Corelabs, GeoSystems Analysis, Daniel B Stephens & Associates. Boreholes within the measured and indicated resource areas are appropriately spaced at a borehole

density of one bore per 4 km². Table 1.3 shows the drainable porosity values assigned to the different geological units for the resource model. The distributions of lithium and potassium concentrations in the model domain are based on a total of 501 brine analyses (not including QA/QC analyses).

Table 1.3 Results of drainable porosity analyses

Lithology	S _y Average
Blanca Lila	0.5%
Alluvium	13.9%
Saline Lacustrine	4.1%
Clastic Central	5.4%
Base Gravels	12.5%

The resource estimation for the Project was developed using the Stanford Geostatistical Modelling Software (SGeMS) and the geological model as a reliable representation of the local lithology. The principal author was closely involved with the block model development; all results have been reviewed and checked at various stages and are believed to be valid and appropriate for these resource estimates. Table 1.4 shows the mineral resource estimate for lithium and potassium for the Pastos Grandes Project.

Table 1.4 Mineral Resources of the Pastos Grandes Project – Dated April 30, 2023

	Measured (M)		Indicated (I)		M+I		Inferred (I)	
	Li	K	Li	K	Li	K	Li	K
Aquifer volume (km3)	13.45		8.81		22.26		6.14	
Mean specific yield (Sy)	0.11		0.11		0.11		0.08	
Brine volume (km3)	1.48		0.97		2.45		0.49	
Mean grade (g/m3)	49	495	13	134	35	352	34	350
Concentration (mg/l)	438	4419	167	1722	331	3352	403	4234
Resource (tonnes)	662,000	6,660,000	118,000	1,180,000	780,000	7,840,000	208,000	2,150,000

Notes to the resource estimate (Table 1.4):

1. CIM definitions were followed for Mineral Resources.
2. The Qualified Person for this Mineral Resource estimate is Frederik Reidel, CPG
3. No cut-off values have been applied to the resource estimate.
4. Numbers may not add due to rounding.
5. The effective date is April 30, 2023

1.8 Conclusion and Recommendations

Based on the analyses and interpretation of the exploration work carried out for the Pastos Grandes Project between 2011 and 2023, the following concluding statements are prepared:

- The entire Project area has been covered by exploratory drilling between 2011 and 2023 at an approximate borehole density of one exploration borehole per 4 km²; it is the opinion of the author that such borehole density is appropriate for the mineral resource estimate described herein.
- The results of drilling 18 core holes and 30 rotary boreholes and the analysis of 501 primary brine samples (excluding QA/QC samples) identify distinct brine composition and grade at specific depth intervals, showing a relatively uniform distribution of lithium bearing brines throughout the Project to a depth of 635 m. The brine composition for the Project is summarized in Table 1.1.
- The lithium bearing brine contains sufficient levels of lithium and potassium to be potentially economic for development.
- Pumping tests carried in production wells completed in this lower brine aquifer supported brine production rates of 25 L/s over 30-day durations indicating favorable hydrogeological conditions and that brine can be commercially produced with conventional wellfield techniques.
- Geophysical surveys and brine exploration drilling carried out within the Project area indicate that the limits of the lower brine aquifer remain open laterally and at depth so that important exploration potential exists to significantly increase the lithium resources documented in the report.
- It is the opinion of the author that the Salar geometry, brine chemistry composition, and the specific yield of the Salar sediments have been adequately defined to a depth 635 m to support the mineral resource estimate described in Table 1.4.

The following technical work is recommended to further advance the Project towards construction and into production.

- Incorporate the lithium resources hosted on the AMSA properties into the resource estimate for the Project so that these resources can be properly incorporated in the numerical groundwater flow and transport modeling for final brine production wellfield design, evaluation of potential environmental constraints, and the estimation of updated reserves.
- Carry out a 30-day pumping test on AMSA production well PW-1 to characterize the southern extent of the lower brine aquifer.
- Drill three deep core holes into the lower brine aquifer to improve the confidence level of geological and drainable porosity parameters in the central clastics and basal gravel /breccia units. These holes should be completed as deep monitoring wells for additional observations point during the additional pumping tests recommended.
- Carry out 30-day pumping tests in existing brine production wells PGPW18-15 and PGPW18-17 with water level monitoring in the above-mentioned new observations points.

- Carry out 7-day pumping test on water production wells PGMW19-2 and PGPW19-3 along with additional groundwater exploration work to secure future water supply requirements from freshwater resources within the Pastos Grandes and Sijes basins.
- Numerical modelling should be resumed with the AMSA-developed 3D FEFLOW groundwater flow and transport model for the basin to carry out predictive simulations for the design and layout of the future brine production wellfield, evaluation of potential environmental effects, and the preparation of updated lithium reserves for the Project.
- Based on the results of the predictive model simulations drill and complete three additional brine production wells in the lower brine aquifer.
- Implement systematic hydro(geo)logical monitoring programs of surface water and groundwater features to reinforce the baseline characterization of the Pastos Grandes basin. Continue with the surveys and studies to improve the quantification of the water balance components of the basin.
- Drill 7-10 deep exploration core holes aimed at increasing the lithium resource base of the Project.
- Drill 4 industrial water exploration wells to evaluate the resources and optimize the production strategy, including Arena Minerals' blocks to the North and East of the basin.

2 INTRODUCTION

2.1 Terms of reference

LAC acquired the Pastos Grandes Project from Millennial in January 2022. LAC subsequently acquired additional mining concessions (LAC Norte and Sur) during 2022. LAC retained Atacama Water to prepare this Technical Report for the Pastos Grandes Project with the objective of updating the mineral resource estimate for lithium contained in brine for the LAC properties in the Pastos Grandes basin based on the consolidation and integration of available information.

LAC completed the acquisition of all the shares of AMSA in April 2023. AMSA owns 65% of the Sal de la Puna Project through a joint venture interest in Sal de la Puna Holdings Ltd. the 100% owner of the Argentine subsidiary, PASAU, the owner of the claims forming part of the Sal del la Puna Project. The remaining 35% of Sal de la Puna Holdings Ltd. is owned by joint venture partner Ganfeng New Energy Technology Development (Suzhou) Co., Ltd. The mineral resource estimate presented herein does not include any resource on the Sal de la Puna properties. LAC anticipates conducting additional work to evaluate consolidating the Pastos Grandes basin to include potential upside from the Sal de la Puna Project.”

This report has been prepared in conformance with the requirements of NI 43-101 and the associated Companion Policy 43-101CP and Form 43-101F1 of the Canadian Securities Administrators and the associated Best Practice Guidelines for Industrial Minerals and Mineral Processing as issued by the Canadian Institute of Mining and Metallurgy. The Report also includes technical judgment of appropriate additional technical parameters to accommodate certain specific characteristics of minerals hosted in liquid brine as outlined in CIM Best Practice Guidelines for Resource and Reserve Estimation for Lithium Brines and as discussed by Houston (Houston et al, 2011).

2.2 Sources of information

The following technical reports have been previously prepared for the Project by the previous owners:

- Technical Report on Pastos Grandes Project. Prepared for LSC Lithium Corporation by Hains Engineering Company Limited. Dated October 2018
- Technical Report: Phase III Measured, Indicated, and Inferred Lithium and Potassium Resource Estimate, Pastos Grandes Project, Salta Province, Argentina. NI 43-101 report prepared by Montgomery & Associates for Millennial Lithium Corporation. Dated May 2019.
- Technical Report: Feasibility Study of the Pastos Grandes Project, Salta Province, Argentina, Technical Report No. 209020-00055-000-GE-TEN-0003 prepared to Canadian Standard NI43-101. Report prepared by WorleyParsons and Montgomery & Associates for Millennial Lithium. Dated July 2019.
- Technical Report: Sal de la Puna Lithium Project, Pastos Grandes Salt Lake, Salta Province, Argentina prepared for Arena Minerals by independent consultants Murray Booker and Pablo Gómez. Dated September 29, 2021.

The author was provided full access to the Project’s database including drill core and cuttings, drilling and testing results, brine chemistry and porosity laboratory analyses, aquifer testing results, geophysical surveys, and all other information available from the work carried out on the Project area between 2011 and 2023. The documentation reviewed and other sources of information are listed at the end of this report in Section 27

References. Various site visits were carried out to the Project area between 2021 and 2022 by Atacama Water and the author to review drilling progress, brine sampling protocols, and related QA/QC procedures. The report was prepared by Frederik Reidel, CPG, “qualified person” (QP) who is independent of LAC as such terms are defined by NI 43-101. The author has relevant experience in the evaluation of brine deposits in South America.

3 RELIANCE ON OTHER EXPERTS

The author has relied on the legal opinion, dated April 12, 2023, prepared by Mr. Rafael Argañaraz Olivero of the firm Argañaraz & Associates for all matters related to the legal title and status of the properties of the Pastos Grandes Project (Chapters 4 and 23).

4 PROPERTY DESCRIPTION AND LOCATION

4.1 Property location

The Pastos Grandes Project is situated within the Department of Los Andes, approximately 10 km south of the village of Santa Rosa de Los Pastos Grandes, and 130 km west of the city of Salta, the capital of the Salta Province in Argentina. The property's location is defined by its center point, which is situated at approximately 3,428,966 mE, 7,283,194 mN (POSGAR 04 / Argentina zone 3). The Project encompasses a surface area of more than 24,000 hectares in Salar de Pastos Grandes at an elevation of roughly 3,785 masl.

The Project site is situated near Highway 129 which connects 40 km north with Highway 51. Highway 51 traverses from Salta to the international border with Chile at the Sico Pass and connects further west to the major mining center of Calama, as well as the ports of Antofagasta and Mejillones in northern Chile. Both ports are major transportation hubs for the importation of mining equipment and the exportation of mineral commodities. Figure 4.1 shows the general location map of the Project.

4.2 Mining license

The location of LAC mining concessions is shown in Figure 4.2, and the property information is summarized in Table 4.1. Tenement coordinates are given in the Argentine coordinate system which uses the Gauss Krueger Transverse Mercator projection and the Argentine Posgar 94 datum. The properties are in Argentine GK Zone 3. All other map coordinates used in this report are Posgar 94 except where noted.

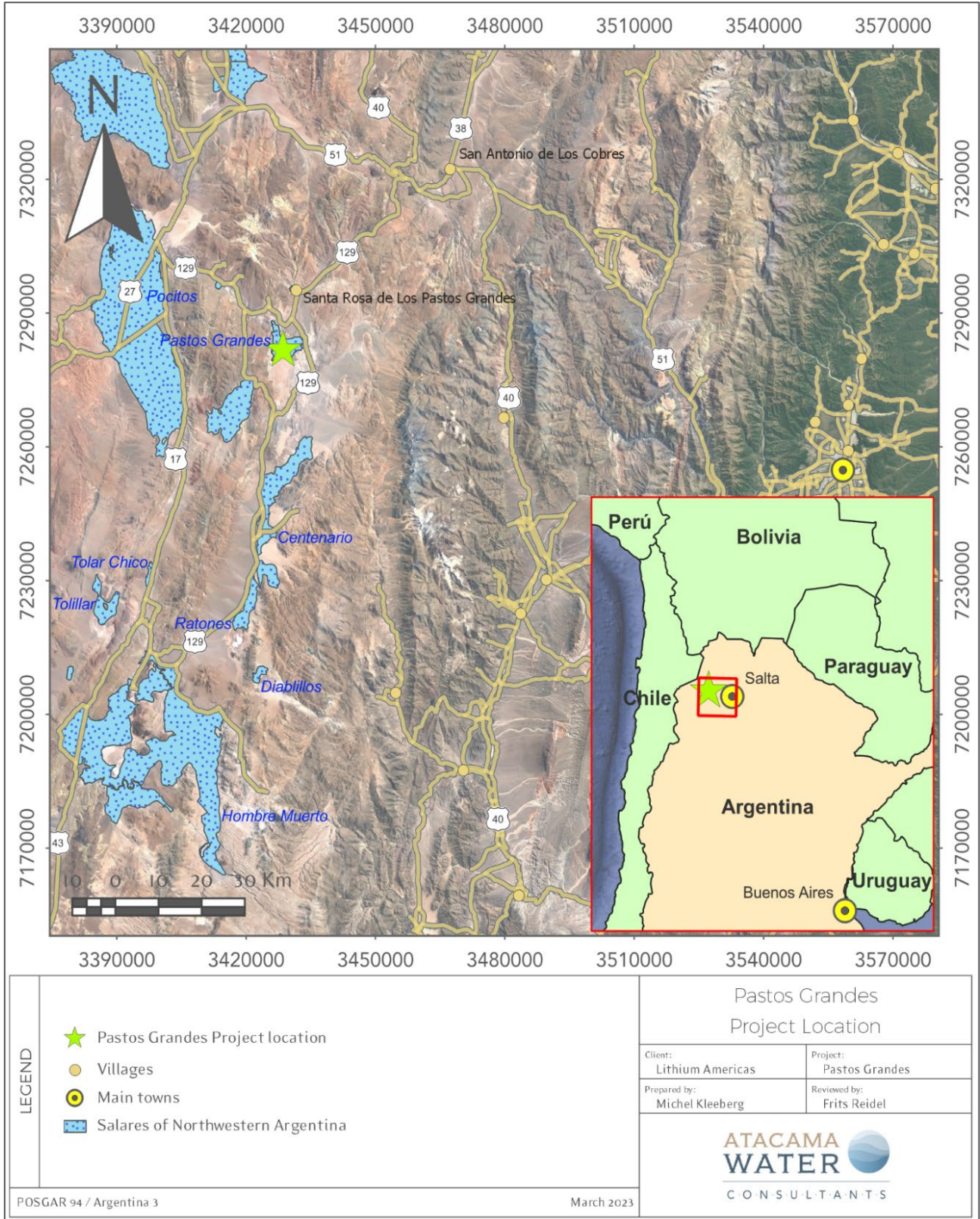
The Argentine mining regulations recognize two types of tenements. Cateos, also known as Exploration Permits, grant permission to explore the tenement for a period that is proportional to its size. The duration of an Exploration Permit is determined by the size of the tenement, with a 1 unit (500 hectares) permit lasting 150 days, and additional units (500 hectares) extending the permit by 50 days each. The largest permit allowed is 20 units (10,000 hectares) and lasts for 1,100 days, starting 30 days after issuance of the permit. The permit holder must submit an exploration work plan and an environmental impact assessment and pay a fee of \$1,600 Argentine pesos per unit (500 hectares). Additionally, the permit holder must make relinquishments after 300 and 700 days.

On the other hand, mining exploitation concessions/licenses are known as "Mines" or "Claims". This kind of permits grant authorization to exploit the tenement, subject to regulatory environmental approval. These licenses have no time limit, provided that the property holder fulfils their obligations under the Mining Code. These obligations include, among others:

- Paying the annual rent (canon);
- Completing a survey of the property boundaries;
- Submitting a mining investment plan; and
- Meeting the minimum investment commitment.

The LAC properties are registered as "Mines" under the file numbers listed in Table 4.1 in the Department of Los Andes (Salta Province). It should be noted that the recently acquired AMSA properties are not included in this list.

Figure 4.1 Location map of the Pastos Grandes Project



4.3 Ownership and title

Through its 100% percent ownership of PGSA, LAC controls the mining concessions of the Pastos Grandes Project. A legal opinion was provided by Mr. Rafael Argañaraz Olivero that indicated the following:

- No key issues have been found. Therefore, there is no foreseeable obstacle to Proyecto Pastos Grandes SA (“PPG”) maintaining ownership on these titles, with the caveat (i) on those areas that were claimed by multiple parties that a lottery may be held, and that area be awarded to a third party (Title 37).
- All patent (canon) payments are up to date on all those claims where the patent is due.
- All claims are free from any evidence of mortgages, encumbrances, prohibitions, interdictions, or litigation.

The following considerations regarding the status of the mining titles were identified in the opinion. The numbering of the observations follows the sequence in Table 4.1.

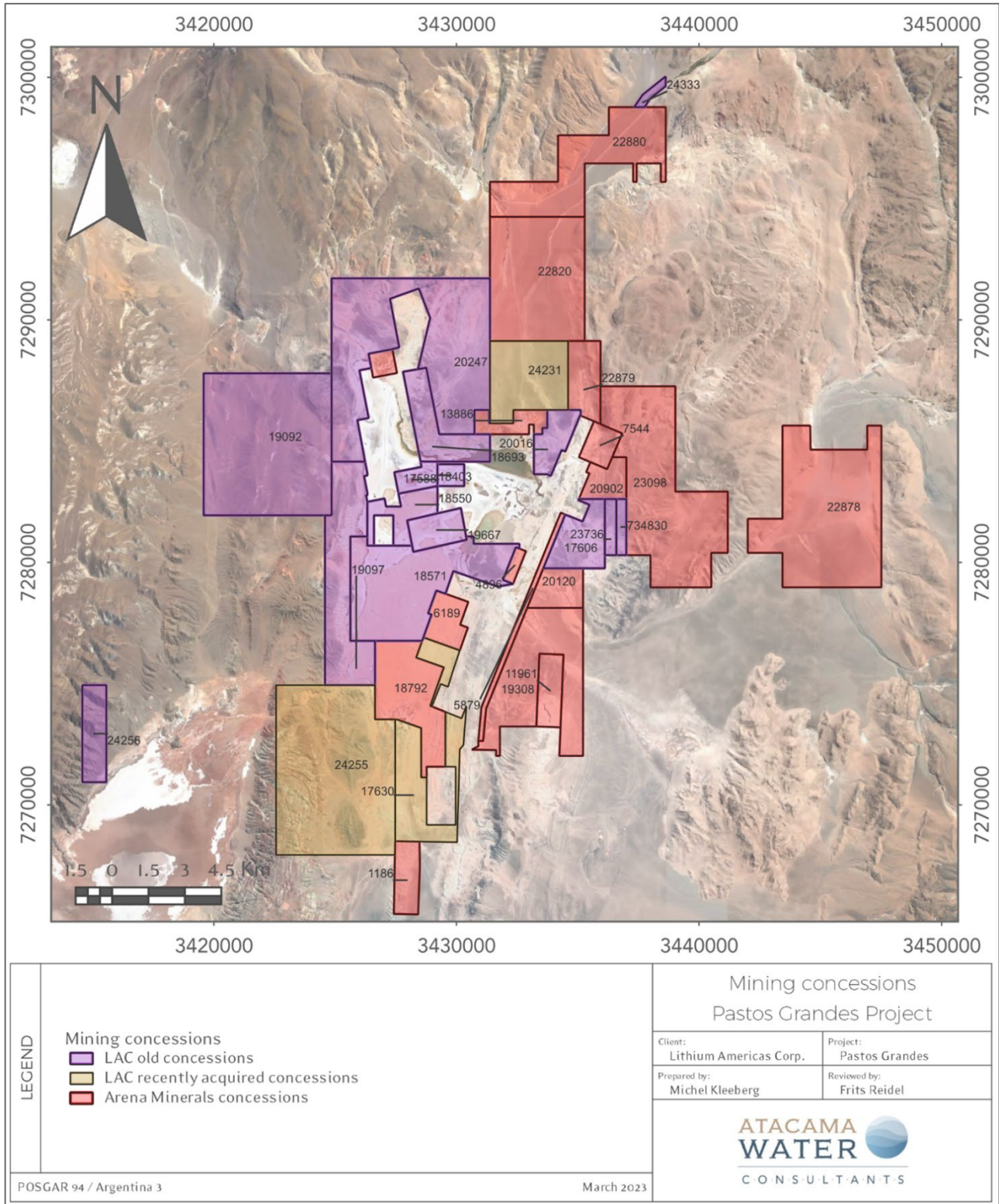
Table 4.1 Mining tenement of the Pastos Grandes Project

PROYECTO PASTOS GRANDES S.A.						
Salta	Loc	Name	File Nº	Granted Area	Under Application	Royalties
1	PG	El Milagro	17588	99		1,5% Gross
2	PG	Neptali II	18403	165		1,5% Gross
3	PG	Norte Argentino	18550	356		1,5% Gross
4	PG	Jorge Eduardo	18693	599		1,5% Gross
5	PG	Aguamarga 15	19097	1,298.00		-
6	PG	TabaPG	20016	317		-
7	PG	Papadopulos LXXIV	20247	3,038.00		-
8	PG	REMSA Investigation Area	22765			-
9	PG	Ignacio	17606	500.05		-
10	PG	Ignacio IV	17630	1,026.84		-
11	PG	Daniel Ramon	18571	1,833.48		-
12	PG	Aguamarga 10	19092	3,087.28		-
13	PG	Nueva Sijesyta 01	23736	109.4423		-
14	PG	Papadopulos XXXII	19667	300		-
15	PG	Easement - Ponds (L_U)	23763		935.56	-
16	PG	Easement - Ponds (A)	23764		486.07	-
	PG	Easement - Ponds (B)	23764		264.36	-
	PG	Easement - Ponds (C)	23764		459.16	-
	PG	Easement - Camp (D)	23764		91.38	-
17	PG	Easement - Ponds (Tar)	23765		83.58	-
18	PG	Easement - Water (A)	23767		7.85	-
	PG	Easement - Water (B)	23767		57.11	-
	PG	Easement - Water (A)	23767		64.27	-
	PG	Easement - Water (B)	23767		60.67	-
	PG	Easement - Water (A)	23767		23.63	-
19	PG	Easement - Road (A)	23768			-
	PG	Easement - Road(B)	23768			-

PROYECTO PASTOS GRANDES S.A.						
Salta	Loc	Name	File Nº	Granted Area	Under Application	Royalties
20	POC	Easement - Storage (Pocitos)	24186		10.00	-
21	PG	Easement - Gas Pipeline	24423			-
22	PG	Easement - Road	20277			-
23	PG	Easement - Brine Duct 01	723917			-
24	PG	Easement - Brine Duct /Pil. Plant 02	723921			-
25	PG	Easement - Ponds 03	723923		422.53	-
26	PG	Easement - Brine Duct /Camp 04	723927		24.11	-
27	PG	PPG 01	24231		968.66	-
28	PG	PPG 02	24255		3,317.50	-
29	POZ	PPG 03	24256		394.80	-
30	PG	Quarry - Agregates - Corral Colorado	24333		50.00	-
31	PG	PPG 04	734830		94.00	-
32	PG	Easement - Brine Duct	740242			-
33	PG	Easement - Brine Duct	740243			-
34	PG	Easement - Ponds (Cas)	741366		100.00	-
35	PG	PPG 05 (UlX)	741363		245.80	-
36	POZ	Amancay VIII	748926		1,447.56	
37	PG	Centenario 208	20259		1,411.25	-

1. **Titles 01 to 04:** the files are fully owned by PPG and in good standing. The Company owns 100% interest in these core properties (the “Pastos Grandes Property”) in Salta Province, Argentina. The Pastos Grandes Property mineral rights, acquired from Mr. Moreno and Mrs. Salas, are subject to a royalty due to the vendors equal to 1.5% of the gross annual sales of lithium from the project, which the Company had the option to purchase for US\$3,000,000 until October 6, 2019, but did not exercise. For clarity, it is noted that the “Pastos Grandes Property” referred to in this paragraph does not include the Contiguous Acquisitions as defined in this document.
2. **Titles 05 to 07:** the files are fully owned by PPG and in good standing. The Company acquired these additional, contiguous mining licenses of 4,653 hectares from the Rojas family-controlled company, Argentina Mining S.A., (the “Rojas Properties”, collectively with the Papadopulos Property, the “Contiguous Acquisitions”).

Figure 4.2 Location map of LAC mining concessions



3. **Title 08:** this is the file started by REMSA in which the tender process for the REMSA area was conducted. This file reflects all the events of the tender which concluded in the signing of an agreement with REMSA aiming at the acquisition and exploration of the area comprised in this file. In August 2017, the Company successfully participated in the tender process and was awarded the opportunity to acquire 2,492 hectares of claims (the “Additional Property”) from the Salta Provincial Energy and Mining Company (“REMSA”). In December 2017, the Company entered into a definitive agreement (“Final Agreement”) with REMSA. On May 29, 2020 PPG and REMSA signed the Closing Deed, in which REMSA confirmed that PPG had strictly complied with each and every one of the obligations derived from the Contract and the 1st and 2nd Addendum Agreements, not having any claim against PPG, and that, consequently, once the remaining Payments were made, the contractual relationship that united them would be extinguished, thus extinguishing all the obligations of PPG towards REMSA. Final payment was executed on June 1, 2020, issuing REMSA a receipt for it on June 2, 2020. The Additional Property is strategically located contiguous to the Company’s current claims.

- As per the Final Agreement, the Company’s commitment to REMSA for the Additional Property included the following:
- a stage 1 spending commitment of US\$15.54 million to maintain its interests and rights in the Additional Properties within twelve months of obtaining the Environmental Impact Report (obtained April 2018). This spending commitment was exceeded within the time frame stipulated in the Final Agreement;
- a guarantee for the US\$1.55 million required bond (obtained); and
- US\$3,000 per hectare for a total purchase price of US\$7,476,150 to be paid as:
 - an initial payment of US\$1,869,038 to REMSA (Cdn\$2,362,153 paid); and
 - payments of US\$1,869,038 to REMSA on each of the first (Cdn\$2,522,864 paid), second, and third anniversary of the signing date of the Final Agreement. On December 18, 2019, REMSA agreed to suspend the terms of the agreement until five mining licenses were registered to the Company. The five licenses were registered with the Company in June 2020; as such, the Company paid the remaining US\$3,738,076 (Cdn\$5,019,862) upon registration of the licenses.

To secure a guarantee for the US\$1.55 million bond required for the stage 1 spending commitment per the terms of the Final Agreement, the Company entered into an insurance contract in August 2017, which was renewed in August 2018 for an annual premium of approximately US\$7,800 (Cdn\$10,365), and provided a guarantee to the insurance company over a bank deposit in the amount of US\$300,000 (Cdn\$398,671), which was included in restricted cash. Having fulfilled the spending commitments, the US\$300,000 deposit was returned to the Company in December 2019.

Having the Company completed all its obligations under the Final Agreement, the same was mutually terminated between PPG SA and REMSA on May 29, 2020.

4. **Titles 09 to 13:** these claims were filed within the REMSA area, which contained vacant mines and free areas. The award of the area on title 08 gave PPG a priority right to claim those vacant mines and free areas. As a result, titles 09 to 13 were claimed by PPG. All these titles have been fully granted to PPG.
5. **Title 14:** Through its Argentine subsidiary, PPG SA, the Company secured an additional 300 hectares of core salar mining rights at Pastos Grandes. Mining rights to the central salar property, Papadopulos XXXII (the “Papadopulos Property”) are contiguous to the Company's holdings, and were fully granted by the Provincial mining authority, the Mining Court of Salta, to the Company.
6. **Titles 15 to 26 and 32 to 34:** these easements were claimed to obtain (i) surface usage rights on areas beyond the boundaries of PPG’s claims and (ii) as well within PPG’s mining concessions. In the case of Title 20, it was claimed to secure a stocking area next to the railway station in Pocitos. Even though PPG’s mining

concessions legally grant PPG priority to the use of the surface, a discussion with a potential claimant of easements within PPG’s concessions wanted to be avoided. The easements are currently in the process of being granted. There is a possibility that those easements claimed on the surface of mining concessions that belong to third parties might be challenged by those third parties, since the Mining Court will notify them of the existence of PPG’s claims. These notifications will open, if a challenge arises, a formal round of negotiations supervised by the Court, after which the Court will rule whether it grants the easement to PPG or not.

7. **Titles 27 to 31:** these claims were filed upon the liberation of these areas by the Mining Court. These are adjacent to the Project and awaiting the granting in full by the Mining Court. In the case of Title 30, it was claimed to secure the provision of aggregates during the construction and production stages of the project.
8. **Title 35:** this mine was filled overlapping a camp easement that belongs to Ulex and a water easement that belongs to Borax, both borates companies, aiming to obtain the mineral rights under the surface, without disturbance to Ulex’s nor Borax’s operations. The Court has notified the companies of PPG’s claims. PPG has not received to date notice of any submission made by these two companies. In case of opposition to our claim, the Court may notify a hearing to all parties to negotiate, or it could plainly reject PPG’s claim.
9. **Title 36:** this claim was acquired in full from Mr. Castañeda on August 2, 2022. The agreement provides for the following installments:

	DATE	USD	DUE
1	Signing	\$250,000	02/08/2022
2	4 Months	\$125,000	02/12/2022
3	4 Months	\$125,000	02/12/2022
4	8 Months	\$250,000	02/04/2023
5	12 Months	\$250,000	02/08/2023
	Total	\$1,000,000	

Installments 3,4 and 5 are subject to the condition that a deed of transfer from Mrs. Romero to Mr. Castañeda is registered on title at the Court. This registration took place on February 9, 2023. Following this transfer, PPG is starting the process to sign the deed and have the title registered to it.

This title is in a very early stage of the process, awaiting its full granting by the Court.

10. **Title 37:** this claim was filed upon the liberation of this area by the Mining Court. Many claimants filled for this area on the same date and time as PPG. Consequently, the Court will eventually notice all claimants to a hearing where a lottery of the area will be conducted, and the area awarded to the drafted claimant.

4.4 Royalties

The Argentine federal government regulates ownership of mineral resources, although mineral properties are administered by the provinces. In 1993 the federal government established a limit of 3% on mining royalties to

be paid to the provinces as a percentage of the “pit head” value of extracted minerals. ANG is expecting a 3% royalty payable to the Salta Province based on earnings before income tax if a brine mining operation is established.

4.5 Environmental liabilities

The author is not aware that the Project is subject to any material environmental liabilities.

4.6 Other significant factors and risks

Several normal risk factors are associated with the property. These risks include but are not limited to the following:

- Mining properties may not be renewed by the provincial authorities.
- Final environmental approvals may not be received from the local authorities.
- Obtaining all necessary licenses and permits on acceptable terms in a timely manner or at all.
- Changes in federal or provincial laws and their implementation may impact planned activities.
- The company may be unable to meet its obligations for expenditure and maintenance of property licenses.
- Activities on adjacent properties may have an impact on the Project.

5 ACCESSIBILITY, CLIMATE, LOCAL RESOURCES, INFRASTRUCTURE AND PHYSIOGRAPHY

5.1 Accessibility

From the city of Salta the Project is reached via the town of Campo Quijano, then continuing along National Route 51 (RN-51) through Quebrada del Toro, the town of San Antonio de los Cobres, and a further 15 km to the junction with Provincial Route 129 (RP-129). 45 km to the Southwest is the village of Santa Rosa de Los Pastos Grandes, which is located 8 km in a straight line to the north of the Salar. Total driving time from Salta to the Project is approximately 4 hours.

The distance between San Salvador de Jujuy and the Project is approximately 330 km and takes about 5 hours by car. The access from Jujuy is via National Route 9 (RN 9) for approximately 60 km to the north until reaching the town of Purmamarca, from there National Route 52R (RN52) for a further 150 km, passing the village of Susques to RP 40 reaching San Antonio de Los Cobres, where the same route described above leads to the village of Santa Rosa de los Pastos Grandes and then to the Salar.

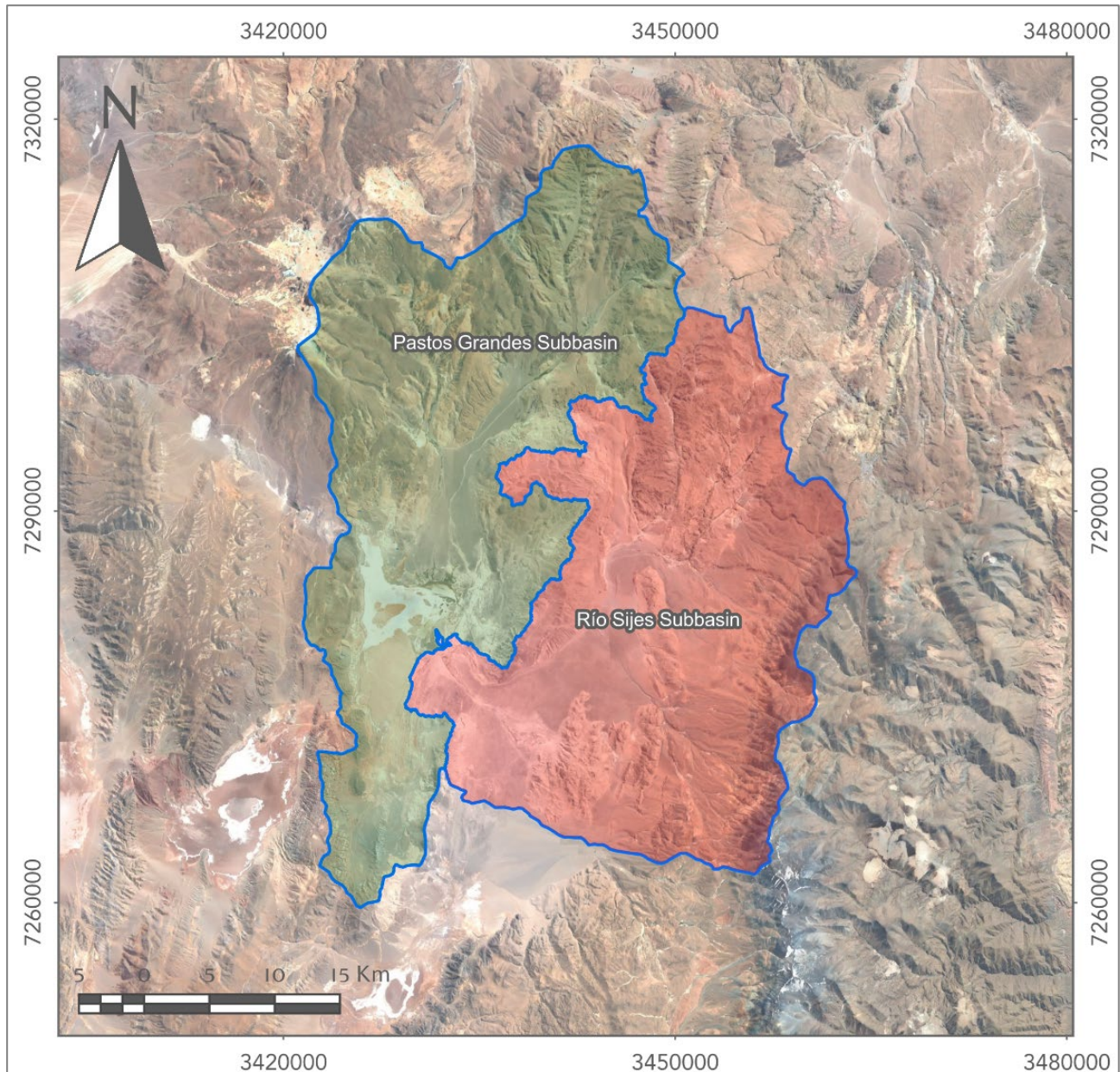
San Antonio de los Cobres is 50 km to the northeast from the Project with a population of approximately 5,500. It hosts the regional administration and has a hospital, petroleum and gas services, and several hotels. The village of Pocitos with a population of approximately 100 is located some 40 km to the northwest of the Project. It is envisaged that some labour force will be contracted from these localities.

5.2 Physiography

The hydrographic basin of the Salar de Pastos Grandes covers 16,901 km² in the Altiplano of Northwestern Argentina. The average elevation of the basin is 4,301 masl while the maximum and minimum elevations are 6,004 masl and 3,767 masl respectively. The Pastos Grandes Basin has been divided into two subbasins according to topographic criteria, the Río Sijes sub-basin at the east and Pastos Grandes sub-basin at the west as shown in Figure 5.1. The active saline crust of the Salar is in the western section of the hydrographic basin and covers near 31.4 km². The salar nucleus sits at an approximately elevation of 3,767 masl.

Unlike other salars of the region, the topography of the nucleus of the Salar the Pastos Grandes is irregular. The current saline crust flat is disrupted over approximately 15% of its area by elevated outcrops of Blanca Lila Formation, which have been interpreted as slightly older salar sediments that have been eroded yet remained as more resistant "islands".

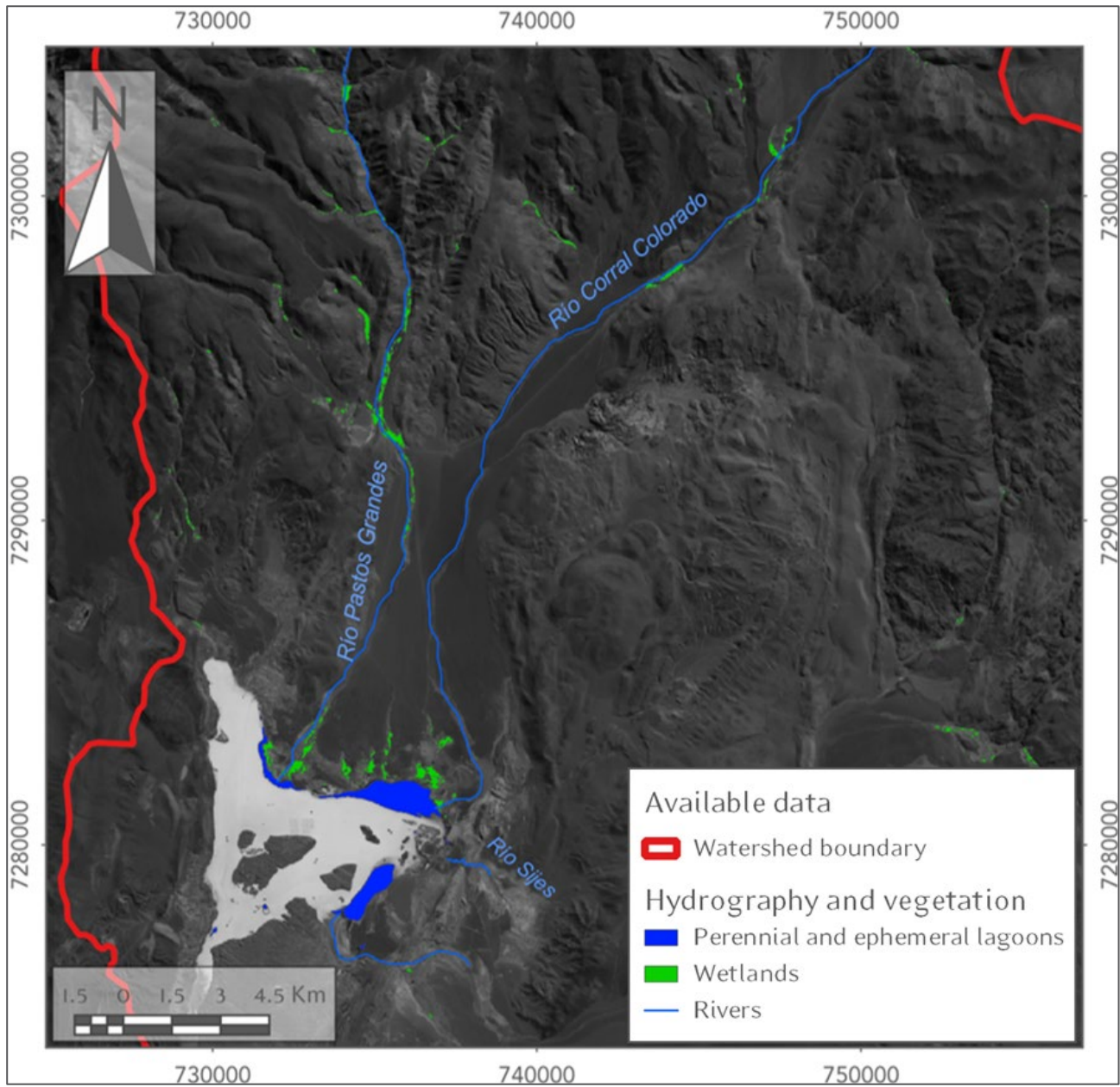
Figure 5.1 Hydrological subdivisions of the Pastos Grandes Basin



Surface runoff is mainly restricted to the rainy season during summer. Three intermittent to ephemeral rivers enter the Salar, Río Sijes from the east, Río Pastos Grandes from the north, and Río Corral Colorado from the northeast. Flow in Río Sijes may originate from groundwater discharge to the surface system near the exit point of the Sijes subbasin into the Pastos Grandes. Average flow of Río Sijes has been measured at 160 l/s. Flow in Río Corral Colorado has been measured at 44 L/s and in Río Pastos Grandes at 38 L/s. A systemic surface monitoring is being implemented during 2023 to obtain a better understanding of the flow regimes in these rivers throughout the different seasons of the year.

Three semi-permanent lagoons occur near the discharge areas of the three above-mentioned rivers into the nucleus of the Salar. Springs and wetlands occur towards the north of the Salar over the interface between the alluvium and evaporitic crust in the lower parts of the Río Pastos Grandes and Río Corral Colorado.

Figure 5.2 Surface water features within Pastos Grandes basin



5.3 Climate

The climate in the Project area is severe and can be described as a typical continental, cold, high-altitude desert, with resultant scarce vegetation. Daily temperature variations may exceed 25°C. Solar radiation is intense, especially during the months of October through March leading to high evaporation rates. The rainy season occurs between the months of December and March when occasional flooding can develop in the Salar and may limit certain exploration activities.

Limited historical climate data are available for the Project and the surrounding areas and is mainly derived from public government-operated stations. These records extend from 1950 to 1990 with 30 years of complete information for most stations. Private data from other companies operating in the region have shorter recording periods including 10 years at El Fénix station from FMC in Salar de Hombre Muerto. Locally, the Project maintained a meteorological station during 2017-2018, completing 10 months of measurements to help building a preliminary water balance for the basin. Mean annual precipitation measured at these stations range from 48 to 121 mm/year while the mean temperature is between 4.7 – 8.1 °C. Eramine also installed in 2012 a station within the Salar with 18 months of records.

Figure 5.3 shows the location of the meteorological stations that were used to characterize the climate for the region.

5.3.1 Temperature

It has been observed that due to the relative proximity and similar elevation, the temperature of Salar de Pastos Grandes exhibits a similar pattern to the San Antonio de Los Cobres and Mina Concordia stations (Dworzanowski et al., 2019). The data between 1950 and 2001 show a mean temperature of these stations of about 7°C, ranging from 1.7°C in winter to 11°C in summer. Daily variations are close to 20°C.

5.3.2 Rainfall

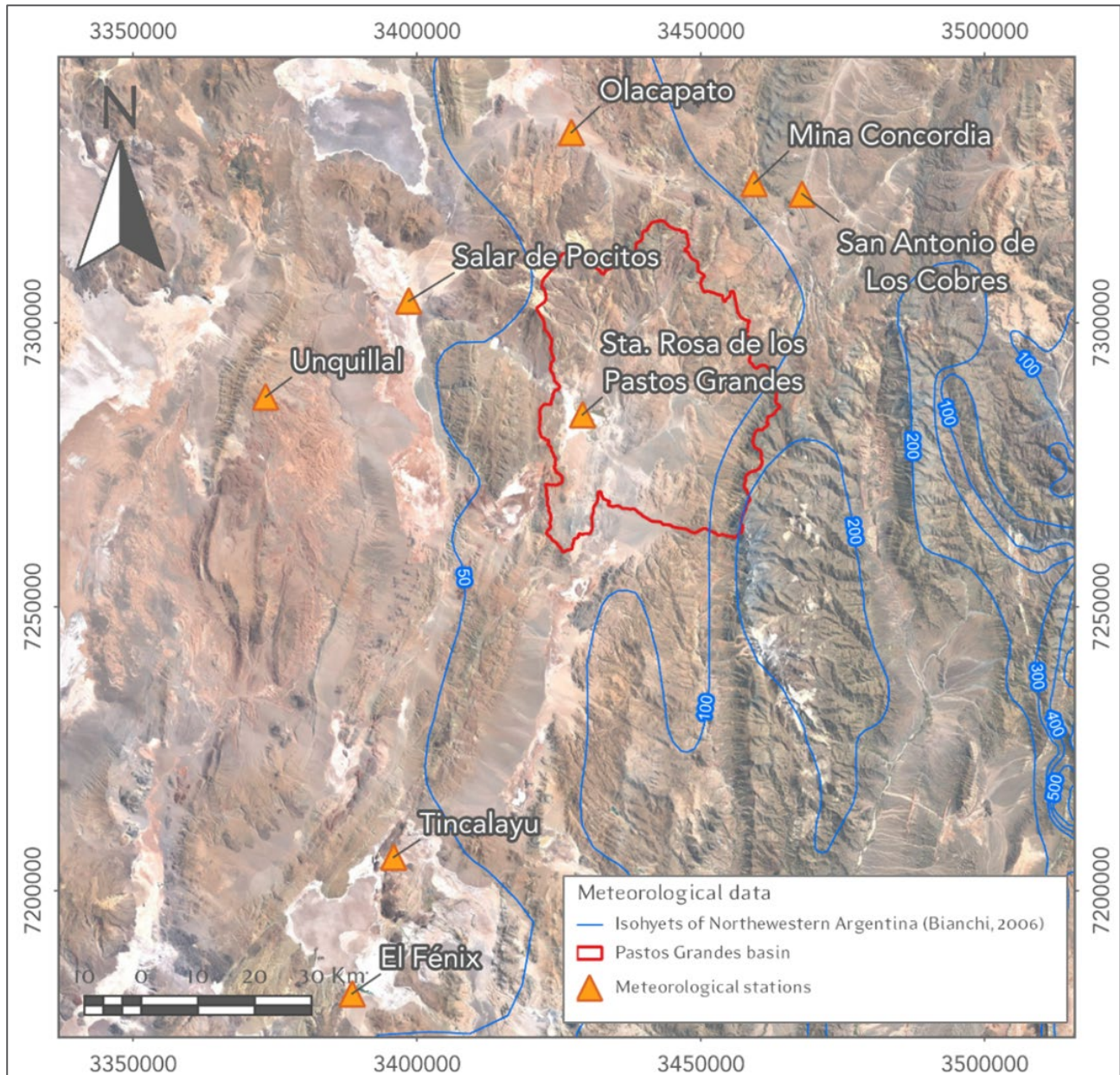
The rainy season occurs between the months of December and March, where most of the annual rainfall occurs often in brief convective storms that originate from Amazonia to the northeast. The period between April and November is typically dry. Annual rainfall tends to increase towards the northeast, especially at lower elevations. Significant control on annual rainfall is exerted by ENSO (El Niño-Southern Oscillation) (Houston, 2006) with significant yearly differences in rainfall linked to ENSO events.

Mean annual precipitation is estimated from a relationship between precipitation and geographical location (M&A, 2018), based on historical meteorological records in for the vicinity of the Pastos Grandes basin. This relation considered latitude and elevation of each station, and was described by the following equation:

$$Pp = 0.0687 * Z + 85.691 * L - 5,540.37 \quad (1)$$

Where Pp: mean annual precipitation (mm), Z: elevation (masl), L: geographical longitude expressed in degrees.

Figure 5.3 Isohyet map for Salar de Pastos Grandes



The result of this approximation is shown in Figure 5.4 where a correlation factor R^2 of 0.86 was obtained which is considered adequate for the scopes of this report.

After dividing the Pastos Grandes basin into elevation bands and applying equation (1) to each different band, a mean precipitation value of 137 mm/year was estimated for the basin as shown in Figure 5.5. This magnitude of rainfall is consistent with annual precipitation estimated for several basins of the region, as well as with the isohyet map of northwest Argentina in Figure 5.3.

Figure 5.4 Correlation between observed and predicted annual precipitation (M&A,2018)

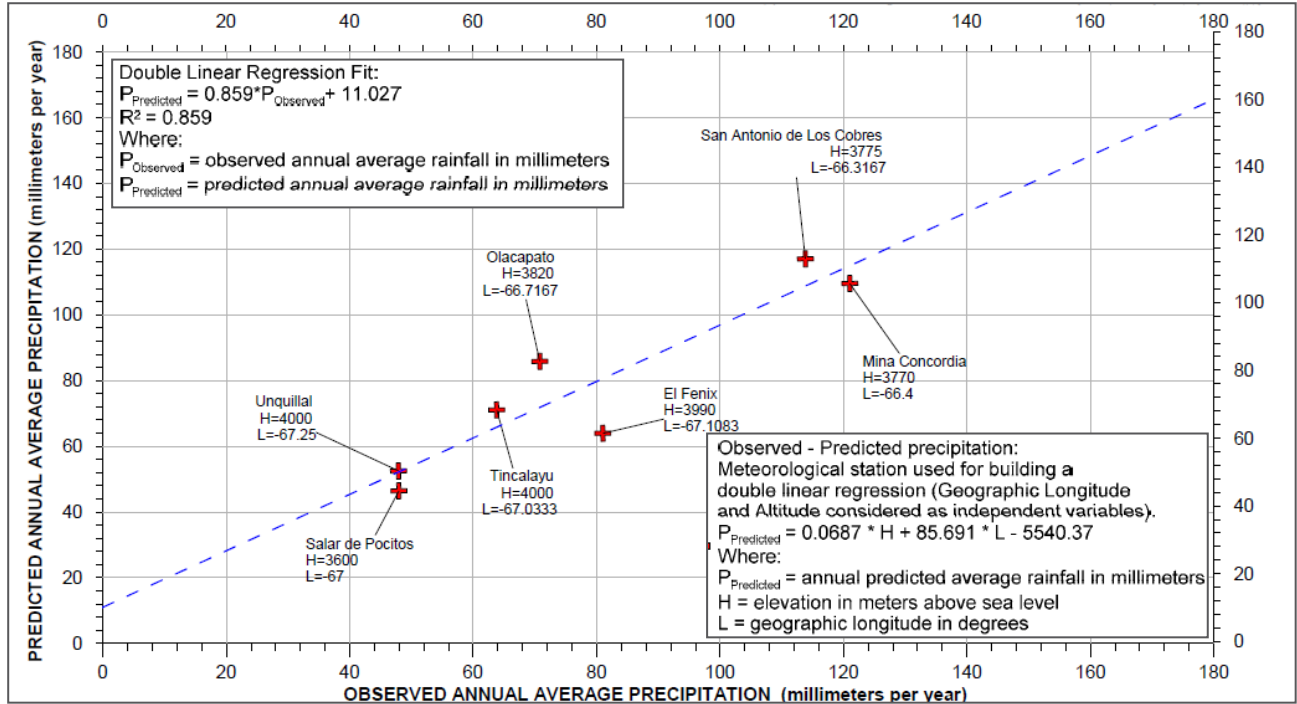
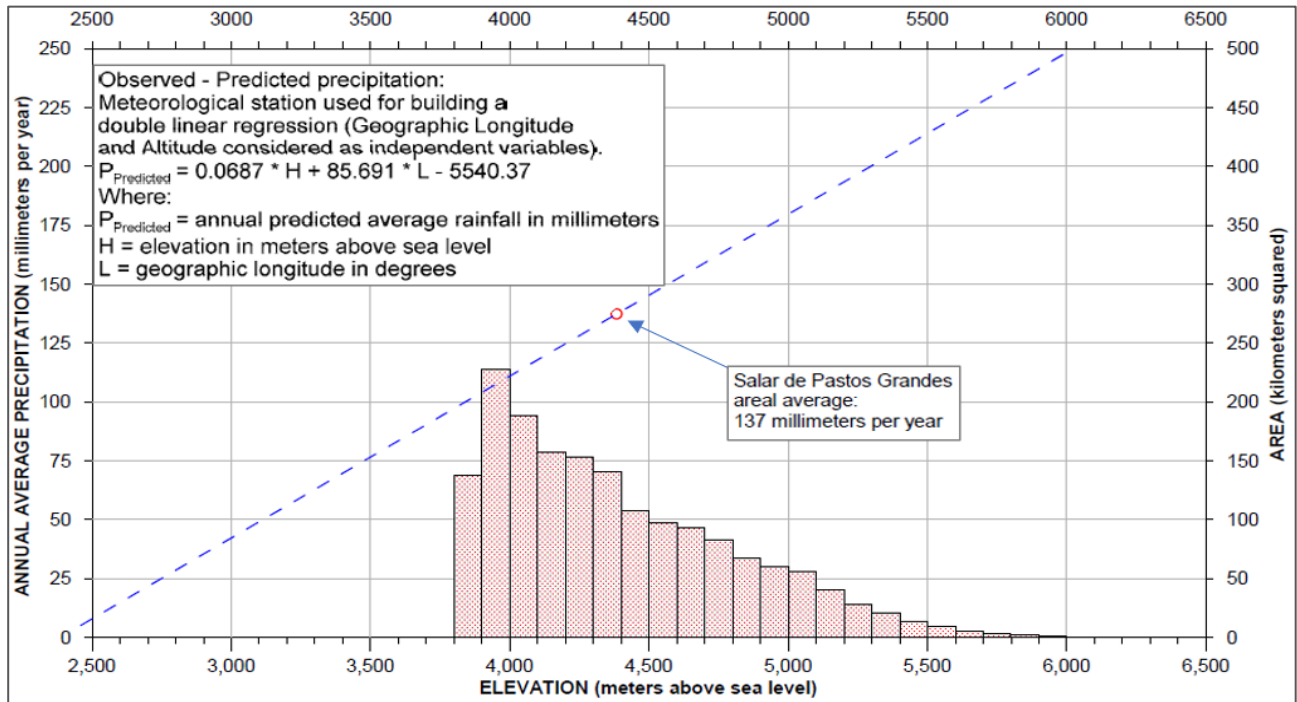


Figure 5.5 Predicted annual precipitation for the Salar de Pastos Grandes (M&A,2018)



5.3.3 Solar radiation

Solar radiation is the most important energy input for evaporation. Long-term solar radiation data is not available for the Salar de Pastos Grandes directly. Local solar radiation measurements were taken from the meteorological station installed in 2017 which registered maximum values between 750 to 1.550 W/m² and mean values between 200-400 W/m² as shown in Figure 5.6.

5.3.4 Wind

Strong winds are frequent in the Puna, reaching speeds of over 100 km/h on rare occasions with an average near 15 km/hour. The wind during summer is generally pronounced after noon and usually calmed during the night. During winter wind velocities are generally higher than in summer. A summary of wind speeds measured by the Pastos Grandes meteorological station during 2017 – 2018 is shown in Figure 5.7.

Figure 5.6 Solar radiation measured at Salar de Pastos Grandes (M&A,2018)

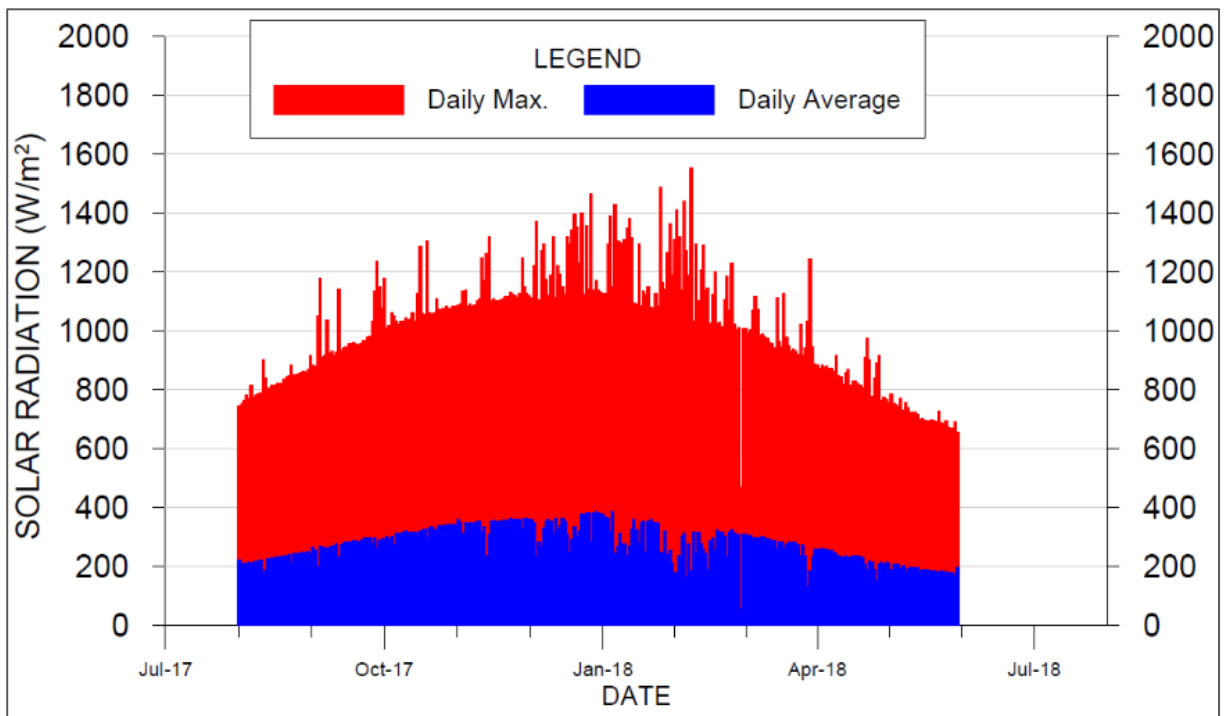
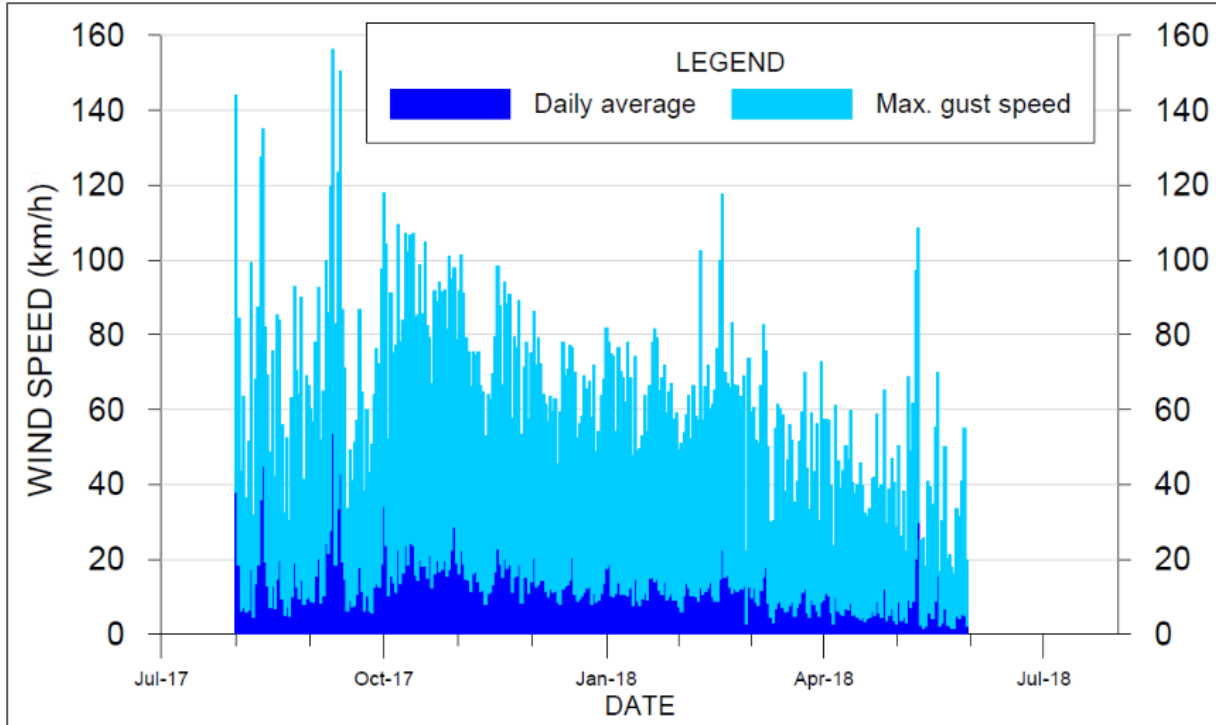


Figure 5.7 Wind speed measured at Salar de Pastos Grandes (M&A,2018)



5.3.5 Evaporation

Evaporation was estimated using empirical relations between evaporation and elevation derived from measured data across several salars in the Atacama Desert. Houston (2006) proposed the following equation for freshwater pan evaporation:

$$\text{Pan freshwater evaporation} \left(\frac{\text{mm}}{\text{year}} \right) = 4,364 - 0.59 * Z \quad (2)$$

Where Z is the elevation of the evaporating feature.

From relation (2), and assuming mean elevation of 3,785 masl for the salar crust, pan freshwater evaporation was estimated to be 2.130 mm/year. To estimate pan brine evaporation a salinity factor (K_s) was used which is dependent on density. According to Ide (1978) this factor is described by the following equation:

$$K_s = -3.7625d^2 + 6.3353d - 1.5725 \quad (3)$$

Where d: fluid density (g/cm^3)

Assuming the brine of Pastos Grandes has a homogeneous density of $1.2 \text{ g}/\text{cm}^3$, the salinity correction factor reaches 0.61, leading to a pan brine evaporation of 1,299 mm/year. This rate can be broken monthly using the monthly fractional values of annual pan evaporation found in Houston (2006) as shown in Table 5.1.

5.3.6 Summary of meteorological parameters

A summary of the measured and estimated meteorological parameters in the Salar de Pastos Grandes is shown in Table 5.1.

Table 5.1 Principal meteorological parameters of Salar de Pastos Grandes

Month	Pp ¹ (mm)	T ² (°C)	Mean solar radiation ³ (W/m ²)	Maximum solar radiation ⁴ (W/m ²)	Pan-A freshwater evaporation ⁵ (mm)	Pan-A brine evaporation ⁶ (mm)
Jan	59	11	304	1,489	244.6	149.2
Feb	50	10.8	271	1,552	227.8	138.9
Mar	2	10	275	1,245	217.2	132.5
Apr	0	7.5	230	976	168.7	102.9
May	0	4.2	191	786	130.8	79.8
Jun	0	2.3	#N/D	#N/D	113.9	69.5
July	0	1.7	#N/D	#N/D	111.8	68.2
Aug	0	3.9	227	916	132.9	81.0
Sep	0	6	276	1,239	154.0	93.9
Oct	0	8.2	321	1,306	198.2	120.9
Nov	0	10	346	1,322	204.6	124.8
Dec	3	10.8	338	1,466	225.7	137.6
Total	113	7.2	278	1,552	2,130	1,299

5.4 Local Infrastructure

5.4.1 Railroad

The Project is in the vicinity of the existing railroad between Salta and Antofagasta that is administrated by two different companies: The Chilean Ferrocarril Antofagasta – Bolivia (Luksic Group) and the Argentinean state owned Ferrocarril Belgrano. It consists of a narrow-gauge railway connecting Antofagasta (Chile) on the Pacific coast to the northern part of Argentina with connections to Buenos Aires on the Atlantic coast. The connection between Pocitos – Antofagasta has been reinstated in cooperation between the regional governments and is currently active shipping product for Livent’s lithium operation in Salar del Hombre Muerto.

¹Annual mean precipitation observed in the Salar 2017-2018 (M&A, 2018)

²Data taken from San Antonio de los Cobres weather station (Bianchi et al., 2005), available in https://anterior.inta.gob.ar/prorenea/infoprorenea/resultados/Precip_NOA/base_precipitaciones_noa.asp

³Solar radiation observed in the Salar 2017-2018 (M&A, 2018)

⁴Solar radiation observed in the Salar 2017-2018 (M&A, 2018)

⁵Estimated by using the assumptions found in Houston (2011) and Houston (2006)

⁶Estimated by using a salinity correction factor on pan freshwater evaporation (IDE, 1978)

5.4.2 Natural gas

A natural gas line (Gas de la Puna) with a distribution terminal is in the village of Pocitos. Here gas is redistributed to Livent in Salar del Hombre Muerto and other lithium operations in the Puna currently being developed. It is planned that the Project will connect to this terminal with a dedicated pipeline for the supply of natural gas during operations.

5.4.3 Water

It is expected that all industrial water supply requirements for the Project can be developed from groundwater resources hosted in the alluvial fans surrounding Salar de Pastos Grandes.

5.4.4 Surface area

The Project controls sufficient surface rights to execute the contemplated mining and processing activities.

5.5 Vegetation

Due to the extreme weather conditions in the region, the predominant vegetation is of the high-altitude xerophytic type adapted to high levels of solar radiation, winds, and severe cold. The vegetation is dominated by woody herbs of low height from 0.40 - 1.5 m, grasses, and cushion plants. The nucleus of the salar is devoid of vegetation due to its high salinity surface.

6 HISTORY

Borate mining has taken place in the general vicinity of Salar de Pastos Grandes since the early 1960s. Borax Argentina, recently divested by Allkem, extracts colemanite, hydroboracite, and ulexite from the Sijes Formation located on tenements situated on the southern and eastern edges of the Pastos Grandes basin. These minerals are processed at the Sijes borates plant.

In 1979, DGFm (a state-owned Argentine arms manufacturer) conducted a lithium exploration program that covered several salars in northwestern Argentina, including Salar de Pastos Grandes (Nicolli et al., 1982). The exploration included surface mapping and sampling of six brine samples from surface, eight from hand-dug pits, and four from streams around the Salar. The sampling campaign found lithium and potassium concentration anomalies with average values of 384 parts per million (ppm) Li and 4,066 ppm K for the pit samples, and 327 ppm Li and 3,518 ppm K for the surface samples. The stream samples reported lithium concentration below detection limits.

In 1987 ULEX began borate production at the Sol de Mañana Mine in the southeastern portion of the Salar near the Rio Sijes reaching a production of near 1,000 tonnes of colemanitehydroboracite- ulexite per year (Hains et al., 2018). Tramo SRL has mined borates (colemanite) at the Quebracho property on the southern border of Salar de Pastos Grandes and common salt (halite, NaCl) on the Salar's surface since 2006. Other smaller mining companies have also carried out salt exploitation over various properties in the Salar (Dworzanowski, 2019).

During 2011 and 2012, Eramet through its subsidiary Eramine Sudamerica SA ("Eramine") carried out exploration activities in the Salar including geophysical surveys (VES, TEM and CSAMT campaigns), drilling (exploration and production wells to maximum depth of 160 m), testing, and geochemical sampling. This work has been referred to as the Stage One investigation of the Pastos Grandes Project and identified a lithium-enriched brine aquifer with lithium concentrations ranging between 330-560 mg/L and a ratio Mg:Li of between 5.35 – 7.87.

LSC Lithium undertook an exploration program between 2016 and 2018 focused on the western and central portion of Salar de Pastos Grandes with a reported mineral resource estimate in 2018 of measured and indicated resources of 344 kt Li and of inferred resources of 58kt Li.

Millennial conducted an extensive program of field work across the Salar from 2016 to 2021 known as the Stage Two and Three investigations of the Pastos Grandes Project. These programs delineated measured and indicated resources of 4,120 Kt of LCE (Montgomery & Associates 2019). A positive NI 43-101 Feasibility Study (FS) was completed (Worley 2019) for a 24 KTPY battery lithium carbonate production plant with a 40-year mine-life using conventional lithium processing technology based on 943 Kt of proven and probable Mineral Reserves. In January of 2022 LAC completed the acquisition of Millennial including the Pastos Grandes Project. LAC is not treating the mineral reserve estimate as a current mineral reserve estimate and no qualified person has done sufficient work to classify this historical mineral reserve estimate as a current mineral reserve. While the mineral reserve estimate was reported in accordance with CIM categories, the qualified person is unable to verify the relevance and reliability of the estimate at this time.

Centaur Resources ("Centaur") carried out lithium exploration activities on the 'Alma Fuerte' mining claim of its Sal de la Puna Project immediate to the south and east of the LAC mining claims during 2018/2019. This program included drilling of three boreholes including a pumping well to around 600 m depth, pumping tests, and seismic & TEM geophysical surveys. On October 19, 2021, AMSA announced the results of the maiden mineral resource estimate (effective as of September 9, 2021) conducted on its Sal de la Puna Project. An Inferred mineral resource consisting of 560,000 t LCE was defined on the Almafuerte property. The resource estimate utilized ordinary kriging for estimation of the lithium and other element concentrations. The porosity model was developed using

geological logs and inverse distance squared estimation of natural gamma log data from holes, which was used to constrain the distribution of an upper halite unit and a lower clastic sediment unit. The halite unit thickens to the east across the Almafuerte property and a hard boundary for porosity data was applied at the contact.

The block model was developed with dimensions of 500 x 500 x 20 m (E, N, RL respectively). The plan dimensions were chosen as they are around a third of the drill hole spacing, and the shorter vertical dimension was chosen to reflect downhole data spacing. The search criteria used for the brine assay ordinary kriging estimates consisted of 2,000, 4,000 and 7,000 m and 100, 100 and 300 m in the horizontal and vertical respectively between the first and third estimation passes.

SDLP Project Lithium Resource

Volume Sediments (m3)	Specific Yield Porosity	Volume Brine (m3)	Brine liters	Li (mg/l)	K (mg/l)	Mg (mg/l)	B (mg/l)	grams lithium	Tonnes Li
3,735,000,000	6.25%	230,000,000	230,000,000,000	460	3,894	2,490	619	1.058E+11	106,000

SDLP Project Lithium Resource

Tonnes Li	Tonnes LCE
106,000	560,000

Work carried out by AMSA on the Sal de la Puna Project prior to its merger with LAC is further described in Sections 10 and 24 below.

7 GEOLOGICAL SETTING AND MINERALIZATION

7.1 Regional geology

7.1.1 Tectonic context

According to Turner (1972) and Isacks (1988), the main lithium-containing region of South America is in the Puna Plateau of the central Andes. The Puna Plateau is approximately 2,000 km long, 300 km wide and has an average elevation of 3,700 m. The eastern volcanic arc and centers have been active from the Miocene to the present (Jordan & Gardeweg, 1989) and are the source of mineralized fluids throughout the plateau. The uplift of the Puna Plateau is the result of the crustal shortening that occurred in the Tertiary and magmatic accumulation (Isacks, 1988).

The section of the Puna which developed in Argentina shows distinct features of the Altiplano than those seen in Bolivia and Peru. Alonso et al. (1984) divided this zone into Southern Puna and Northern Puna according to their relative position with respect to the Olacapato lineament. This lineament corresponds to a regional megafault on a WNW-ESE course that crosses other geological provinces of the Andean axis. The observed geological differentiation in the upper crust is a response to the deep segmentation of the subducted Nazca plate which, and according to Alonso et al. (1984), would condition a different metallogenic development. The southern Puna is considered the *plateau* region associated with the volcanic arc developed between 24° and 27° S and the Northern Puna to the region between 24° and 22° S.

The volcanic arc limits the Puna hydrological basin to the west while the Eastern Cordillera limits this basin to the east. Towards the Puna Austral (Southern Puna), a combination of east-west striking volcanic chains with uplifted blocks caused by north-south striking reverse faults limit numerous hydrological sub-basins (Alonso, 1986; Alonso et al., 1991; Vandervoort, 1995), with numerous and extensive salt flats covering their bases, frequently surrounded by important alluvial systems. Thick sections of Neogene strata (up to 5 km) are present within depositional basins (Jordan & Alonso, 1987; Alonso et al., 1991), which contain evaporites (mainly halite, gypsum, and borates) and alluvial clastic material with smaller tuff horizons (Alonso, 1986). Exposed Neogene strata is present along the margins of the salars due to reverse faulting or as intra-basin uplift within the salt flats (Vandervoort, 1995).

7.1.2 Stratigraphy

The stratigraphy of the Pastos Grandes area (Blasco et al. 1996) are summarized in Figure 7.1 and Figure 7.2. The units that outcrop in the region correspond only to rocks of Ordovician and Cenozoic age.

The Ordovician outcrops are represented by leptometamorphic shales and greywackes, green to grey, strongly folded and fractured that make up the Cordón de Copalayo (Coquena Fm.), on the western flank of the depression, as well as its basement. Additionally, Ordovician plutonites and metamorphites assigned to the Oire Eruptive Complex are found in a conspicuous northern prolongation of the Oire ridge and on the eastern edge of the depression.

In strong angular unconformity and with an inclination towards the east, a thick sequence of tertiary continental sedimentary rocks developed which outcrop across the width of the basin (17 km), although in many cases without continuity. Turner (1960), based on chromatic and lithological differences, subdivided these tertiary sedimentary rocks into Fm. Geste, Fm. Pozuelos and Fm. Sijes, components of what are called the Pastos Grandes Group. Alonso and Gutierrez (1986) identified the Fm. Singuel and separated it from the top originally assigned to the Fm. Sijes of this thick sequence of sparsely consolidated conglomerates with increasing gradation. Figure

7.3 shows a schematic cross-section of the outcrop units in Salar de Pastos Grandes, modified from Alonso (1992).

Figure 7.1 Stratigraphic chart (modified from Blasco et al., 1996)

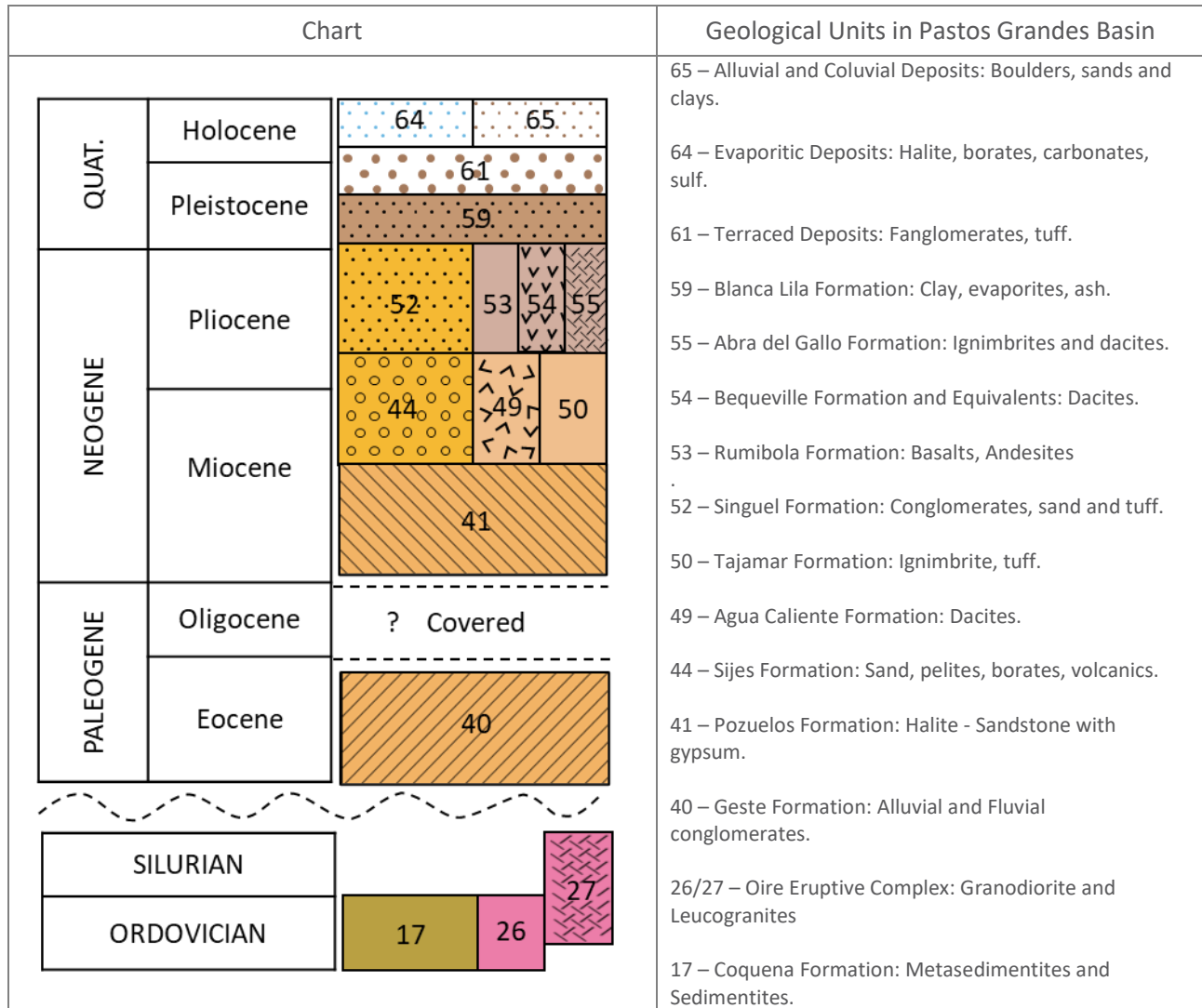


Figure 7.2 Regional geological Scheme (modified from Blasco et al., 1996)



The Oire eruptive complex is mainly constituted by fine-grained and porphyroid varieties of granodiorities which are followed chronologically by leucogranites and rhyodacitic porphyries that intrude into the granodioritic facies. A complex of aplitic and lamprophyric dykes complete the sequence.

Tertiary

Pastos Grandes Group

Turner (1964) defines this group as a set of continental clastic sediments with evaporite intercalations, which varies from coarse-grained at the base to fine-grained, advancing to claystones and limonites with pyroclastic intercalations in the upper third. Based on lithological differences this author recognizes three formations, Geste, Pozuelos and Sijes. The Sijes Fm was later subdivided by Alonso and Gutierrez (1986), separating the Singuel Formation (Figure 7.2).

40 – Geste Formation

This formation consists of fluvial deposits, alluvial fans and conglomerates. It crops out unconformably on Paleozoic units on the western edge of Salar de Pastos Grandes in which two sections are recognized. The lower section is characterized by tabular bodies of thick, poorly selected, light red polymictic conglomerates with clasts of quartz, quartzite, granite, phyllite, vulcanite, schist, hornfels, and limestone. They were interpreted as proximal alluvial fans originated by mud flows. The upper section transitional over the previous one is characterized by fine polymictic conglomerates, light red in color, poorly selected with clasts of quartz, quartzites, granites, phyllite, vulcanite, and schists. It was interpreted as alluvial deposits of distal facies compared with the lower section with passage in the upper part to braided fluvial deposits of the basal part of the overlying Formation. Based on mammal ages, this Unit was assigned a Middle to Upper Eocene age.

41 – Pozuelos Formation

Halite - Sandstone with gypsum interbeds

It outcrops to the north of Salar de Pozuelos and to the east of Salar de Pastos Grandes and is characterized by thick sequences, up to 5m, of halite (rock salt) dominance. It is composed of a succession of rock salt with intercalations of fine sandstone, siltstone, claystone, gypsum, and a small proportion of tuff and tuffite. The upper section, approximately 100 m thick, is dominated by silty claystones, sandstones, and tuffs. The top of the Pozuelos Fm passes transitionally to the Sijes Fm. There are no direct elements that allow dating the Pozuelos Fm; however, based on the 6.8 Ma Sijes Fm and the mammal ages of the upper part of the Geste Fm, it can be delimited between the Middle to Late Eocene and Lower Miocene.

44 – Sijes Formation

Sandstones and shales with borates and pyroclastics

This formation crops out to the east of Campo de la Paciencia in the Colorados range to the southeast of the Salar de Pocitos in the depression of the Salar de Pastos Grandes, and in the Salar de la Laguna up to the northwestern latitude of Salar Centenario.

Three members are recognized in the Pastos Grandes region for the Sijes Formation: Monte Amarillo, Monte Verde and Esperanza.

The Monte Amarillo member is constituted by yellowish-green flakes and has a guide bank of red claystones at the base that integrates the contact unit with the Pozuelos Fm. It has a section with intercalations of pelites with ulexite, gypsum and rhythmic intercalations of hydroboracite and gypsum with disseminated ulexite. It is thought that each sequence represents a lacustrine cycle.

The Monte Verde Member has a lower mudstone section with a gray tuff bank at the base. The upper section of light brown to greenish flakes has rhythmic intercalations of inyoite, colemanite, and gypsum. There is abundant disseminated ulexite and scattered levels of gray tuffs and tuffites. It has a tight folding style, but softer than the underlying member.

The Esperanza Member has the highest pyroclastic content and begins with a normally graded conglomerate that ends with interbedded sandstones and friable shales, as well as two levels of white tuffs. This member contains both diatom and gastropod levels.

Additionally, the upper section is predominantly pyroclastic and contains carbonate levels. Towards the top there are intercalations of coarse sandstone and fine friable conglomerates. The folding style consists mainly of broad folds with homocline deformations found only on the top. These facies were classified as continental endorheic with an arid climate and active explosive volcanism with salt flat beaches and brackish or saltwater lagoons, like the environment that currently prevails in the Puna salars, like Salar de Pastos Grandes nowadays.

Based on radiometric dating, carried out in tuffs located at its base (6.81 Ma) and top (4.0 Ma), it can be deduced that the depositional cycle of the Sijes Fm took place between the upper Miocene and the lower Pliocene.

49 - Agua Caliente Formation y Equivalentes

Dacites

All lava spills and subvolcanic bodies of predominantly dacitic composition belonging to the volcanic cycle that began in the Late Miocene which have been eroded and are integrated under this name. The formation crops out in numerous points and proximities within the Salar de Pastos Grandes. Below the Queva lava flows and volcanic edifices and in the Antuco river creek, south and west of Santa Rosa de los Pastos Grandes. These rocks have grayish tones and a porphyritic structure of abundant phenocrysts of very close feldspars interposed by aphanitic paste. Under the microscope one can see biotitic quartz content, dacites, and andesites with a low proportion of quartz. An intense hydrothermal alteration is often associated with this Formation, particularly in the cases in which it is traversed by northwesterly trending fractures. Based on radiometric dating and stratigraphic relationships (it overlies the Pozuelos Formation), and it is estimated that the top of the Formation dates to the Upper Miocene.

50 – Tajamar Formation

Tuff and ignimbrites

The various outcrops of tuffs, ignimbrites and volcanic agglomerates in the area are closely related to each other, as they are associated with the same volcanic cycle and grouped under this name. Dacitic compositions are prevalent among these extrusive rocks. The Tajamar Fm crops out to the west of Salar de Pocitos. This region is characterized by alternating andesitic agglomerates with a tuff matrix, white dacitic tuffs, and gray and purple conglomeradic sandstones that overlie Tertiary sedimentites of the Pastos Grandes Group and the Batín Fm or on different Palaeozoic units. Based on radiometric dating and stratigraphic relationships the Upper Miocene to Pliocene age is inferred for this unit.

52 – Singuel Formation

Conglomerates and sandstones with tuffs and gypsum

It outcrops to the north of Salar Centenario and can be followed to the south of the Sijes river basin, in the Salar de Pastos Grandes depression. This Formation consists of sandy conglomerates and conglomeradic sandstones of reddish color, arranged in layers formed by Ordovician sedimentary rocks from the Oire Eruptive Complex and ignimbrites and tuffs. In the upper part there are frequent intercalations with tuffs and volcanic agglomerates. The authors who studied this Unit in detail suggest a typical fluvial environment, related to restricted lagoon environments evidenced by the presence of diatoms. Based on the stratigraphic relationships, as well as the dating of ignimbrites and tuffs, it is estimated that the sedimentation of the Singuel Fm and Equivalents could have occurred between the Upper Miocene and the Lower Pliocene.

53 – Rumibola Formation

Andesites and basalts

This Unit includes hypersthene basalts, partly with olivine and hornblend andesites from the Tul Tul del Medio and Pocitos volcanoes, as well as Nevado Queva and the Pastos Grandes mountain range. The andesite lavas and subvolcanic bodies of the Rumibola Fm frequently have a characteristic reddish alteration color. The lower levels of the Chivinar and Guanaquero hills are made up of hypersthene phenobasalts, which may present olivine. The Tul Tul y del Medio and Pocitos volcanoes have a main body formed by hornblendiferous or lamprobolite, hypersthene andesites. In the Nevados de Queva area there are two main pulses of andesitic lavas. A Pliocene age is inferred for this unit extending its lower limit to the upper Miocene.

54 – Bequeville Formation and Equivalents

Dacites

It constitutes a succession of dacitic and andesitic outcrops to the west of Salar Centenario, originally assigned to the Miocene and later inferred to the Pliocene. The Formation corresponds to lavas and subvolcanic bodies, mainly dacitic in composition, with a reddish color in the surface and greenish-gray color in fresh fractures. The rock structure is porphyric with a microgranular holocrystalline paste with quartz, feldspar and mafic phenocrystals.

Based on its morphology, its unconformity stratigraphic relationships with respect to the previous volcanic cycle, its lithological similarities with the tuffs of the Abra del Gallo Fm, as well as alteration dating in volcanites with similar levels of erosion, this Formation is assigned to the Pliocene.

55 – Abra del Gallo Formation

Ignimbrites and dacites

Designated based on the outcropping Unit in the homonymous locality and designated Abra del Gallo Fm. Its deformation is less than the ignimbrites/tuffs of the previous cycle and regarding its morphological aspect can be distinguished by its relatively smooth surface extension, as well as being less dislocated than the ignimbrites of the Tajamar Fm and its equivalents. The Formation crops out in the spring of the Pastos Grandes River and can be seen to the north of the town of Santa Rosa de los Pastos Grandes. The outcrops are composed of hypersthene biotite, phenodacitic tuffs and ignimbrites of yellowish white color. The age of the tuffs and ignimbrites found within this Formation can be assigned to the Upper Miocene to Pliocene.

Quaternary

59 – Blanca Lila Formation

Pelites, evaporites, travertine and borates

The outcrops of this Unit are distributed on the edges of Salar de Pastos Grandes reaching its greatest expression to the north and south, forming slabs towards the center of the Salar. The total outcrops cover 140 km² with an approximate thickness of 30 meters.

In unconformity above the Sijes Fm, light gray gravel, sand and tuffites were deposited in banks 20 to 50 cm thick. Occasionally, carbonate veins are present, and cross-bedding and convoluted lamination are observed. Sands and clays continue upward, sometimes with rhythmic stratification. Borate banks are also present, followed by silts and clays. Layers of caliche, which contain bird footprints and plant remains, are intercalated with calcium carbonate cemented levels. The entire unit is covered by a coherent sandy caliche layer that protects the relief from erosion. The depositional environment corresponds to a depression with centripetal drainage, muddy beaches and a predominantly seasonal evaporation body as indicated by the rhythmites. The footprints of birds and diatoms indicate a shallow lagoon environment. These conditions are the same that currently exist in Salar de Pastos Grandes and in some other salars in the region. Fission traces from gray tuff in the middle to upper part of the Blanca Lila Fm indicate a Lower Pleistocene age (1.6 Ma).

61 – Terrace Deposits

Fanglomerates with tuff layers

Under this name are the haulage deposits that constitute the highest terraces. They are described by different authors according to the area in which they are distributed.

They are essentially developed on tertiary deposits of the Pastos Grandes Group reaching Salar de Pocitos to the east. Other smaller deposits which could not be represented due to the scale of the map are found in the vicinity of Salar de Pastos Grandes. They consist of alluvial deposits that generally correspond to the outcrops from which they come. It is made up of medium to coarse fanglomerates, moderately selected with coarse stratification, and a yellowish color that is well differentiated from the reddish deposits of the Tertiary. Clasts of volcanites and metamorphites predominate over the older schists and sediments. In the Salar de Pastos Grandes the piedmont layers are shallow, up to 8 m, and formed by gypsiferous red argillaceous sandstones and light gray argillaceous sandstones, distinguishable from the Blanca Lila Fm. The deposits are sub horizontal and cover tertiary or older units. Considering that the last ignimbritic levels represented by the Abra del Gallo Fm and equivalents are interbedded in the terraced levels, these deposits are inferred to be from the Pleistocene to Early Holocene. The terraced deposits are covered by Holocene basalts.

64 – Evaporitic Deposits

Halite, borates, carbonates and sulfates

The presence of salars in the Puna area is one of its several relevant features, occupying tectonic-type depressions with a general north-south orientation. The basins are endorheic, and their water input has a seasonal distribution. Given the dry climate prevailing in the region, the main output of water occurs through evaporation, along with the consequent formation of salts. Generally, evaporite deposits are intercalated with clayey layers as well as borates and gypsum. The endorheic basins occupied by the salars were already formed during the Pliocene. Thus, volcanism divided primitive basins (as in the case of the Pocitos, Tul tul and Medio volcanoes). Therefore, although the process of formation of vents continues up to the present, it is not ruled out that its accumulation began in the Upper Tertiary.

65 – Alluvial and Coluvial Deposits

Boulders, sands and clays; mudflats

They constitute the modern detrital accumulations and comprise various origins and are widely distributed throughout the region. They present variable thicknesses and are unevenly distributed over all the underlying units. In general they are unconsolidated deposits of highly variable granulometry which cover depressions forming alluvial fans or constitute fluvial deposits in various creeks. Locally there are accumulations of dune forming sands with eolic origin, such as at the southern end of the Salar de Pozuelos. The ejection cones that converge towards the great depressions are composed of clastic elements of variable granulometry, generally sandy silt or fine clastic material. Finally, vertical and horizontal granulometric selection can be observed while superficial and thin layers of angular fragments are common, settled on silt or sand, leaving thick clasts accumulated on the surface.

7.1.3 Structures

The Andean tectonic evolution in the region was conditioned by the Paleozoic structuring and, to a lesser extent, by the extensional regime present during the Upper Paleozoic. Three main compressional stages are recognized during the evolution of Andean tectonics in the region. The first being the pre-Oligocene stage, which folded the

Neopaleozoic strata with crossed orientations respect to the orogenic front, due to the uplift and rotation of blocks controlled by ancient structures. The second stage consists of the foreland basin, which was already installed during the Oligocene, with its deposits slightly deformed into open folds. Finally, the third stage corresponds to the advance of the orogenic front and the recycling of the foreland basin. The elevation of basement blocks was accentuated from 6 Ma (Seggiaro et al., 2006) generating a folded belt of thick skin with double vergence. Towards the end of this stage, out-of-sequence structures developed between the main thrusts of ages less than 4 million years. Since the last 2 million years, an important extensional and transcurrent tectonic activity began in the Southern Puna, related to the recent volcanism. Finally, the modern sedimentary deposits were formed by alluvial fans, debris flows, ephemeral fluvial deposits, and mudflats that make up the filling of basins restricted to intermontane valleys.

The dominant structures in the Puna trending N-S to NNE-SSW are generally compressional or transgressive in nature formed mainly during the Neogene. Other structures are lineaments of regional magnitude, transversal to the Andean strike with a northeast and northwest direction along with displacements that occur in the strike direction and changes in the orientation of the Neogene folds and faults as well aligned volcanic flows of Cretaceous, Miocene-Pliocene and Quaternary ages. Some of the transversal lineaments have a well-documented pre-Cenozoic history, such as the Calama-El Toro-Olacapato lineament (Figure 7.4). South of this lineament, the deepest levels of the crust are exposed in both the Puna and Calchaquenia suggesting that the pre-Neogene deformation was dominated by vertical movements, descending towards the north. In addition, immediately north of the lineament, the western edge of the Cretaceous rift basin undergoes a marked westward displacement (Gorustovich et al, 2011). Figure 7.5 illustrates the regional structural evolution of the Altiplano-Puna Zone.

Figure 7.4 Structural setting of the Puna

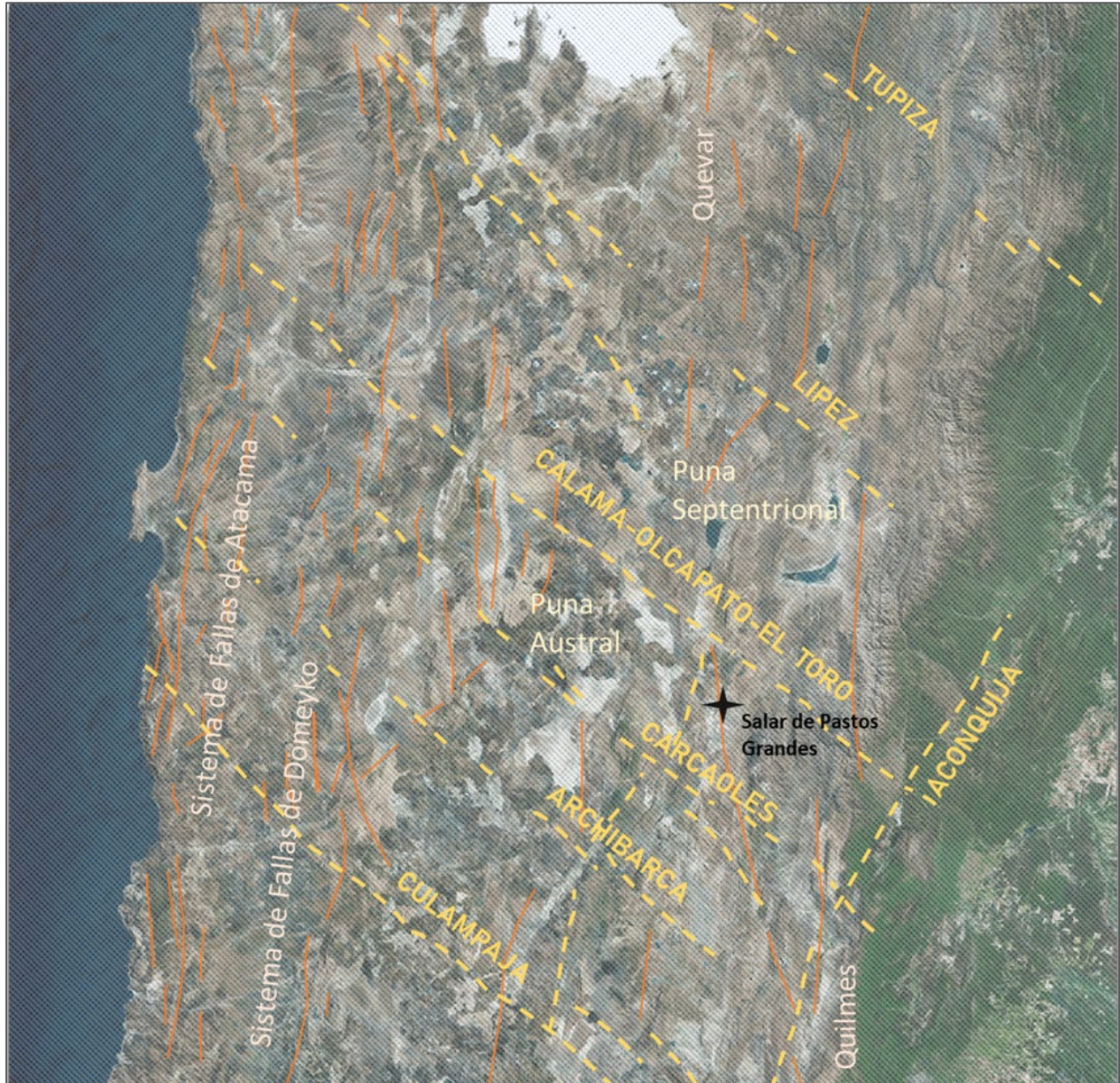
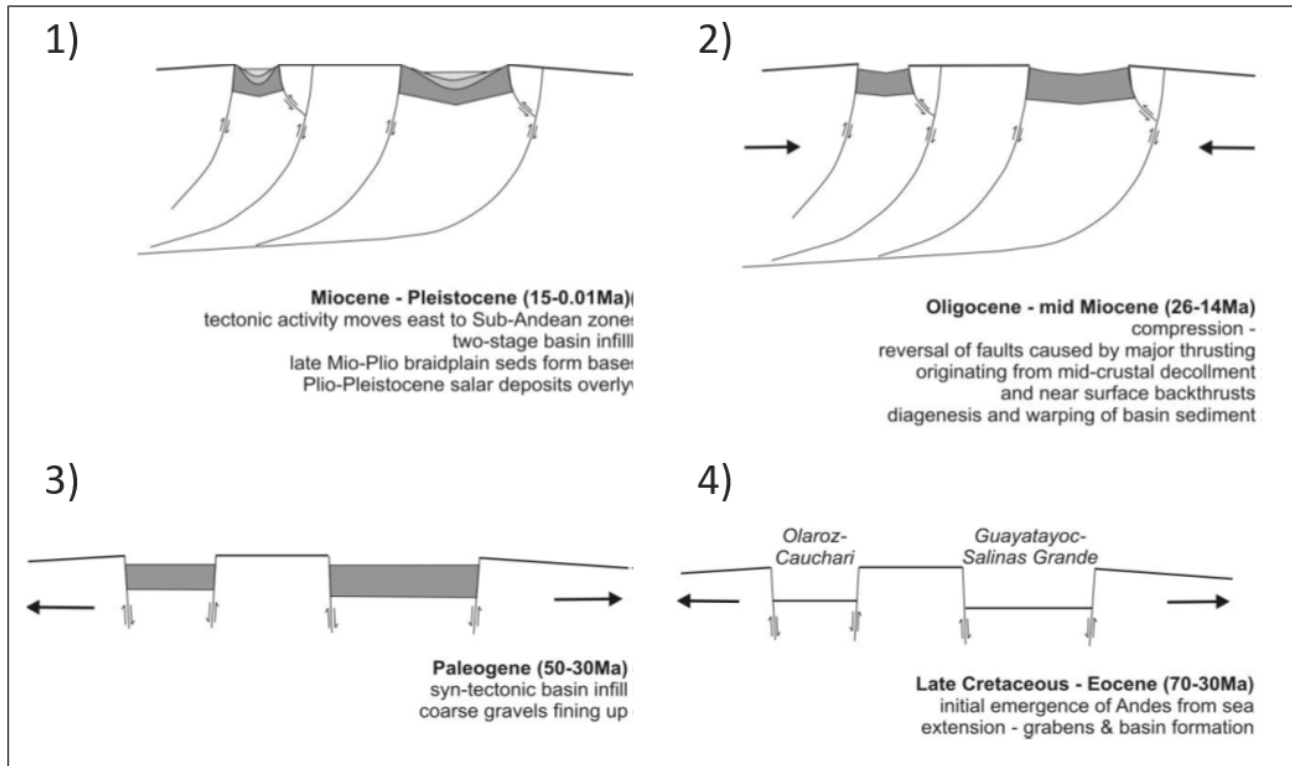


Figure 7.5 Generalized evolution of the structures of the Puna (Houston, 2010)



7.2 Local geology

After reviewing the available historical information associated with the Pastos Grandes Sub-basin, the following sources of information were mainly used for the interpretation and correlation of local geology:

- Drilling records available in the study area, integrating the drilling data from the Project with those reported by third parties in their respective feasibility reports (Millennial and LSC, respectively reported in Dworzanowski et al., 2019 and Hains et al., 2018).
- TEM and seismic sections developed for the Project.
- Shallow seismic refraction tomography survey carried out by Millennial (Dworzanowski et al., 2019).
- Geological sheet and stratigraphic map HG 2566-I San Antonio de los Cobres (Blasco et al., 1996).

7.2.1 Borehole information

As part of this resource update, geological descriptions were reinterpreted and the redundant information of each platform was consolidated in a single drilling record (for example, different boreholes within a few meters, of different depths and different drilling methodologies). The interpretations originally set forth in the core samples descriptions were reconciled with the observations made from field visits to adjust the lithological descriptions with the interpretation of the units.

Table 7.1 lists the detail of the boreholes considered in the reinterpretation while Figure 7.6 shows their spatial distribution.

Table 7.1 Boreholes incorporated in the geological model.

BHID	East (m) ⁷	North (m)	Elevation ⁸ (masl)	Final depth (m)	Drilling method	Source
PGMW16-01	3,429,218	7,283,662	3,775.6	190	DDH	Millennial
PGMW16-01b	3,429,221	7,283,655	3,775.6	355	MR	Millennial
PGMW16-02	3,427,731	7,283,257	3,785	400	DDH-181-MR	Millennial
PGMW17-03	3,428,367	7,283,805	3,773.6	154	DDH	Millennial
PGMW17-04	3,427,853	7,280,921	3,789.8	245.5	DDH	Millennial
PGMW17-04b	3,427,849	7,280,949	3,786.9	564	MR-401-DDH	Millennial
PGMW17-05	3,428,922	7,281,677	3,773.9	121	DDH	Millennial
PGMW17-05b	3,428,927	7,281,683	3,773.9	387	DDH	Millennial
PGMW17-05c	3,428,918	7,281,672	3,773.9	601	MR	Millennial
PGMW17-06	3,429,497	7,281,016	3,785	455	DDH-387.5-MR	Millennial
PGMW17-06b	3,429,497	7,281,016	3,785	424	MR	Millennial
PGMW17-06c	3,429,497	7,281,016	3,785	571	MR	Millennial
PGMW17-07	3,426,888	7,282,228	3,763.1	203.3	DDH	Millennial
PGMW17-07b	3,426,888	7,282,228	3,763.1	203.3	MR	Millennial
PGMW17-07c	3,426,888	7,282,228	3,763.1	412	DDH-283-MR	Millennial
PGMW17-07d	3,426,901	7,282,217	3,763.1	510	MR	Millennial
PGMW17-08	3,429,941	7,281,596	3,785	425.5	DDH	Millennial
PGMW17-08b	3,429,941	7,281,596	3,785	446	MR	Millennial
PGMW17-09	3,428,156	7,283,107	3,785	595	DDH-268-MR-475-DDH-548.5-MR	Millennial
PGMW17-10	3,429,822	7,283,569	3,773.7	601	DDH-178-MR	Millennial
PGMW17-11	3,429,826	7,285,591	3,817.6	568	MR	Millennial
PGMW18-12	3,428,224	7,280,087	3,787.7	554	MR	Millennial
PGMW18-13	3,428,223	7,278,696	3,795.3	559	MR-524-DDH	Millennial
PGMW18-14	3,428,234	7,277,357	3,797.1	635	MR	Millennial
PGMW18-15	3,426,687	7,278,678	3,792.7	594	MR	Millennial
PGMW18-16	3,429,618	7,279,568	3,790.4	641	MR	Millennial
PGMW18-17	3,426,685	7,280,094	3,767.5	605	MR	Millennial
PGMW18-18	3,426,656	7,277,421	3,798.7	605	MR	Millennial
PGMW18-19	3,429,083	7,280,529	3,787.7	602	MR	Millennial
PGMW18-20b	3,430,661	7,279,511	3,777.3	575	MR	Millennial
PGMW19-21	3,426,079	7,279,867	3,784.5	574.3	MR-180-DDH	Millennial
PGMW19-22	3,431,009	7,288,304	3,832.5	464.5	MR-102-DDH- 347.5-MR	Millennial
PGPW16-01	3,429,204	7,283,655	3,775.6	351	MR	Millennial

⁷ POSGAR94, Projection G-K Argentina Zone 3

⁸ Acquired with Handheld GPS

BHID	East (m) ⁷	North (m)	Elevation ⁸ (masl)	Final depth (m)	Drilling method	Source
PGPW17-04	3,427,842	7,280,941	3,788.5	475	MR	Millennial
PGPW18-15	3,426,687	7,278,707	3,792.7	610	MR	Millennial
PGPW18-17	3,426,666	7,280,153	3,767.5	606	MR	Millennial
PGWW18-01	3,428,857	7,286,244	3,781.2	42	MR	Millennial
PGWW19-02	3,431,200	7,288,950	3,874.7	62	MR	Millennial
PGWW19-03	3,431,279	7,287,953	3,821.7	62	MR	Millennial
PGWW19-04	3,431,032	7,288,305	3,831.5	62	MR	Millennial
PGWW19-05	3,430,916	7,287,889	3,844	62	MR	Millennial
PGWW19-06	3,430,545	7,288,054	3,842.5	62	MR	Millennial
SPG-2018-01	3,431,609	7,283,171	3,776.9	601	DDH-50?-MR	LSC
SPG-2017-02	3,426,955	7,285,189	3,775.5	121	DDH	LSC
SPG-2017-02B	3,427,203	7,284,055	3,769.4	572.5	DDH-50?-MR	LSC
SPG-2017-04 ^a	3,243,076	7,282,489	3,774.2	553	MR	LSC
SPG-2017-05	3,429,294	7,282,107	3,780.8	279.5	DDH	LSC
SPG-2017-05B	3,429,344	7,282,088	3,778.7	500.5	DDH	LSC
PP-01-2018	3,427,028	7,275,405	3,805.7	611	MR	Centaur
PP-02-2019	3,427,171	7,273,819	3,772.5	650	MR	Centaur
PP-03-2019	3,428,251	7,276,673	3,803.2	542	MR	Centaur
DD-01	3,429,329	7,278,639	3,793.5	700	DDH	Arena Minerals
DD-02	3,427,651	7,275,815	3,802.5	646	DDH	Arena Minerals
R-01	3,434,507	7,279,732	3,794.7	601	MR	Arena Minerals
R-02	3,435,359	7,283,016	3,813	411	MR/DDH	Arena Minerals
R-03	3,435,050	7,288,856	3,836	617	MR	Arena Minerals

Table 7.1 (Continuation)

7.2.2 Geophysical surveys

The results of a seismic refraction survey helped improve the understanding of the local geology and the development of the 3-D geological model by allowing to define the limits between some subsurface units. The interface between the fine sediments that underlie the halite crust within the Salar is represented within sections and is clearly correlated with the descriptions of the Project's boreholes. On the other hand, due to the resolution of the study, the deeper units in the basin under the halite crust show some noise and the correlation with borehole information is not direct.

7.3 Local geology description

Based on the lithological descriptions of the drill core and cuttings together with the interpretation of the available geophysical information and field observations five major geological units were defined and correlated, these units were incorporated into a 3-D geological model of the Pastos Grandes sub-basin. Figure 7.6 shows the

geological units at surface and Figure 7.7 shows a view of the geologic model from the southwest. The geological units are described hereafter:

7.3.1 Fluvial/Alluvial Unit

The Fluvial/Alluvial Unit is characterized by a heterogeneous sequence of alluvial and fluvial sediments of variable texture, dominated by clastic sediments formed by gravel and sand that surround the Salar. These fractions may present low proportions of fine sediments (sands or clays) which develop mainly along the northern and southern edges of the Salar de Pastos Grandes, prograding in depth towards the center, to interdigitate with finer silt sediments formed by clay and sandy clays from the Central Clastics Unit. Figure 7.8 shows the spatial distribution of this unit.

7.3.2 Upper clay unit (Blanca Lila Formation)

Formed by a superficial sequence of clays with a wide distribution in the center-south of the basin, as well as in the western margins where, according to field observations, it occurs in outcrop. This clay dominated unit intercalates with layers of evaporites, halites and borates, while in the bibliography travertine and tuff horizons were also described. Figure 7.9 shows the spatial distribution of this unit.

7.3.3 Saline/Lacustrine unit

Immediately below the Blanca Lila Fm and in the north-central sector from the surface, a thick halite sequence is recognized. This Unit is characterized by a massive and compact halite body with the presence of interstitial clastic material and occasional intercalations of finer levels of clay. The average thickness of this Unit ranges between 200 m and 300 m, reaching maximum thicknesses of 700 m in the central-eastern sector of the basin, which is interpreted as an ancient depocenter. Figure 7.10 shows the spatial distribution of this unit.

7.3.4 Central clastic unit

This Unit consists of clay and clayey sands and occurs within the central sector of the basin underneath the halite deposits, as shown in Figure 7.11. This Unit is poorly characterized due to limited and low-quality borehole information but seems to represent a distal sector of an alluvial fan and its interaction with marginal lacustrine deposits of the Salar. Additional core drilling is planned during 2023 to improve the hydrogeological characterization of this Unit.

7.3.5 Base Breccia/Gravels unit

Based on Millennial’s lithological description, a sedimentary breccia unit of coarse fragments of silicified conglomerate and ignimbrites was recognized in borehole PGMW19-21. This Unit corresponds to intermixed levels of sand and gravel with a thickness of 200 m on the western edge of the basin and deepening towards the north-central limit of the model where due to limited information its thickness becomes uncertain. Figure 7.12 shows the spatial distribution of this unit.

Three cross sections through the geological model are shown in Figure 7.13 and Figure 7.14. to demonstrate the lateral relation between the geological units across the basin Figure 7.7 shows the location of the sections.

Figure 7.6 Plan view of the interpreted geological units

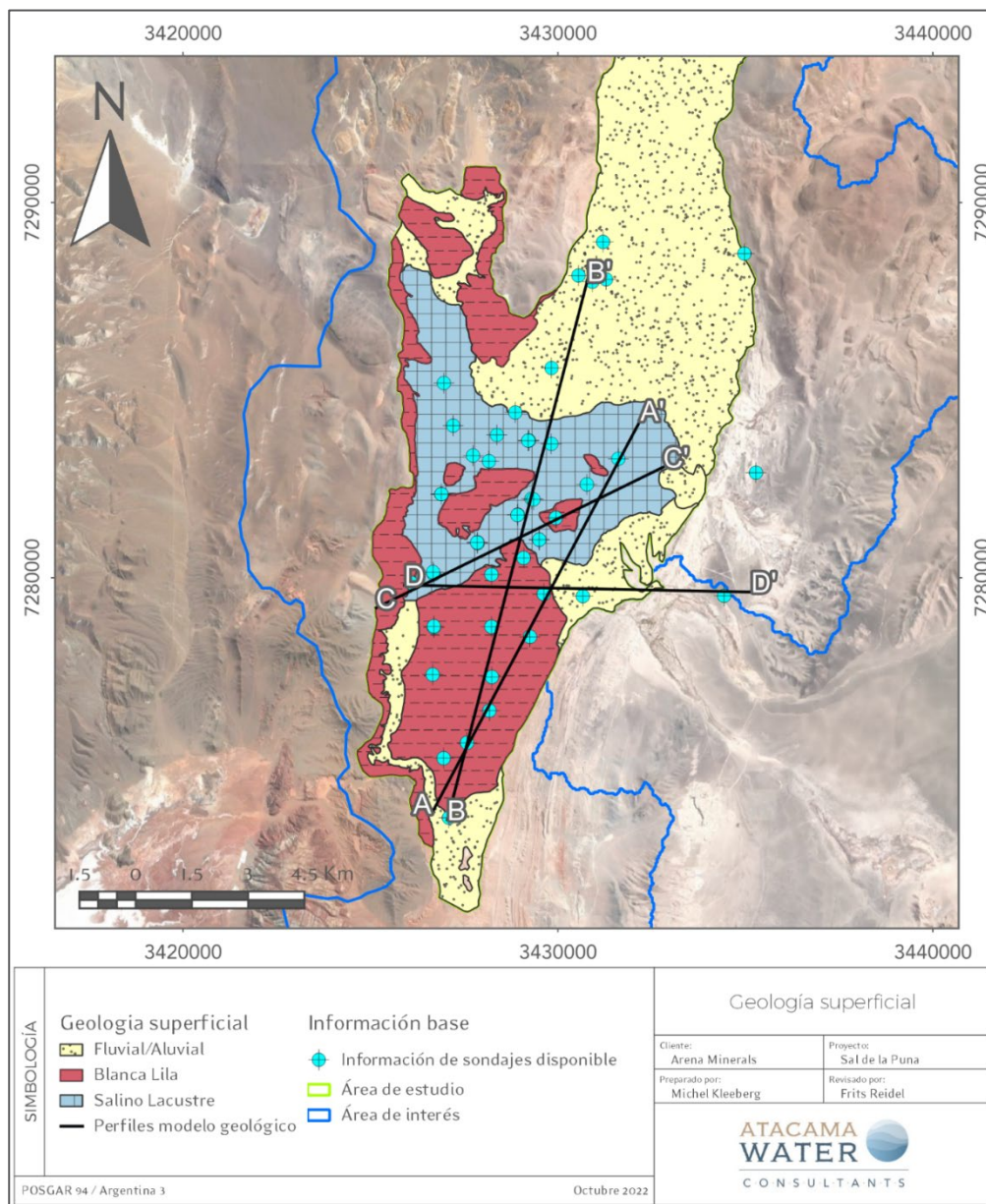


Figure 7.7 N-S section, through the geological model looking from the NW)

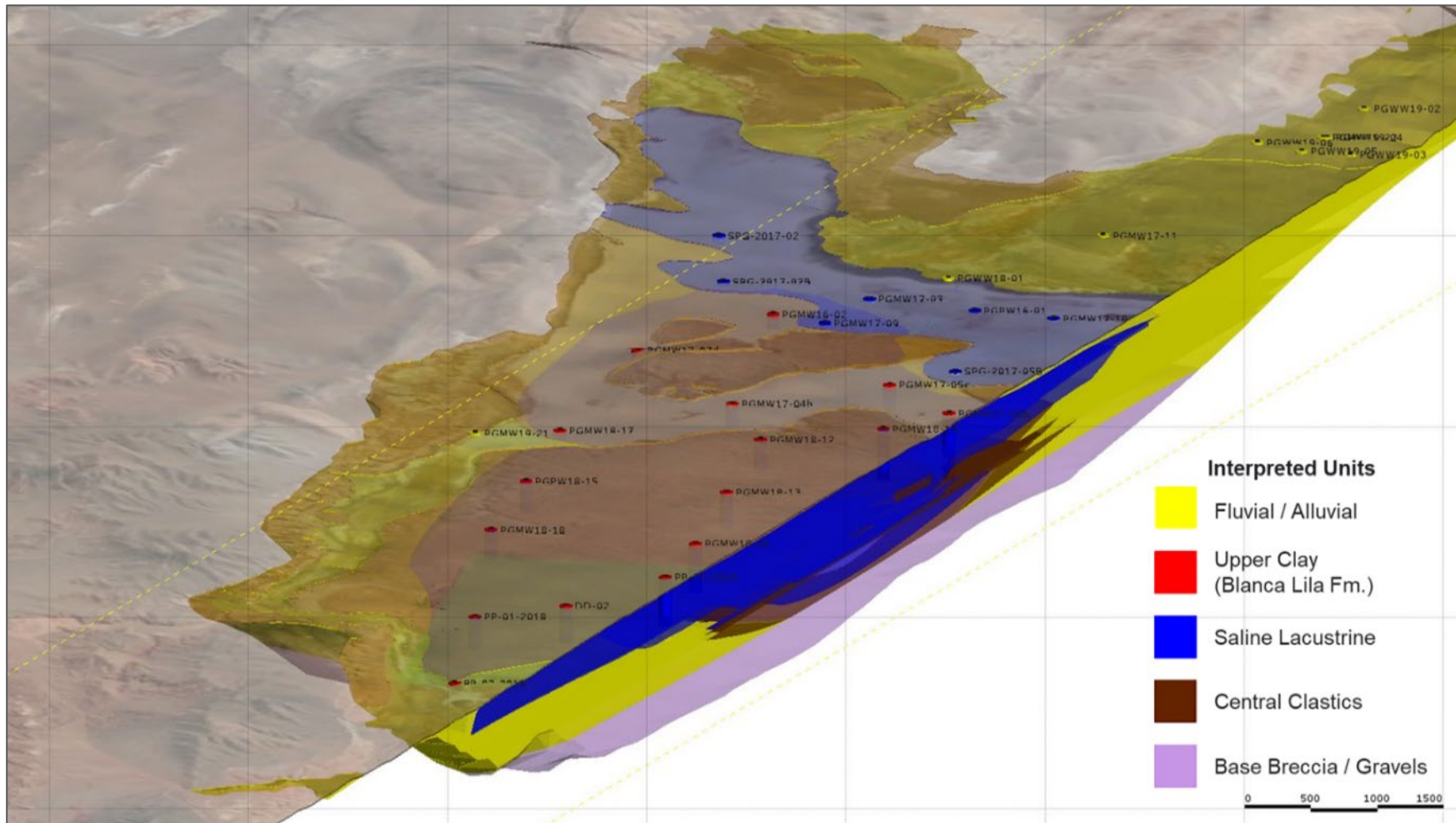


Figure 7.8 Spatial distribution Fluvial/Alluvial Unit

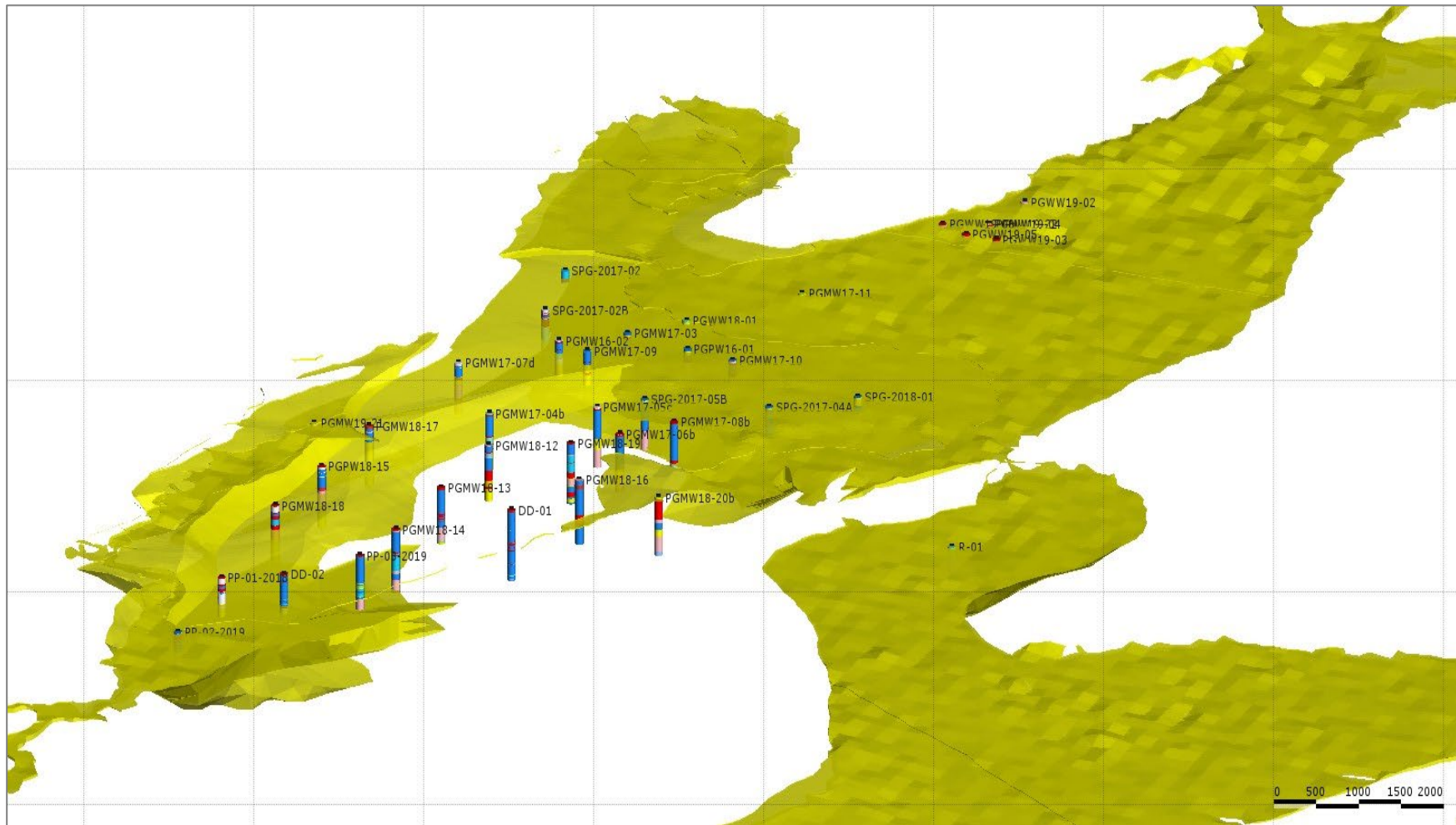


Figure 7.9 Spatial distribution Upper Clay Unit (Blanca Lila Formation)

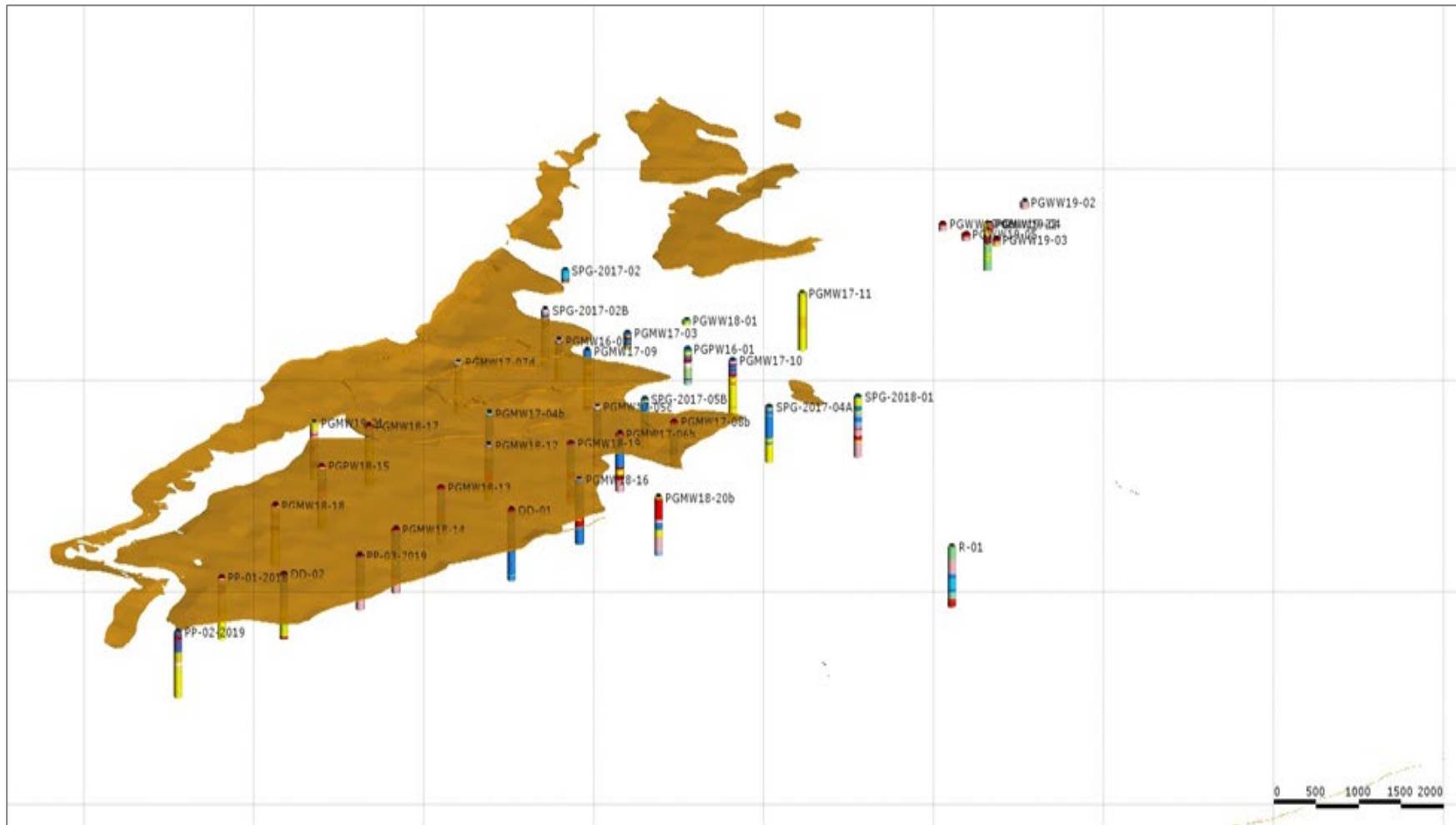


Figure 7.10 Spatial distribution Saline-Lacustrine Unit

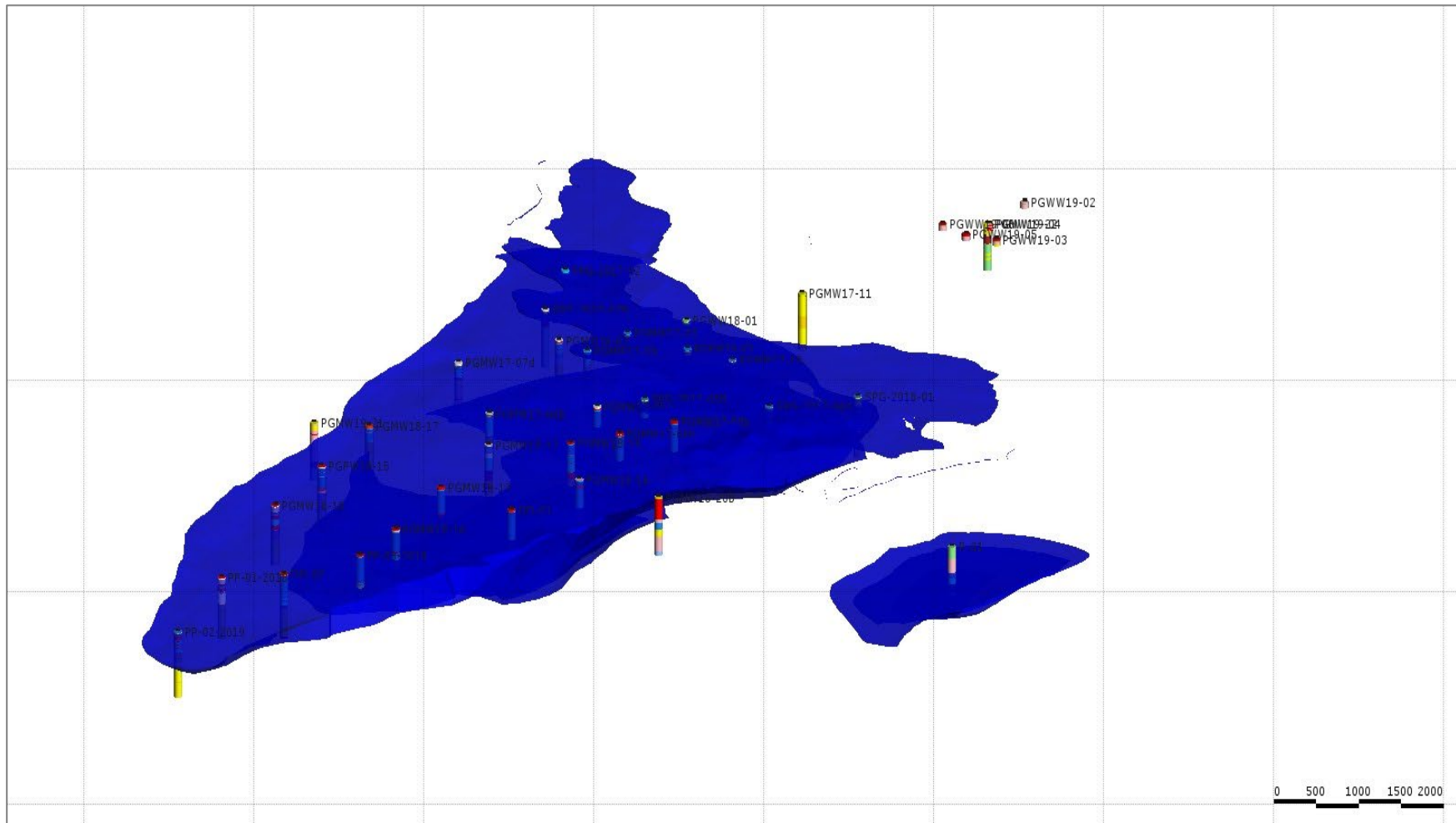


Figure 7.11 Spatial distribution Central Clastic Unit

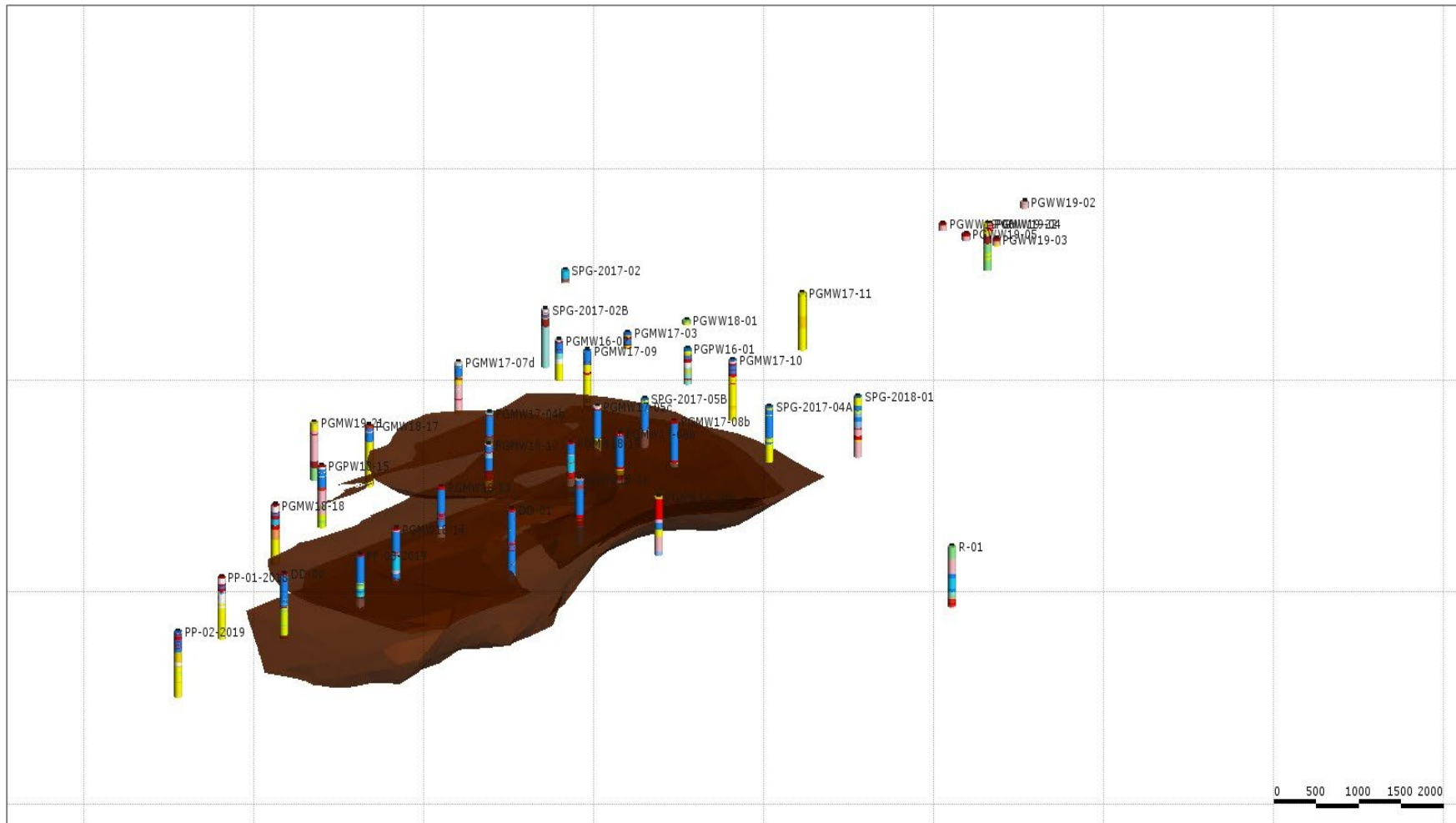


Figure 7.12 Spatial distribution Base Breccia/Gravel Unit

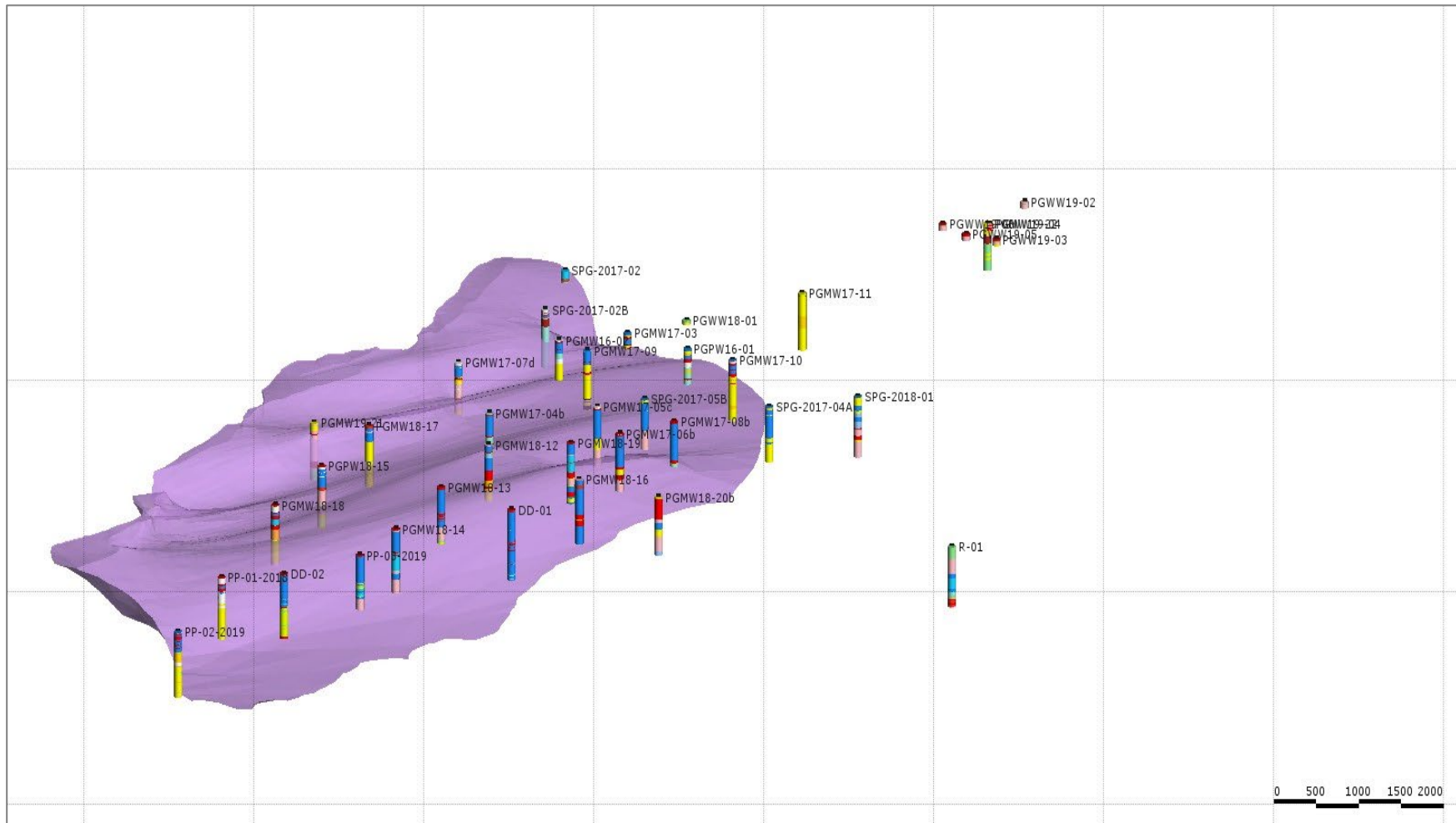


Figure 7.13 Cross sections AA' and BB' through the of the Pastos Grandes basin

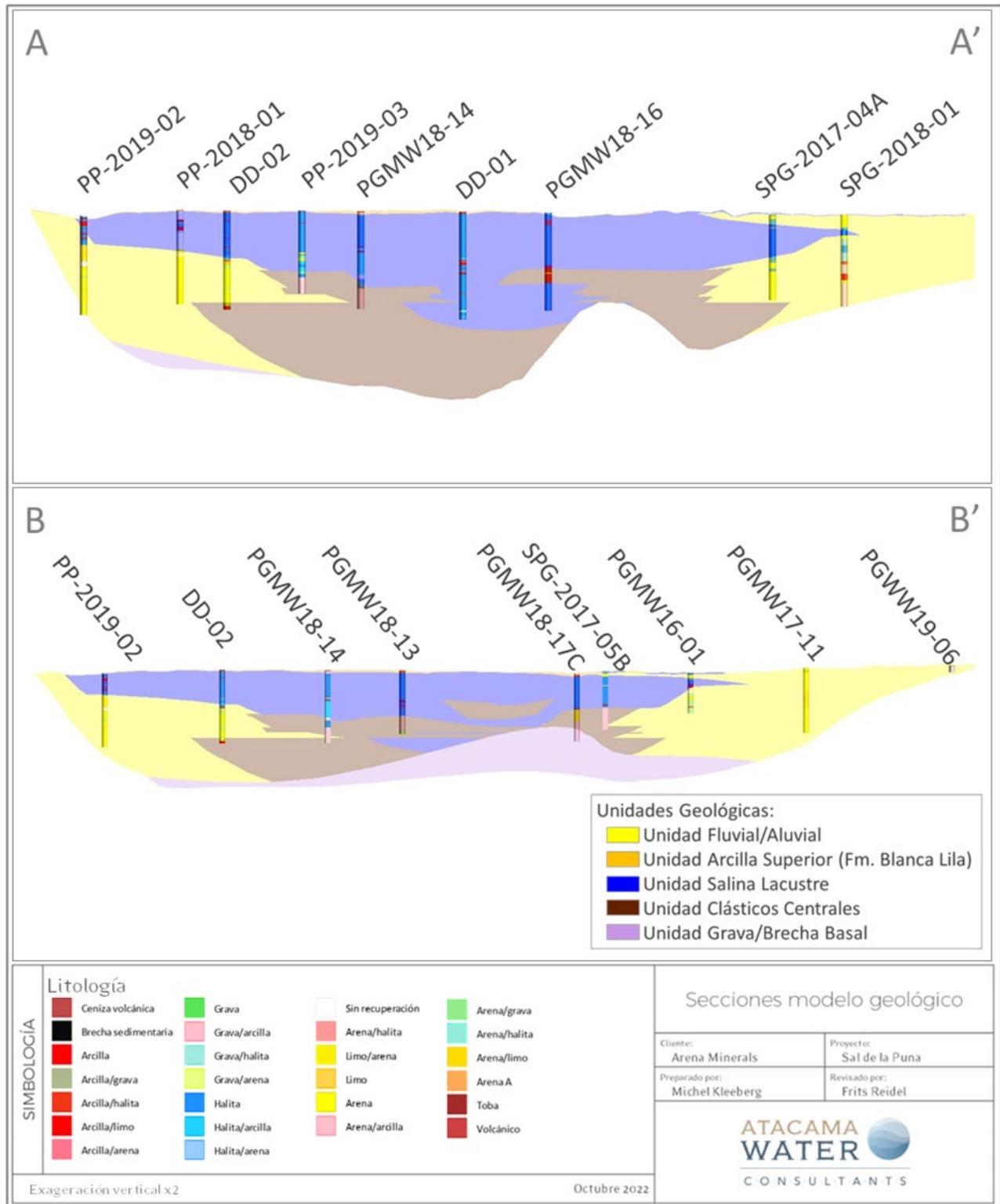
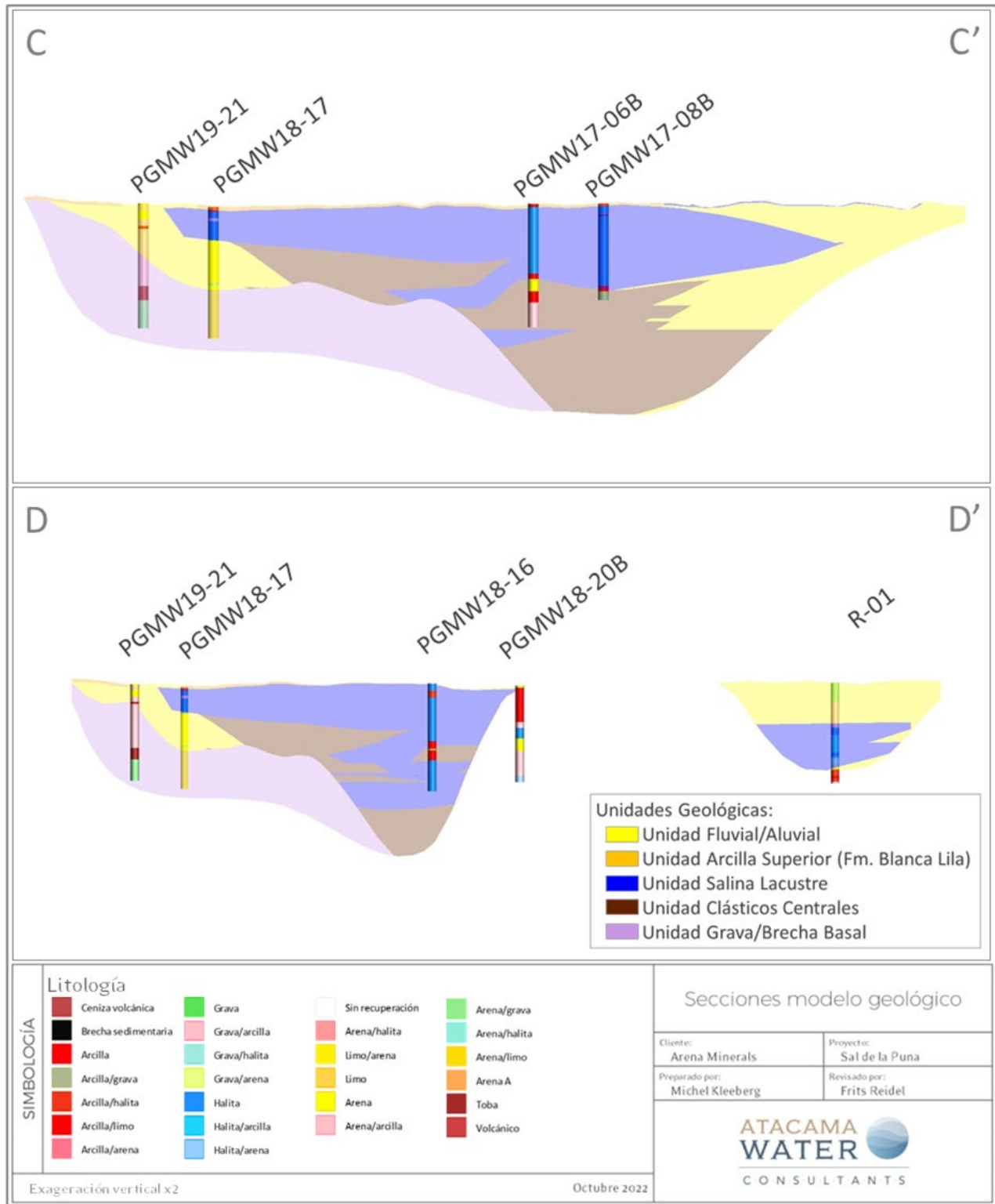


Figure 7.14 Cross section CC' and DD' through the Pastos Grandes basin



7.4 Mineralization

The brines from Pastos Grandes are solutions saturated in sodium chloride with an average concentration of total dissolved solids (“TDS”) of 302 g/L and an average density of 1.19 g/cm³. The other components present in the Pastos Grandes brine are K, Li, Mg, SO₄, Cl and B with relatively low Ca. The brine can be classified as a sulphate-chloride type with anomalous lithium. Lithium concentrations in Salar de Pastos Grandes have an average value of 392 mg/L, with some samples reaching up to 700 mg/L.

Table 7.2 shows a breakdown of the principal chemical constituents in the Pastos Grandes brine including maximum, average, and minimum values, based on 501 primary brine samples collected between 2017 and 2022.

Table 7.2 Maximum, average and minimum elemental concentrations of the Pastos Grandes brine

	B	Ca	Cl	Li	Mg	K	Na	SO ₄	Density
Units	mg/L	mg/L	mg/L	mg/L	mg/L	mg/L	mg/L	mg/L	g/cm ³
Maximum	938.00	1,707	196,869	701.00	5,130	6,660	130,032	13,998	1.22
Average	557.62	821	169,838	391.76	2,257	3,733	102,381	7,547	1.19
Minimum	20.20	11.00	116.00	8.75	23.20	18.00	196.00	12.00	1.00

Brine quality is evaluated through the relationship of the elements of commercial interest, such as lithium and potassium, with those components that constitute impurities, such as Mg, Ca and SO₄. The calculated ratios for the averaged chemical composition are presented in Table 7.3.

Table 7.3 Average values (mg/L) of key components and ratios for the Pastos Grandes brine

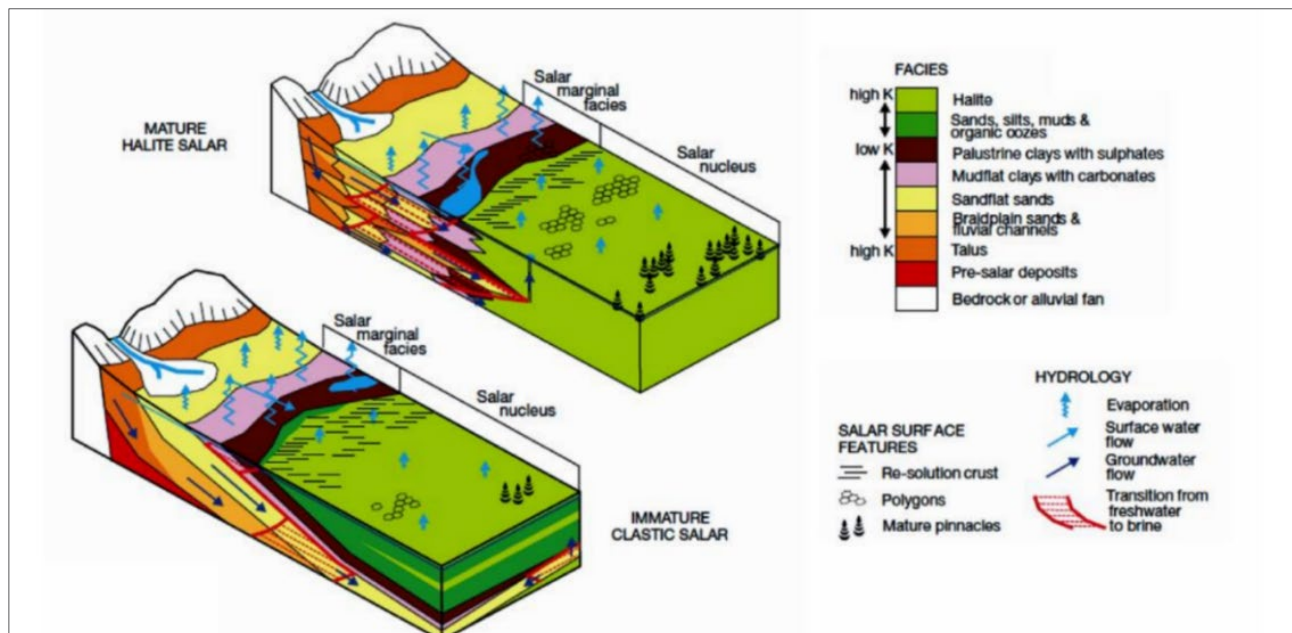
K	Li	Mg	Ca	SO ₄	B	Mg/Li	K/Li
3,733	392	2,257	821	7,547	558	5.76	9.53

8 DEPOSIT TYPE

8.1 General

Salars occur in closed (endorheic) basins without external drainage in dry desert regions where evaporation rates exceed stream and groundwater recharge rates, preventing lakes from reaching the size necessary to form outlet streams or rivers. Evaporative concentration of surface water over time in these basins leads to residual concentration of dissolved salts (Bradley et al., 2013) to develop saline brines enriched in one or more of the following constituents: sodium, potassium, chloride, sulphate, carbonate species, and, in some basins, metals such as boron and lithium. Houston et al. (2011) identified two categories of salars: 1) mature, halite dominant; and 2) immature, clastic dominant. Figure 8.1 shows the conceptual model for each salar type.

Figure 8.1 Conceptual model for mature and immature (Houston et al., 2011)



Immature salars are characterized by increased humidity (increased precipitation, less evaporation) and are more frequent at higher elevations and in the wetter northern and eastern parts of the region. They are characterized by alternate sequences of fine-grained sediments and evaporitic beds of halite and/or ulexite, indicating the changes in sediment supply due to variable tectonic and climate history (Houston, et al., 2011). Immature salars include Olaroz, Cauchari, Diablillos and Centenario.

Mature salars are less humid and tend to be more common in lower and drier areas of the region. They are characterized by a relatively thick and uniform sequence of halite deposits in variable sub-aquatic and sub-aerial conditions. Nevertheless, ancient floods leading to widespread silty clay deposits and volcanic fallout have led to thin intercalated beds that can be recognized in drill core and geophysical surveys. The central portion of Salar de Atacama is a typical mature setting.

Salar de Pastos Grandes is a mature salt flat, with a well-developed halite crust. In the central portion of the salar, the crust can reach a thickness of several hundred meters, with a thin clay layer that is constantly being generated through evaporation in the shallower beds.

8.2 Hydrogeology

The Salar is the lowest topographic point in the Pastos Grandes Basin. The salt flat itself is surrounded by alluvial fans which drain into the Salar and tertiary rocks that may act as impermeable boundaries, although further hydrogeological characterization work of the Tertiary is recommended. The surface of the Salar in the north is composed of mainly chloride facies (halite crust) with active evaporation occurring since the brine level occurs within 5 cm from the surface. The Salar surface in the south is covered by the Blanca Lila Fm with an average thickness of 3 m. Depth to brine in the southern part of the Salar is between 3 m and to 4 m, below the evaporation extinction depth that is estimated around 2.5m.

Based on the interpretation of drilling and testing work in the basin, four hydrogeological units have been identified as shown in Figure 8.2 and are described below:

- UH-1 Fine Grained Shallow Deposits: These sediments belong to the Blanca Lila formation and are in conformity with the underlying Saline Lacustrine Unit, reaching a maximum thickness of 30 m at the northeast of the Salar. Because of the fine texture, permeability and storage properties for this Unit are estimated to be low with a hydraulic conductivity (K) ranging between 0.1 – 0.01 m/d, a specific storage (Ss) of 1×10^{-6} 1/m and drainable porosity below 2%. Geophysics and field sampling suggests that this Unit is saturated with brine inside the Salar and with brackish water around the margins.
- UH-2 Evaporitic Deposits: Massive evaporitic unit, intercalated with lenses of fine-grained sediments that can have a thickness up to 700 m. This relatively homogeneous Unit includes the saline lacustrine material that forms the surface of the salar nucleus and is overlain by the Blanca Lila Fm (UH-1) in the south. Based on drilling and testing results this Unit has a relatively low permeability and could limit hydraulic connectivity between the upper and deeper hydrogeological units in the basin. The hydraulic conductivity of this Unit is estimated to be lower than 0.01 m/d, the specific storage is estimated to be near 10^{-6} 1/m and the specific yield could reach 4%. Geophysics and field sampling suggests that this Unit is saturated with brine.
- UH-3 Alluvial and Colluvial Deposits: This hydrogeological unit includes the alluvial fans identified at the margins of the Salar which are composed of unconsolidated gravels and sand. This Unit overlies and is in lateral contact with UH-2 and locally appears interfingering with UH-4. The hydraulic conductivity ranges between 30 m/d and 50 m/d. The average drainable porosity is 14%. Groundwater flow in the Alluvial and Colluvial Deposits is generally unconfined; however, locally semi- confined to confined flow conditions occur where this unit is overlain by UH-1 and UH-2. The unit hosts freshwater resources in the alluvial fans on higher ground above the margin of the Salar and significant brine resources in the southern portion of the Salar where it is partially overlain by UH-1
- UH-4 Lower Deposits: Overlaying basement rock, this hydrogeological unit includes the Central Clastics and Base Gravels. It is composed of sandy gravels with a high fraction of fine material in a sedimentary matrix and some clayey to silty lenses that decrease the bulk vertical hydraulic conductivity. This unit is constrained to the central portion of the basin, underlies UH-2, and is in lateral contact with the

unconsolidated deposits of UH-3. The hydraulic conductivity of this unit is estimated to range between 0.1 – 1 m/d, the specific storage at 10⁻⁶ 1/m, and the drainable porosity near 8%. This unit forms part of the confined lower brine aquifer from which future brine production will likely not affect the freshwater resources hosted in the alluvial system due to the overlying low-permeability halite unit.

8.3 Water balance

A water balance for the Pastos Grandes Basin was prepared as part of the conceptual hydrogeological model and is summarized in Table 8.1. In closed endorheic basins such as Salar de Pastos Grandes recharge is in long-term equilibrium with evaporation in the absence of any brine production. Recharge is composed of direct recharge from precipitation and lateral groundwater in lows from adjacent subbasins (Sijes subbasin) and was estimated within a range of 300 - 1000 L/s. Discharge occurs mainly through evaporation in the form of 1) soil evaporation where the water table is above the extinction depth; 2) evapotranspiration from wetlands at the margins of the Salar; and 3) free water (or brine) evaporation from perennial or ephemeral lagoons over the surface of the Salar. Table 8.1 provides a detail of the water balance estimate for the Salar de Pastos Grandes Basin.

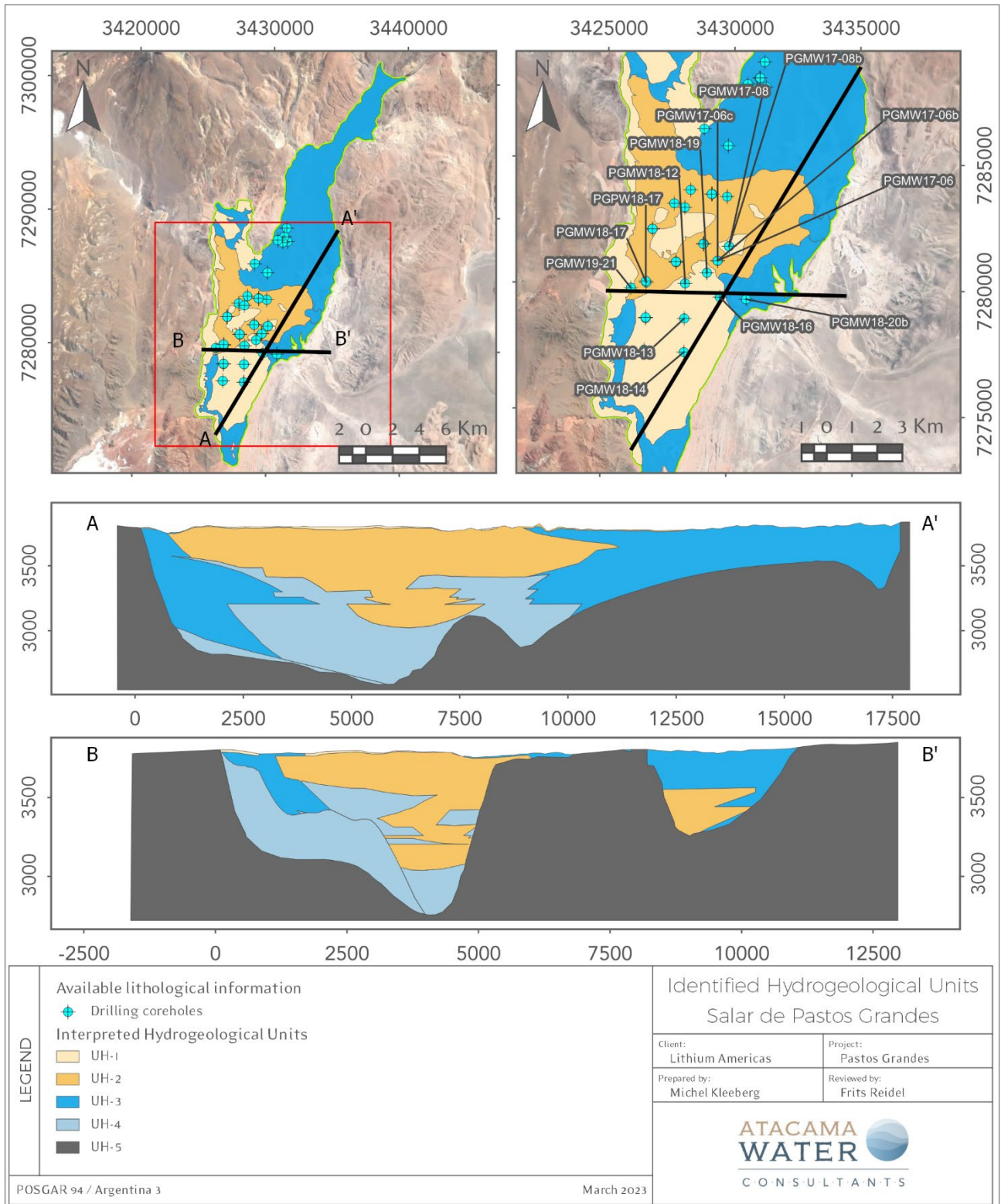
Table 8.1 Water balance for Salar de Pastos Grandes

Inflows (L/s)		
Direct recharge from precipitation		150 - 600
Lateral recharge from Sijes Subbasin		150 – 400
Total inflows		300 - 1000
Outflows (L/s)		
Evaporation	Lagoon evaporation	100 – 300
	Evapotranspiration	100 - 300
	Soil evaporation	100 - 300
Total outflows		300 - 900

8.4 Drainable porosity

Porosity is highly dependent on lithology. Total porosity is generally higher in finer grained sediments than coarser grained sediments, whereas the reverse is true for drainable porosity or specific yield, since finer grained sediments have a high specific retention. The lithology within the Salar is variable with halite and halite mixed units, clay and gravel-sand-silt-clay sized mixes spanning the full range of sediment types.

Figure 8.2 Hydrogeological cross section



Based on the results of drainable porosity analyses carried out on 76 undisturbed samples from HQ core by GeoSystems Analysis it was possible to assign drainable porosity values to the specific lithological units encountered during the various drilling programs between 2016 and 2022. Table 8.2 summarizes the results of the porosity analysis. The analysis of drainable porosity is further discussed in Section 14.

Table 8.2 Results of drainable porosity analyses

Lithology	S _y Average
Blanca Lila	0.5%
Alluvium	13.9%
Saline Lacustrine	4.1%
Clastic Central	5.4%
Base Gravels	12.5%

8.5 Permeability

Permeability (or hydraulic conductivity) is also a parameter that is dependent of lithology. Generally finer grained and well-graded sediments have a lower permeability than coarser grained poorly graded sediments. Eight pumping tests have been carried out within the Salar and the surrounding alluvial sediments. The results of the interpretation of these pumping tests, integrated with literature information on similar lithologies are summarized in Table 8.3. Vertical anisotropy of 10% is proposed for these units according to different references of classical hydrogeology (Freeze & Cherry, 1979; Domenico and Schwartz, 1990; Custodio y Llamas. 1993). Further test work is recommended to improve the characterization of the hydrogeological units. The analysis of the pumping tests is further discussed in Section 10 below.

Table 8.3 Summary of permeability values

Unit	K _x (m/d)	K _y (m/d)	K _z (m/d)
Blanca Lila	0,01	0,01	0,001
Alluvium	10	10	1
Saline Lacustrine	0,01	0,01	0,001
Clastic Central	0,1	0,1	0,01
Base Gravels	0,1	0,1	0,01

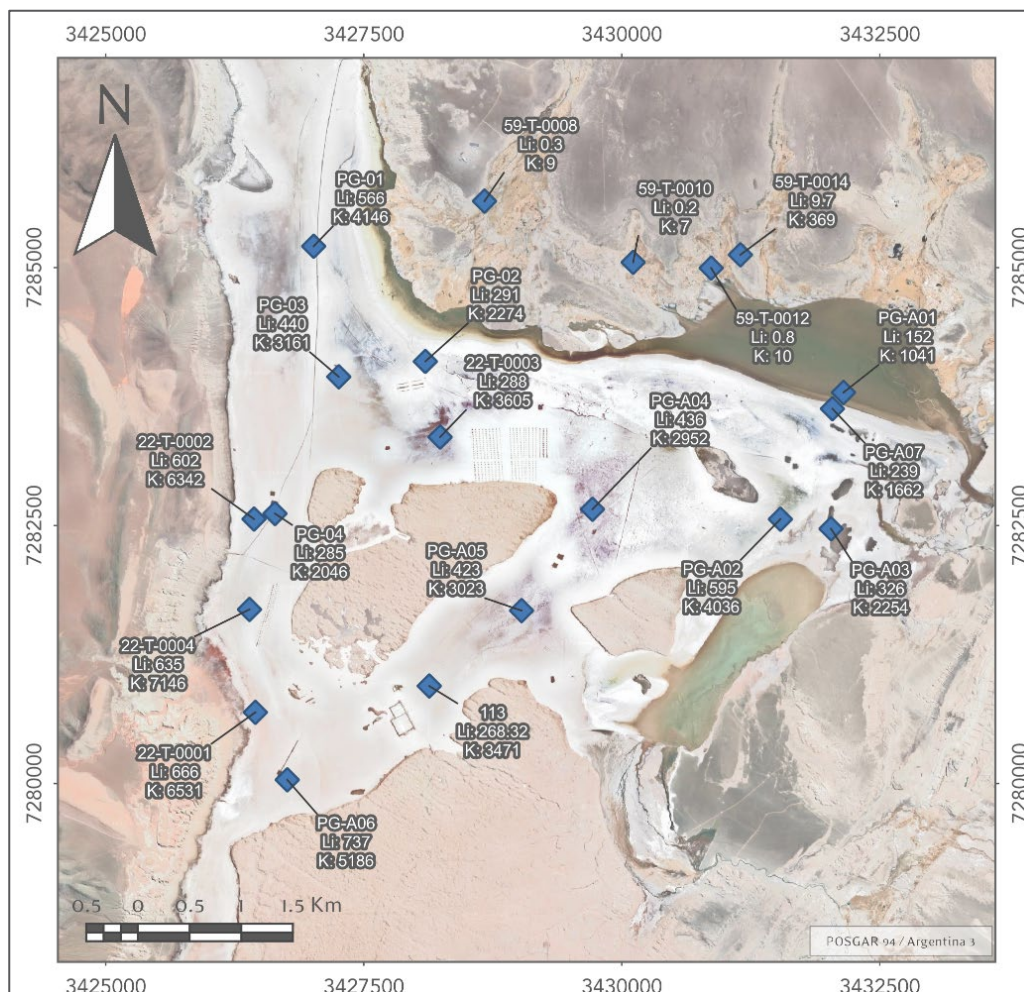
9 EXPLORATION

This section provides a description of the exploration work that has been carried out in the Salar between 2011 and 2021 by various owners prior to LAC.

9.1 Surface brine sampling

In 2011, Eramet took a total of nine samples from shallow hand-dug auger holes within the eastern section of the Salar and the wetlands as shown in Figure 9.1. Three brine samples toward the west of the Salar had lithium concentrations near 600 mg/L and potassium concentrations near 7,000 mg/L while samples at the center of the Salar had lithium and potassium concentrations near 200 and 2,000 mg/L, respectively. LSC completed a second surface sampling program in 2016 which included 11 sampling sites (shallow brine bodies and hand dug pits) with similar results as Eramet in 2011. The results of the brine chemistry analysis of these samples were not used in this current resource estimate due to the uncertainty related with the quality of the sampling protocols.

Figure 9.1 Historical surface brine samples in Salar de Pastos Grandes



9.2 Geophysical studies

9.2.1 Eramet (2011-2013)

Eramet carried out a Transient Electromagnetic (“TEM”), Vertical Electrical Soundings (“VES”), and Controlled Source Audio Magnetotellurics (“CSAMT”) surveys in Salar de Pastos Grandes between 2011 and 2013. The locations of the VES and CSAMT surveys are shown in Figure 9.2; no information is available for the TEM survey. The objectives of these surveys were to map the occurrence of brine versus freshwater, and the distribution and relative continuity of lithological units.

9.2.2 Millennial exploration (2017 – 2019)

9.2.2.1 VES survey (2017)

Millennial conducted a VES survey in 2017, focused on the alluvial deposits in the northern portions of the Salar. This study included 10 VES stations which were interpreted into three vertical sections whose locations are shown in Figure 9.2. The objective of this survey was to map the saline interphase, identify potential brine resources in the north, and help define new exploration drilling sites.

9.2.2.2 Seismic survey (2018-2019)

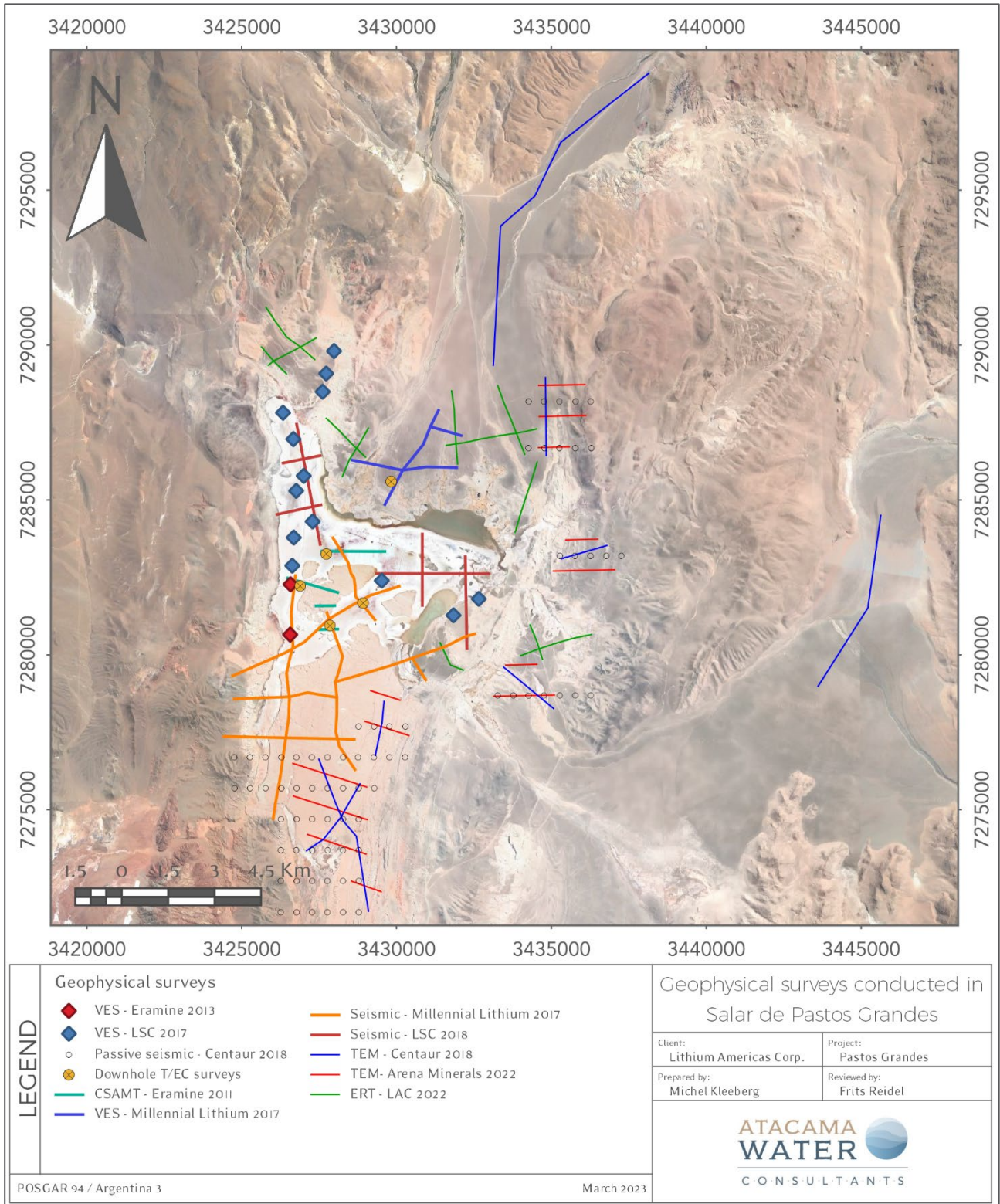
Millennial carried out a two-phase seismic investigation program during 2018-2019 to help refine the understanding of the lithology in the Salar and help define new exploration targets. The locations of the seismic lines are shown in Figure 9.2.

The seismic tomography survey provided valuable information on the vertical distinction and lateral continuity of lithological layers. Additionally, several structures were interpreted, especially in the north to south profile, suggesting north to northwest dipping beds.

9.2.2.3 Downhole temperature and electrical conductivity surveys

Down-hole electrical conductivity profiling was conducted in boreholes PGMW16-02, PGMW17-04b, PGMW17-05c, PGMW17-07d, and PGMW17-11 which were completed with 2-inch diameter PVC casing on completion of drilling. Figure 9.2 shows the location of these boreholes. Temperature and electrical conductivity were recorded at 3-m intervals using an In-Situ brand Aquatroll 100 downhole probe and brine samples were taken to measure laboratory density. The results showed a reasonably good correlation between the Aquatroll specific conductivity and the laboratory density measurements on the depth-specific samples.

Figure 9.2 Geophysical surveys conducted in Salar de Pastos Grandes



9.3 LSC exploration (2017 – 2018)

9.3.1 VES survey (2017b)

LSC Lithium carried out a VES study in 2017 to map lithology and the freshwater/ brine interface. The survey consisted of 13 soundings as shown in Figure 9.2. The results of this survey identified five geoelectrical units: 1) conductive gravels and sands; 2) a semi-conductive fine grained unit (silt and clays and/or halite gypsum and borates), probably related to the Blanca Lila Formation; 3) a highly conductive zone of evaporates and mixed halite/clastics saturated with brine; 4) a more resistive layer representing again the Blanca Lila Fm or other Tertiary sequences and; 5) a resistive zone interpreted as the hydrogeological basement composed of thick clastic facies (conglomerates) and/or facies of volcanic rocks (andesites).

9.3.2 Seismic survey (2018)

LSC undertook a seismic tomography survey consisting of six lines for a total of 15 km as shown in Figure 9.2. The interpretation of the results of this survey was based on a combination of literature values, regional geological information, and specific correlation to boreholes SPG-2017-02B and SPG-2017-04A and is summarized below.

To the west of the Salar seven seismic units were identified without structure to a depth of 600 m: 1) dry alluvial deposits; 2) halite crust; 3) saturated sand, clay and/or organic material; 4) crystalline halite; 5) saturated sand, clay and/or organic material; 6) gravels and 7) breccia.

To the center and east of the Salar 11 seismic units were identified without structure to a depth of 600 m, from top to bottom: 1) dry to partially saturated sediments and alluvial material (saturated sand, clay and/or organic material); 2) halite crust; 3) saturated sand, clay and/or organic material; 4) halite with scarce matrix; 5) halite with abundant matrix; 6) halite with scarce matrix; 7) sand; 8) alternation of halite and sand bands; 9) gravel, sand and/or clay; 10) halite with interbedded sand; 11) gravel and/or sand.

9.4 Centaur/AMSA exploration (2018 – 2022)

9.4.1 TEM survey (2018)

Centaur conducted several TEM surveys to evaluate the presence of brine beyond the margins of the Salar in the Corral Colorado river valley, the Sijes subbasin, and in the southern portion of the Salar. Figure 9.2 shows the location of the TEM lines.

The TEM lines in the north and east confirmed the existence of a deeper conductive anomaly associated with brine and the overlaying freshwater hosted in the alluvial sediments.

The southern lines over the Blanca Lila Fm showed a conductive unit close to the surface interpreted as the halite unit saturated with brine, based on drilling.

9.4.2 Passive seismic survey (2019)

A passive seismic survey was conducted by Centaur in 2019 to map basement and confirm interpreted fractures to the south and east of the Salar. This study consisted of 78 stations arranged in 10 east-west orientated lines (Figure 9.2). The survey did not consistently identify basement rocks due to depth and the poor seismic contrast between the massive halite body and basement rocks.

9.4.3 TEM survey (2022a)

AMSA carried out a TEM survey during 2022 along the eastern boundary of the Salar to refine the delineation of the overburden and hydrogeological basement, and to further investigate the freshwater/brine interface in this portion of the Salar based on Centaur's 2018 survey. The profile locations are shown in Figure 9.2. The survey helped identify the limit between the unconsolidated sediments and basement rock. These results and interpretations were correlated to lithological information of boreholes DD-01, DD-02 and DD-03.

9.5 LAC exploration (2022)

9.5.1 ERT survey (2022b)

LAC conducted a ERT survey to refine the delineation of freshwater resources suitable for industrial water supply in the alluvial deposits in the north-eastern portion of the Project. The survey consisted of 12 lines (Figure 9.2) with a vertical maximum resolution of 160 m -200 m.

Three geoelectrical units were identified 1) fine grained sediments with abundant interstitial clay and saturated with brine of high electrical conductivity; 2) fine to coarse grained sediments saturated with water; and 3) medium to coarse grained sediments partially or not saturated.

10 DRILLING

10.1 Overview

Three drilling campaigns have been carried out for the Project since 2011⁹. Eramet conducted the first exploration program in 2011 including 11 shallow exploration boreholes (“SW” series), two diamond drill holes (DW01PGDDH and DW02PGDDH), four shallow exploration holes completed with 6-inch diameter casing (“PMP” series), and three exploration wells of varying depths completed with 6-inch diameter casing (DW03PG, DW04PG, DW05PG). Detailed information of these boreholes has not been published and is mostly unavailable, although according to Dworzanowski et al. (2018) maximum depths reached at this stage rarely exceeded 100 m. The second and third campaign conducted by Millennial included 32 brine exploration boreholes (PGMW16-01 through PGMW19-22), 6 freshwater exploration wells (PGWW18-01 to PGWW19-06) and 4 brine production wells (PGPW16-01 to PGPW18-17) with drilling depths of up to 600 m. Most of the monitoring wells were completed as piezometers with 2-inch diameter PVC slotted casing, while production wells were constructed with 6 to 8-inch diameter screened casing.

AMSA and Centaur carried out drilling programs on the Sal de la Puna Project in between 2018 and 2022. These programs consisted of two diamond core holes (DD-01 and DD-02), five combination core /rotary holes (PP-01-2018, PP-02-2018 and R-01 through R-03), two production wells (PP-03-2019 and PW-1), and several piezometer installations.

The objectives of the drilling program can be broken down into three general categories:

1. Exploration drilling to allow the estimation of “in-situ” brine resources: The drilling methods were selected to allow for 1) the collection of continuous cores to prepare “undisturbed” samples from specified depth intervals for laboratory porosity analyses and 2) the collection of depth-representative brine samples at specified intervals. Additional details of the sampling process can be found in the following chapters 11 and 12 of this report.
2. Test well installations: 8 rotary holes (PGPW16-01 to PGPW18-17; PGWW18-01 to PGWW19-03, and PW-1) which were drilled and completed as production wells to carry out pumping tests and additional selective brine sampling. Monitoring wells were installed adjacent to most of these production wells for use during the pumping tests as observation points.
3. Pumping tests: Eight pumping tests had been completed in the Salar of Pastos Grandes. These tests included three short-term tests (PGWW18-02, PGWW19-02 and PGWW19-03), each lasting about one day and conducted on freshwater wells; three three-day tests conducted on brine wells (PGPW16-01, PGPW18-15 and PGPW18-17); and two long-term pumping tests (PGPW16-01 and PGPW17-04) with 23- and 30-day duration.

Figure 10.2 shows the location of the drilling carried out for the Project and Table 10.1 includes a summary of the construction details of each completed borehole.

⁹All holes drilled at the Salar were drilled vertically.

Figure 10.1 Borehole locations in Salar de Pastos Grandes

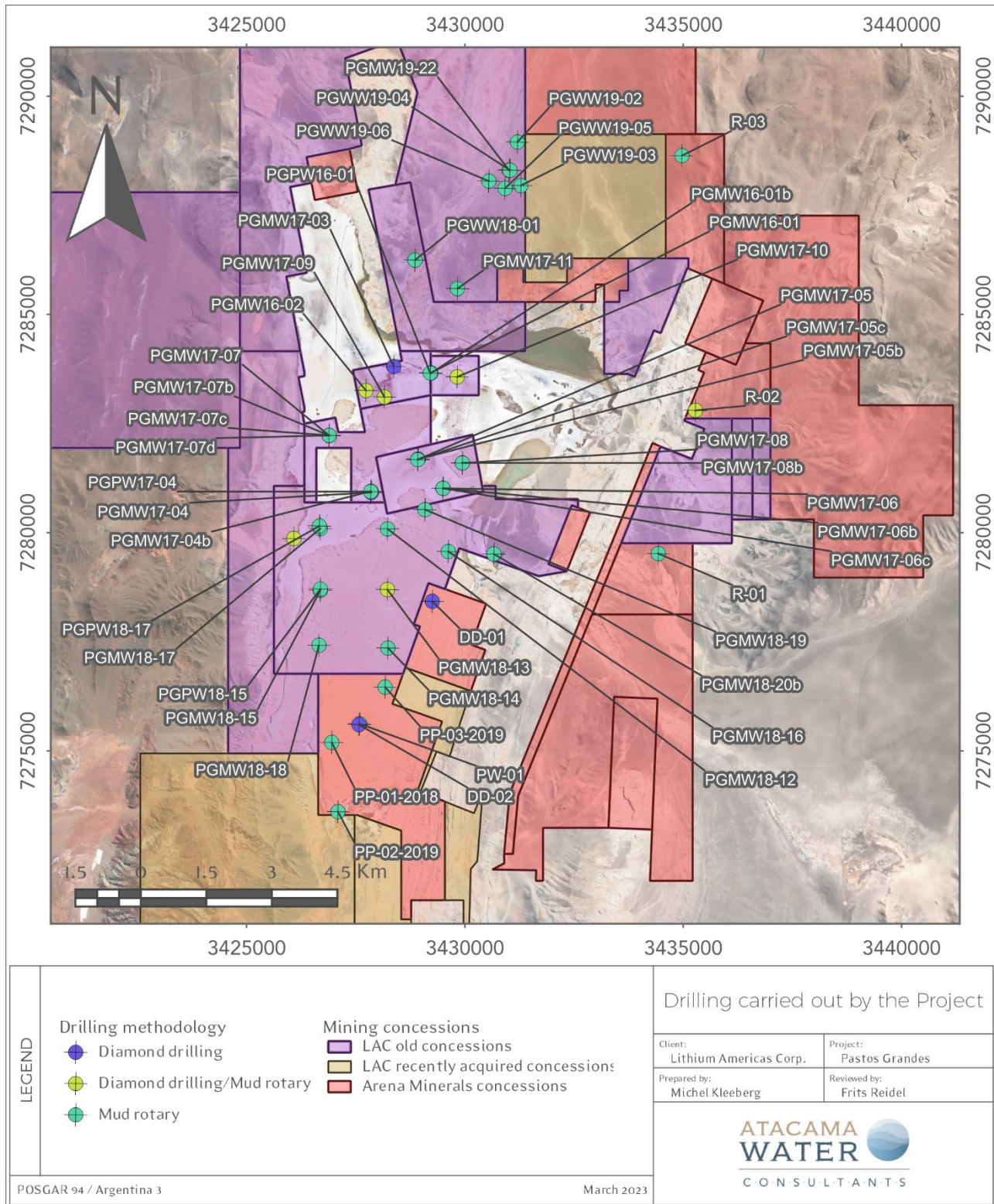


Table 10.1 Summary of 2016-2022 boreholes

Borehole	East (m)	North (m)	Elevation (masl)	TD (m)	Method	Year	Completion	
							Diameter (inches)	Screened interval (m)
PGMW16-01	3,429,218	7,283,662	3,775.60	190	DDH	2016	2"	8.6-91.7
PGMW16-01b	3,429,221	7,283,655	3,775.60	355	MR	2016	2"	0-283.6
PGMW16-02	3,427,731	7,283,257	3,785	400	DDH/MR	2016	2"	8.5-386.9
PGMW17-03	3,428,367	7,283,805	3,773.6	154	DDH	2017	-	-
PGMW17-04	3,427,853	7,280,921	3,789.80	245,5	DDH	2017	-	-
PGMW17-04b	3,427,849	7,280,949	3,786.90	564	DDH/MR	2017	2"	4.2-206.0
								211.6-389.4
								395.0-519.5
PGMW17-05	3,428,922	7,281,677	3,773.9	121	DDH	2017	-	-
PGMW17-05b	3,428,927	7,281,683	3,773.9	387	DDH	2017	-	-
PGMW17-05c	3,428,918	7,281,672	3,773.9	601	MR	2017	2"	14.2-180.6
								186.6-371
PGMW17-06	3,429,497	7,281,016	3,785	455	DDH/MR	2017	-	-
PGMW17-06b	3,429,497	7,281,016	3,785	424	MR	2017	-	-
PGMW17-06c	3,429,497	7,281,016	3,785	571	MR	2017	-	-
PGMW17-07	3,426,888	7,282,228	3,763.1	203,3	DDH	2017	-	-
PGMW17-07b	3,426,888	7,282,228	3,763.1	203,3	MR	2017	-	-
PGMW17-07c	3,426,888	7,282,228	3,763.1	412	DDH/MR	2017	-	-
PGMW17-07d	3,426,901	7,282,217	3,763.1	510	MR	2017	2"	12-17.95
								29.70-249.88
								261.64-499.73
PGMW17-08	3,429,941	7,281,596	3,785	425,5	DDH	2017	-	-
PGMW17-08b	3,429,941	7,281,596	3,785	446	MR	2017	-	-
PGMW17-09	3,428,156	7,283,107	3,785	595	DDH/MR	2017	2"	11.7-198.8
								204.7-397.3
								403.3-583.0
PGMW17-10	3,429,822	7,283,569	3,773.7	601	DDH/MR	2017	-	-
PGMW17-11	3,429,826	7,285,591	3,817.60	568	MR	2017	2"	278.95-546.66
PGMW18-12	3,428,224	7,280,087	3,787.70	554	MR	2018	2"	71.61-543.61

Borehole	East (m)	North (m)	Elevation (masl)	TD (m)	Method	Year	Completion	
							Diameter (inches)	Screened interval (m)
PGMW18-13	3,428,223	7,278,696	3,795.30	559	DDH/MR	2018	2"	82.49-314.85
								320.81-553.16
PGMW18-14	3,428,234	7,277,357	3,797.10	635	MR	2018	2"	70.79-313.69
								319.66-628.57
PGMW18-15	3,426,687	7,278,678	3,792.70	594	MR	2018	2"	74.23-321.96
								327.85-587.38
PGMW18-16	3,429,618	7,279,568	3,790.40	641	MR	2018	2"	73.19-321.38
								327.28-629.08
PGMW18-17	3,426,685	7,280,094	3,767.50	605	MR	2018	2"	17.63-129.24
								135.21-170.61
								200.43-306.32
								312.28-595.05
PGMW18-18	3,426,656	7,277,421	3,798.70	605	MR	2018	2"	8.35-273.46
PGMW18-19	3,429,083	7,280,529	3,787.70	602	MR	2018	-	
PGMW18-20b	3,430,661	7,279,511	3,777.30	575	MR	2018	2"	0.40-64.79
								111.99-336.11
PGMW19-21	3,426,079	7,279,867	3,784.50	574,3	DDH/MR	2019	2"	26.15-285.16
								291.01-567.71
PGMW19-22	3,431,009	7,288,304	3,832.50	464,5	DDH/MR	2019	2"	37.8-363
PGPW16-01	3,429,204	7,283,655	3,775.60	351	MR	2016	6"	20-351
PGPW17-04	3,427,842	7,280,941	3,788.50	475	MR	2017	6"	113.37-464.31
PGPW18-15	3,426,687	7,278,707	3,792.70	610	MR	2018	6"	76.88-592.8
PGPW18-17	3,426,666	7,280,153	3,767.50	606	MR	2018	8"	50.43-594.4
PGWW18-01	3,428,857	7,286,244	3,781.20	42	MR	2018	6"	4-34
PGWW19-02	3,431,200	7,288,950	3,874.70	62	MR	2019	6"	29.53
PGWW19-03	3,431,279	7,287,953	3,821.70	62	MR	2019	6"	17-53
PGWW19-04	3,431,032	7,288,305	3,831.50	62	MR	2019	-	-
PGWW19-05	3,430,916	7,287,889	3,844	62	MR	2019	-	-
PGWW19-06	3,430,545	7,288,054	3,842.50	62	MR	2019	-	-
PP-01-2018	3,427,028	7,275,405	3,805,70	611	MR	2019	2"	No data

Borehole	East (m)	North (m)	Elevation (masl)	TD (m)	Method	Year	Completion	
							Diameter (inches)	Screened interval (m)
PP-02-2019	3,427,171	7,273,819	3,772,50	650	MR	2019	2"	No data
PP-03-2019	3,428,251	7,276,673	3,803,2	542	MR	2019	10"-212-8"	No data
DD-01	3,429,329	7,278,639	3,793,5	700	DDH	2022	2"	6m every 12m
DD-02	3,427,651	7,275,815	3,802,50	646	DDH	2022	2"	380-440
R-01	3,434,507	7,279,732	3,794,70	601	MR	2022	2"	497-515
R-02	3,435,359	7,283,016	3,813	411	DDH/MR	2022	2"	6m every 12m
R-03	3,435,050	7,288,856	3,836	617	MR	2022	2"	18m every 18m
PW-01	3,427,651	7,275,815	3,802,50	503	MR	2022	10"-200-8"	350-500

Table 10.1 (continuation)

10.2 Exploration drilling

Hidrotec S.R.L. was contracted to carry out the drilling program for Millennial during 2016-2019 (PG-PW/PG-MW series). This program totaled 16,882 meters distributed in 42 vertical holes with depths ranging from 121 m to 641 m (Table 10.1). Most boreholes were drilled using a diamond core rig, but loss-circulation conditions required several locations to be re-drilled or to be drilled with a combination of core and mud rotary techniques to reach target depths (Table 10.1).

The following guidelines were followed during the diamond drilling and mud rotary program:

- Core recovery calculated and was recorded.
- Cores were described and stored in labeled cardboard core boxes.
- Drill cuttings were collected from rotary holes, described, and stored in cuttings boxes.
- Most boreholes were completed with 2-inch diameter blank and slotted PVC casing (0.75mm slot size).

The majority of brine sampling was conducted with a packer system. Packer samples were collected at specific intervals during drilling and occasionally upon completion of the drilling. Drive point sampling was used for five samples. The brine sampling procedures are further described in Section 11 below.

10.3 Production well drilling

Four production wells (PGPW16-01 to PGPW18-17) were drilled by Hidrotec S.R.L. during 2016-2019 using conventional mud rotary methodology following these general guidelines during the process:

- Drilling fluid was polymer mixed with brine.
- Unwashed and washed drill cuttings were described and stored in labeled plastic cutting boxes.

- Once drilling was finished PGPW16-01 was completed with 10-inch diameter blank PVC casing and 6-inch diameter slotted PVC well screen; PGPW17-04 and PGPW-15 were completed with 10-inch diameter blank steel casing and 6-inch diameter slotted steel well screen; and PGPW18-17 was completed with 12-inch diameter blank steel casing, 12 and 8-inch diameter slotted steel well screen.
- Gravel pack (1-3 mm diameter) was installed in the annular space surrounding the well screen.

After the installation of casing, gravel pack, and fill materials, polymer mud was broken down by emplacing sodium hypochlorite solution into the well. The developing process was completed using compressed air and by airlift pumping water and sediment from the well. The sand content of produced brine was monitored during development using an Imhoff cone.

10.4 Freshwater Exploration Drilling

A freshwater exploration program was carried out during 2018-2019 and included conventional mud rotary drilling of 6 wells to depths from 42 m to 62 m (PGWW series). The following guidelines were followed during the drilling process:

- Drilled mud rotary using conventional circulation.
- Drilling fluid was polymer mixed with brine.
- Unwashed and washed drill cuttings were described and stored in labeled plastic cutting boxes.
- PGWW18-01, PGWW19-02 and PGWW19-03 were completed with 6-inch diameter blank and slotted steel casing and gravel pack (1-3 mm diameter).
- PGWW19-04, PGWW19-05 and PGWW19-06 remained uncased.

10.5 Hydraulic testing

Millennial completed eight pumping tests between 2017 and 2019. These tests included three one-day tests on the freshwater wells; three three-day tests on brine wells; and two long-term pumping tests (23- and 30-day duration) also on brine wells. Figure 10.2 includes the layout of each of these pumping tests.

10.5.1 Brine Well Pumping Tests

10.5.1.1 PGPW16-01 (2017)

A 3-day pumping test was carried out on well PGPW16-01 at an average pumping rate of 27.7 L/s. The configuration of the test and its results are shown in Table 10.2 and Figure 10.3. The production well is screened across the saline halite unit and the underlying brine aquifer. This test included four observation wells but only SW03PG-1 (without completion information) reacted to pumping. Drawdown and recovery data were interpreted, respectively with Cooper & Jacob (1946) and Theis (1935) recovery solutions leading to a hydraulic conductivity (K) estimate of about 3 m/d.

Figure 10.2 Location map of the pumping tests conducted in Salar de Pastos Grandes

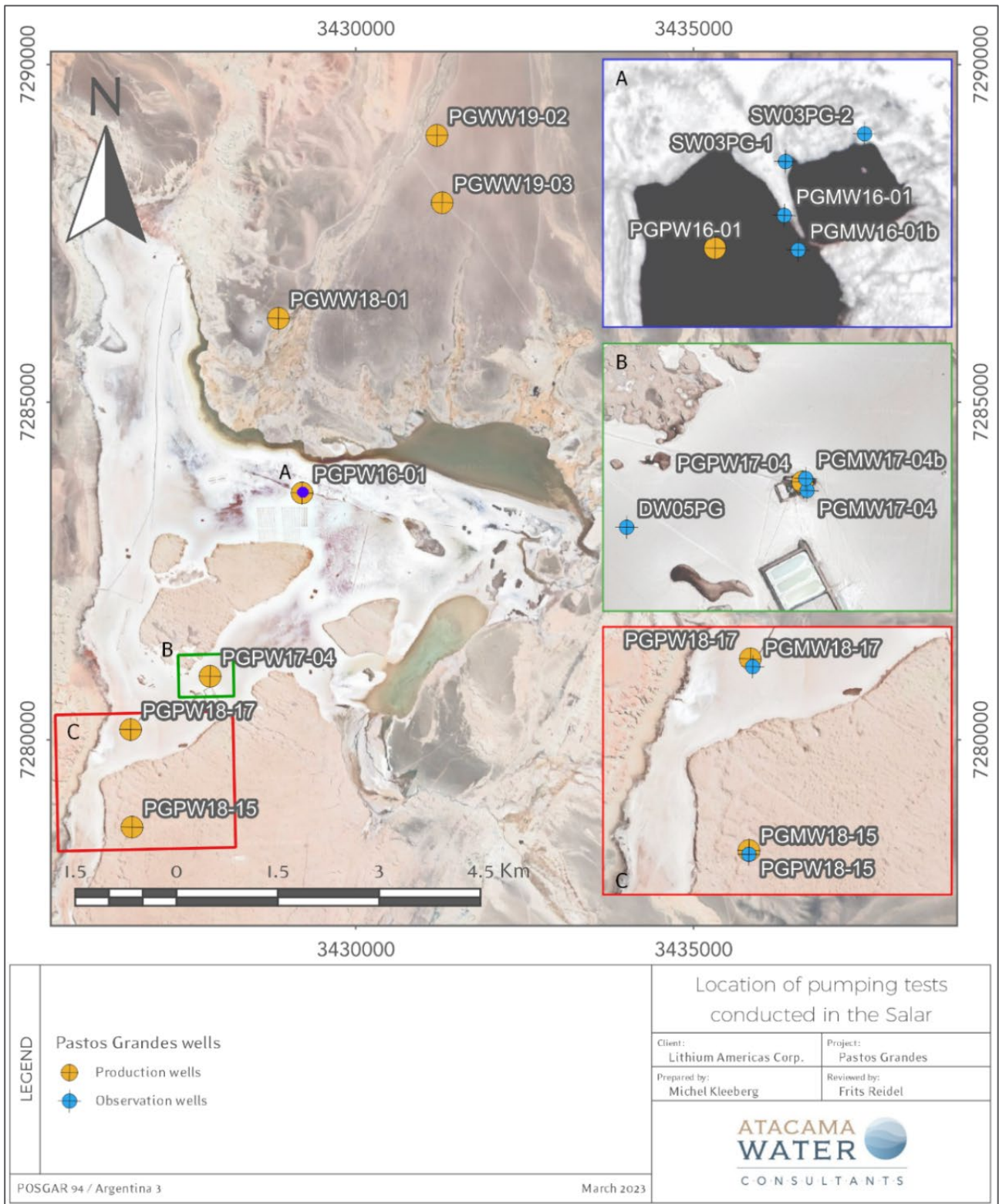


Table 10.2 Summary of pumping test PGPW16-01 (2017)

PGPW16-01 (2017)									
Well	Type	Q (L/s)	Duration (days)	Lithology	Minimum saturated thickness (m)	Maximum drawdown (m)	Fit	T (m ² /d)	K (m/d)
PGPW16-01	P	27.7	3	Mixed halite, sand, silt	224	9.04	C&J	1.100	4.91
							Theis Rec.	500	2.23
SW03PG-1	O	27.7	3	Mixed halite, sand, silt	#N/D	1.19	C&J	1.100	#N/D
							Theis Rec.	1	#N/D

10.5.1.2 PGPW17-04

A 23-day pumping test was completed on PGPW17-04 at a pumping rate of 15.23 L/s in 2019. The production well is screened across halite, sand, and silt; because of the low permeability of the halite it is believed that the drawdown response is mainly related to the unconsolidated clastic sediments beneath it. Drawdown data during the pumping stage was discarded due to an apparent non-related water level recovery observed during test. Therefore, only recovery data were adjusted to the Theis (1935) recovery solution, leading to a transmissivity estimate of 40 m²/d, or a hydraulic conductivity 0.12 m/d assuming a saturated thickness of 329 m. The configuration of the test and its results are shown in Table 10.3 and Figure 10.4.

Table 10.3 Summary of pumping test PGPW17-04

PGPW17-04									
Well	Type	Q (L/s)	Duration (days)	Lithology	Minimum saturated thickness (m)	Maximum drawdown (m)	Fit	T (m ² /d)	K (m/d)
PGPW17-04	P	15.23	23	Mixed halite, sand, silt	329	57.11	Theis Rec.	40	0.12

10.5.1.3 PGPW18-15

A pumping test (variable and constant rate, and recovery) was carried out in PGPW18-15 during April of 2019. The well was screened in the same lithological unit as PGPW-17-04. The configuration of this test and its results are shown in Figure 10.6 and Figure 10.5. Water levels during the test were also monitored in PGMW18-15. The hydraulic conductivity was estimated to range between 0.15 - 0.22 m/d.

Table 10.4 Summary of pumping test PGPW18-15

PGPW18-15									
Well	Type	Q (L/s)	Duration (days)	Lithology	Minimum saturated thickness (m)	Maximum drawdown (m)	Fit	T (m ² /d)	K (m/d)
PGPW18-15	P	24.1	3	Mixed halite, sand, silt	456	38.7	C&J	90	0.2
							Theis Rec.	70	0.15
PGMW18-15	O			Mixed halite, sand, silt	453	6.5	Theis	100	0.22

10.5.1.4 PGPW18-17

A three-day pumping test was conducted on well PGPW18-17 well with an average pumping rate of 19.4 L/s. The configuration of the test and its results are shown in Table 10.5 and Figure 10.6. Drawdown data was measured only in the pumping well and was adjusted to the Cooper and Jacob (1946) and Theis (1935) recovery solutions. The estimated hydraulic conductivity ranges between 0.17 – 0.22 m/d, which is consistent with previous results for the same lithologies in the Salar.

Table 10.5 Summary of pumping test PGPW18-17

PGPW18-17									
Well	Type	Q (L/s)	Duration (days)	Lithology	Minimum saturated thickness (m)	Maximum drawdown (m)	Fit	T (m ² /d)	K (m/d)
PGPW18-17	P	19.4	3	Mixed halite, sand, silt	589	30.31	C&J	130	0.22
							Theis Rec.	100	0.17

10.5.1.5 PGPW16-01 (2019)

A 15-day pumping test was conducted on well PGPW16-01 at an average pumping rate of 23.2 L/s during Mau 2019. The results of this 2019 test are summarized in Table 10.6 and Figure 10.7 and are quite similar to the results of the 2017 test. Drawdown and recovery data were interpreted with the Theis (1935) recovery solution, leading to a hydraulic conductivity estimate of about 2 m/d.

Table 10.6 Summary of pumping test PGPW16-01 (2019)

PGPW16-01 (2019)									
Well	Type	Q (L/s)	Duration (days)	Lithology	Minimum saturated thickness (m)	Maximum drawdown (m)	Fit	T (m ² /d)	K (m/d)
PGPW16-01	P	23.2	15	Mixed halite, sand, silt	224	15.15	Theis Rec.	400	1.79

10.5.2 Pumping tests conducted in freshwater wells

10.5.2.1 PGWW18-01

A variable rate and a 1-day constant rate tests with an average flow rate of 0.85 L/s was carried out on well PGWW18-01 in May 2019. No hydraulic parameters could be obtained from this test because of the short test duration and the low pumping rate as shown in Table 10.7.

Table 10.7 Summary of pumping test PGWW18-01

PGWW18-01									
Well	Type	Q (L/s)	Duration (days)	Target lithology	Minimum saturated thickness (m)	Maximum drawdown (m)	Adjust	T (m ² /d)	K (m/d)
PGWW18-01	P	0.85	1	Gravels and sands	10.96	5.13	-	-	-

10.5.2.2 PGWW19-02

Well PWGWW19-02 was pump tested in 2019 (a variable rate, a constant rate and a recovery). The layout of this test and results are shown in Figure 10.8 and in Table 10.8. Drawdown and recovery trends were adjusted with the Cooper and Jacob (1946) and Theis (1935) recovery solutions, respectively. Estimated hydraulic conductivity values ranged from 20 to 60 m/d which is considered reasonable for these types of coarse-grained unconsolidated sediments. The pumping test configuration didn't include observation wells; therefore, no storage estimates could be obtained.

Table 10.8 Summary of pumping test PGWW19-02

PGWW19-02									
Well	Type	Q (L/s)	Duration (days)	Lithology	Minimum saturated thickness (m)	Maximum drawdown (m)	Fit	T (m ² /d)	K (m/d)
PGWW19-02	P	24	0.8	Gravels and sands	15.5	5.32	C&J	1.6	66.67
							Theis Rec.	500	20.83

10.5.2.3 PGWW19-03

A variable rate, constant rate test and recovery test were carried out on Well PWWW19-03. The layout of this test and main results are shown in Figure 10.9 and in Table 10.9. Drawdown and recovery trends were adjusted with the Cooper and Jacob (1946) and Theis (1935) recovery solutions, respectively. Estimated hydraulic conductivity ranges from 6 to 11 m/d, which is reasonable for this type of coarse-grained unconsolidated sediments with a higher fine fraction. The pumping test configuration didn't include any observation wells; therefore, no storage estimates could be obtained from this test.

Table 10.10 and Table 10.11 include summary information on the pumping tests conducted in the Salar.

Table 10.9 Summary of pumping test PGWW19-03

PGWW19-03									
Well	Type	Q (L/s)	Duration (days)	Lithology	Minimum saturated thickness (m)	Maximum drawdown (m)	Fit	T (m ² /d)	K (m/d)
PGWW19-03	P	3.41	1	Gravels and sands	36	3.46	C&J	250	6.94
							Theis Rec.	400	11.11

Figure 10.3 Location, setup and results of pumping test well PGPW16-01 (2017)

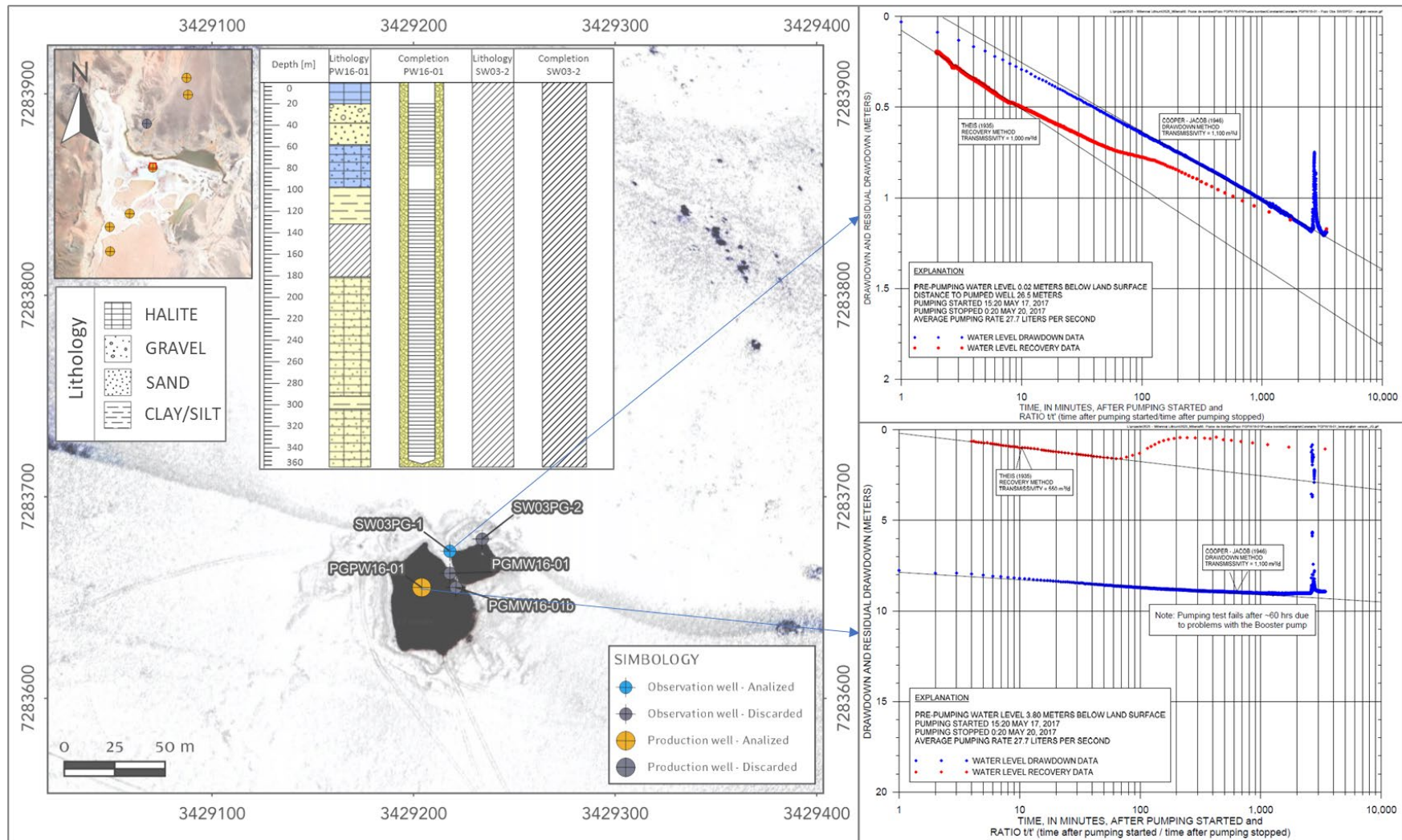


Figure 10.4 Location, setup and results of pumping test PGPW17-04

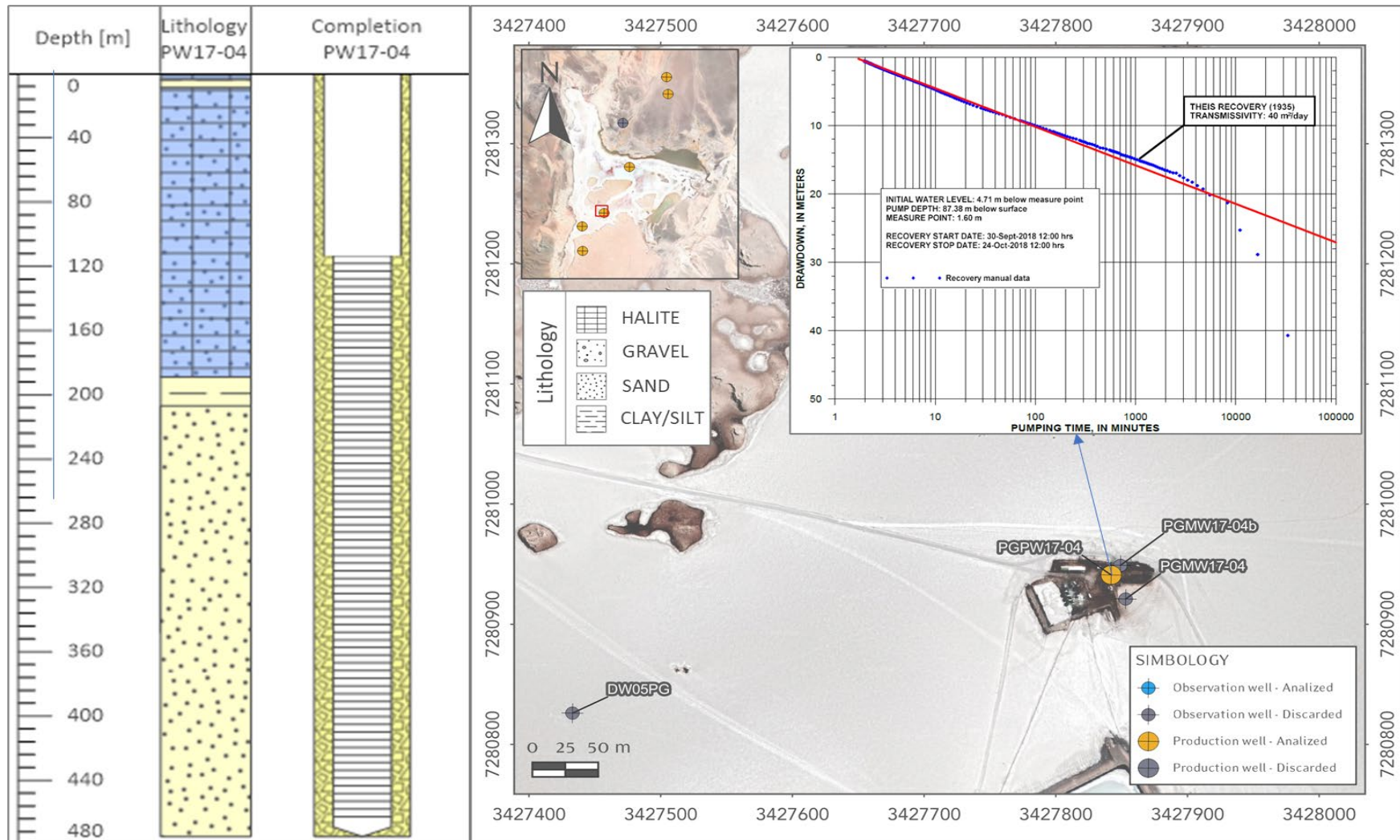


Figure 10.5 Location, setup and results of pumping test PGPW18-15

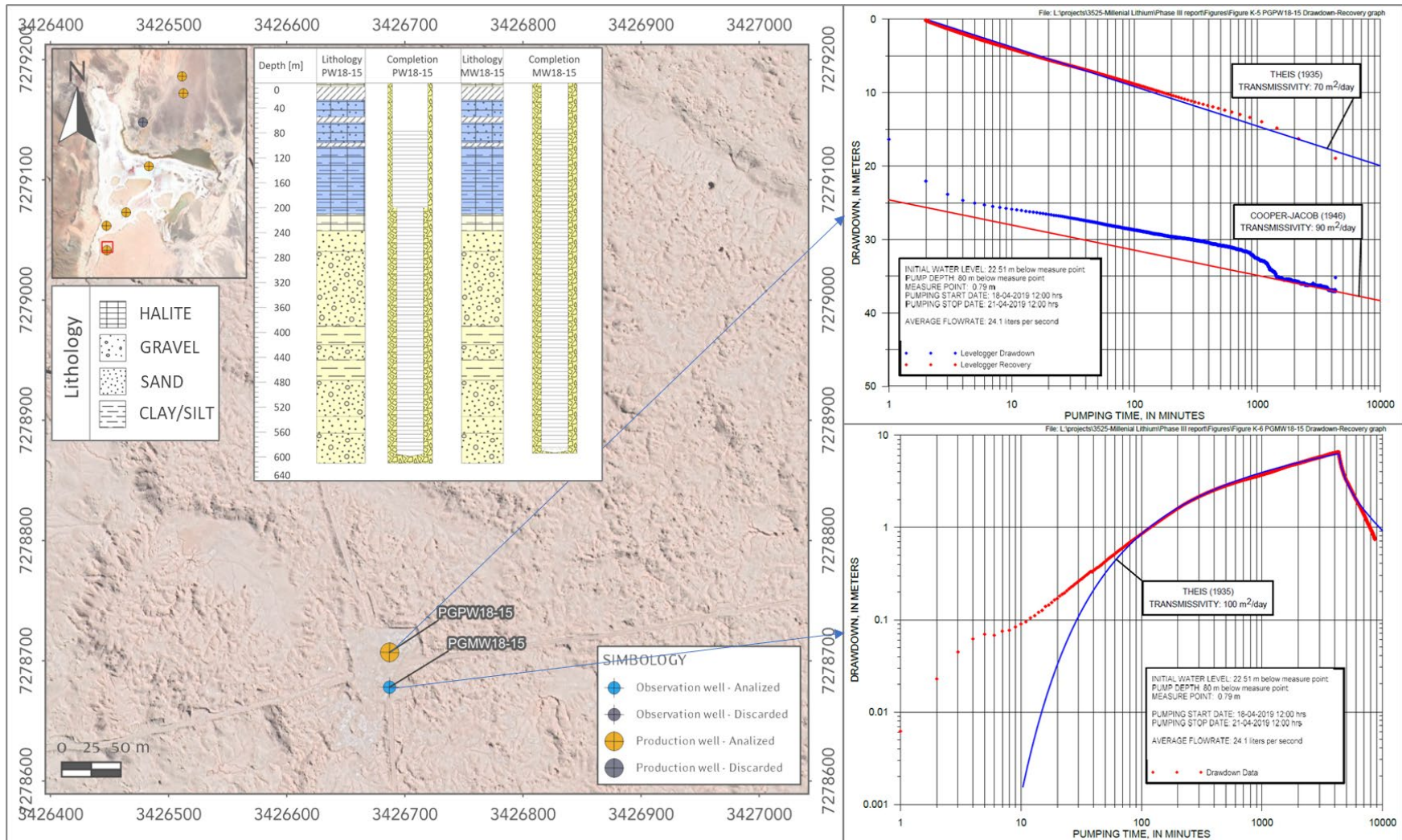


Figure 10.6 Location, setup and results of pumping test PGPW18-17

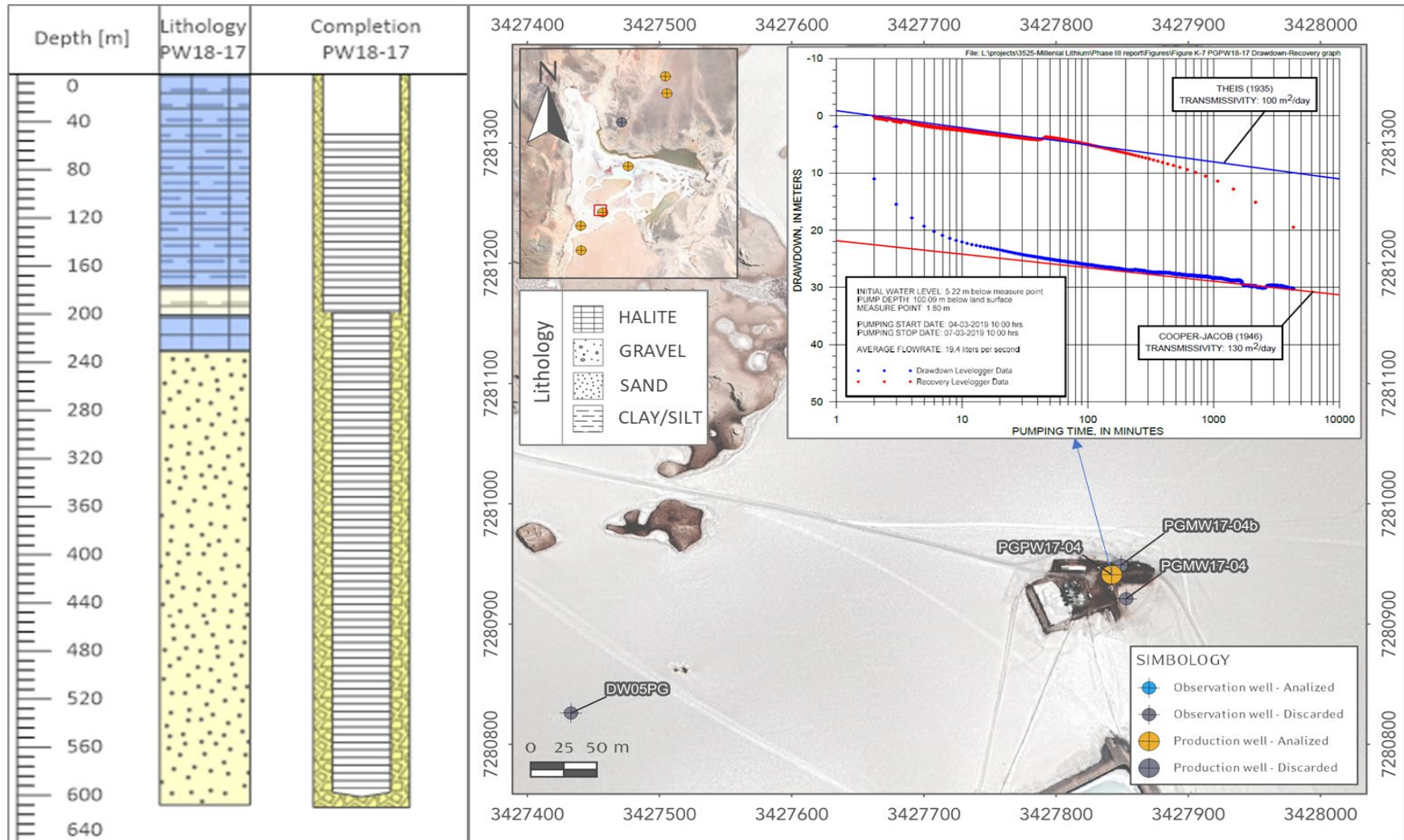


Figure 10.7 Location, setup and results of pumping test PGPW16-01 (2019)

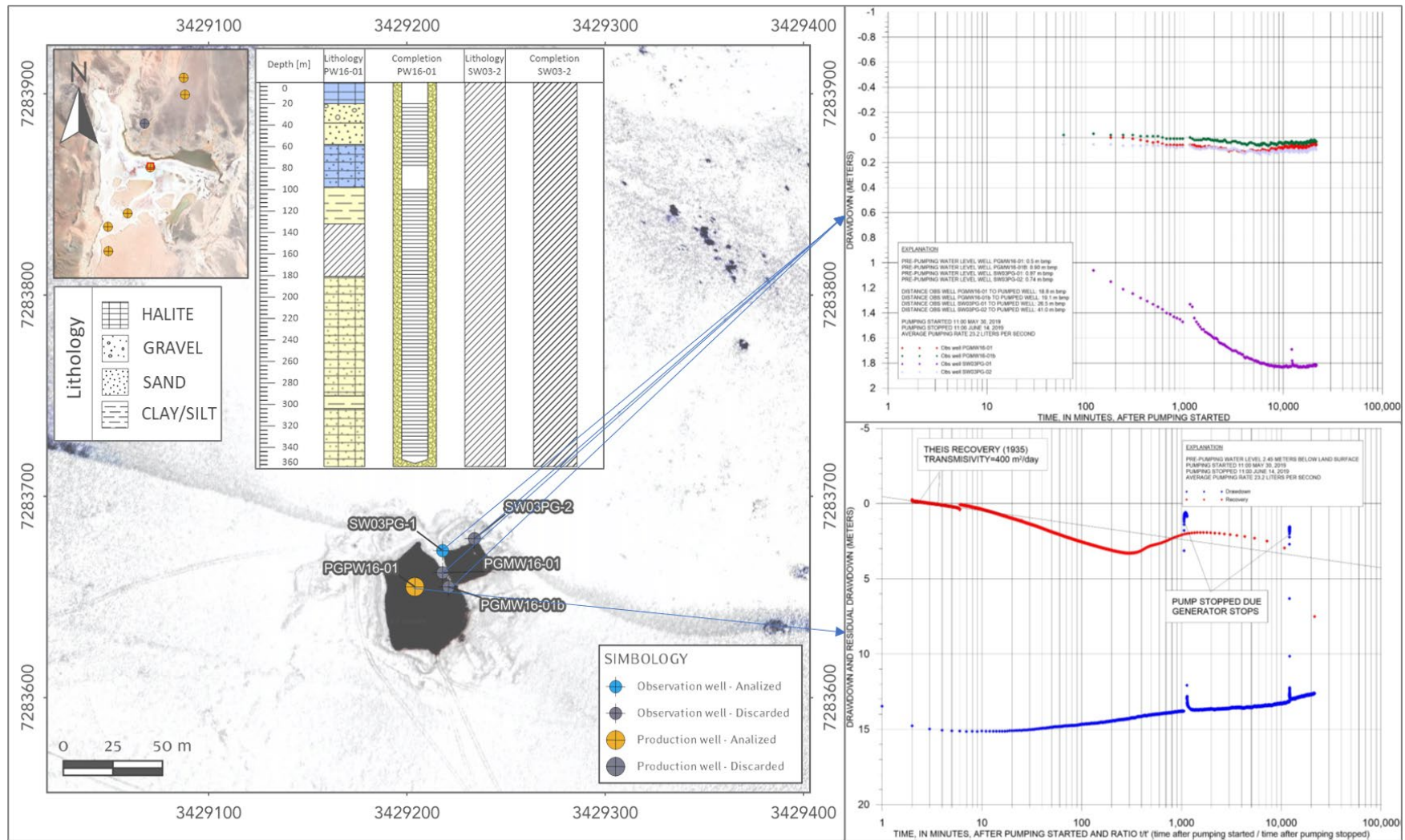


Figure 10.8 Location, setup and results of pumping test PGWW19-02

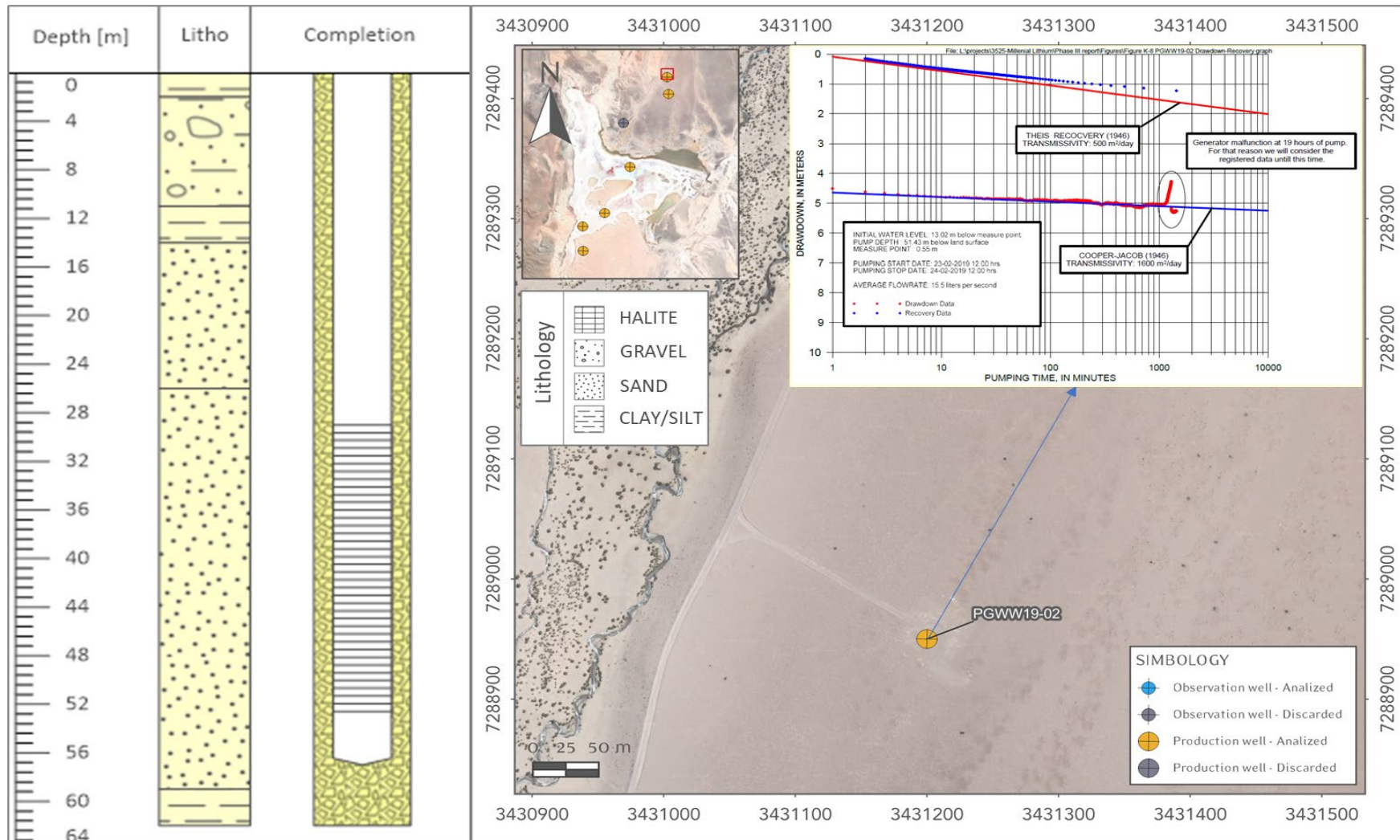


Figure 10.9 Location, setup and results of pumping test PGWW19-03

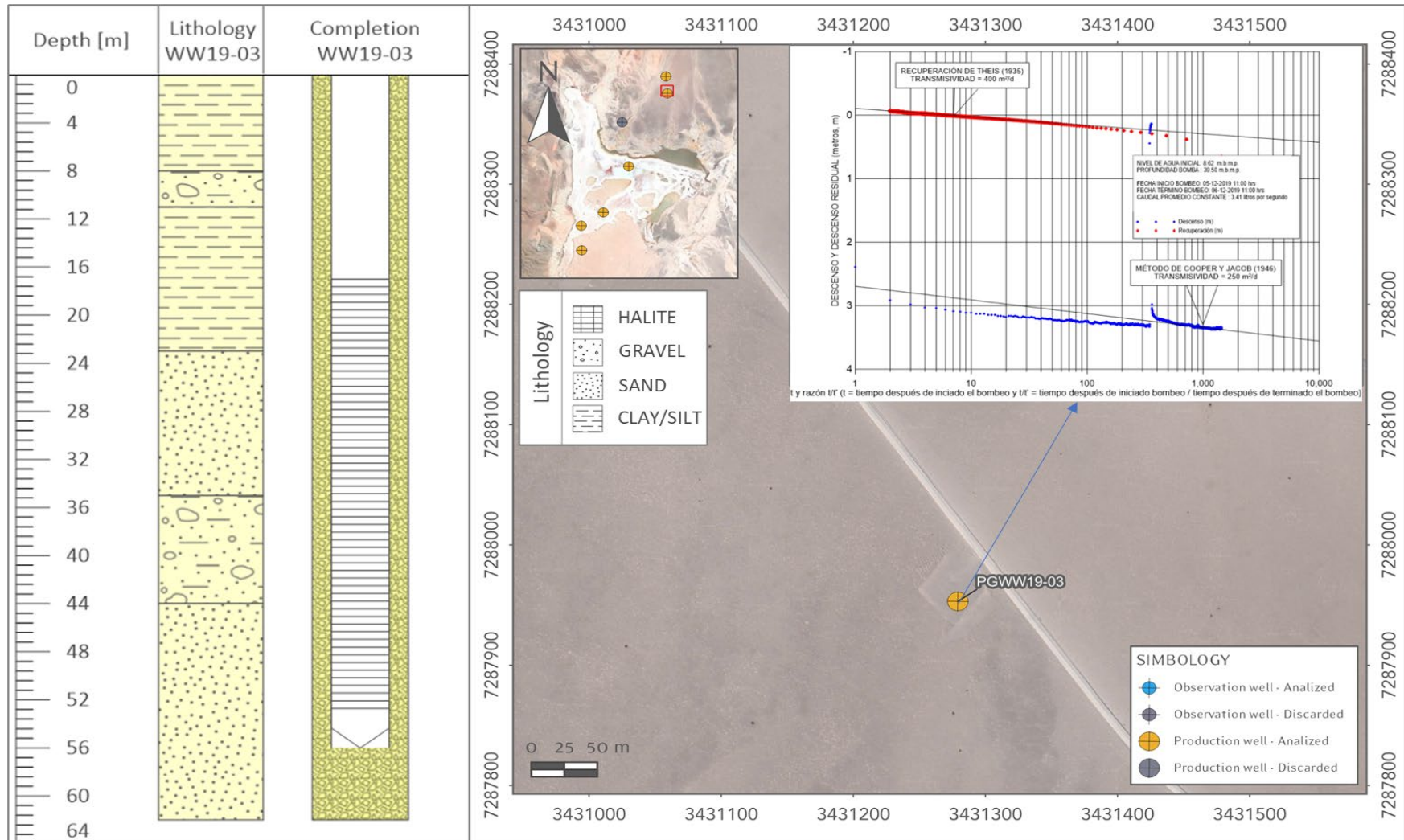


Table 10.10 Summary of brine well tests

Test	Well	Type	Q (L/s)	Duration (days)	Lithology	Minimum saturated thickness (m)	Maximum drawdown (m)	Fit	T (m ² /d)	K (m/d)	Specific capacity (L/s/m)
PGPW16-01 (2017)	PGPW16-01	P	27.7	3	Mixed halite, sand, silt	224	9.04	C&J (1946)	1.1	4.9	3.1
								Theis Rec. (1935)	500	2.2	-
	PGMW16-01	O			Mixed halite, sand, silt	38	0.13	-	-	-	-
	PGMW16-01b	O			Mixed halite, sand, silt	189	0.08	-	-	-	-
	SW03PG-1	O			Mixed halite, sand, silt	No data	1.19	C&J (1946)	1.1	-	-
Theis Rec. (1935)			1	-	-						
SW03PG-2	O	Mixed halite, sand, silt	No data	0.03	-	-	-	-			
PGPW17-04	PGPW17-04	P	15.2	23	Mixed halite, sand, silt	329	57.11	Theis Rec. (1935)	40	0.12	0.27
	PGPW17-04b	O			Mixed halite, sand, silt	484	3.88	-	-	-	-
	DW05PG	O			Mixed halite, sand, silt	No data	0.12	-	-	-	-
PGPW18-15	PGPW18-15	P	24.1	3	Mixed halite, sand, silt	456	38.70	C&J (1946)	90	0.20	0.68
								Theis Rec. (1935)	70	0.15	-
	PGMW18-15	O			Mixed halite, sand, silt	453	6.50	Theis (1935)	100	0.22	-
PGPW18-17	PGPW18-17	P	19.4	3	Mixed halite, sand, silt	589	30.31	C&J (1946)	130	0.22	0.64
								Theis Rec. (1935)	100	0.17	-
PGPW16-01 (2019)	PGPW16-01	P	23.2	15	Mixed halite, sand, silt	224	15.15	Theis Rec. (1935)	400	1.8	1.5
	PGMW16-01	O			Mixed halite, sand, silt	38	0.12	-	-	-	-
	PGMW16-01b	O			Mixed halite, sand, silt	189	0.07	-	-	-	-
	SW03PG-1	O			Mixed halite, sand, silt	No data	1.83	-	-	-	-
	SW03PG-2	O			Mixed halite, sand, silt	No data	0.14	-	-	-	-

Table 10.11 Summary of freshwater pumping tests

Test	Well	Type	Q (L/s)	Duration (days)	Lithology	Minimum saturated thickness (m)	Maximum drawdown (m)	Fit	T (m ² /d)	K (m/d)	Specific capacity (L/s/m)
PGWW19-02	PGWW19-02	P	15.5	0.8	Gravels and sands	24	5.32	C&J (1946)	1.6	66.6	2.9
								Theis rec. (1935)	500	20.8	-
PGWW19-03	PGWW19-03	P	3.1	1	Gravels and sands	36	3.46	C&J (1946)	250	66.6	0.9
								Theis rec. (1935)	400	11.1	-
PGWW18-01	PGWW18-01	P	0.85	1	Gravels and sands	10.96	5.13	-	-	-	0.2

11 SAMPLE PREPARATION, ANALYSIS, AND SECURITY

11.1 Sampling Methods and Assays

11.1.1 Millennial drainable porosity analysis (2016-2019)

Samples were obtained from ‘undisturbed’ core during the 2016-2019 Millennial drilling programs and analyzed for drainable porosity by Core Laboratories-Petroleum Services in Houston, Texas (“Corelabs”). In addition, rotary drill cuttings were sent to Geosystems Analysis in Tucson, Arizona (“GSA”) for repacking, triaxial testing, and drainable porosity analysis.

Both Corelabs and GSA offer advanced petrophysical and geological analysis and interpretation services for core samples. These laboratories operate in compliance with ISO 9001:2008 Certification ensuring that processes and procedures adhere to internationally recognized quality standards. The analytical procedures for determining drainable porosity for each laboratory are further described below.

Corelab drainable porosity analysis are based on centrifuge methodology and involve the following:

1. 38 mm (1.5-inch) diameter cylindrical plugs were cut from the sample material.
2. Samples were frozen with dry ice to maintain their integrity, if required.
3. Sample weight and thickness were measured.
4. The plugs were encapsulated in Teflon and nickel foil as required, and nickel screens were placed on the ends of the plugs. The encapsulated samples were then weighed.
5. Bulk density was calculated as: $(\text{Mass of plug before encapsulation}) / (\text{Calliper bulk volume})$.
6. The plugs were placed in brine and saturated under vacuum to ensure full saturation. Corelabs utilized a standard sodium chloride brine with a NaCl concentration of 244,000 ppm with a density of 1.184 gm/cm³.
7. The weight of the saturated cores was recorded.
8. The samples were desaturated in a high-speed centrifuge for 4 hours. Spin rates were calculated to provide a drainage pressure of 1 pound per square inch (psi) for poorly cemented or loose sands and 5 psi for clay and halite.
9. The drainage was collected, and the volume was recorded. The effluent was saved for possible analysis. However, it should be noted that the fluid collected from these cores may not be representative of in situ brines if re-saturation with NaCl was required.
10. Plugs were removed from the centrifuge and weight was recorded. Drained fluid volume was calculated as: $(\text{saturated plug weight} - \text{drained plug weight}) / 1.184$. Drainable porosity was calculated as $(\text{Drained fluid volume}) / (\text{Calliper bulk volume})$.
11. Total porosity was calculated after drying the samples for 5 days at 115.6 degrees Celsius to record dry weight.
12. All weight loss is assumed to be water lost from pore space where volume of water loss is calculated as: $((\text{Drained plug weight}) - (\text{Oven-dried plug weight})) / (\text{Water density of } 1 \text{ g/cc})$.
13. Total porosity is calculated as $((\text{Drained fluid volume}) + (\text{Oven drying fluid loss})) / (\text{Calliper bulk volume})$.

GSA drainable porosity analysis procedures for repacked sediment samples include the following steps:

1. All loose and sandy samples were packed into test cells with moderate effort without prior knowledge of bulk density or other consolidation tests. Additional repacking was performed on some samples with minimum and maximum effort to evaluate the effectiveness and variation of hand-packing at higher and lower densities. Bulk densities approximately 0.1 g/cm³ lower and higher than the initial density were achieved, respectively.

2. The sandy material was packed into a stainless-steel ring in several small lifts. The weight and packing height of the first lift were used to guide the subsequent lifts to ensure consistent density packing. Scales were used to track the equipment, cell, and sample weights throughout the process, and the final packed and assembled core weight was recorded.
3. Plastic air tubing, approximately 6 inches in length, was inserted into the top of each core to monitor saturation and prevent brine solution spillage. The cores were then assembled and saturated slowly from the bottom up using provided brine. A combination of gravity feed and vacuum suction was used to achieve the target saturation. If the target saturation could not be reached using gravity feed alone, vacuum suction was applied. The saturation process lasted for up to 24 hours. Once fully saturated, the cores were closed at the bottom with a hose clamp to prevent brine solution loss and disconnected from the saturation setup.
4. Each cell assembly underwent three pressure steps after being transferred to a test rack. The first step, at 0 mbar pressure, lasted for 24 hours and was applied to remove excess saturation solution. To approximate the release of brine solution at 120 mbar and 1/3 bar of the brine solution, two sequential pressure steps were used at 120 mbar and 1/3 bar, respectively. The 120-mbar pressure step was maintained for 2 days, and the 1/3 bar was continued for another 2 to 4 days. Weight measurements were taken twice a day to determine the loss of brine solution over time. After the final step the cores were disassembled and samples were oven dried to determine total porosity following the procedure described in MOSA, 2002, Part 4 Ch. 2, 2.3.2.1.
5. To estimate the brine solution release volumes at the 120 millibar and 1/3 bar pressure steps, the difference was calculated between the measured total porosity and the moisture retained after the pressure plate measurements as outlined in MOSA (2002), Part 4, Chapter 3, Section 3.3.3.5. The solution's release volume obtained at 1/3 bar was regarded as an approximation of the maximum solution drainage that could occur under gravity or pumping conditions, and hence was used to determine the specific yield.

After completing the tests, the estimated particle density and weight data from core samples at various pressure steps were entered into a spreadsheet. The spreadsheet was programmed to automatically calculate the salt weight left in the sample after drying, estimated porosity, and water content change. Furthermore, particle density was optimized during data processing by utilizing all prior test measurements and using a solver in Microsoft Excel. The laboratory report presented the calculated particle density for each sample.

11.1.2 AMSA drainable porosity samples (2021-2022)

36 samples from the AMSA 2021-2022 drilling program were sent to GSA for drainable porosity analysis. All samples were tested using the 'Rapid Brine Release' method (Yao et al., 2018) to measure specific yield (Sy) and total porosity (Pt). Brine release drainable porosity was measured at 120 mbar and 333 mbar of pressure, where:

1. Brine release at 120 mbar represents drainable porosity from sand dominated sediments and rapid brine release from macropores (Nwankwor et al., 1984).
2. Brine release at 333 mbar represents the Sy for intermediate to finer texture sediments (Cassel and Nielsen, 1986).

Brine release values at 120 mbar were provided for reference and 333 mbar values were presented as the estimated Sy (drainable porosity). A subset of paired samples representative of the range in lithology types were selected by AW and GSA for testing using the Relative Brine Release Capacity (RBRC, Stormont et. al., 2011) method by Daniel B. Stephens & Associates, Inc. in Albuquerque, NM (DBSA). The goals of the test work were to

provide S_y and P_t values for each sample, summary statistics of S_y and P_t by lithological group, and to compare the S_y and P_t values derived for paired core samples using the RBR and RBRC methods.

Table 11.1 lists the physical properties analyses carried out by GSA. In addition to the RBR testing, physical property tests were run by GSA to assist in lithologic characterization and interpretation of results including bulk density testing (ASTM D2937-17e2) on all RBR samples.

Table 11.1 Summary of laboratory tests conducted by GSA

Test Type	Sample Type and Number	Test Method	Testing Laboratory	Standard
Physical	36 core samples	Bulk density	GSA Laboratory (Tucson, AZ)	ASTM D2937-17e2
	36 core samples	Estimated Particle Density	GSA Laboratory (Tucson, AZ)	MOSA Part 4 Ch. 2, 2.2
Hydraulic	5 core samples	Relative Brine Release Capacity (RBRC)	DBS&A (Albuquerque, NM)	Stormont et. al., 2011
	36 core samples	Estimated Total Porosity	GSA Laboratory (Tucson, AZ)	MOSA Part 4 Ch. 2, 2.3.2.1
		Estimated Field Water Capacity		MOSA Part 4 Ch. 3, 3.3.3.2
		Rapid Brine Release (RBR)		Modified ASTM D6836-16
MOSA Part 4 Ch. 3, 3.3.3.5				

Three packing methods were used to prepare RBR core samples:

- Stainless steel rings were pushed into intact sediment cores to preserve the structure and retain the original bulk density and porosity distribution in the sample.
- Sediment cores with loose sediment and/or disturbed samples were extruded, and voids were filled in using moderate packing effort to eliminate voids in the test samples.
- Most solid halite and/or rock cores were cut with a rock saw to fit GSA’s RBR test cells and then fit into a 6.35 cm diameter ring and sealed as discussed below.

RBR test cells were prepared by placing a pre-wetted micro-pore membrane (rated 1200 mbar air entry value) into the bottom PVC cap. This membrane maintains a permeable saturated bottom boundary for solution flow and prevents air entry under the target air pressures applied during RBR testing. The PVC caps contain gaskets to create an air-tight test cell that maintains constant air pressure and allows continuous solution outflow through the membrane.

The RBR method is based on the moisture retention characteristic method using the Tempe cell design (Modified ASTM D6836-16), whereby S_y is determined by applying pressures equivalent to gravity drainage to the Test Cell and measuring the amount of brine solution released. P_t is also measured in the RBR method, and is equal to the sum of S_y and S_r .

Each saturated RBR Test Cell was transferred to a test rack for the pressure extraction procedure where no pressure was applied for one day to remove any excess brine solution due to core over-saturation. Two sequential pressure steps were used to approximate brine solution release at 120 mbar and 333 mbar of matric potential (MOSA Part 4 Ch. 3, 3.3.3.2).

The 120-mbar pressure step was maintained for at least two days, and the 333-mbar pressure step was continued for another two to four days. Core assemblies were weighed prior to saturation, after saturation, and then two times daily to determine brine solution loss over time.

All samples were oven dried for three days at 60°C and one day at 105°C after the final step to determine the specific retention (Sr), dry bulk density, and Pt (MOSA Part 4 Ch. 2, 2.3.2.1), where Sr is the volume of water retained by the sample under 333 mbar soil water potential. This drying approach allowed for quantification of the amount of moisture lost due to crystalline water present in gypsum.

Brine solution release volumes at the 120 mbar and at 333 mbar pressure steps were estimated by the weight of brine lost between the initial cell assembly mass and the mass after each pressure plate step divided by the brine specific gravity (Equation 2, MOSA Part 4 Ch3, 3.3.3.5):

$$S_y = \frac{w_s - w_{333 \text{ mbar}}}{A * L * Bsg}$$

where w_s is the saturated weight, $w_{333 \text{ mbar}}$ is the weight at 333 mbar, A is the sample core area, L is sample length, and Bsg is the specific gravity of the brine solution. The S_y is assumed to approximate the solution release volume from saturation to 333 mbar. Particle density was estimated from the measured porosity and bulk density according to:

$$1 - \frac{\text{Bulk density}}{\text{Particle density}}$$

11.1.3 Brine samples

Depth-specific brine samples were collected during core and rotary drilling by packer-system, bailing, or drive-point sampling. Bulk (compound) brine samples were obtained during pumping tests on selected exploration wells.

- Depth-specific packer sampling was the primary method used to collect brine samples during the drilling programs for Phase II and III (2016-2020). Most samples were obtained during drilling, although some were also taken after drilling had concluded. Samples were considered acceptable and representative of the depth interval only if they showed no, or minimal traces of drilling mud. The intervals were typically 3 m long and determined by the site geologist after inspecting drill cores or at predetermined depths. However, the interval length may vary depending on the specific circumstances of a given hole or interval, such as borehole stability. To ensure accurate sampling, intervals were flushed out multiple

times before collecting the actual sample. The flushed brine was then collected in a barrel, and the time taken to fill the barrel was recorded.

- Drive-point sampling: five brine samples were collected using this method where a drive-point was installed onto BT-sized drill rods after removing the core barrel. The drive-point was then lowered past the drill bit with the help of a drop hammer and an impermeable diaphragm was used to prevent filling of the drill rods during the descent. Once the desired depth was reached, an electric water level sounder was used to confirm that the interior was dry before perforating the diaphragm using a weighted pin lowered with the wireline. This piercing allowed the brine to flow into the drive point and fill the BT rods and collect the samples with the use of a bailer.
- Bailing: the borehole was purged by bailing up to three well volumes of brine from the drill casing as calculated from the water level measurement, prior to collecting the final brine sample from the bottom of the hole. The final brine sample was discharged from the bailer into a 20-liter clean bucket from which one-liter sample bottles were rinsed and filled with brine. Each bottle was taped and marked with the borehole number and depth interval. A small sub-sample from the bucket was used to measure field parameters (density, electric conductivity, pH and temperature) at the wellhead.
- Samples from pumping tests: This method involved collecting samples directly from the discharge pipe at regular intervals during pumping tests. Temperature and density were recorded on internal field sheets.

Regardless of the sampling method, samples were collected in 20-liter containers that were washed with distilled water and rinsed with brine several times prior to filling. The temperature and density were recorded before filling 1-liter sample bottles which were also flushed with brine from the 20-liter container. The sample bottles were then sealed with a secure screw top to prevent leakage and labelled clearly with their identification number. Samples did not undergo any further preparation before being shipped to their respective laboratories.

After the sampling process the site geologist would retain possession of the brine samples until they were delivered to the office for shipment to the assay laboratory. Once at the office, duplicates, blanks, and standards were inserted into the assay batches before being sent to the laboratory. Prior to shipment all samples were kept under controlled temperature conditions.

The chemical analysis of brines was conducted by two reputable laboratories: SGS Argentina S.A and Norlab S.R.L, the later partnered with Alex Stewart Assayers (ASA) in 'ASANOVA'. The mentioned laboratories have extensive experience analyzing lithium-bearing brines and hold accreditation to ISO 9001 standards and follow the ISO 17025 guidelines.

For the primary constituents of interest, including boron, calcium, potassium, lithium, and magnesium, both ASANOVA and SGS utilized Inductively Coupled Plasma Analysis (ICP) as the analytical technique, with samples diluted 100:1 prior to analysis. A summary of the analytical methods employed by each laboratory for each physicochemical parameter and analyte is shown in Table 11.2.

Table 11.2 Analytical methods used by ASANOA and SGS for brine assays.

Analysis	ASA Code	ASA Method	SGS Code	SGS Method
Physicochemical Parameters				
Alkalinity	LMFQ167	Volumetric	SM 2320B	Titration
Conductivity	LMFQ01	Potentiometric	SM 2510 B	Resistor Network
Density	LMFQ19	Pycnometer	ASTM D4052-16	Digital Density Meter
Hardness (CaCO ₃)	LMFQ13	Volumetric	SM 2320B	Titration
PH	LMC128	Potentiometric	SM 4500 H B	Potentiometric
TDS	LMFQ08	Gravimetric	SM 2540C	Gravimetric
Inorganic Parameters				
Chlorides (Cl)	LMC101	Argentometric	SGS.ME.108	Ion Chromatography
Sulphates (SO ₄)	LMC107	Gravimetric	SGS.ME.108	Ion Chromatography
Dissolved Metals				
Barium (Ba)	LMMT03	ICP	SGS.ME.113	ICP
Boron (B)	LMMT03	ICP	SGS.ME.113	ICP
Calcium (Ca)	LMMT03	ICP	SGS.ME.113	ICP
Iron (Fe)	LMMT03	ICP	SGS.ME.113	ICP
Lithium (Li)	LMMT03	ICP	SGS.ME.113	ICP
Magnesium (Mg)	LMMT03	ICP	SGS.ME.113	ICP
Manganese (Mn)	LMMT03	ICP	SGS.ME.113	ICP
Potassium (K)	LMMT03	ICP	SGS.ME.113	ICP
Sodium (Na)	LMMT03	ICP	SGS.ME.113	ICP
Strontium (Sr)	LMMT03	ICP	SGS.ME.113	ICP

11.2 Drainable porosity QA/QC

Five duplicate samples were sent to DBSA to serve as check samples to test for accuracy within the drainable porosity analysis. Summary statistics for paired samples by GSA lithologic category for Pt and Sy are provided in Table 11.3 and Table 11.14 respectively. QAQC testing was run on subsamples from the same core, but not on identical samples. Minor differences in material type (sand/silt/clay content) and core physical structure (bulk density, degree of cementation, rock content, macropore content) may result in discrepancies between laboratory measured values. Correlations between GSA and external laboratory measured values of Pt and Sy are provided in Figure 11.1 and Figure 11.2, respectively.

Variations can likely be attributed to sample heterogeneity within cores which result in subsamples with slightly to significantly different material properties, and differences in laboratory methods such as testing duration. The Sy values measured by GSA were often considerably higher than the Sy values measured by DBSA, particularly for the 333 mbar RBR measurement (Table 14.4, Figure 11.2). Differences were most pronounced for halite

samples due to lithological variability within the group (one crystalline sample with large crystals and one massive to crystalline sample with very scarce matrix). In the absence of sample heterogeneity, differences are likely attributable to testing equilibration time and testing method. DBSA’s RBRC method only applied 333 mbar of equivalent pressure for 24 hours and did not use a filter paper to prevent air moving through samples, whereas GSA’s RBR testing was run at 120 mb for two days and then 333 mbar for two to four days no air was allowed to move through samples. Therefore, the lower Sy values reported by DBSA may be due to the samples not reaching equilibrium over the testing period. This may be most pronounced in materials with a greater predominance of macropores such as sands. It should be noted that Sy values measured at 120 mbar were generally in better agreement with DBSA’s measured Sy values for all sediment lithological groups (Table 14.4, Figure 11.3).

Specific gravity was higher for the RBR DD-01 451-451,2 sample (SG = 2.29) compared to the RBRC sample (SG = 2.13). Comparison of average values by lithological group was also limited due to small sample number. Average Pt values measured using the RBRC method (DBSA) were 7% lower for the clastic material group and 129% lower for the halite group. Average Pt values were considerably higher for the clastic group (0.24), with the halite group having a mean Pt value of 0.02.

There was general agreement between the total porosity data (R2 = 0.85). Correlation was slightly lower for the specific yield data (R2 = 0.80). The slope of the line was relatively high, indicating that GSA Sy values were approximately 35% higher than those reported by DBSA. The adjusted correlation coefficient between RBRC Sy and the drainable porosity at 120 mbar was R2 = 0.80.

All the samples tested for Sy fell below the 1:1 line indicating that GSA measured Sy values were typically higher than DBSA measured Sy values. In contrast, while three Pt points were scattered below the 1:1 line, two clastic material samples were plotted on the 1:1 line meaning the measured Pt values were similar for both laboratories.

Figure 11.1, Figure 11.2 and Figure 11.3 compare Pt, Sy, and GSA’s drainable porosity (at 120 mbar) versus DBSA’s Sy (at 333 mbar) respectively, for the 5 check samples. The lithology classification of the plotted data is indicated by color, with green representing clastic material and purple representing halite. The central blue line represents the 1:1 ratio while the two adjacent blue lines indicate the acceptable 33% threshold. The graphs reveal that there is acceptable variation between the laboratories for samples in the clastic material classification, but unacceptable variation for samples in the halite classification.

Table 11.3 Total porosity results for paired samples using GSA lithologic classification.

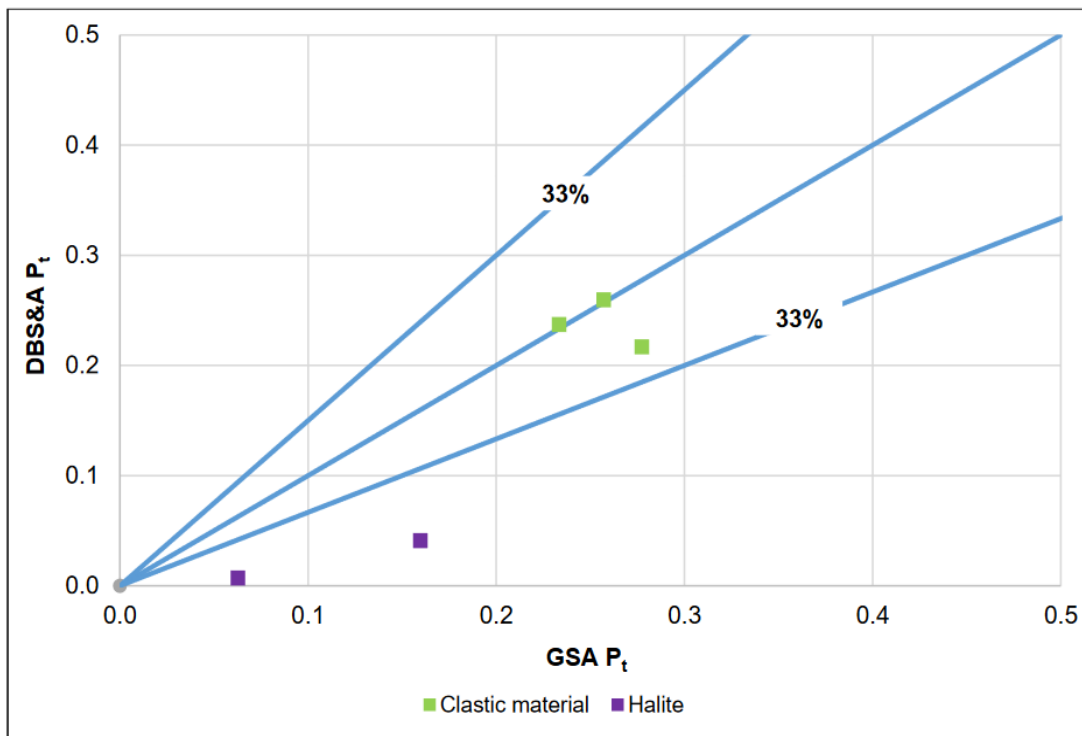
Total Porosity Statistics	Clastic material		Halite	
	RBR	RBRC	RBR	RBRC
N	3		2	
Avg	0.26	0.24	0.11	0.02
StdDev	0.02	0.02	0.07	0.02
Average Relative Percent Difference ¹⁰	7%		129%	

¹⁰ Calculated as 2*absolute value of (RBR-External Lab)/(RBR+External Lab), expressed as a percentage.

Table 11.4 Specific yield results for paired samples using GSA lithological classification.

Specific Yield Statistics	Clastic material			Halite		
	RDR @ 120	RBR @ 333	RBRC	RBR @ 120	RBR @ 333	RBRC
n	3			2		
Avg	0.10	0.14	0.10	0.02	0.07	0.00
StdDev	0.05	0.04	0.03	0.00	0.01	0.00
Average Relative Percent Difference ¹¹	2% (120 mbar), 29% (333 mbar)			123% (120 mbar), 177% (333 mbar)		

Figure 11.1 Pt comparison for check samples DBSA - GSA



¹¹ Calculated as 2*absolute value of (RBR-External Lab)/(RBR+External Lab), expressed as a percentage.

Figure 11.2 Sy comparison for check samples DBSA - GSA

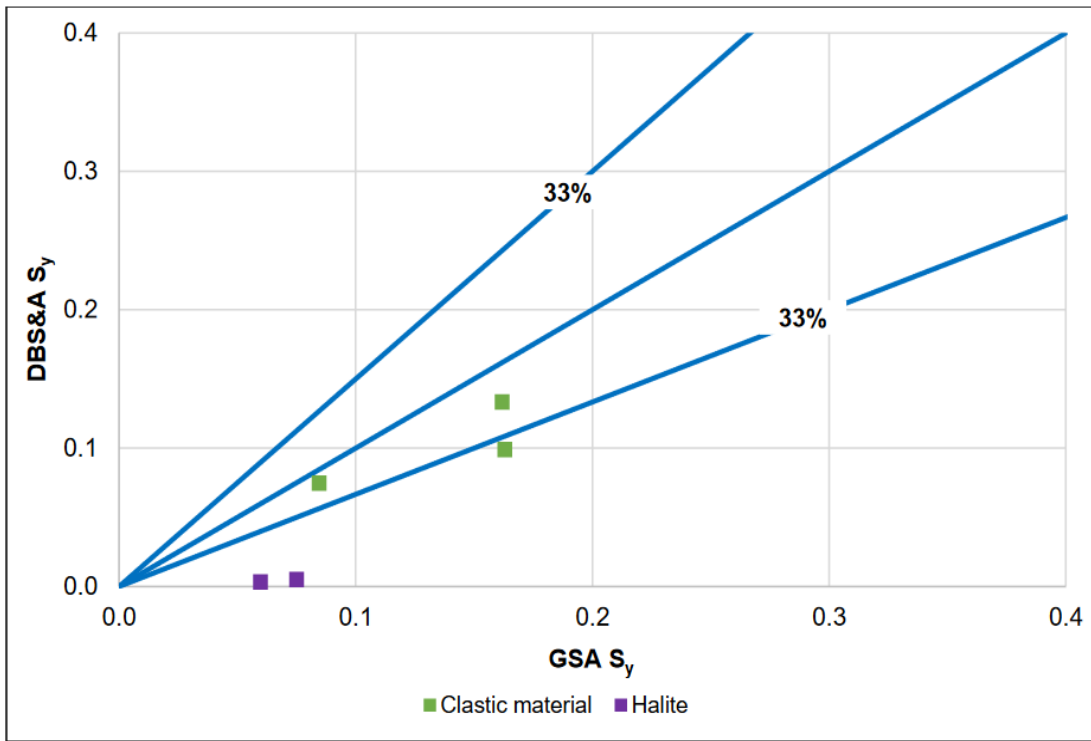
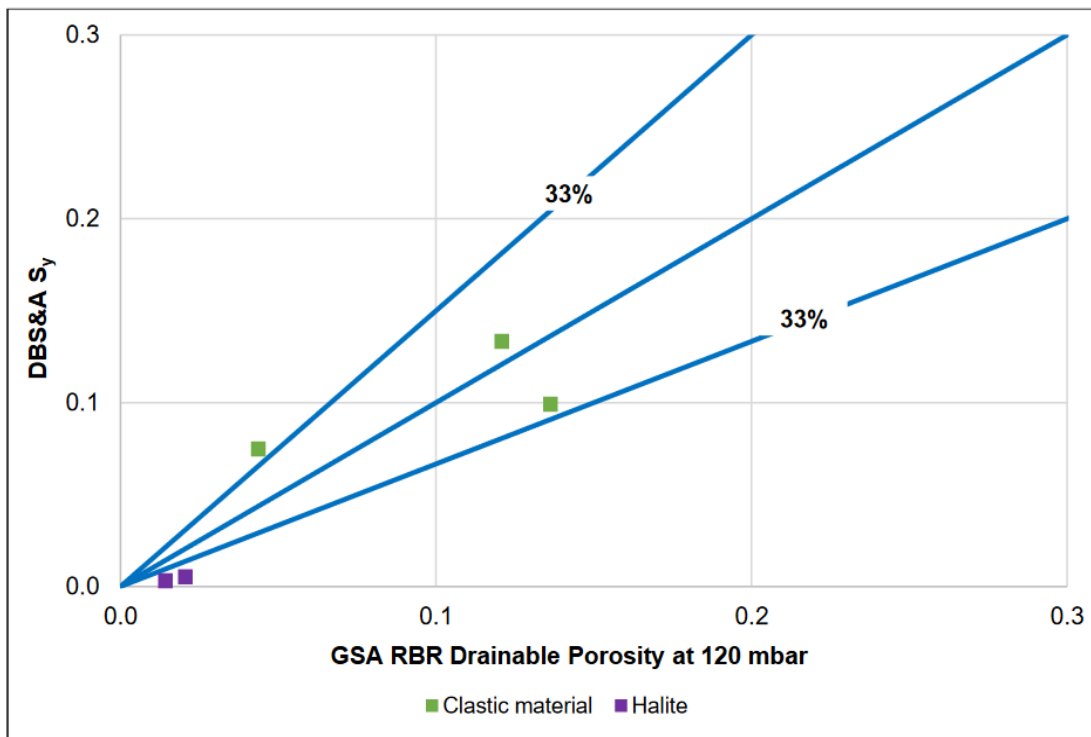


Figure 11.3 Sy and RBR comparison for check samples DBSA - GSA



11.3 Brine QA/QC

This section outlines the quality assurance and quality control (QA/QC) procedures implemented for laboratory chemistry analysis of brine samples obtained during drilling and pumping activities. The section is subdivided according to the exploration campaigns carried out by the various companies: Millennial, AMSA, and Centaur. Each QA/QC program involved randomly inserting duplicates, check samples, field blank, and standards, with the following percent of quality control samples for each party: 21% for Millennial, 21% for AMSA and 17% for Centaur. The purpose each QA/QC program was to confirm the accuracy and precision of the analysis, as well as to detect any potential contamination of the samples.

ASANOVA was the primary laboratory used by Millennial while SGS was used as the secondary lab for check samples. This arrangement was in place until August 21, 2017 when ASANOVA was replaced by SGS as the main laboratory. No registered secondary lab was used for check samples. AMSA used SGS as their primary laboratory throughout the 2021/2 campaign, while ASANOVA was used as the main lab for Centaur throughout the 2019/9 campaign. The insertion rates for blanks, check samples, duplicates, and standards for each QA/QC program are detailed in Table 11.5.

Table 11.5 Summary of QAQC insertion rates for each campaign

Sample Type	Total N°	Millennial	AMSA	Centaur
Originals	635	452	104	79
Duplicates & Checks	66	51	9	6
Blanks	43	32	6	5
Standards	56	39	12	5
Total	800	574	131	95

Accuracy which is the closeness of measurements to the “true” or accepted value was monitored by the random insertion of standards, and the implementation of check samples analyzed by a secondary, independent laboratory. Precision, the ability to consistently reproduce a measurement in similar conditions, was monitored by submitting blind field duplicates to the laboratory, monitoring any variability in the sampling and analytical program. Contamination which is the transference of material from one sample to another was measured by inserting blank samples into the sample stream. By implementing a QA/QC program that monitors these three factors, it is possible to ensure the reliability and accuracy of the laboratory results.

11.3.1 Millennial duplicate brine samples

To ensure the laboratory's precision, duplicate brine samples were submitted to the same facility. Millennial’s Phase II and Phase III exploration programs included a total of 51 duplicate samples, some of these also used as check samples. 16 duplicates and their original samples were submitted to ASANOVA, while 35 were submitted to

SGS. Table 11.6 & Table 11.7 list the main statistics regarding the duplicates versus their original samples for lithium and potassium for each laboratory.

Table 11.6 Statistical analysis of duplicate samples – ASANOVA

Statistic	Li (mg/L)	Duplicate Li (mg/L)	K (mg/L)	Duplicate K (mg/L)
Count	16	16	16	16
Min	247.1	273.8	2783.2	3300.5
Max	579.4	570.7	6092.0	6367.8
Mean	478.5	471.8	5147.9	5047.5
Std Dev	92.0	85.6	926.4	817.1
RPD	1.4		2.0	

Table 11.7 Statistical analysis of duplicate samples – SGS

Statistic	Li (mg/L)	Duplicate Li (mg/L)	K (mg/L)	Duplicate K (mg/L)
Count	35	35	35	35
Min	10.0	10.0	15.0	15.0
Max	701.0	758.0	6,660.0	7,170.0
Mean	415.6	416.2	4,340.5	4,362.1
Std Dev	155.4	162.1	1,574.4	1,653.4
RPD	0.2		0.5	

The assay results for duplicate samples at both ASANOVA and SGS laboratories demonstrate a high degree of precision and consistency for key parameters of lithium and potassium. The highest Relative Percent Difference (RPD) is only 2% for ASANOVA and 0.5% for SGS. This is significantly lower than the commonly accepted 10% cut-off and suggests that the laboratory’s analytical procedures are consistently producing results that are in close agreement with each other.

Max-min plots for each laboratory are displayed from Figure 11.4 to Figure 11.7. These show the maximum versus minimum values for each pair of samples, and the failure line is represented by a hyperbolic function ($Y^2 = m^2X^2 + b^2$), where m is the slope of the asymptote and b the intersection at the y axis. The failure line was calculated based on a 10% relative error allowance.

For each max-min plot, sample pairs (each duplicate and its original) are represented by red circles, while the failure curve is shown in red, and a 45° line is added in green for reference. Additionally, sample pairs that are plotted above the failure line and considered failures are marked in blue circles with an “x” shape in the middle.

The standard threshold for an acceptable number of failures is typically set at 10%. However, given the limited sample size and the observation that there are 2 failures for both lithium and potassium that are marginally

beyond the 10% relative error cut-off, a failure rate of 25% is deemed acceptable in this specific instance. If the failures found on the limit of the failure line were deemed to be acceptable, the percentage of failure would change to 6.25% and 12.5% respectively.

Figure 11.6 and Figure 11.7 show the max-min plots for SGS, and duplicate samples are considered acceptable for both lithium and potassium, as the percentage of failures for each element falls below the 10% cut-off. It is noteworthy that three registered failures for lithium are only marginally beyond the 10% threshold, indicating high precision within the SGS laboratory.

Figure 11.4 Max-min plot for lithium in duplicates - ASANOA

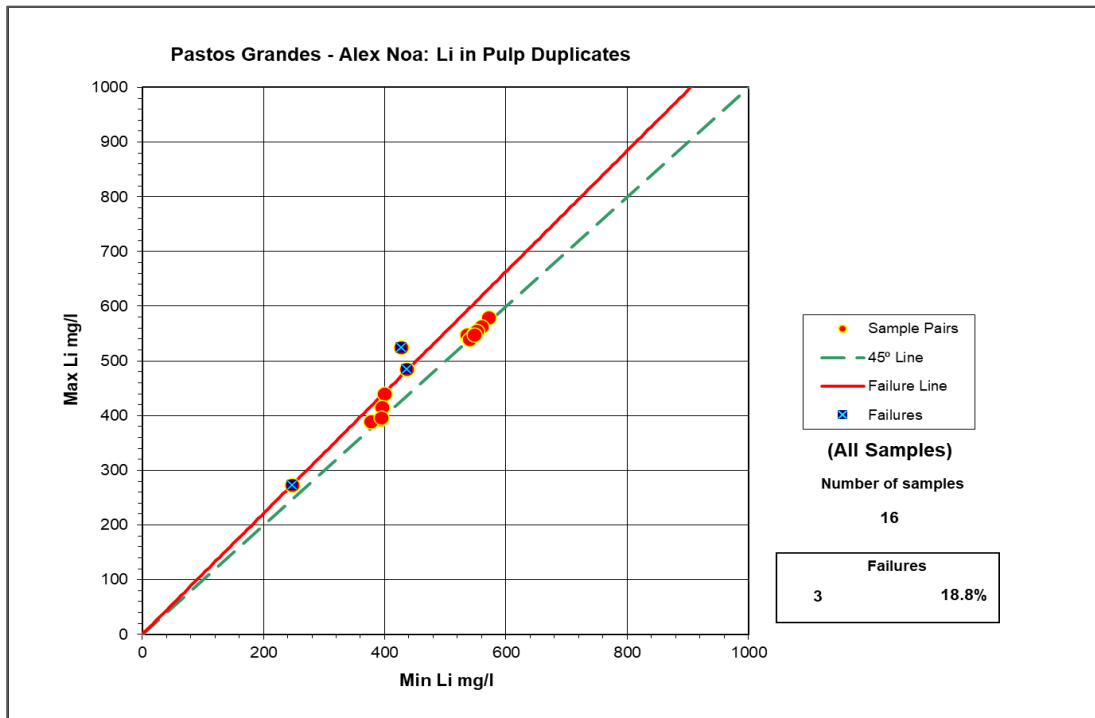


Figure 11.5 Max-min plot for potassium in duplicates - ASANOVA

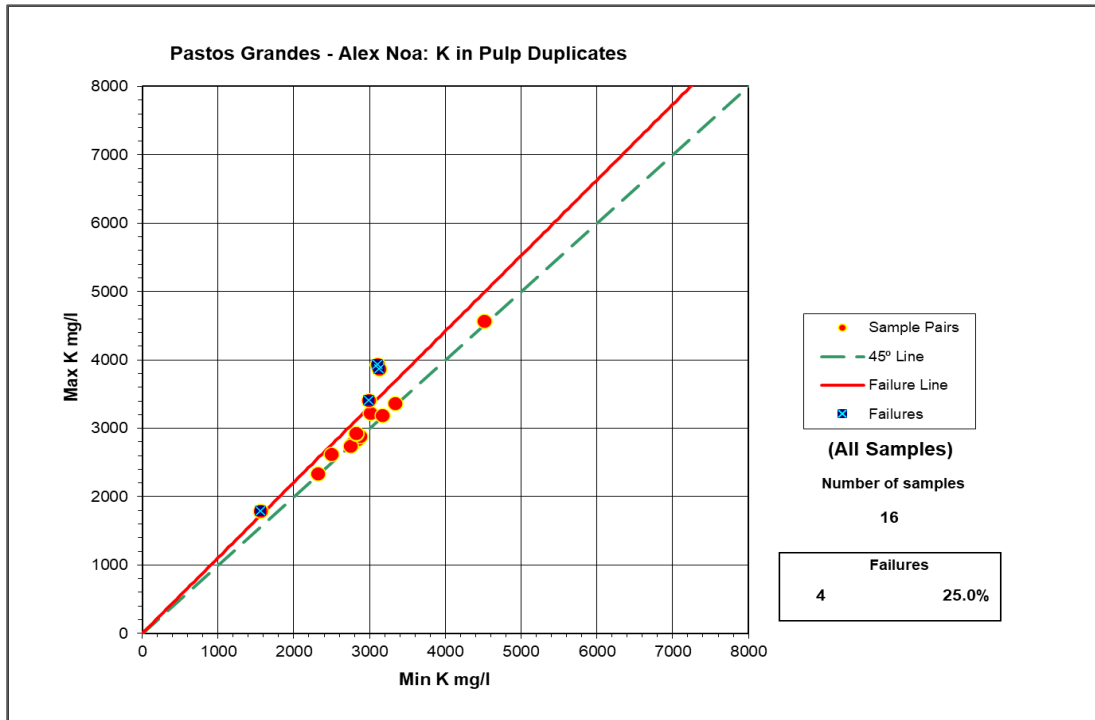


Figure 11.6 Max-min plot for lithium in duplicates - SGS

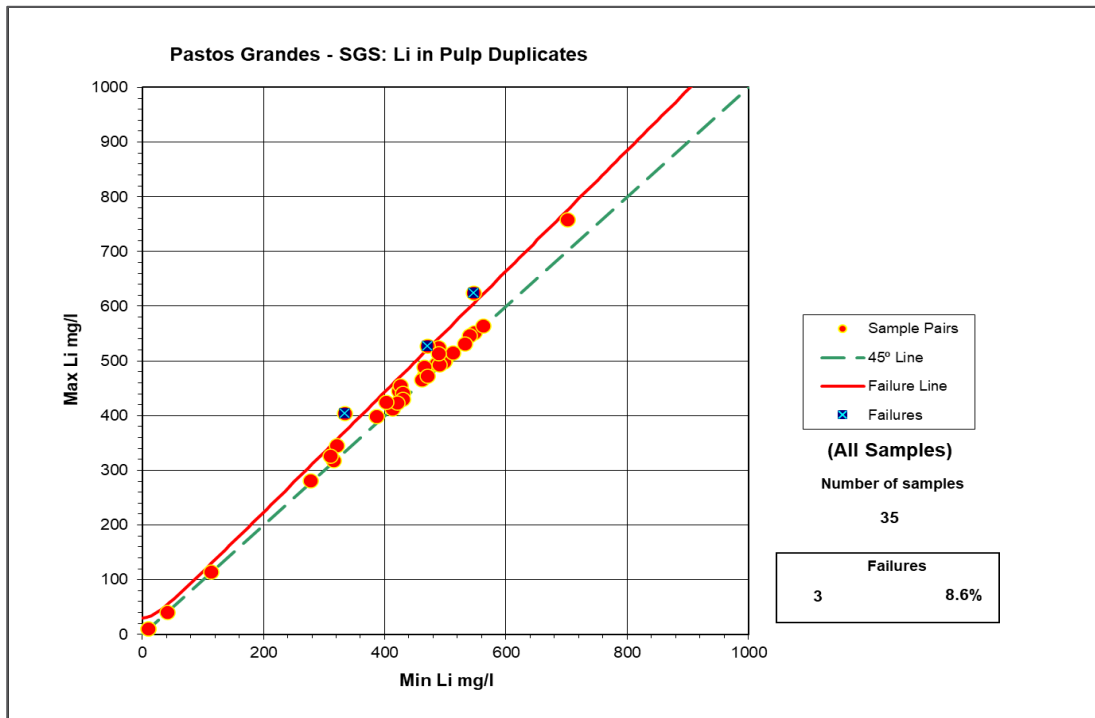
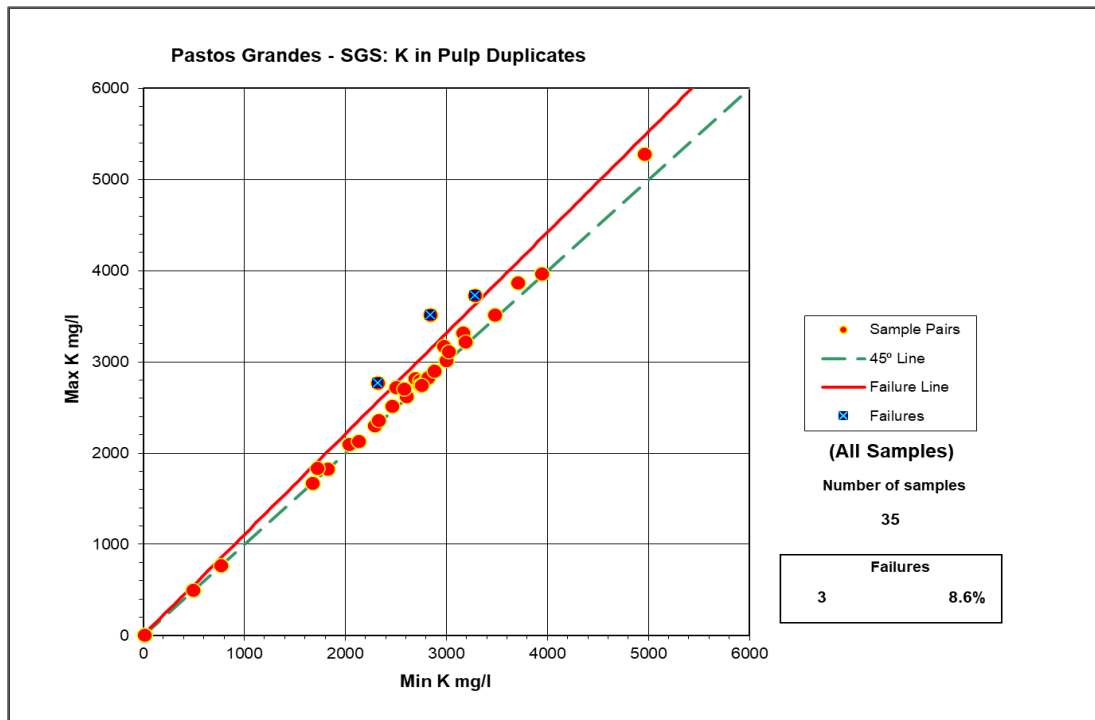


Figure 11.7 Max-min plot for potassium in duplicates - SGS



11.3.1.1 Millennial check samples

To test the laboratory's accuracy, samples were randomly selected and analyzed at a secondary and independent laboratory - SGS. It's important to note that this only occurred before August 21, 2017, when SGS replaced ASANOA as the main laboratory. Since that date, no secondary laboratory has been registered for check samples. Millennial's Phase II and III exploration programs included 29 check samples to both primary and secondary labs. The main statistics regarding the check samples for lithium and potassium are listed in Table 11.8.

Table 11.8 Statistical analysis of check samples – ASANOA & SGS

Statistic	ASANOA-Li (mg/L)	SGS-Li (mg/L)	ASANOA-K (mg/L)	SGS-K (mg/L)
Count	29.0	29.0	29.0	29.0
Min	0.5	10.0	2.5	10.0
Max	554.4	714.0	5424.3	7740.0
Mean	468.8	543.9	4779.2	5916.2
Std Dev	104.1	123.8	970.3	1248.8
RPD	14.8		21.3	

The assay results for check samples between ASANOA and SGS fall within a 20% relative difference for lithium, but slightly over 20% for potassium. A RPD over 20% indicate that there may be an issue with the accuracy of

one or both laboratories testing methods, but this cannot be determined solely by the RPD value, and further investigation is needed to identify the cause of the discrepancy. The RPD value for lithium of 14.8% is within the accepted 20% cut-off, but still suggests there is some difference between the results obtained by the two labs.

Figure 11.8 and Figure 11.9 present the max-min plots for the check samples of lithium and potassium respectively. Like the duplicate section discussed above, these plots display the maximum versus minimum values for each pair of samples. The failure line is represented by a hyperbolic function ($Y^2 = m^2X^2 + b^2$), where m is the slope of the asymptote and b the intersection at the y axis. The failure line was calculated based on a 20% relative error allowance.

Figure 11.8 Max-min plot for lithium in check samples: ASANOVA - SGS

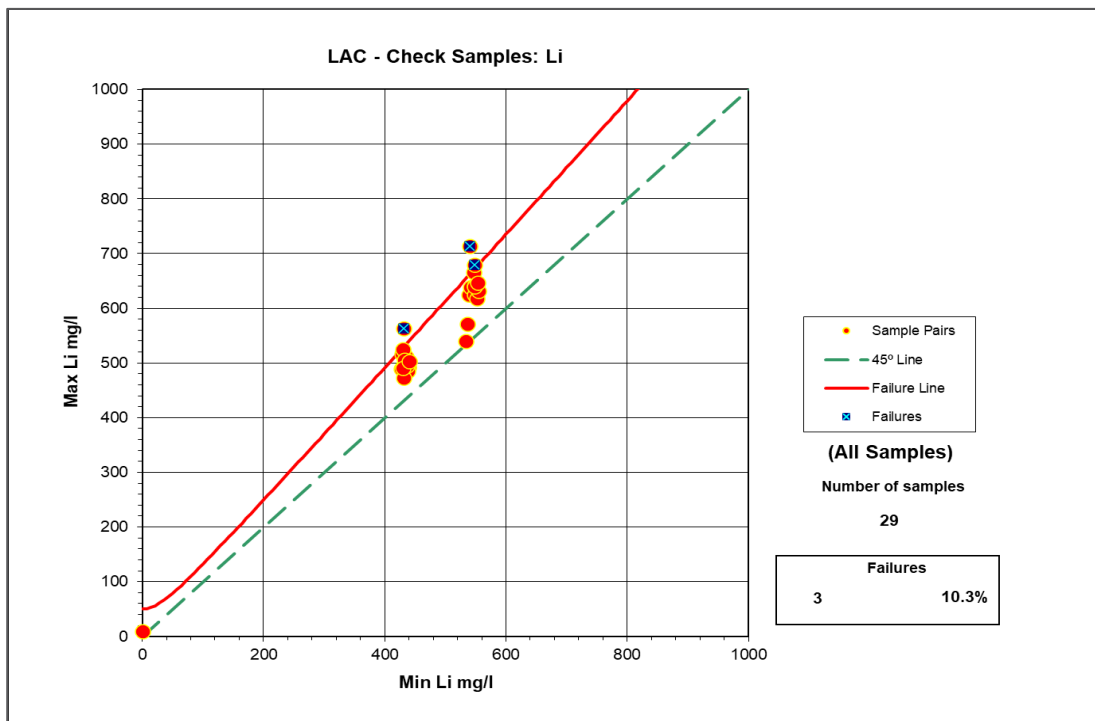
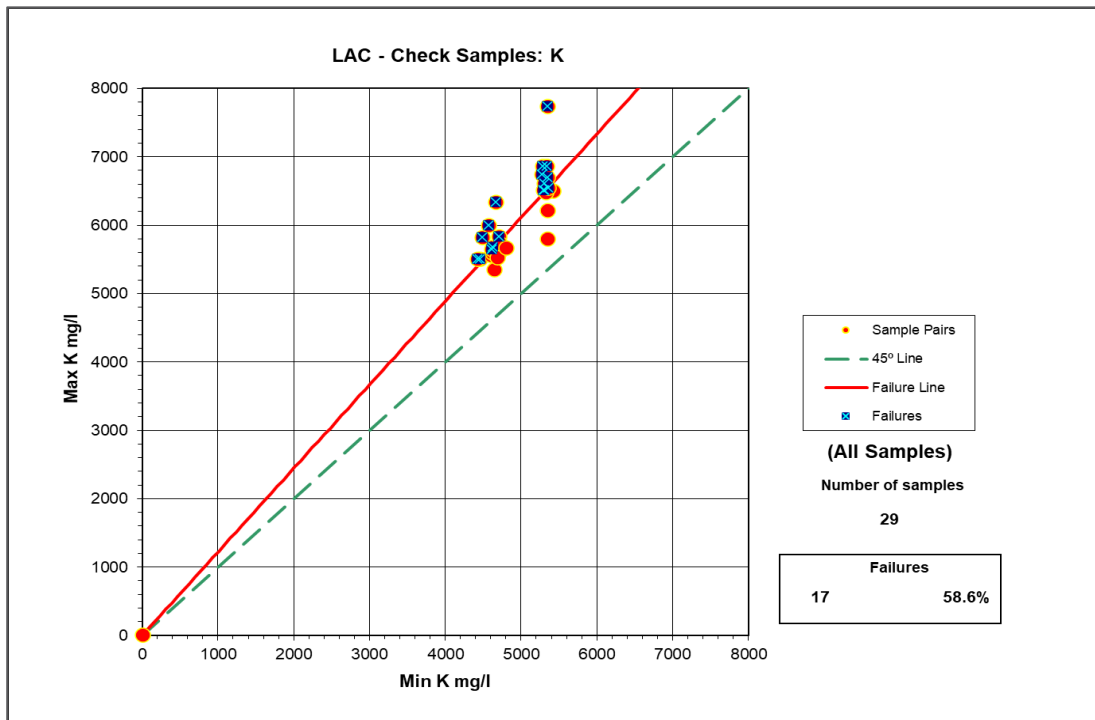


Figure 11.9 Max-min plot for potassium in check samples: ASANOVA - SGS



For each max-min plot, sample pairs (corresponding duplicates sent to each lab) are represented by red circles, while the failure curve is shown in red, and a 45° line is added in green for reference. Additionally, sample pairs that are plotted above the failure line and considered failures are marked in blue circles with an “x” shape in the middle.

The check samples for both lithium and potassium show a failure rate that exceeds the accepted 10% cut-off. However, one of the three failures for lithium falls only marginally beyond the failure line, which, if considered acceptable, would result in a failure rate of 6.9%. In contrast, the failure rate for potassium is 58.6%, with several samples falling beyond the failure line, indicating an unacceptable level of variation.

11.3.1.2 Millennial field blanks

To measure potential contamination 32 blank samples consisting of distilled water were inserted into the sample stream and sent to the laboratories for analysis. ASANOVA received 10 blanks, while SGS received 22. Neither laboratory detected any lithium in the samples, although traces of potassium were detected by ASANOVA. It is important to note that the detected potassium concentrations were below the standard safe limit, which is generally considered to be three times the detection limit.

This data can be visualized with Blank vs Previous graphs where the Y-axis represents the concentrations detected in blanks for each element and the X-axis represents the measured concentration of the same element for the sample assayed just before the blank. Additionally, the graphs feature a regression line for lithium concentrations shown in blue and a red line, representing the safe limit. Figure 11.10 to

Figure 11.13 display these graphs for both lithium and potassium for each lab.

Figure 11.10 Blank vs previous samples for lithium - ASANOA

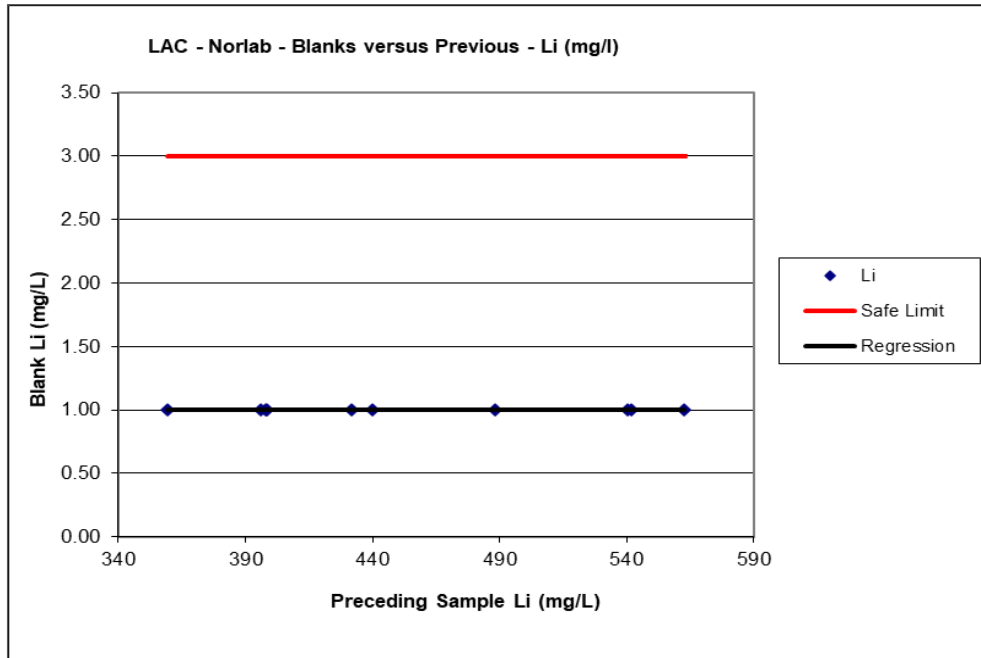


Figure 11.11 Blank vs previous samples for potassium - ASANOA

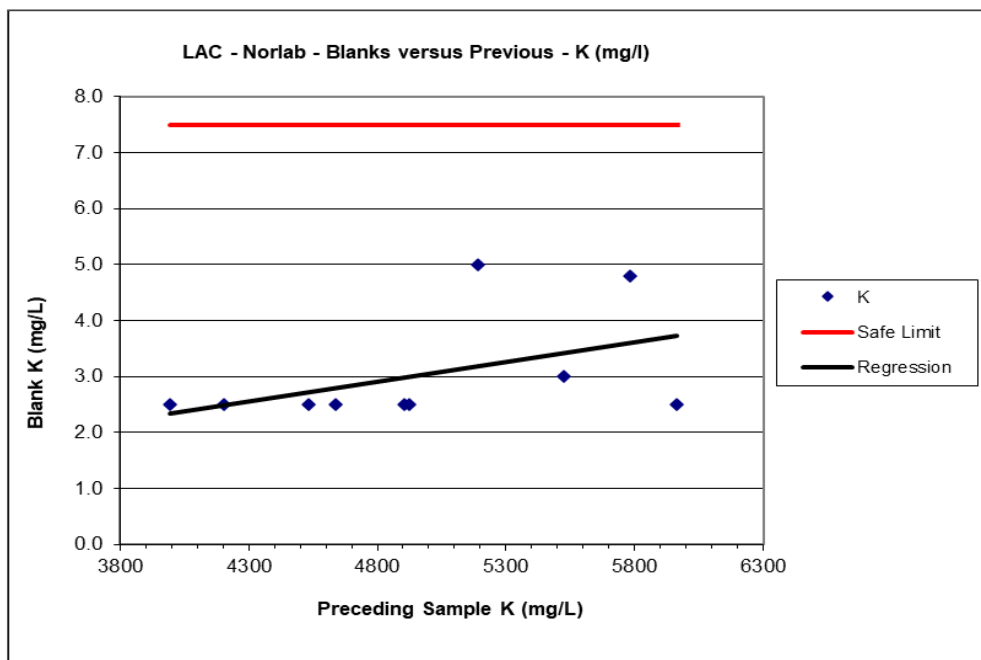


Figure 11.12 Blank vs previous samples for lithium - SGS

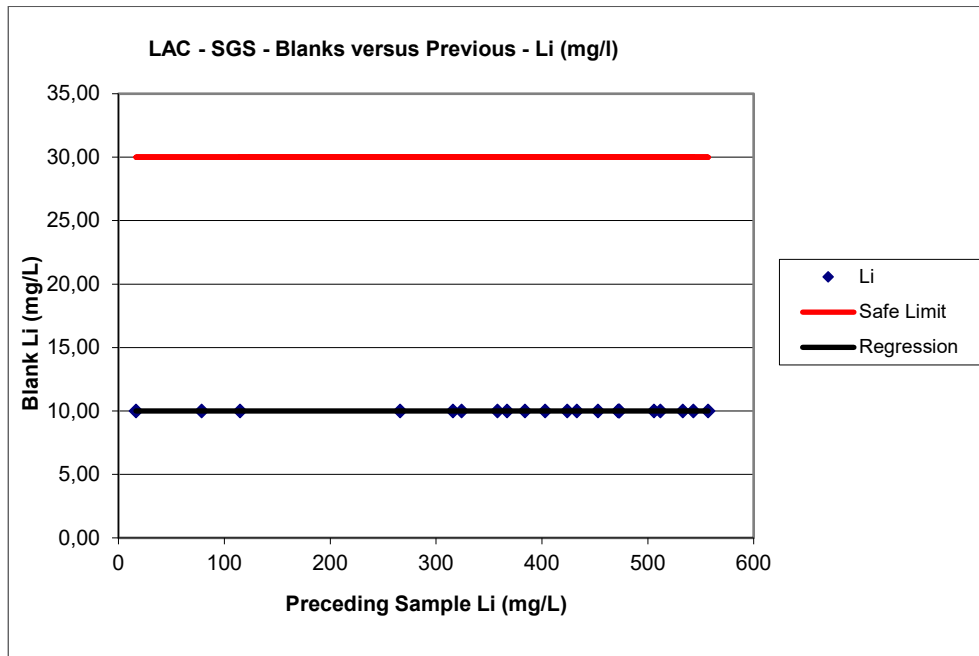
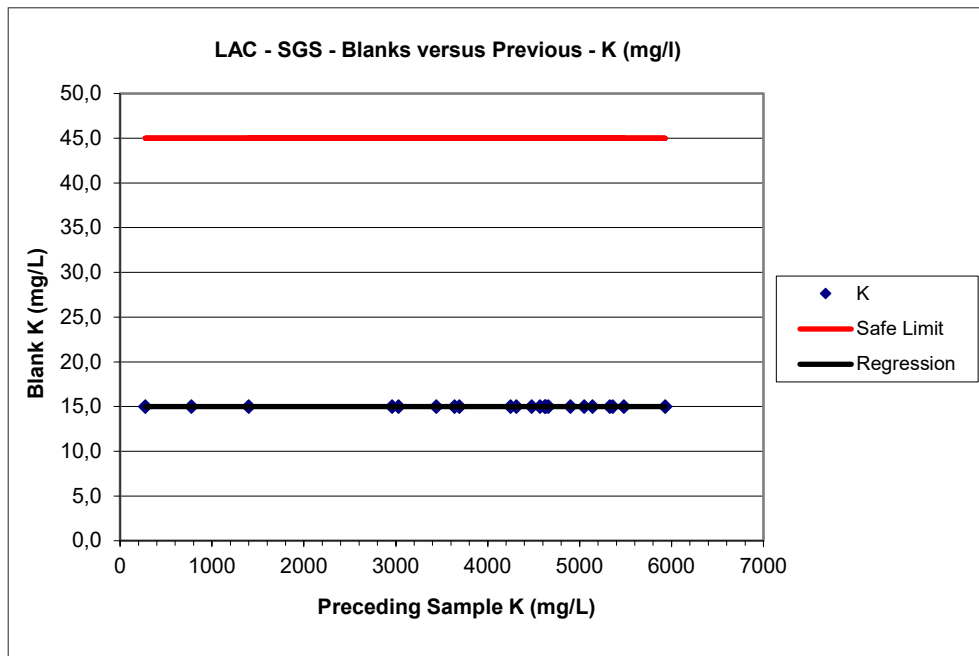


Figure 11.13 Blank vs previous samples for potassium - SGS



11.3.1.3 Standard samples

The Millennial sampling program utilized two types of standards. The first standard, 'RR', consisted of a large sample of brine collected from the Salar de Pastos Grandes during testing at well PGPW16-01 with the concentrations being obtained from a round robin style quality control check. 5 RR standards were sent to ASANOVA for analysis while 26 samples were sent to SGS. The concentrations (best values) of the standard obtained through the round robin are shown in Table 11.9.

Table 11.9 Element concentrations (best values) for Standard RR – Millennial

Sample	Li (mg/L)	Ca (mg/L)	Mg (mg/L)	B (mg/L)	Na (mg/L)	K (mg/L)	Density (g/mL)	EC (mS/cm)	TDS (mg/L)
PGS17153	450.2	618.8	3,033.9	774.9	107,255.0	4,890.0	1.2	189.0	334,800.0

The second type of standard, 'INBEMI', consisted of a synthetic solution prepared by the National University of Salta. INBEMI standards were only sent to SGS for analysis, amounting to a total of 6 samples. The concentration values for this standard are reported in Table 11.10.

Table 11.10 Element concentrations for Standard INBEMI - Millennial

Sample	Li (mg/L)	Ca (mg/L)	Mg (mg/L)	B (mg/L)	Na (mg/L)	K (mg/L)	SO4 (mg/L)	Density (g/mL)
PGS17153	295.0	440.0	189.0	532.0	75,518.0	3,188.0	189.0	1.2

Figure 11.14 to Figure 11.19 present a graphical analysis of the assay results for the samples using both the 'RR' and 'INBEMI' standards for both ASANOVA and SGS laboratories. All graphs account for a 95% confidence interval of the mean and display the element concentration on the Y-axis and the date of sampling on the X-axis. The reference value (best value) of the element for each standard is shown with a purple line along with a $\pm 5\%$ acceptable variation represented by a brown and grey line respectively. The actual data is displayed with black outlined squares while the data's moving average is represented in green. The average plus or minus 2 standard deviations are displayed in yellow lines. In general, a total relative bias higher than $\pm 10\%$ is considered unacceptable.

Figure 11.14 Graphical analysis of lithium within 'RR' Standards assayed by ASANO.A.

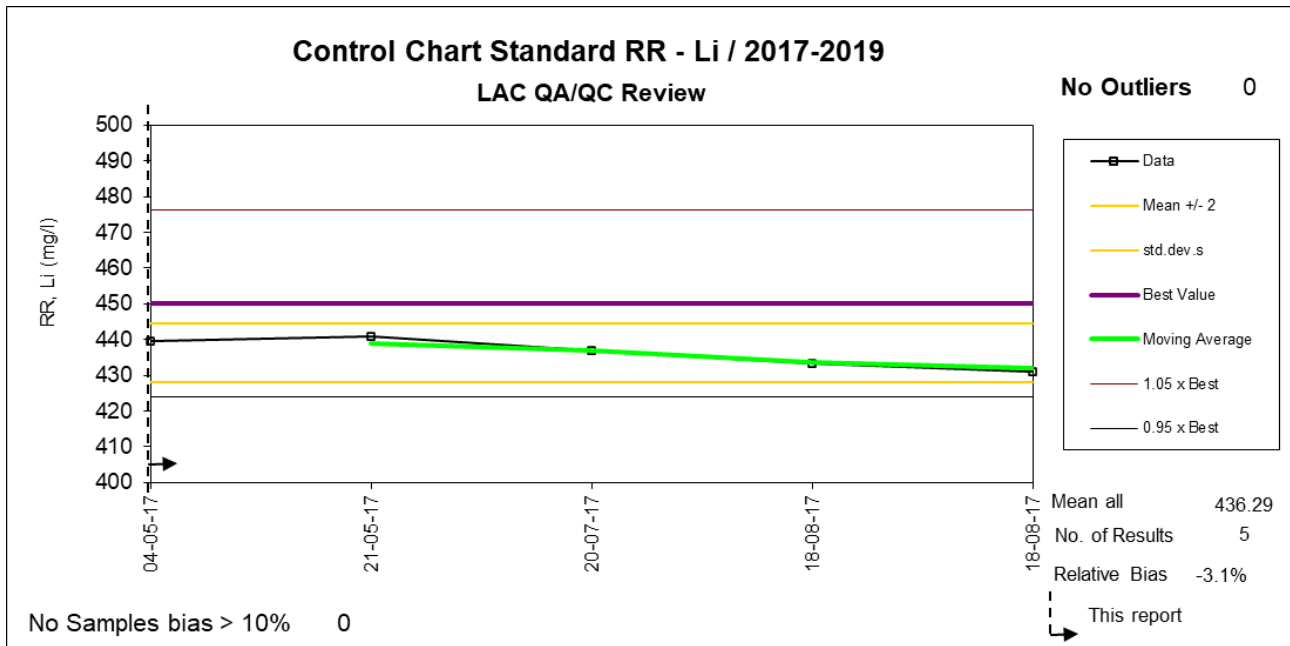
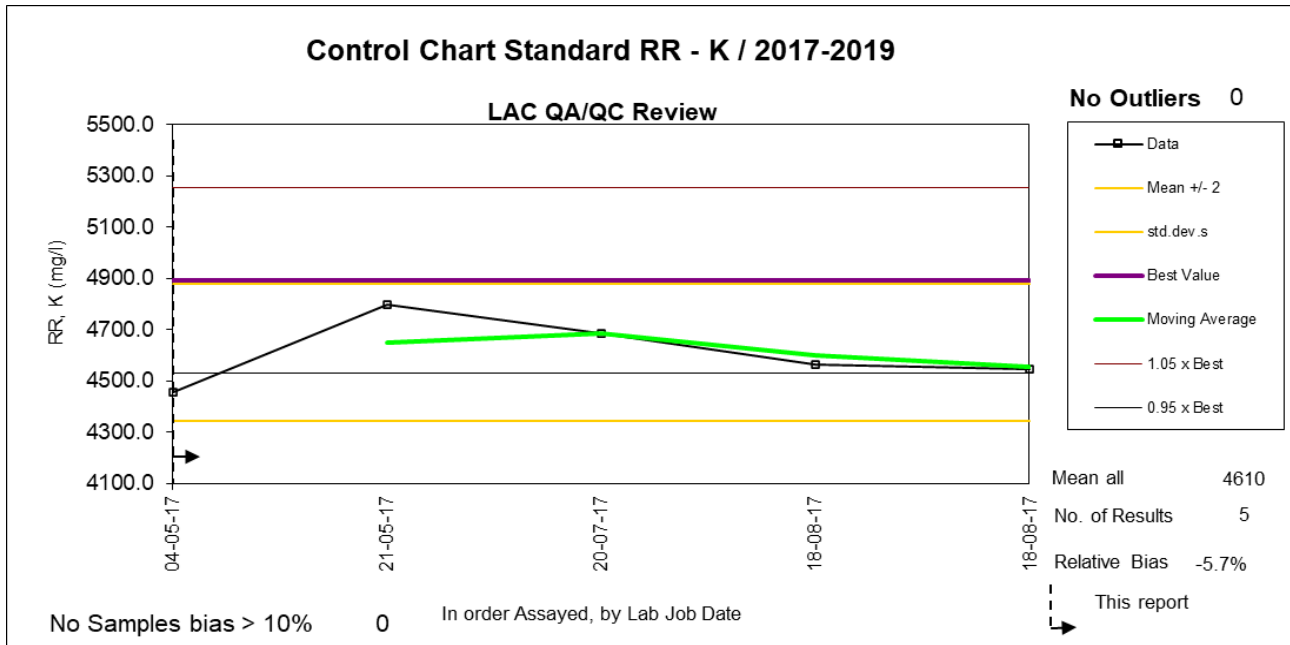


Figure 11.15 Graphical analysis of potassium within 'RR' Standards assayed by ASANO.A.



The RR standards analyzed by ASANOVA show that none of the lithium nor potassium values fall outside the ± 2 standard deviations from the mean. Additionally, all lithium values fall within the $\pm 5\%$ range of the reference values while only one potassium value falls outside this range. There were not enough INBEMI standard samples analyzed by ASANOVA to conduct a graphical analysis as the moving average does not have enough data.

Notably, a bias check for the assay results revealed a negative bias ranging from -3.1% for Li to -5.7% for potassium indicating that the measured values are consistently lower than the expected or reference values. However, this detected bias is well below the accepted 10% and is not considered to be significant.

The RR standards analyzed by SGS show that 6 out of 26 samples had a bias over the accepted limit of 10% bias lithium with no outliers and a total relative bias of -1.9% which is considered acceptable. Similarly, the potassium samples present 4 out of 26 values over 10% bias with one outlier, and a total relative bias of -3.1%, also deemed acceptable.

Regarding the INBEMI standards analyzed by SGS, 2 out of 6 lithium samples showed a bias over 10% with no outliers and a total relative bias of 0%. For potassium samples show 1 out of a total of 6 had a bias over 10%, with no outliers and a total relative bias of 0%.

In summary, while some individual samples showed a bias beyond the generally accepted 10% limit, the overall bias for both lithium and potassium within the standard samples analyzed by both laboratories is considered acceptable with the highest being -5.7% for lithium within the RR standards assayed by ASANOVA.

Figure 11.16 Graphical analysis of lithium within 'RR' Standards assayed by SGS.

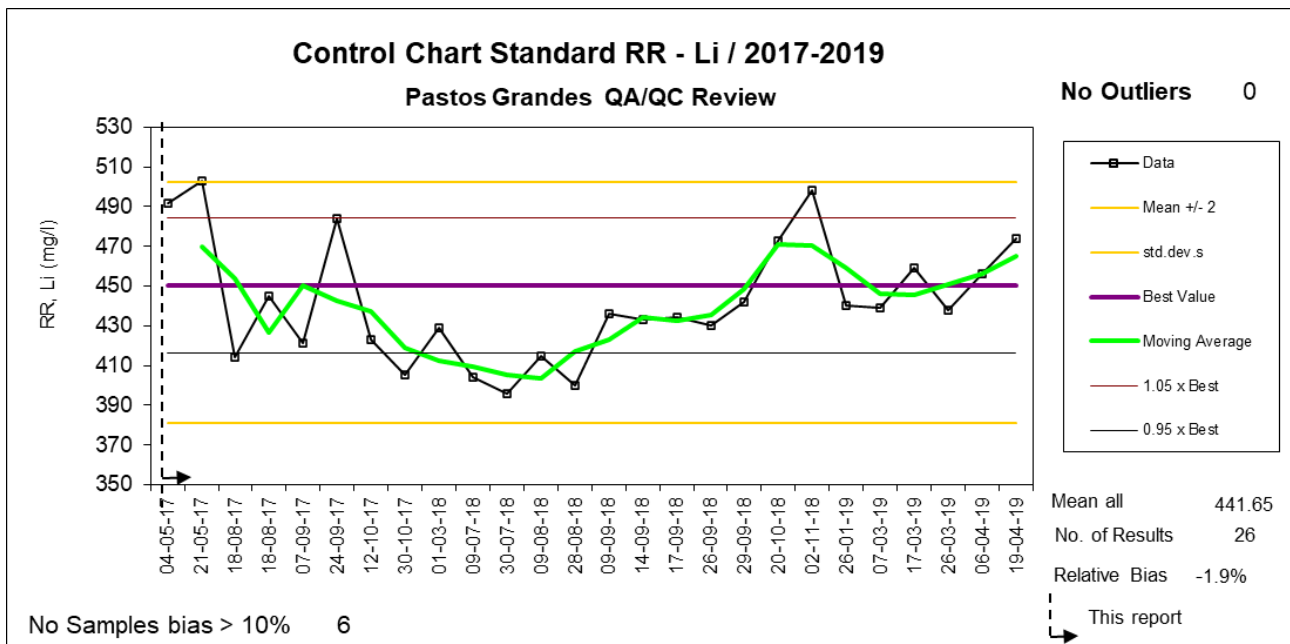


Figure 11.17 Graphical analysis of potassium within 'RR' Standards assayed by SGS.

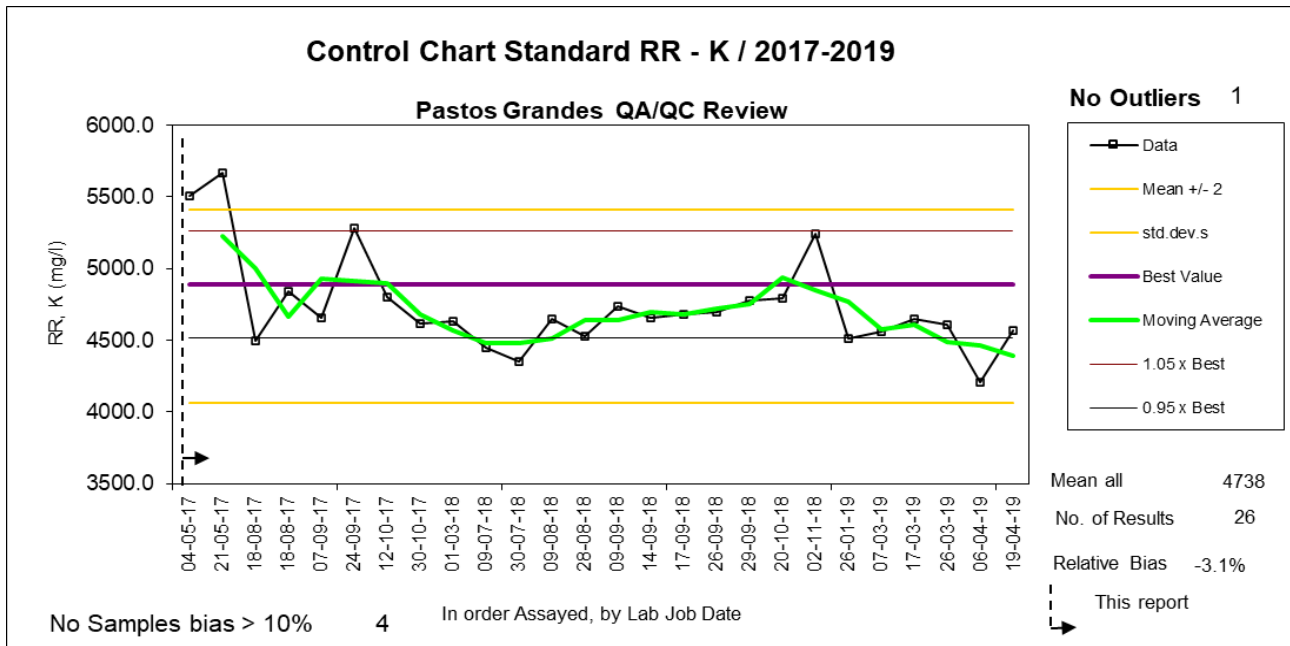


Figure 11.18 Graphical analysis of lithium within 'IBEMI' Standards assayed by SGS.

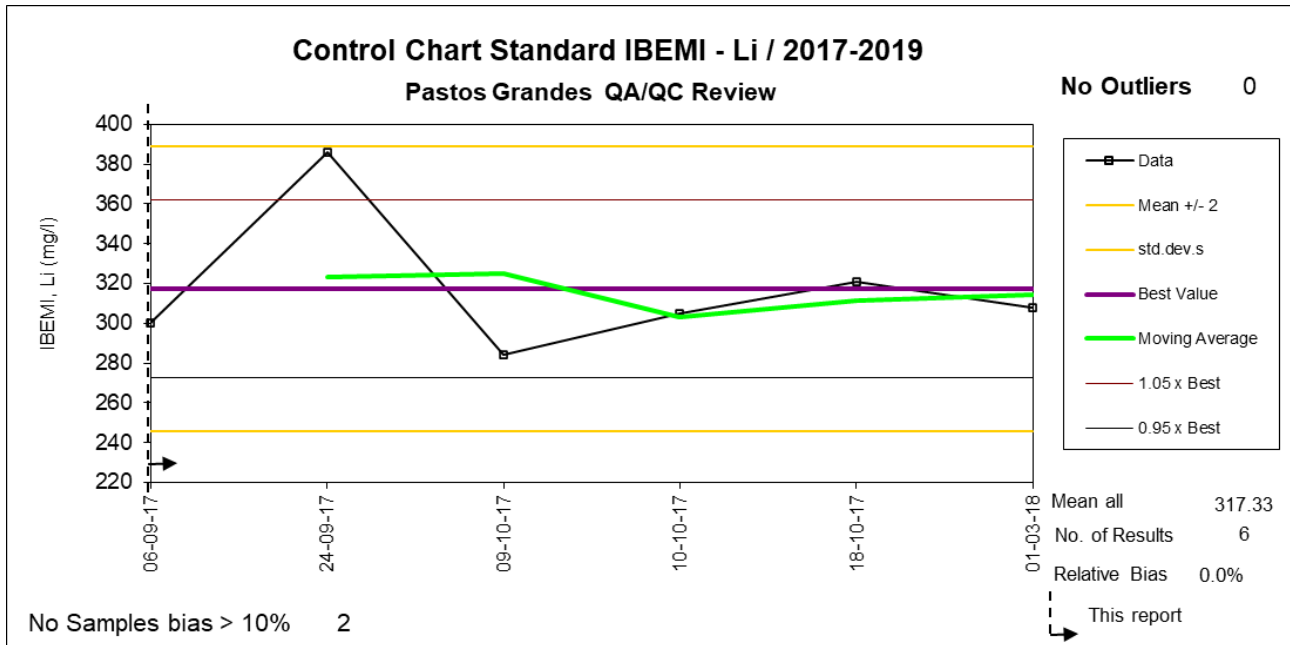
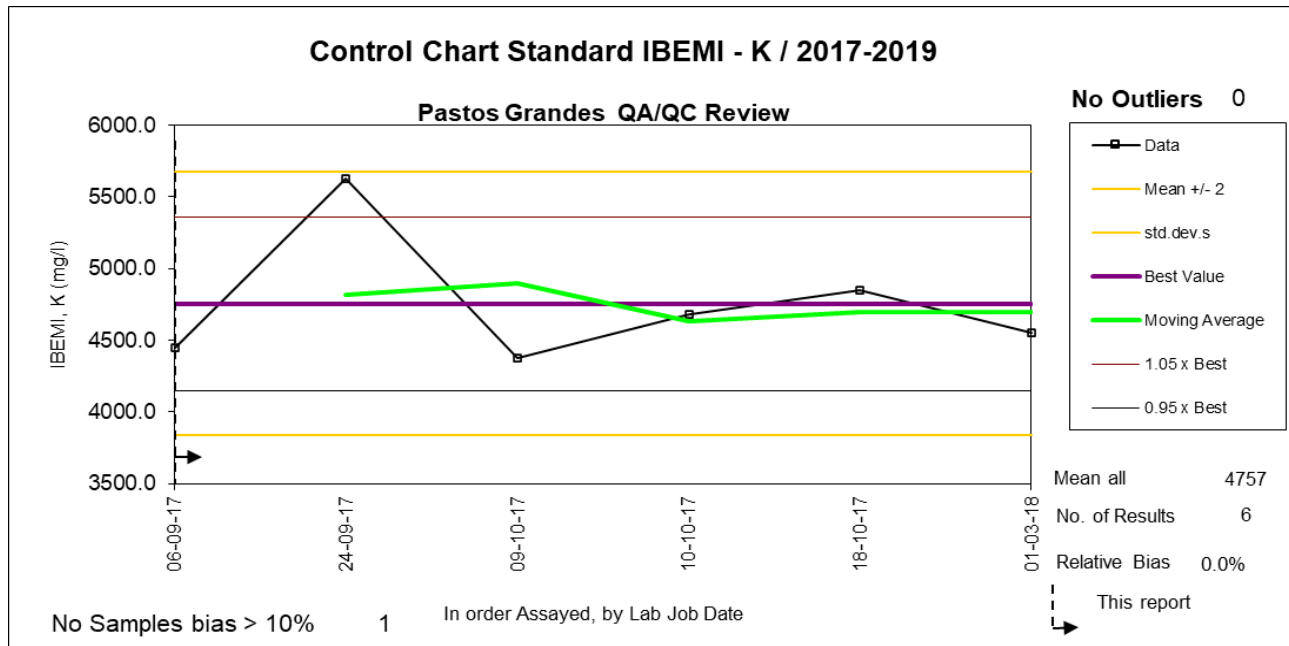


Figure 11.19 Graphical analysis of potassium within 'INBEMI' Standards assayed by SGS.



11.3.2 AMSA duplicate brine samples

SGS was used as the main assay laboratory by AMSA and to ensure that the precision of the lab was acceptable, a total of 9 duplicate brine samples were submitted. There were no check samples used during the AMSA drilling campaign due to C-19 related issues. Table 11.11 lists the main statistics regarding the duplicates for lithium and potassium.

Table 11.11 Statistical analysis of duplicate samples – SGS

Statistic	Li (mg/L)	Duplicate Li (mg/L)	K (mg/L)	Duplicate K (mg/L)
Count	9.0	9.0	9.0	9.0
Min	33.6	31.9	197.0	177.9
Max	658.8	657.8	6022.9	6075.6
Mean	419.1	413.8	3726.1	3686.1
Std Dev	185.0	183.3	1788.9	1757.4
RPD	1.3		1.1	

The assay results for duplicate samples at SGS demonstrate a high degree of precision and consistency for key parameters of lithium and potassium. The Relative Percent Difference (RPD) is low, with values of only 1.3% for lithium and 1.1% for potassium. These are significantly lower than the commonly accepted 10% cut-off and suggests that the laboratory's analytical procedures are consistently producing results that are in close agreement with each other.

Figure 11.20 and Figure 11.21 display max-min plots for each laboratory, showing the maximum versus minimum values for each pair of samples and the failure line is represented by a hyperbolic function ($Y^2 = m^2X^2 + b^2$), where m is the slope of the asymptote and b the intersection at the y axis. The failure line was calculated based on a 10% relative error allowance.

For each max-min plot, sample pairs (each duplicate and its original) are represented by red circles while the failure curve is shown in red and a 45° line is added in green for reference. Additionally, sample pairs that are plotted above the failure line and considered failures are marked in blue circles with an “x” shape in the middle.

There were no failures for neither lithium nor potassium within duplicates analyzed by SGS. The generally accepted threshold for failure rates is 10%, so duplicates are not only considered acceptable, but the lack of failures suggests high precision within the SGS laboratory for the current project.

Figure 11.20 Max-min plot for lithium in duplicates - SGS

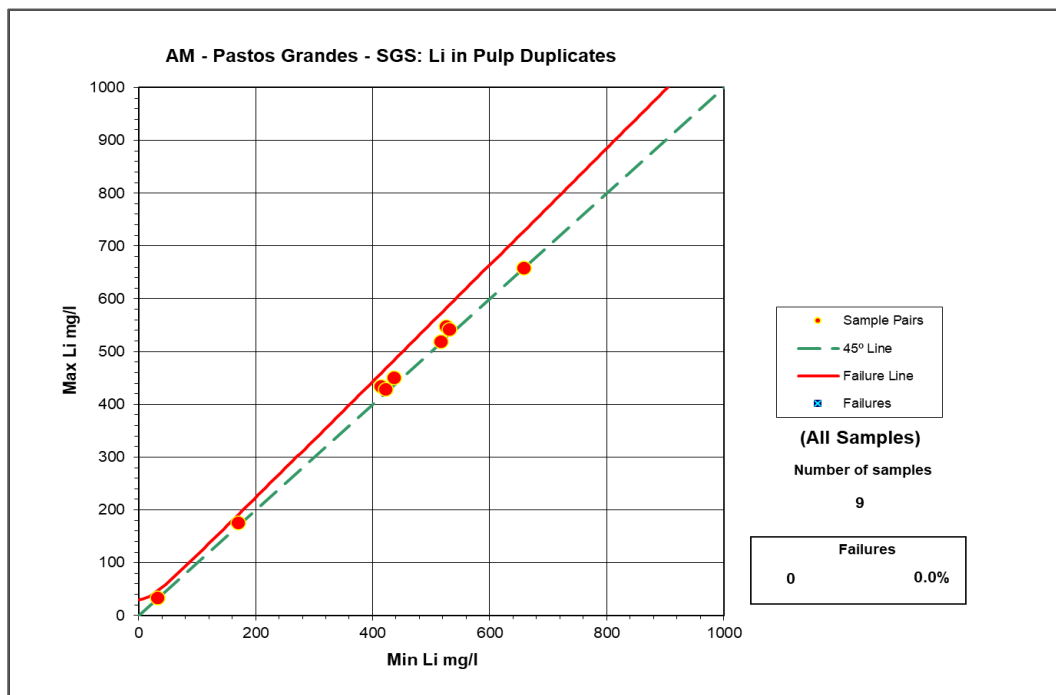
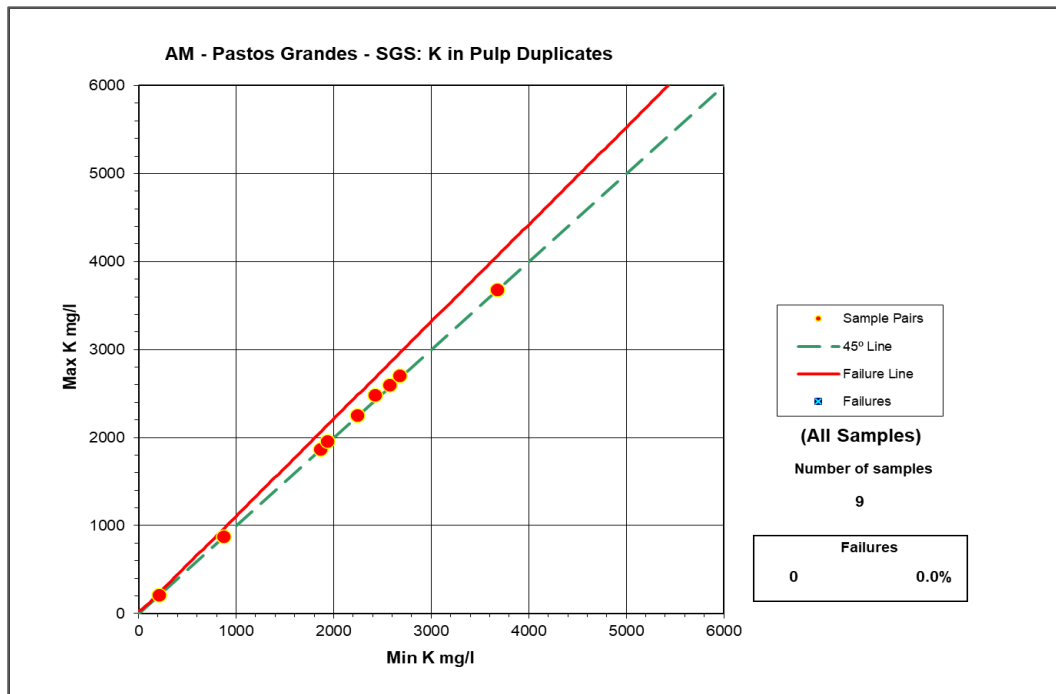


Figure 11.21 Max-min plot for potassium in duplicates - SGS



11.3.2.1 AMSA field blanks

To measure potential contamination within the sampling process a total of 6 blank samples consisting of distilled water were inserted into the sample stream and sent to the SGS laboratory for analysis. Neither lithium nor potassium were detected in any samples, therefore all concentrations were below the standard safe limit, which is generally considered to be three times the detection limit.

This data can be visualized with Blank vs Previous graphs, where the Y-axis represents the concentrations detected in blanks for each element, and the X-axis represents the measured concentration of the same element for the sample assayed just before the blank. Additionally, the graphs feature a regression line for lithium concentrations shown in blue and a red line representing the safe limit. Figure 11.22 and Figure 11.23 display these graphs for both lithium and potassium for each lab.

Figure 11.22 Blank vs previous samples for lithium - SGS

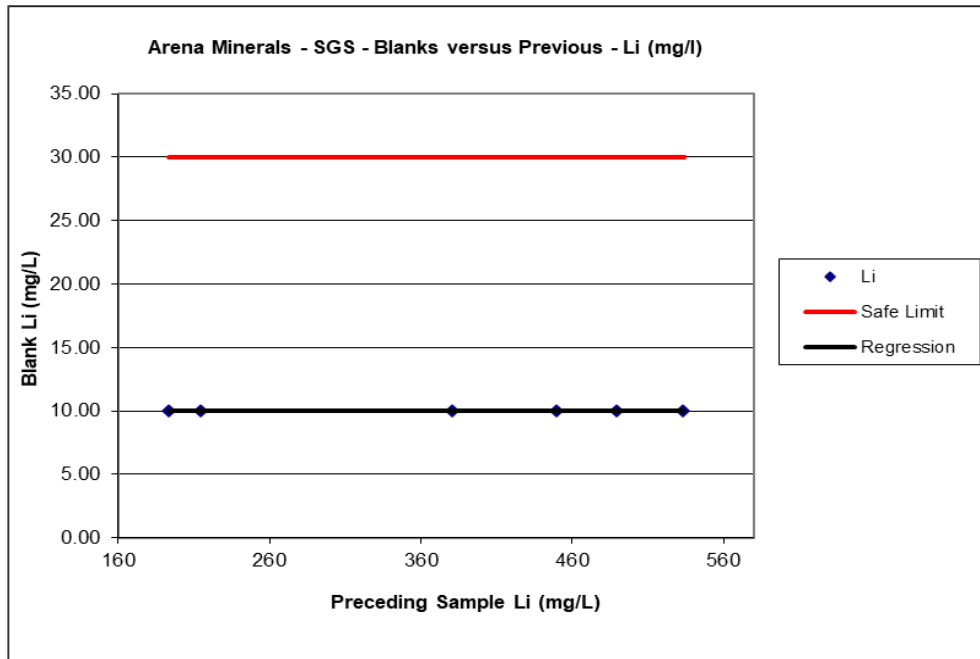
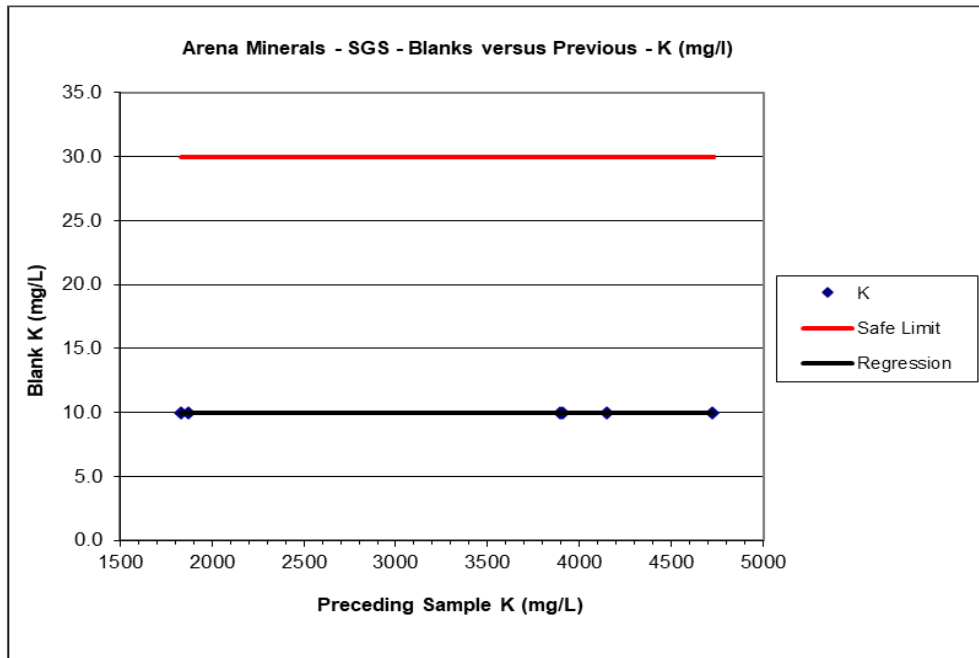


Figure 11.23 Blank vs previous samples for potassium - SGS



11.3.2.2 AMSA standard samples

The AMSA sampling program utilized two different standards, both obtained from brine within Salar de Pastos Grandes and named STD-1 and STD-2. Six samples were sent to SGS for analysis for each standard, amounting to a total of 12 standard samples. Their respective concentrations (best values) were obtained from a round robin style quality control check and are shown in Table 11.12.

Table 11.12 Element concentrations (best values) for Standards 1 & 2 - AMSA

Sample	Li (mg/L)	Mg (mg/L)	Na (mg/L)	K (mg/L)
STD-1	645.7	2,395.5	55,435.8	6,709.8
STD-2	352.6	1,292.0	29,825	3,682.5

Figure 11.24 to Figure 11.24 Figure 11.27 present a graphical analysis of the assay results for lithium and potassium within the samples using both the STD-1 and STD-2 standards. All graphs account for a 95% confidence interval of the mean and display the element concentration on the Y-axis and the date of sampling on the X-axis. The reference value (best value) of the element for each standard is shown with a purple line, along with a $\pm 5\%$ variation, represented by a brown and grey line respectively. The actual data is displayed with black outlined squares while the data's moving average is represented in green. Finally, the average ± 2 standard deviations are displayed in yellow lines. In general, a total relative bias higher than $\pm 10\%$ is considered unacceptable.

The STD-1 standard has no outliers nor values with a bias higher than 10% for neither lithium nor potassium, which suggests high accuracy and precision. Two lithium values fall outside the $\pm 5\%$ variation from the reference value which still can be considered acceptable. The total relative bias for lithium is 6.7% and 2.6% for potassium, indicating that the measured values are consistently higher than the reference values, but are both within the acceptable 10% threshold. Finally, no values of lithium nor potassium fall outside the ± 2 standard deviations from the mean.

The STD-2 standard has no outliers but has one value with a bias higher than 10% for both lithium and potassium. Additionally, the same lithium and potassium value falls outside the $\pm 5\%$ variation from the reference value, although can still be considered acceptable. The total relative bias for lithium is 7.3% and 3.6% for potassium indicating that the measured values are consistently higher than the reference values but are both within the acceptable 10% threshold. Finally, no values of lithium nor potassium fall outside the ± 2 standard deviations from the mean.

In summary, while some individual samples showed a bias beyond the generally accepted 10% limit, the overall bias for both lithium and potassium within the standard samples analyzed by both laboratories is considered acceptable, with the highest being 7.3% for lithium within the STD-2 standard.

Figure 11.24 Graphical analysis of lithium within 'STD-1' Standards assayed by SGS.

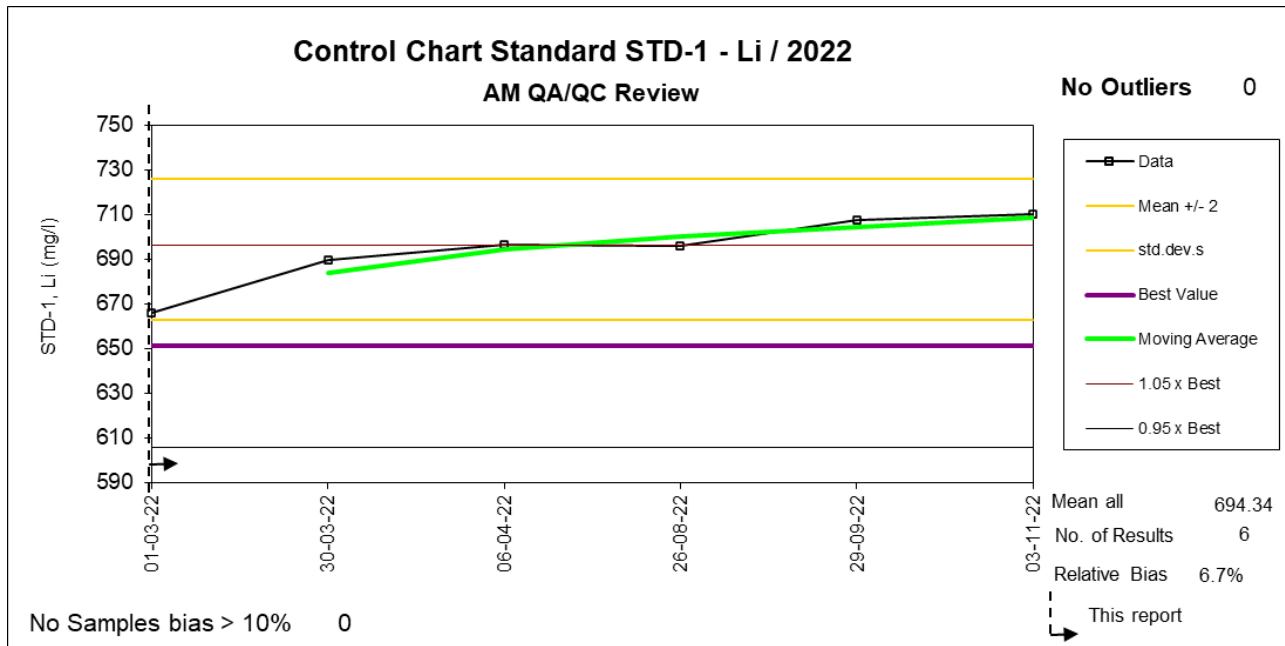


Figure 11.25 Graphical analysis of potassium within 'STD-1' Standards assayed by SGS.

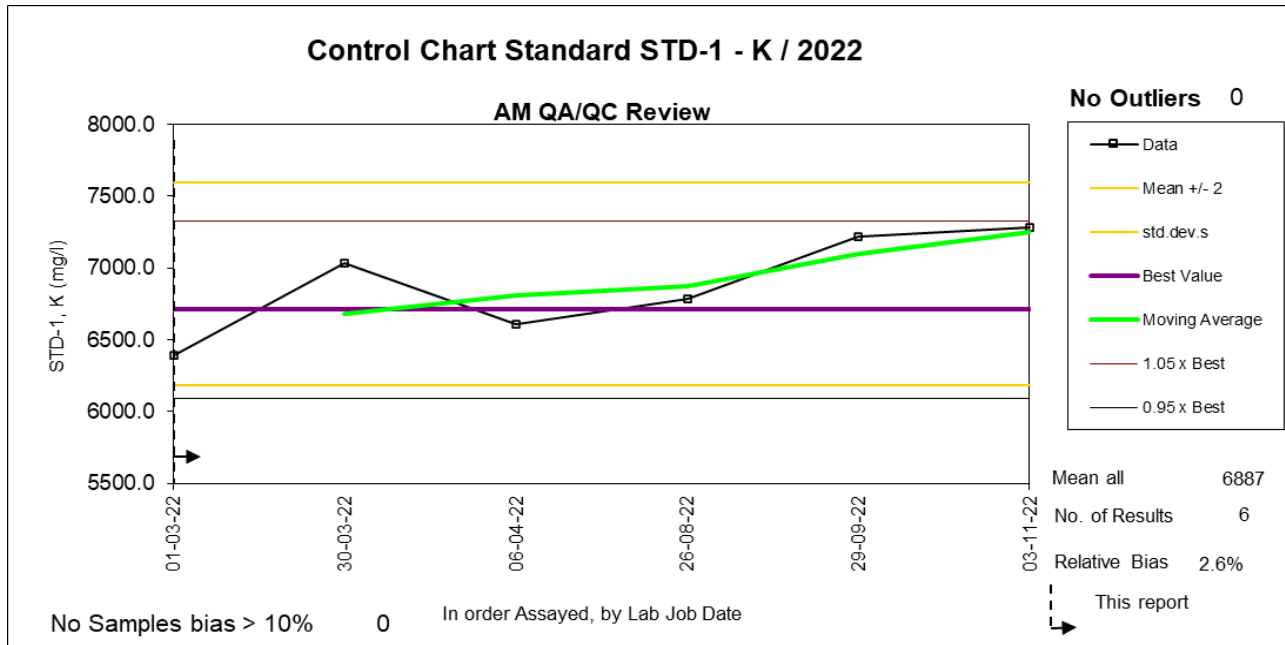


Figure 11.26 Graphical analysis of lithium within 'STD-2' Standards assayed by SGS.

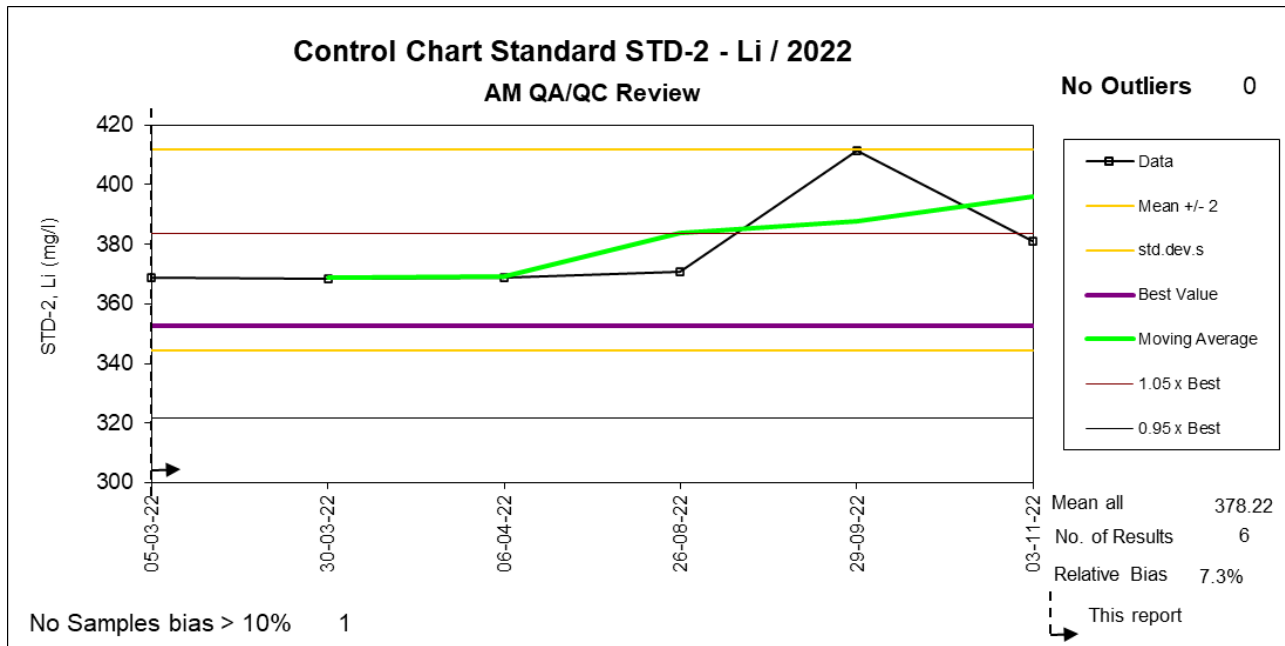
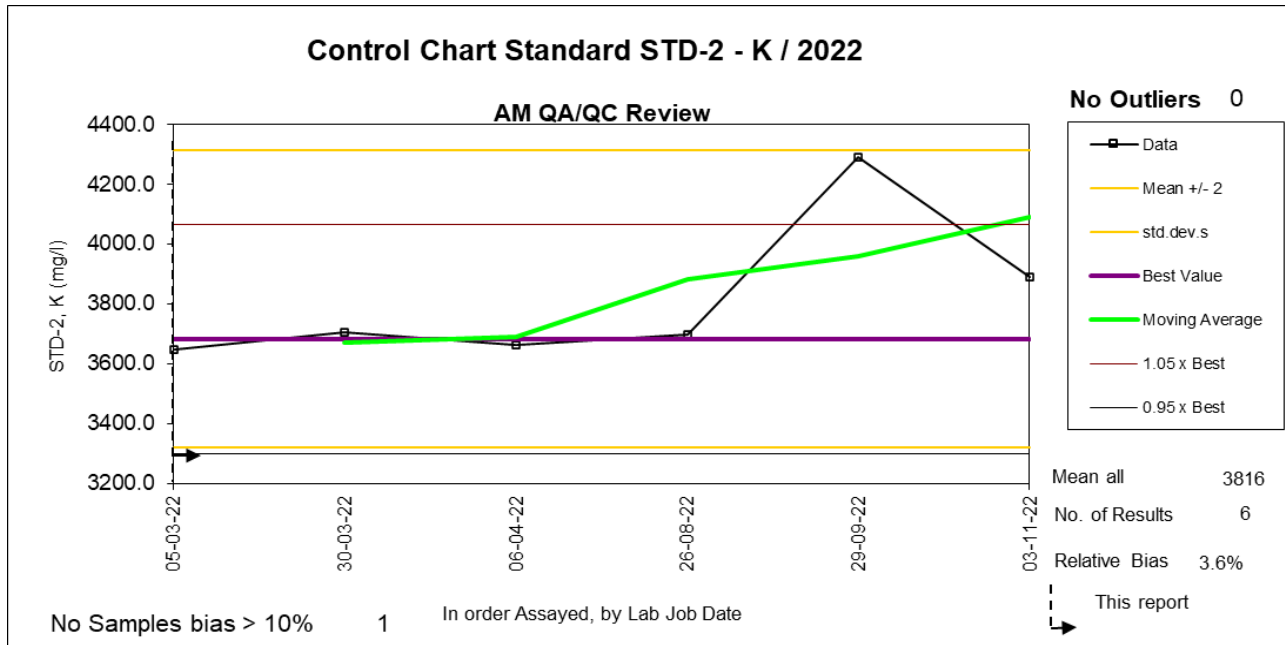


Figure 11.27 Graphical analysis of potassium within 'STD-2' Standards assayed by SGS.



11.3.3 Centaur duplicate brine samples

ASANOVA was used as the main laboratory by Centaur and to ensure acceptable precision within the lab, a total of six duplicate brine samples were submitted to the same facility. Table 11.13 lists the main statistics regarding the duplicates for lithium and potassium.

Table 11.13 Statistical analysis of duplicate samples – ASANOVA

Statistic	Li (mg/L)	Duplicate Li (mg/L)	K (mg/L)	Duplicate K (mg/L)
Count	6.0	6.0	6.0	6.0
Min	409.6	411.5	2,894.1	2,886.7
Max	548.3	627.9	5,093.1	5,213.7
Mean	507.3	543.2	4257.6	4617.1
Std Dev	52.5	65.8	880.1	824.0
RPD	6.8		8.1	

The assay results for duplicate samples at ASANOVA demonstrate a high degree of precision and consistency for key parameters of lithium and potassium. The Relative Percent Difference (RPD) is below the commonly accepted 10% cut-off for lithium and potassium, with values of 6.8% and 8.1% respectively. This suggests that the laboratory’s analytical procedures are consistently producing results that are in close agreement with each other.

Figure 11.28 and Figure 11.29 display max-min plots for each laboratory showing the maximum versus minimum values for each pair of samples and the failure line is represented by a hyperbolic function ($Y^2 = m^2X^2 + b^2$), where m is the slope of the asymptote and b the intersection at the y axis. The failure line was calculated based on a 10% relative error allowance.

For each max-min plot, sample pairs (each duplicate and its original) are represented by red circles while the failure curve is shown in red, and a 45° line is added in green for reference. Additionally, sample pairs that are plotted above the failure line and considered failures are marked in blue circles with an “x” shape in the middle.

The max-min plots showed that out of the six duplicates tested, only one failure occurred for lithium while there were no failures for potassium. This translates to a 16.7% failure rate for lithium and 0% for potassium. The generally accepted failure rate threshold is 10% which means that duplicates are considered acceptable for potassium but unacceptable for lithium. However, it's important to note that the sample size taken under Centaur Resources is limited, with only six duplicates assayed. Therefore, in this case, a single failure surpasses the 10% threshold. Taking this into consideration a 16.7% failure rate is deemed to be acceptable.

Figure 11.28 Max-min plot for lithium in duplicates - ASANO

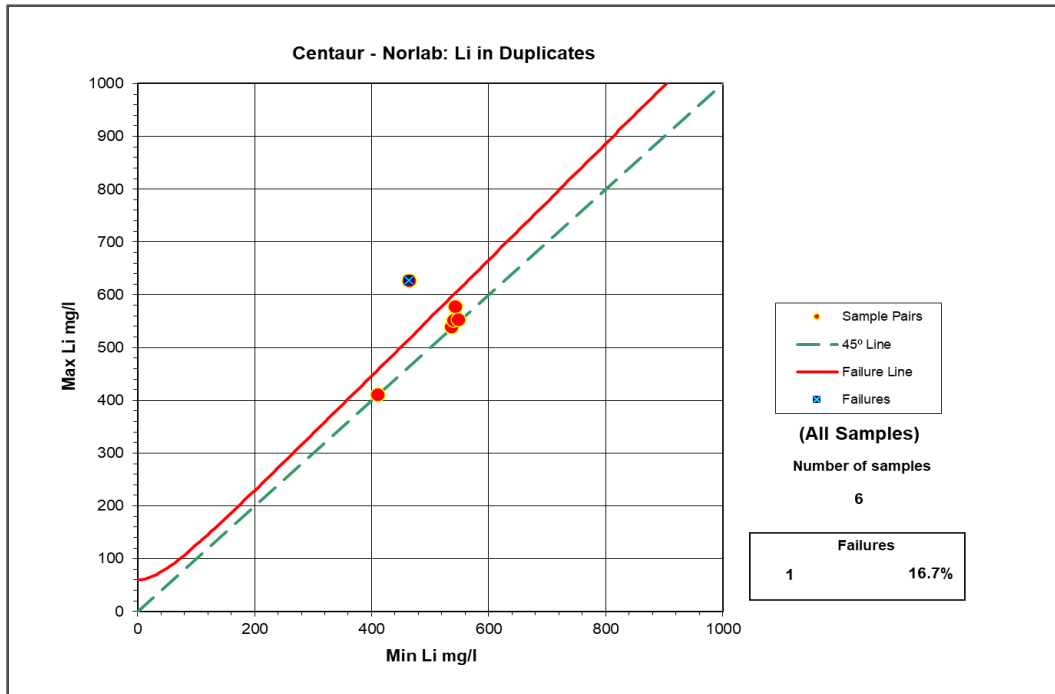
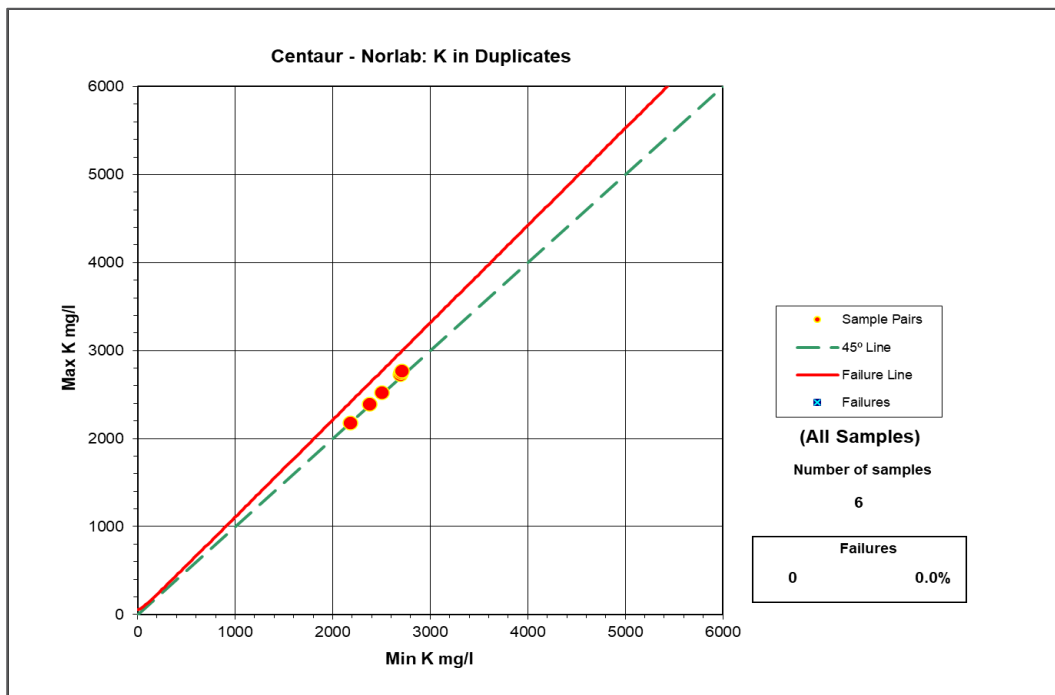


Figure 11.29 Max-min plot for potassium in duplicates - ASANO



11.3.3.1 Centaur field blanks

To measure potential contamination a total of five blank samples consisting of distilled water were inserted into the sample stream and sent to ASANOA for analysis. Neither lithium nor potassium were detected in any samples, which means that all concentrations were below the standard safe limit, generally considered to be three times the detection limit.

This data is presented in Blank vs Previous graphs, where the Y-axis represents the concentrations detected in blanks for each element, and the X-axis represents the measured concentration of the same element for the sample assayed just before the blank. Additionally, the graphs feature a regression line for lithium concentrations shown in blue and a red line representing the safe limit. These graphs are displayed for both lithium and potassium in Figure 11.30 and Figure 11.31.

Figure 11.30 Blank vs previous samples for lithium - ASANOA

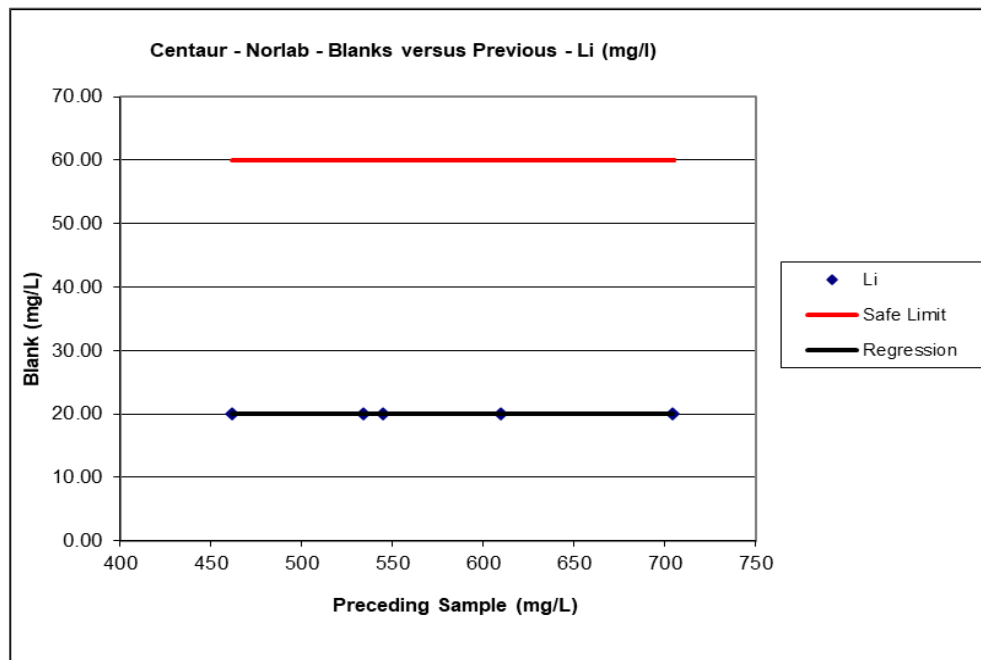
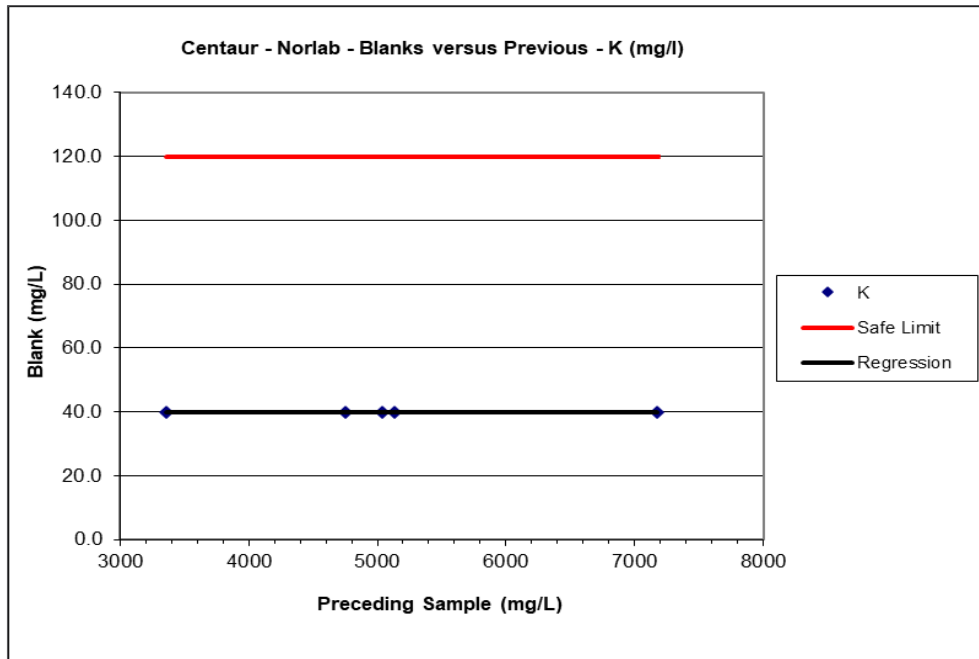


Figure 11.31 Blank vs previous samples for potassium - ASANOA



11.3.3.2 Centaur Standard samples

The Centaur sampling program utilized two different standards both obtained from brine within Salar de Pastos Grandes with their respective concentrations obtained from a round robin style quality control check. These standards were named STD-A and STD-B, and three samples of the former were sent to the lab for analysis while only 2 of the latter were assayed. The concentrations (best values) for each standard obtained through the round robin are shown in Table 11.14.

Table 11.14 Element concentrations (best values) for Standards A & B - Centaur

Sample	Li (mg/L)	Mg (mg/L)	Na (mg/L)	K (mg/L)
STD-A	707.0	4,641.9	111,699.2	7,041.9
STD-B	370.5	2,444.3	58,074.0	3,543.1

Figure 11.32 Graphical analysis of lithium within 'STD-A' Standards assayed by ASANOVA.

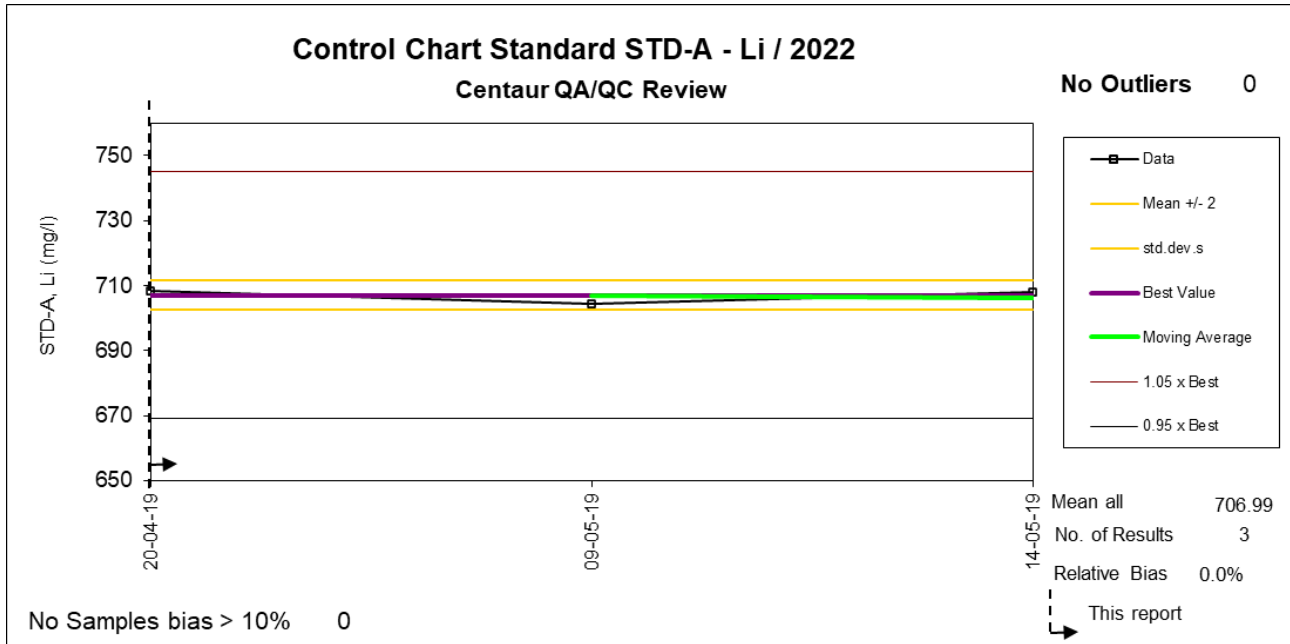
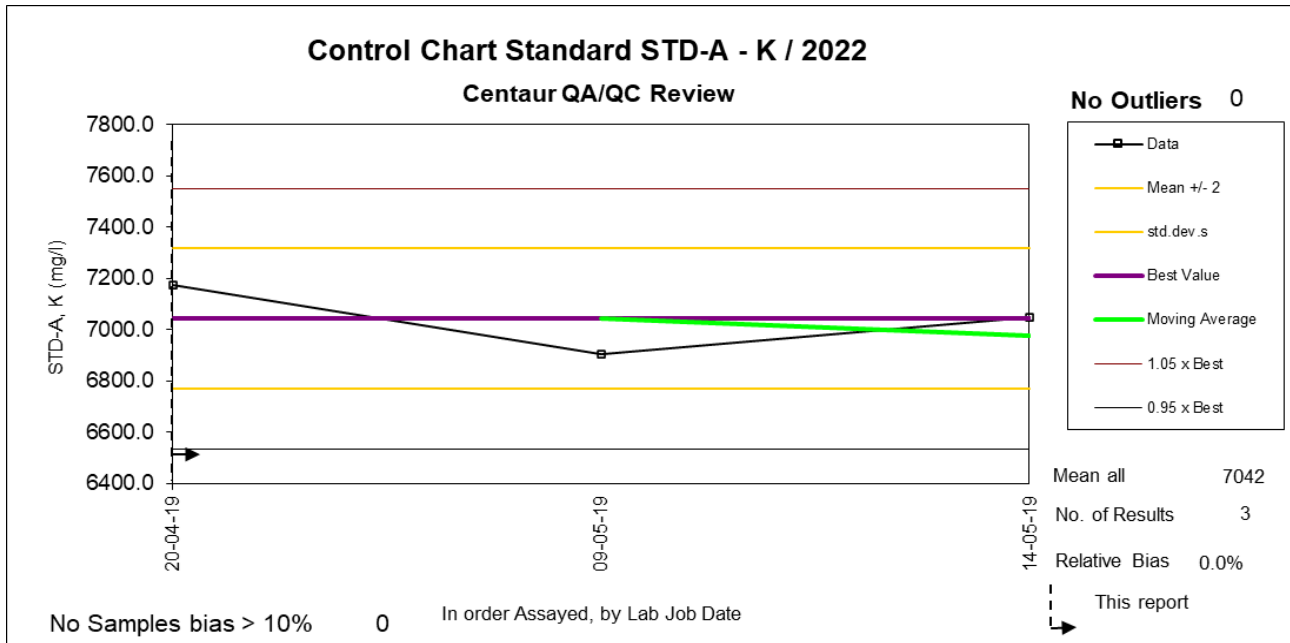


Figure 11.33 Graphical analysis of potassium within 'STD-A' Standards assayed by ASANOVA.



Graphical analysis of the assay results for lithium and potassium for the STD-A standards can be seen in Figure 11.32 and Figure 11.33 while graphical analysis for the STD-B standard was not possible due to a lack of samples. Both graphs account for a 95% confidence interval of the mean and display the element concentration on the Y-axis and the date of sampling on the X-axis. The reference value (best value) of the element for each standard is represented with a purple line, along with a $\pm 5\%$ variation, represented by a brown and grey line respectively. The actual data is displayed with black outlined squares while the data's moving average is represented in green. Finally, the average ± 2 standard deviations are displayed in yellow lines. In general, a total relative bias higher than $\pm 10\%$ is considered unacceptable.

The STD-A standard has no outliers nor values with a bias higher than 10% for neither lithium nor potassium, which suggests high accuracy and precision. Similarly, no lithium nor potassium values fall outside the $\pm 5\%$ variation from the reference value, which is also a good indicator of accuracy and precision. The total relative bias for lithium and potassium is 0% indicating that the measured values are in accordance with the reference values. No lithium nor potassium values fall outside the ± 2 standard deviations from the mean.

12 DATA VERIFICATION

The author was involved with the planning, execution, and oversight of the 2021-2022 AMSA drilling and testing program in Salar de Pastos Grandes. The author was responsible for developing drilling and sampling methodologies and the implementation of field sampling protocols. The author spent a significant amount of time in the field overlooking the implementation and execution of drilling, testing, and sampling protocols.

The author was responsible for the oversight and analysis of the QA/QC programs related to brine sampling and laboratory brine chemistry analysis as well as the laboratory porosity analysis. A significant amount of QA/QC protocols were implemented for the brine chemistry and drainable porosity analysis programs that allowed continuous verification of the accuracy and reliability of the results obtained. As described in Section 11 no issues were found with the results of the brine and porosity laboratory analysis.

It is the opinion of the author that the information developed and used for the brine resource estimate herein is adequate, accurate and reliable.

13 MINERAL PROCESSING AND METALLURGICAL TESTING

No mineral processing nor metallurgical testing studies have been prepared for this Resource Estimate update.

14 BRINE RESOURCE ESTIMATES

14.1 Overview

The essential elements of a brine resource determination for a salar are:

- Definition of the aquifer geometry,
- Determination of the drainable porosity or specific yield (Sy) of the hydrogeological units in the salar
- Determination of the concentration of the elements of interest.

Resources may be defined as the product of the first three parameters. The use of specific yield allows the direct comparison of brine resources from the widest range of environments.

Aquifer geometry is a function of the shape of the aquifer, the internal structure, and the boundary conditions (brine / freshwater interface). Aquifer geometry and boundary conditions can be established by drilling and geophysical methods. Hydrogeological analyses are required to establish catchment characteristics such as ground and surface water inflows, evaporation rates, water chemistry and other factors potentially affecting the brine reservoir volume and composition in-situ. Drilling is required to obtain samples to estimate the salar lithology, specific yield, and grade variations both laterally and vertically.

14.2 Resource model domain and aquifer geometry

The resource model domain is constrained by the following factors:

- Upper Boundary: The upper boundary of the model is determined by the highest elevation samples within the dataset, and/ or the phreatic brine level.
- Lateral Extent: The lateral extent of the resource model covers an area of 56 km² confined within the boundaries of the LAC mining claims in the Salar. Additionally, the extent can be restricted in some cases by the contact between the Quaternary basin and the underlying basement rock.
- Lower Boundary: The lower boundary of the model domain is set to coincide with the basement from the geological model or the total depth of 650 m when the basement is not present.

14.3 Specific Yield

The specific yield values were derived from 76 valid drainable porosity analyses of undisturbed samples. The samples were analyzed by GeoSystems Analysis. In comparison to lithium concentration data, which exhibits spatial correlation due to the geological processes that influence its distribution, drainable porosity data shows no such correlation. This is primarily because Sy values are highly dependent on the lithology of the project area, resulting in considerable stochastic variability. After conducting exploratory data analysis, it was concluded that assigning representative values to each geological unit would be more accurate than using interpolation methods like kriging.

The variability is shown in Figure 14.1 which displays the range of confidence intervals and the standard error for both units. This underscores the necessity for additional drilling and sample collection to reduce uncertainty and improve understanding of drainable porosity values within these geological units.

Table 14.1 Summary statistics of drainable porosity for geological units

Unit	2019 Data	2019 Average	2023 Data	2023 Average	Confidence -95%	Confidence +95%	Variance	Std. Error
Blanca Lila	1	0.5%	1	0.5%				
Alluvium	17	14.2%	27	13.9%	11.0%	16.7%	0.5%	1.4%
Saline Lacustrine	2	5.6%	20	4.1%	2.9%	5.4%	0.1%	0.6%
Central Clastics	0		3	5.4%	-4.1%	14.9%	0.1%	2.2%
Base Gravels	25	12.5%	25	12.5%	9.0%	16.1%	0.7%	1.7%
All Grps	45	12.6%	76	10.1%	8.6%	12.2%	0.6%	0.9%

14.4 Brine Concentrations

The distributions of lithium and potassium concentrations in the model domain are based on a total of 501 brine analyses (not including QA/QC analyses)

Table 14.2 shows a summary of the brine chemical composition.

Table 14.2 Summary of brine chemistry composition

	B	Ca	Cl	Li	Mg	K	Na	SO ₄	Density
Units	mg/L	mg/L	mg/L	mg/L	mg/L	mg/L	mg/L	mg/L	g/cm ³
Maximum	938.00	1,707	196,869	701.00	5,130	6,660	130,032	13,998	1.22
Average	557.62	821	169,838	391.76	2,257	3,733	102,381	7,547	1.19
Minimum	20.20	11.00	116.00	8.75	23.20	18.00	196.00	12.00	1.00

14.5 Resource category

The CIM Council (May 10, 2014) adopted the following definition standards for minerals resources:

Inferred Mineral Resource

An Inferred Mineral Resource is that part of a Mineral Resource for which quantity and grade or quality are estimated based on limited geological evidence and sampling. Geological evidence is sufficient to imply but not verify geological and grade or quality continuity.

An Inferred Mineral Resource has a lower level of confidence than that applying to an Indicated Mineral Resource and must not be converted to a Mineral Reserve. It is reasonably expected that most of the Inferred Mineral Resources could be upgraded to Indicated Mineral Resources with continued exploration.

An Inferred Mineral Resource is based on limited information and sampling gathered through appropriate sampling techniques from locations such as outcrops, trenches, pits, workings, and drill holes. Inferred Mineral Resources must not be included in the economic analysis, production schedules, or estimated mine life in publicly disclosed Pre-Feasibility or Feasibility Studies, or in the Life of Mine plans and cash flow models of developed mines. Inferred Mineral Resources can only be used in economic studies as provided under NI 43-101.

There may be circumstances, where appropriate sampling, testing, and other measurements are sufficient to demonstrate data integrity, geological and grade/quality continuity of a Measured or Indicated Mineral Resource, however, quality assurance and quality control, or other information may not meet all industry norms for the disclosure of an Indicated or Measured Mineral Resource. Under these circumstances, it may be reasonable for the Qualified Person to report an Inferred Mineral Resource if the Qualified Person has taken steps to verify the information meets the requirements of an Inferred Mineral Resource.

Indicated Mineral Resource

An Indicated Mineral Resource is that part of a Mineral Resource for which quantity, grade or quality, densities, shape and physical characteristics are estimated with sufficient confidence to allow the application of Modifying Factors in sufficient detail to support mine planning and evaluation of the economic viability of the deposit.

Geological evidence is derived from adequately detailed and reliable exploration, sampling and testing and is sufficient to assume geological and grade or quality continuity between points of observation.

An Indicated Mineral Resource has a lower level of confidence than that applying to a Measured Mineral Resource and may only be converted to a Probable Mineral Reserve.

Mineralization may be classified as an Indicated Mineral Resource by the Qualified Person when the nature, quality, quantity and distribution of data are such as to allow confident interpretation of the geological framework and to reasonably assume the continuity of mineralization. The Qualified Person must recognize the importance of the Indicated Mineral Resource category to the advancement of the feasibility of the project. An Indicated Mineral Resource estimate is of sufficient quality to support a Pre-Feasibility Study which can serve as the basis for major development decisions.

Measured Mineral Resource

A Measured Mineral Resource is that part of a Mineral Resource for which quantity, grade or quality, densities, shape, and physical characteristics are estimated with confidence sufficient to allow the application of Modifying Factors to support detailed mine planning and final evaluation of the economic viability of the deposit.

Geological evidence is derived from detailed and reliable exploration, sampling and testing and is sufficient to confirm geological and grade or quality continuity between points of observation.

A Measured Mineral Resource has a higher level of confidence than that applying to either an Indicated Mineral Resource or an Inferred Mineral Resource. It may be converted to a Proven Mineral Reserve or to a Probable Mineral Reserve.

Mineralization or other natural material of economic interest may be classified as a Measured Mineral Resource by the Qualified Person when the nature, quality, quantity, and distribution of data are such that the tonnage and grade or quality of the mineralization can be estimated to within close limits and that variation from the estimate would not significantly affect potential economic viability of the deposit. This category requires a high level of confidence in, and understanding of, the geology and controls of the mineral deposit.

The resource classification method used is based on the use of distinct domains, including the unsaturated zone, northern transitional zone, eastern transitional zone, upper zone, central brine zone, lower zone, and central clastic zone.

- The unsaturated zone contains no resources.
- The northern and eastern transitional zones, which show low lithium concentrations and represent the transition between brine and freshwater, were classified as indicated resources. A drill hole spacing of less than 3 km and vertical sampling of about 20 m were used.
- The upper zone has a very limited number of samples, with unsampled intervals of up to 200 m. Because of the lack of systematic sampling, this zone is therefore classified as an inferred resource. It is also worth mentioning that several drillholes have unsampled intervals of up to 300 m.
- The central brine zone has the highest sample density and best characterization and was classified as a measured resource with a borehole spacing of less than 2 km and a vertical sampling of about 20 m.
- The lower zone was incorporated due to lithium samples showing a tendency to improve with depth and was classified as an inferred resource to a depth of 700 m or 3,096 masl.
- The central clastic zone was reclassified to an indicated resource within the central brine zone due to the uncertainty of its drainable porosity values.

The different zones used in this classification are schematically illustrated in Figure 14.2.

Figure 14.1 Schematic section illustrating resource categories based on data density for different zones

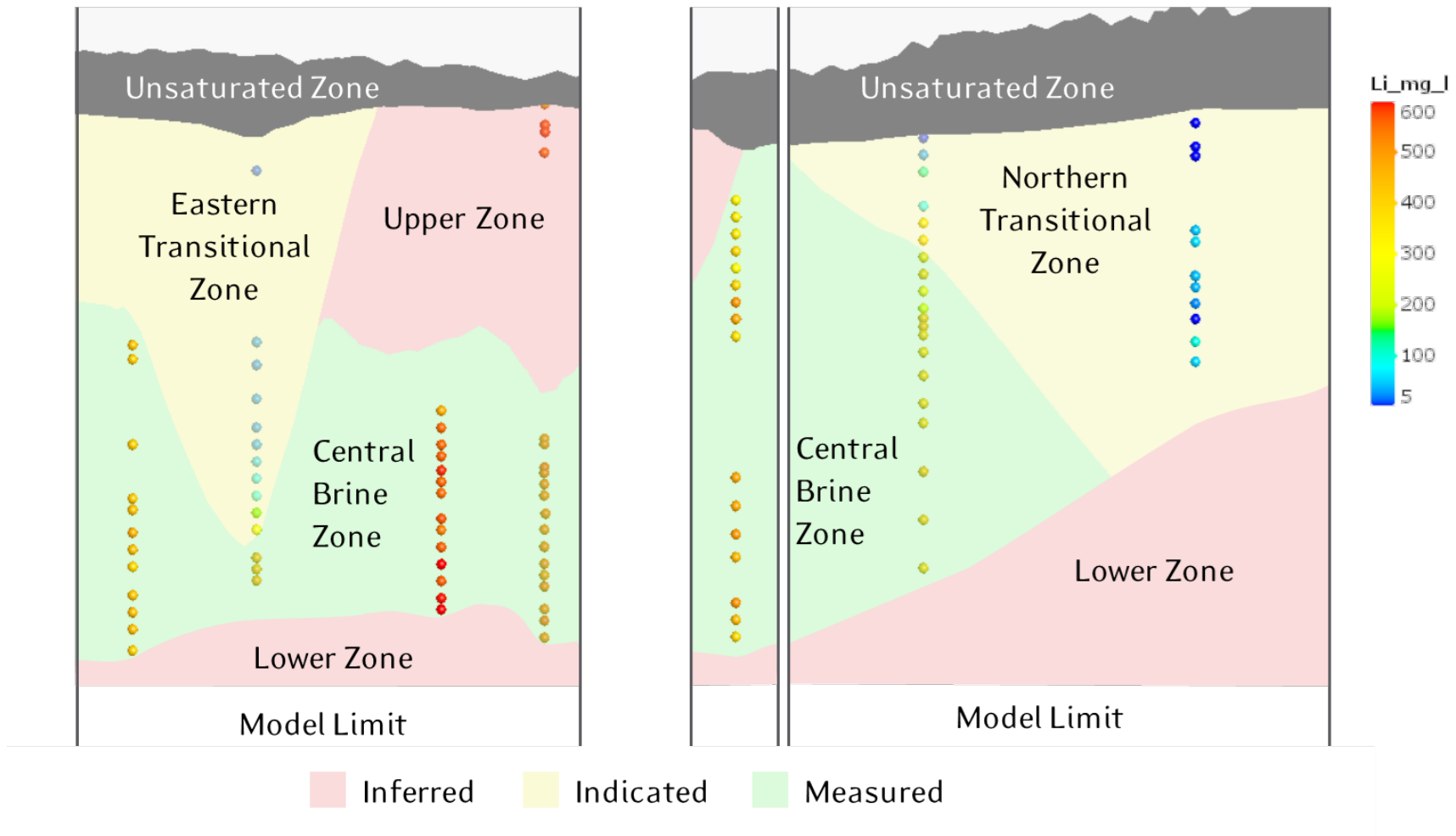
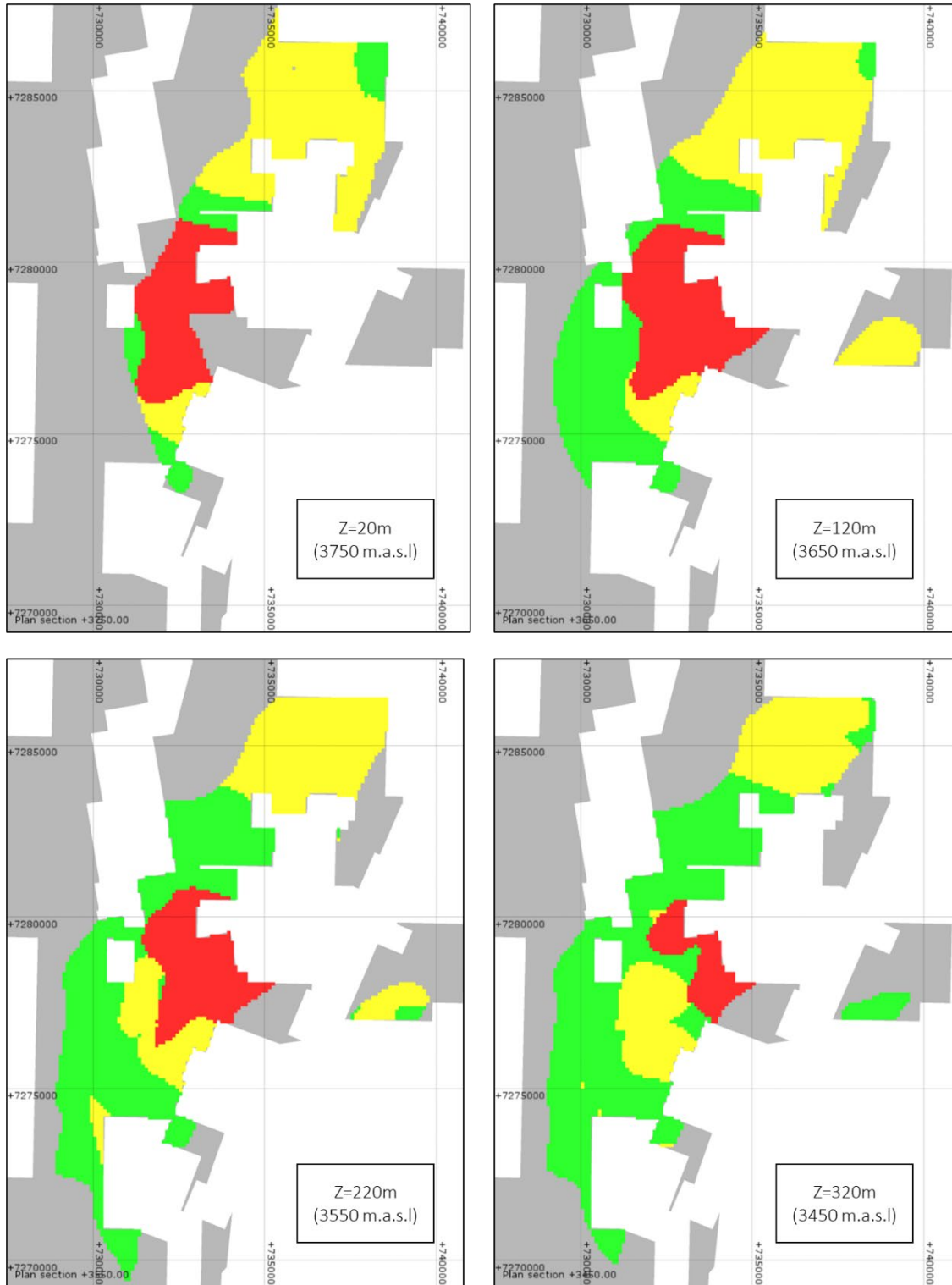


Figure 14.2 Spatial distribution of resource classification by depth



14.6 Resource model methodology and construction

The resource estimation for the Project was developed using the Stanford Geostatistical Modeling Software (SGeMS). Brine concentrations showed two clear groups of data spatially distributed in two regions: region I and II. Region I is associated with high concentrations of potassium and lithium, whereas Region II is associated with low concentrations of potassium and lithium. Region II is mostly located close to the boundaries of the reservoir, where brine is affected by mixing with fresh water. The delineation of these two regions was estimated through geostatistical indicator kriging. For this the following indicator function is defined:

$$I(x) = \begin{cases} 1 & C(x) \geq 2000 \text{ mg/L} \\ 0 & \text{Otherwise} \end{cases}$$

The conditional expected value of the indicator function is exactly the probability that the potassium concentration is larger or equal to 2,000 mg/L (or the probability that region I prevails at that location). Given the high correlation between potassium and lithium concentrations (coefficient of correlation of 0.93), one can delineate the probability that region I prevails by considering either potassium or lithium concentrations. That is because the ratio between potassium and lithium concentrations is about 10, similar results will be obtained by considering a lithium cut-off of 200 mg/L. Note that the lithium histogram shows two groups of data with a cut-off of 200 mg/L. By definition, the probability of occurrence of a given region is a continuous variable ranging between 0 and 1. In order to separate the data into regions a cut-off in the estimate of the indicator variable must be developed. Ritzi et al. (1994) has suggested to define the boundary between regions by the isoline $\text{Prob}\{C \geq 2000\} = p$, where p is estimated as either the global mean of the indicator values or the empirical relative volumetric fraction of the region. In this case, both conditions yield similar results and $p=0.8$ was selected which is close to the data volumetric fraction. Once the two regions were defined kriging was applied within each region. Kriging interpolation within each specific region is sequentially performed using the semivariogram model and the closest primary data samples within the region. The following steps were carried out to calculate the lithium and potassium resources.

- Definition of the block model (15,985,800 blocks) and block size ($x=100$ m, $y=100$ m, $z=20$ m). The block size has been chosen for being representative of the geological model.
- Delineate regions of high and low brine concentrations based on geostatistical indicator kriging. Spatial definition of region I with potassium concentrations larger or equal to 2,000 mg/L and region II with potassium concentrations smaller than 2,000 mg/L.
- For each region, generation of histograms, probability plots and box plots for the Exploratory Data Analysis (EDA) for lithium and potassium. No outlier restrictions were applied, as distributions of the different elements do not show anomalously high values. The experimental variograms were calculated with their respective variogram models for lithium and potassium in three orthogonal directions. Variography revealed that the variogram model is axisymmetric with respect to the z coordinate direction; the variogram model is isotropic in the horizontal direction and anisotropic in the vertical.

- For each region, lithium and potassium concentrations were interpolated for each block in mg/L using ordinary kriging with the variogram models shown in Figure 14.6 and Figure 14.7.
- Validation using a series of checks including comparison of univariate statistics for global estimation bias, visual inspection against samples on plans and sections in the north, south and vertical directions to detect any spatial bias.
- Calculation of total resources using the average drainable porosity value for each geological unit, based on the boreholes data and results of the laboratory drainable porosity analysis as shown in Table 14.1. The total resources are shown in Table 14.6.

14.6.1 Univariate statistical description

The univariate statistical description of lithium and potassium concentrations are based on histograms, probability plots and box plots. Table 14.3 presents a summary of the univariate statistics of potassium and lithium. As described in the methodology, these statistics contain the information of all geological units. The mean concentration of potassium is about 10 times that of lithium. Both exhibit a similar high degree of variability with coefficients of variation of 2.46 and 2.48 for the potassium and lithium, respectively. The concentrations of potassium range between 18 mg/L and 6,660 mg/L, and the concentrations of lithium range between 9 mg/L and 701 mg/L.

Table 14.3 Summary of univariate statistics of Li and K

	Li mg/L	K mg/L
Valid N	501	501
Mean	392	3,733
Minimum	9	18
Maximum	701	6,660
Variance	26,149	2,503,050
Upper Quartile	519	5070
Median	437.8	4,471.8
Lower Quartile	357	3,180
CV	2.46	2.48

Figure 14.4 shows the lithium and potassium distribution and their cumulative distribution. Results show that the data do not strictly follow a normal distribution and that the distribution is markedly bimodal. This suggests two different groups of data that should be treated separately: one defined by potassium concentrations larger or equal to 2,000 mg/L (region I), and another associated with potassium concentrations smaller than 2,000 mg/L (region II). From a physical perspective, the first group is located within and nearby the nucleus of the Salar,

whereas the second group is close to the boundaries of the resource. In the latter, brine concentrations are relatively low, reflecting the mixing with freshwater at the salar boundaries. Once data is separated into groups, the corresponding histograms of the potassium and lithium concentrations follow a Gaussian shape (see Figure 14.5). This gives confidence in the kriging estimate of the concentrations, which is known to be the best linear and nonlinear estimator of the concentrations when the data follow a multivariate normal distribution.

Figure 14.3 lithium and potassium histograms and cumulative distributions

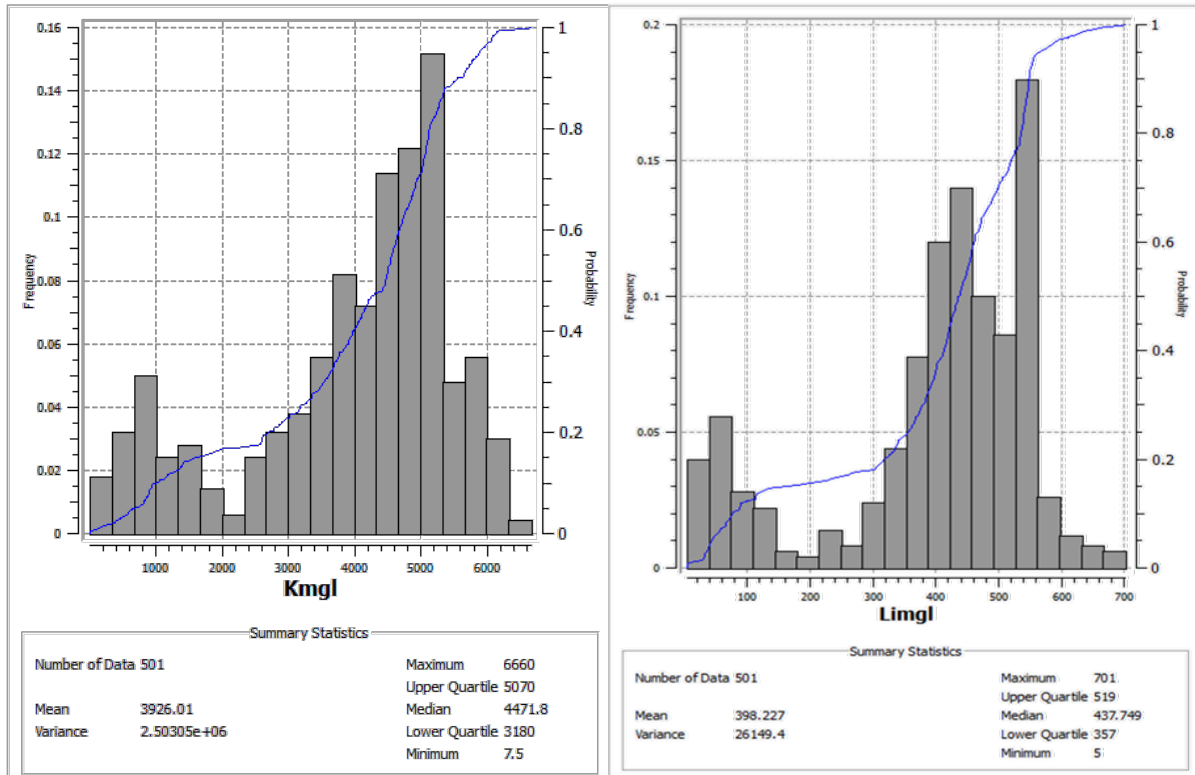
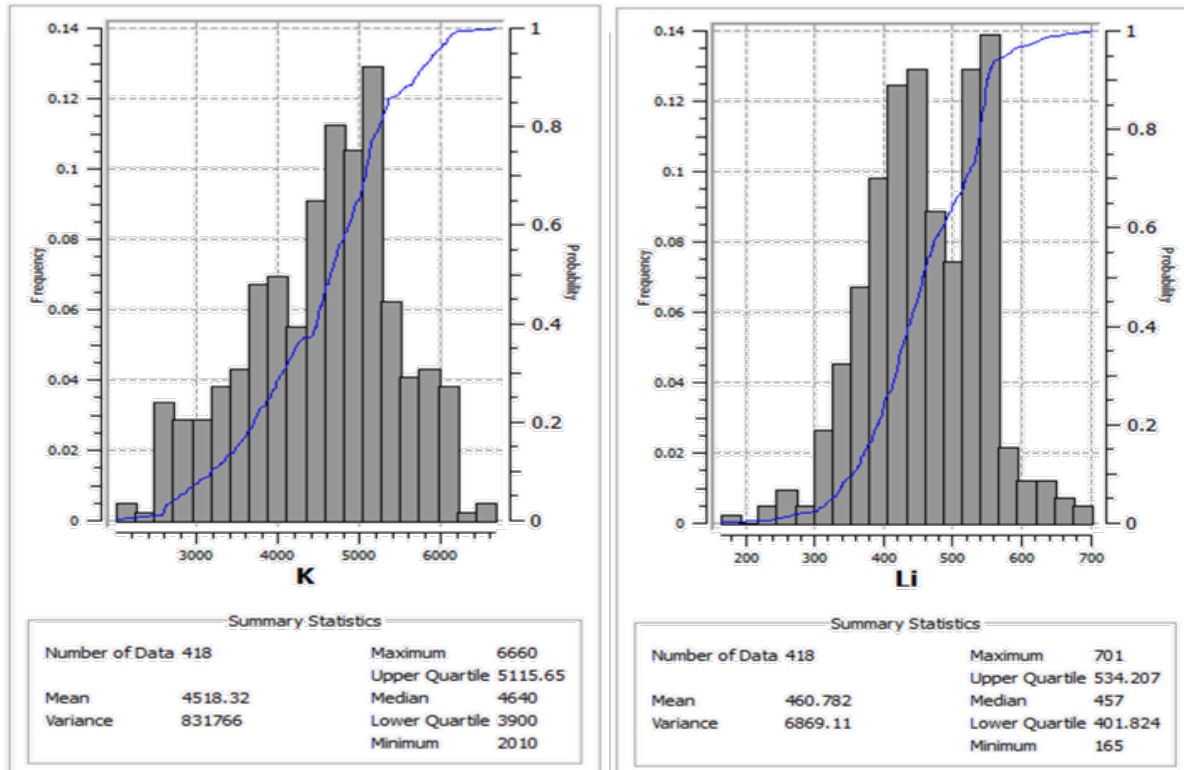


Figure 14.4 Lithium and potassium histograms and cumulative distributions for region I



14.6.2 Variography

The spatial correlation for the indicator variable $I(x)$, defined previously to delineate regions of different concentration groups, was reviewed using experimental variograms with the parameters shown in Table 11.4. Variogram models are axisymmetric with a simple exponential structure characterized by a horizontal range a_h and a vertical range a_z . Consequently, the spatial variability was modelled using two experimental directions. The horizontal range is $a_h=10,200$ m and the vertical range is $a_z=1,836$ m. The anisotropy ratio is about $a_h/a_z=5$, which suggest that the indicator variables is only slightly stratified. The variogram ranges obtained for the indicator variable are substantially larger (double) than those obtained for the potassium and lithium concentrations, meaning that the indicator variables are more continuous in space compared with concentrations. The experimental variograms for the indicator variable with their respective variogram models are shown in Figure 14.5 and Figure 14.6.

$$\gamma_I = 0.23 \gamma_{Exp}(a_h = 10,200 \text{ m}, a_z = 1,836 \text{ m})$$

Table 14.4 Parameters for the calculation of the experimental variograms of the indicator variable

Variogram Parameters				Tolerance	
Lag (m)	Max. No. Of Lags	Azimuth (°)	Dip (°)	Bandwidth (m)	Angular (°)
600	50	70	0	50	45
600	50	70	0	50	45
18	50	0	90	100	45

The spatial correlation for the lithium and potassium concentrations for each region were reviewed using experimental variograms with the parameters shown in Table 14.5. Variogram models are axisymmetric with multiple structures characterized by a horizontal range a_h and a vertical range a_z . Consequently, for each region, the spatial variability was modelled using two experimental directions. Lithium and potassium concentrations are expressed in mg/l. The variograms are expressed in mg/l squared. In general, a good correlation was found between the sample concentrations of lithium and potassium in all regions. Consequently, results show that the lithium and potassium concentrations can be represented by the combination of similar fundamental structures.

Table 14.5 Parameters for the calculation of the experimental variograms of the K and Li concentrations

Variogram Parameters				Tolerance	
Lag (m)	Max. No. Of Lags	Azimuth (°)	Dip (°)	Bandwidth (m)	Angular (°)
400	50	70	0	50	45
400	50	70	0	50	45
18	50	0	90	100	45

The region I of the formation characterized by higher potassium concentrations not influenced by fresh water were represented by the sum of two exponential variograms with a different vertical range. In this case, two structures are needed to represent the vertical variability of the concentrations. The first exponential variogram describes the short-scale spatial continuity with a vertical range of $a_z=100$ m, which contrasts with a range of $a_h=4,700$ m in the horizontal direction. This means that the ratio of anisotropy is $a_h/a_z=47$, which expresses that the geological system is highly stratified as typically observed in most sedimentary formations. The second structure reflects the appearance of more variability in the vertical direction at larger scales.

Variogram models for region I:

$$\gamma_K(h) = 0.24 \times 10^6 \gamma_{Exp}(a_h = 4700 \text{ m}, a_z = 100 \text{ m}) + 0.69 \times 10^6 \gamma_{Exp}(a_h = 4700, a_z = 3700 \text{ m})$$

$$\gamma_{Li}(h) = 2400 \gamma_{Exp}(a_h = 4700 \text{ m}, a_z = 100 \text{ m}) + 6900 \gamma_{Exp}(a_h = 4700, a_z = 2200 \text{ m})$$

Variogram models for region II:

$$\gamma_{Li}(h) = 5148 \gamma_{Sph}(a_h = 5700 \text{ m}, a_z = 400 \text{ m})$$

$$\gamma_K(h) = 0.22 \times 10^6 \gamma_{Sph}(a_h = 5100 \text{ m}, a_z = 180 \text{ m})$$

The region II of the formation characterized by lower potassium concentrations was represented by an anisotropic axisymmetric spherical variogram. The range in the vertical direction is 180 m for potassium and 400 m for lithium which seems to be more continuous in this direction. In the horizontal direction, the range is 5,100 m and 5,700 m for potassium and lithium, respectively. The anisotropy ratio a_h/a_z ranges between 18 and 28, meaning that potassium and lithium is slightly less stratified in region I compared to region II. The variogram contributions are like region I but the vertical variogram model does not reflect multiple structures.

The experimental variograms with their respective variogram models are shown in Figure 14.5 and Figure 14.6.

The lithium and potassium concentrations were estimated within each specific region using the corresponding variogram models and the closest concentration data samples within the region. The interpolation methodology for estimating lithium and potassium was Ordinary Kriging (OK). The estimation was carried out separately for each parameter using their respective variogram models as appropriate.

Figure 14.5 Experimental variogram and variogram model for the indicator variable

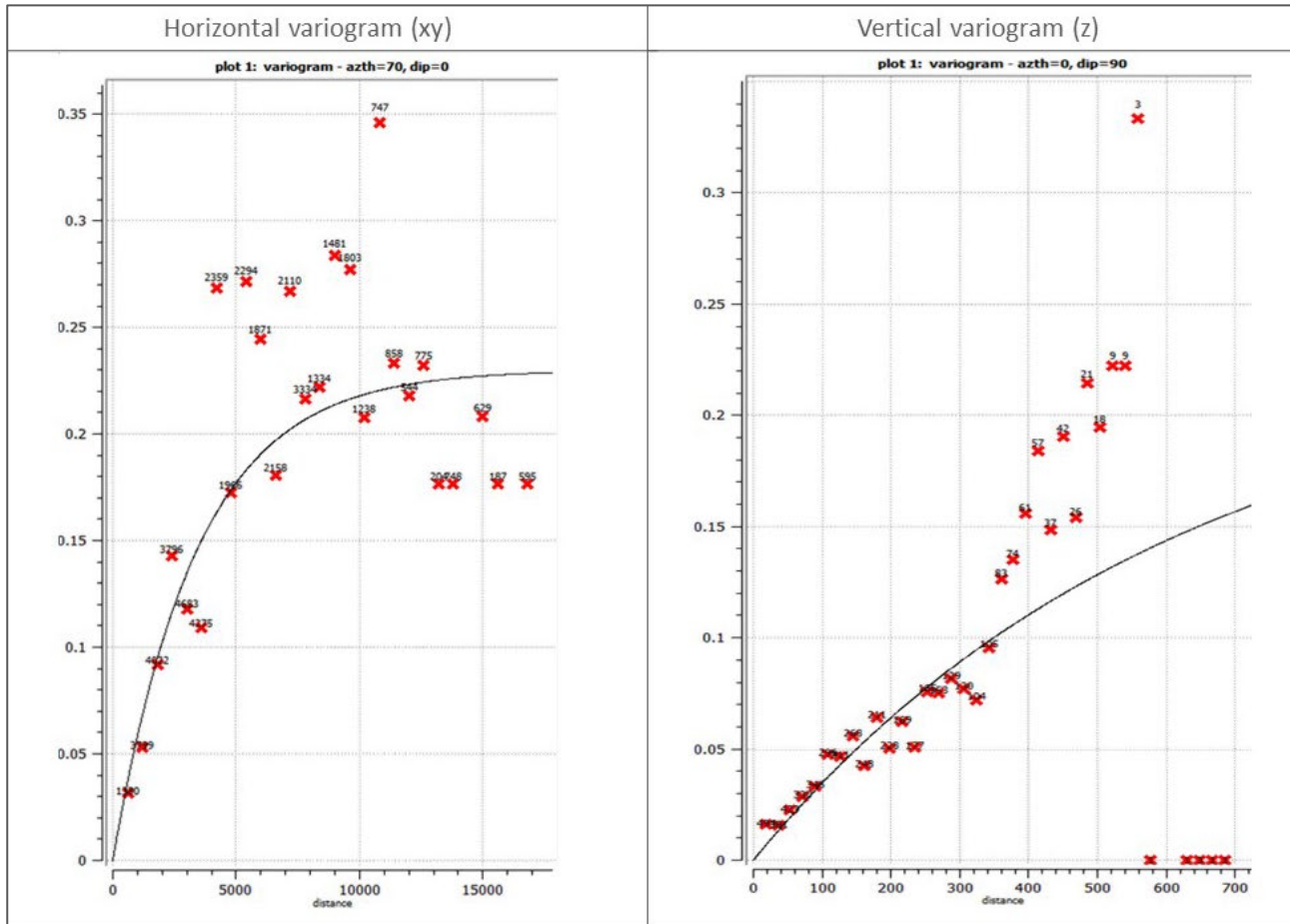
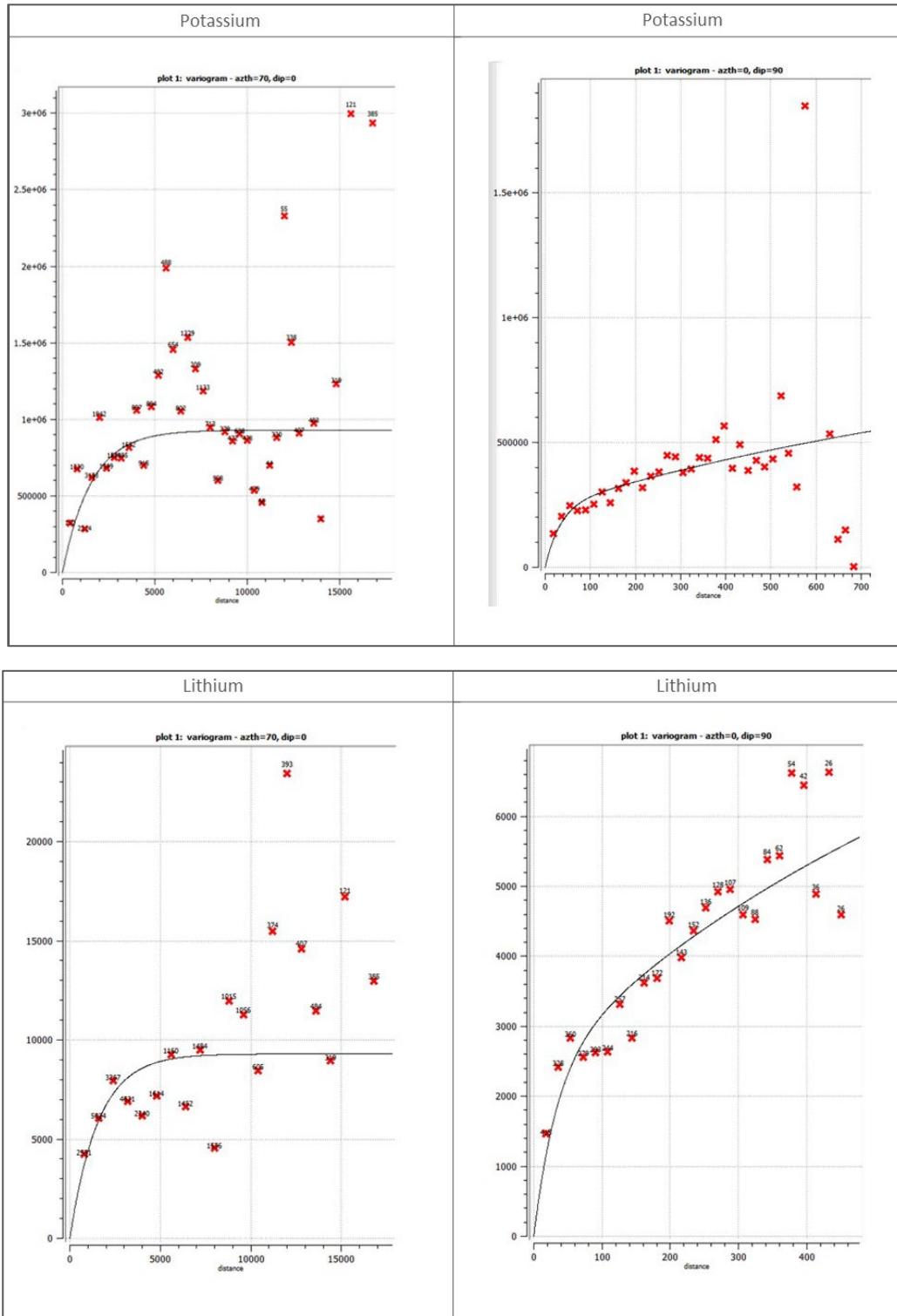


Figure 14.6 Experimental variogram and variogram model for potassium and lithium in region I



14.7 Grade estimate

The grade estimates of lithium and potassium in each block inside the model were calculated applying the following operation:

$$R_i = C_i \cdot Sy_i$$

Where: i is the indice of the block, going from 1 to 15,985,800

R_i : Grade value to be assigned (g/m³)

C_i : Concentration value assigned from the estimation (mg/L)

Sy_i : Specific yield value assigned from the estimation (%)

Figure 14.7 through Figure 14.9 shows N-S, W-E, and SW-NE sections through the resource model showing lithium grade distributions in g/m³. The resource classification was made within the limits of the block model.

Figure 14.7 N-S section through the resource model showing the lithium grade distribution

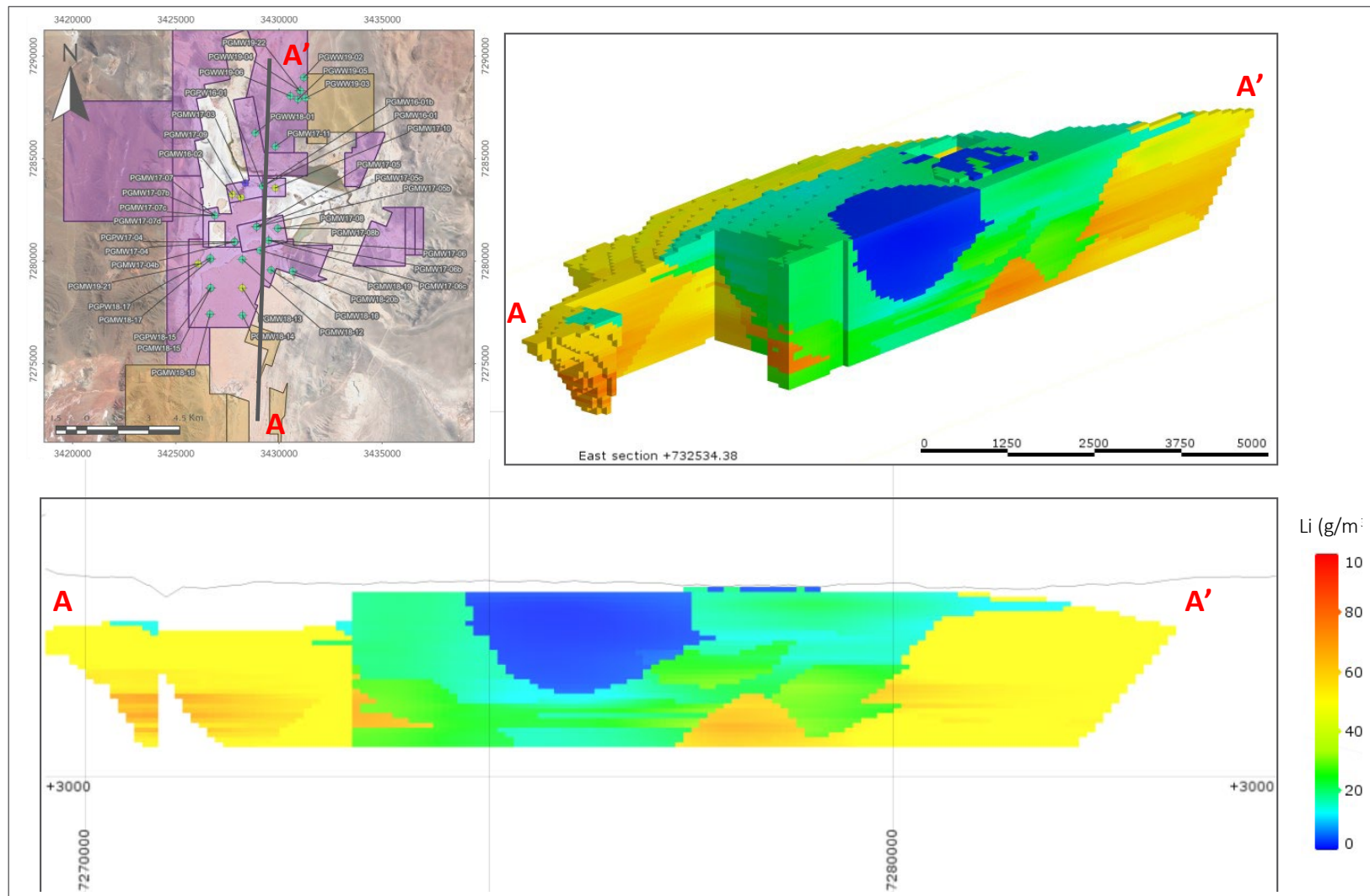


Figure 14.8 W-E section through the resource model showing the lithium grade distribution

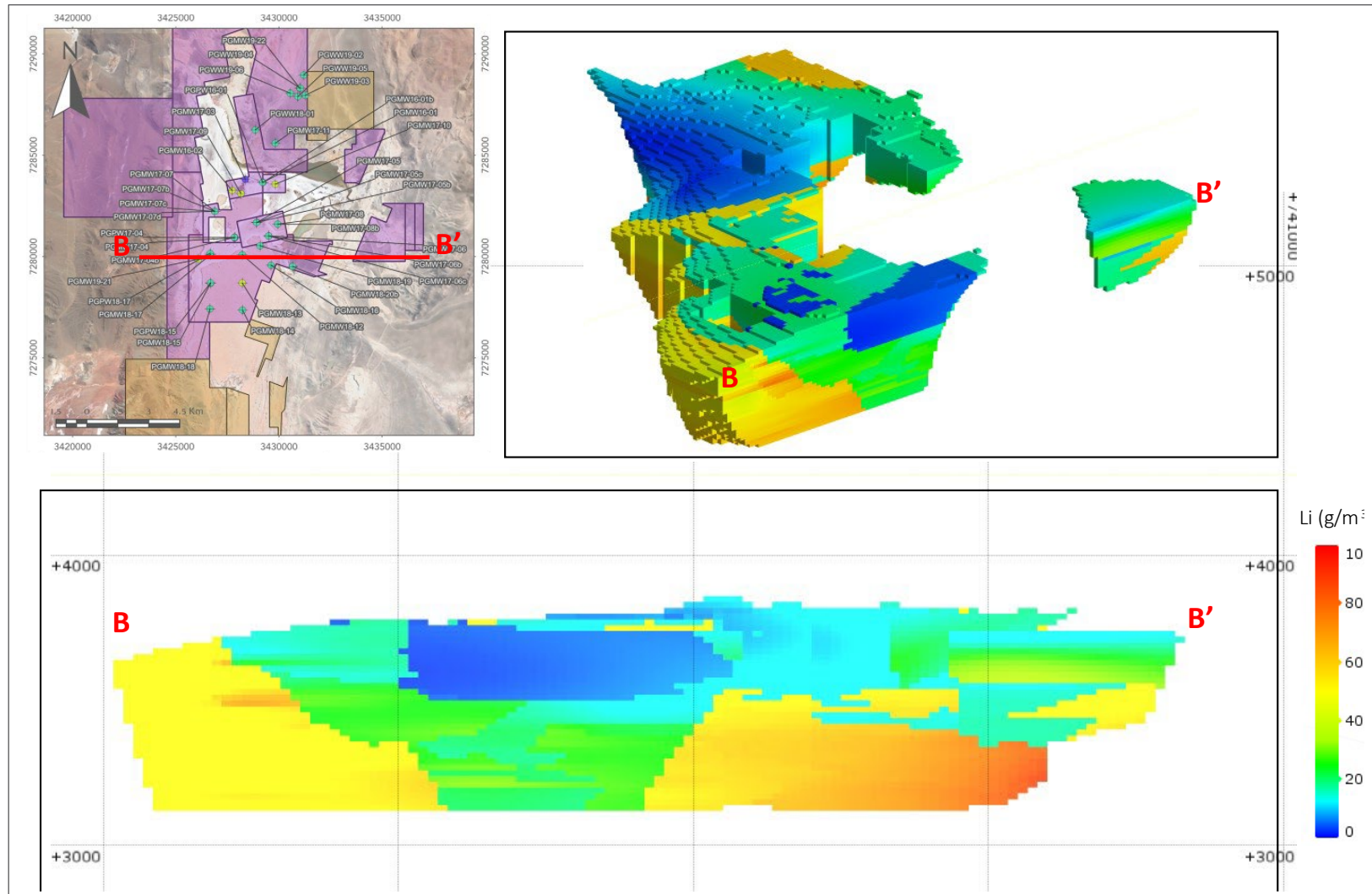
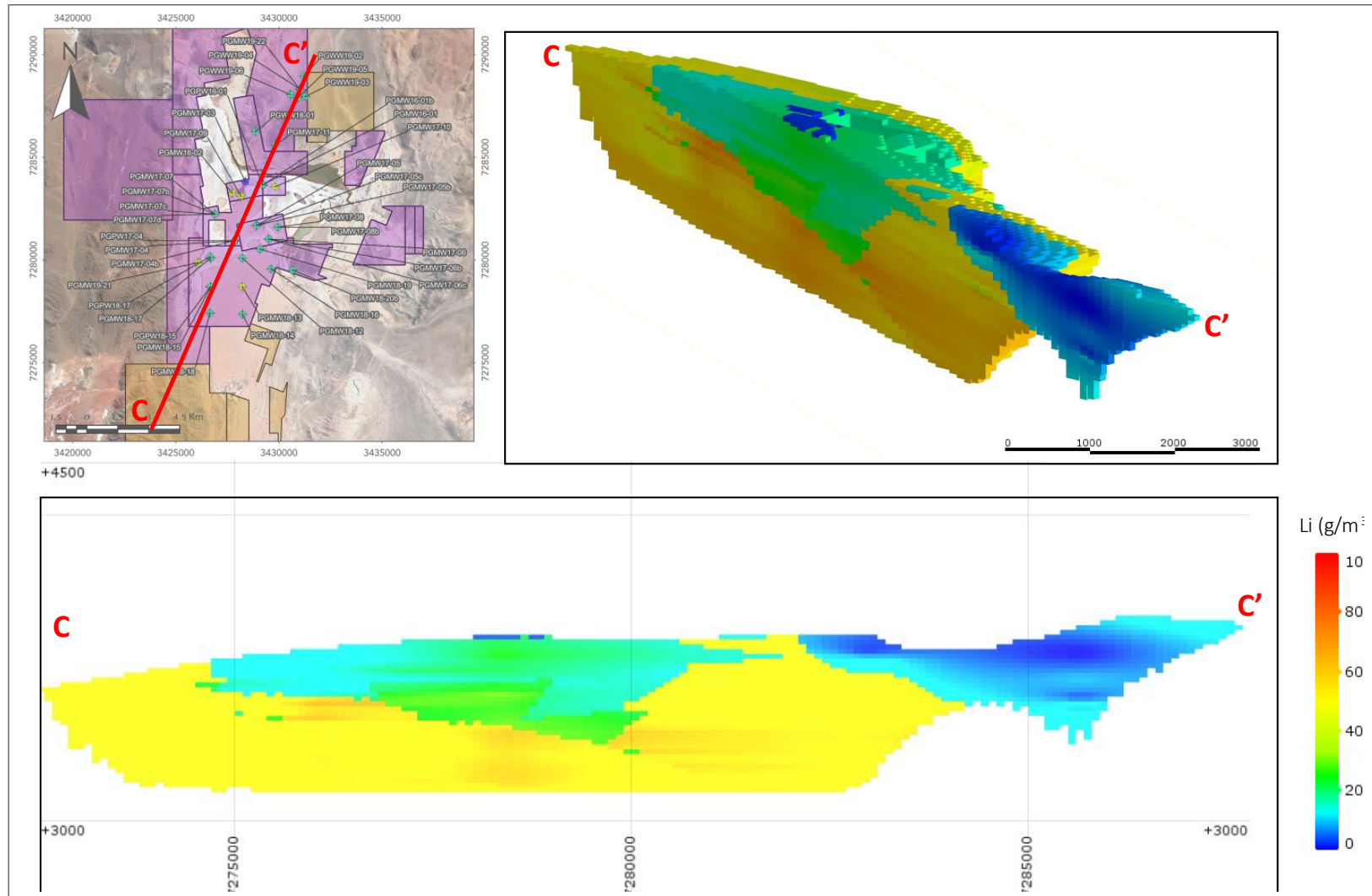


Figure 14.9 SW-NE section through the resource model showing the lithium grade distribution



14.8 Resource estimate

The resource estimate for the Pastos Grandes Project was prepared in accordance with the guidelines of the National Instrument 43-101 and uses the best practices methods specific to brine resources. The lithium and potassium resources are summarized in Table 14.6. The effective date for the estimate is April 30, 2023.

Table 14.6 Mineral Resources of the Pastos Grandes Project – Dated April 30, 2023

	Measured (M)		Indicated (I)		M+I		Inferred (I)	
	Li	K	Li	K	Li	K	Li	K
Aquifer volume (km ³)	13.45		8.81		22.26		6.14	
Mean specific yield (Sy)	0.11		0.11		0.11		0.08	
Brine volume (km ³)	1.48		0.97		2.45		0.49	
Mean grade (g/m ³)	49	495	13	134	35	352	34	350
Concentration (mg/l)	438	4419	167	1722	331	3352	403	4234
Resource (tonnes)	662,000	6,660,000	118,000	1,180,000	780,000	7,840,000	208,000	2,150,000

Notes to the resource estimate (Table 14.6):

1. CIM definitions were followed for Mineral Resources.
2. The Qualified Person for this Mineral Resource estimate is Frederik Reidel, CPG
3. No cut-off values have been applied to the resource estimate.
4. Numbers may not add due to rounding.
5. The effective date is April 30, 2023.

Table 14.7 shows the mineral resources of the Pastos Grandes Project expressed as lithium carbonate equivalent (LCE) and potash (KCl).

Table 14.7 Pastos Grandes Project resources expressed as LCE and KCl

	Measured and Indicated Resources	
	LCE	KCl
Tonnes	4,200,000	14,900,000

Notes to Table 14.7

1. Lithium is converted to lithium carbonate (Li₂CO₃) with a conversion factor of 5.32.
2. Potassium is converted to potash with a conversion factor of 1.91.
3. Numbers may not add due to rounding.

It is the opinion of the author that the Salar geometry, brine chemistry composition, and the specific yield of the Salar sediments have been adequately characterized to support the Measured, Indicated, and Inferred Resource estimate for the Project herein.

It is the opinion of the author the resource estimated and described in the current report meet the requirements of reasonable prospects for eventual economic extraction, as defined in Form 43-101F1. The resource described herein has similar lithium concentrations, chemical composition, and hydraulic parameter values (drainable porosity values between 0.05 and 0.11 and hydraulic conductivities values between 0,5 m/d and 300 m/d) to resources currently in commercial production such as those in Salar de Atacama in Chile or Salar de Olaroz located in the Puna region of Northern Argentina. The hydraulic parameters of the resource area determined from the results of the pumping tests suggests that it is reasonable to expect brine extraction by a conventional production wellfield at a commercially viable rate, while the geochemical characteristics of the brine suggest that conventional processing techniques may be employed to produce saleable lithium products in an economically profitable manner. These conventional processing techniques are employed in most lithium brine operations, including the two operations at Salar de Atacama (Chile), one at Salar de Olaroz (Argentina), and one at Clayton Valley (USA). The author is not aware of any known environmental, permitting, legal, title, taxation, socio-economic, marketing, political or other relevant factors which could materially affect the mineral resource estimate.

15 MINERAL RESERVE ESTIMATES

No mineral estimates have been prepared as part of this resource estimate.

16 MINING METHODS

Based on the results of the pumping tests carried out for the Project (as described in Section 10 above) brine abstraction from the Salar will take place by installing and operating a conventional production wellfield. Pumping rates of individual wells could range between 20 l/s and 45 l/s. Well completion depths will vary between 200 m and 600 m (lower brine aquifer). The brine wellfield configuration will be finalized as part of the on-going Project optimization during 2023.

17 RECOVERY METHODS

No mineral recovery methods have been described for this Resource Estimate update.

18 PROJECT INFRASTRUCTURE

No new studies have been carried out for Project's infrastructure requirements as part of this resource update.

19 MARKET STUDIES AND CONTRACTS

No market studies have been prepared for this Resource Estimate update.

20 ENVIRONMENTAL STUDIES, PERMITTING AND SOCIAL OR COMMUNITY IMPACT

20.1 Environmental studies

Millennial contracted Ausenco to prepare the initial Environmental Baseline Study for the Project in 2018. This study formed the basis for the Project's Environmental Impact Assessment in 2019. Elisa Cozzi y Asociados (EC) updated the Environmental Baseline report in September 2022 as required by law. Currently regional hydrogeological studies are being carried out by the Universities of Alaska and Massachusetts to refine the quantification of recharge to the Pastos Grandes Basin. A significant surface water and groundwater monitoring network is being implemented throughout the Pastos Grandes and Sijes sub-basins.

20.2 Permits

LAC has secured all required permits to continue with exploration activities described hereinafter in Section 26. Further EIA updates will be carried out as required for Project construction and operations.

20.3 Social and community

The closest community to the Project is Santa Rosa de Los Pastos Grandes. The habitants are mostly descendants of Andean Indigenous People (Kollas). Very few people live within the Project area, only five isolated houses have been identified. In the area of influence of the Project, the predominant economic activity is the breeding of llamas and small ruminants that include goats and sheep. LAC has a proactive approach in its relationship with the local communities and other stakeholders. The Company is continuously updating its social management strategy to follow international standards, including Local Employment, Local Suppliers, Grievance Mechanism and Participatory Environmental Monitoring (MAP). The Company has developed a Stakeholders Engagement Plan that promotes numerous activities with the local community.

LAC actively employs people directly from the local communities as well as extends as contract services. The Company participates in the "Coordination Tables" between companies, communities, and the Province for Santa Rosa de los Pastos Grandes and Estacion Salar de Pocitos. LAC has supported the construction of an Integration Center and a freshwater well for the community, amongst other initiatives, in Santa Rosa de los Pastos Grandes.

Argentina joined and ratified the International Agreement concerning Indigenous and Tribal Peoples in Independent Countries of the International Labor Organization (ILO) Convention 169 in March 1992. This Convention calls on governments to develop systematic actions to protect the rights of indigenous and tribal peoples, including their social, economic, and cultural rights, customs, traditions and institutions. LAC is complying with the application of this convention in Argentina.

21 CAPITAL AND OPERATING COSTS

No capital and operating costs have been prepared for this Resource Estimate update.

22 ECONOMIC ANALYSIS

No economic analyses have been prepared for this Resource Estimate update.

23 ADJACENT PROPERTIES

Third-party ownership of mining properties in the vicinity of the Project are outlined in Table 23.1 and shown in Figure 23.1. Third-party owners include Ganfeng Lithium Co dedicated to lithium production and Borax Argentina S.A. and ULEX S.A focused on borates production.

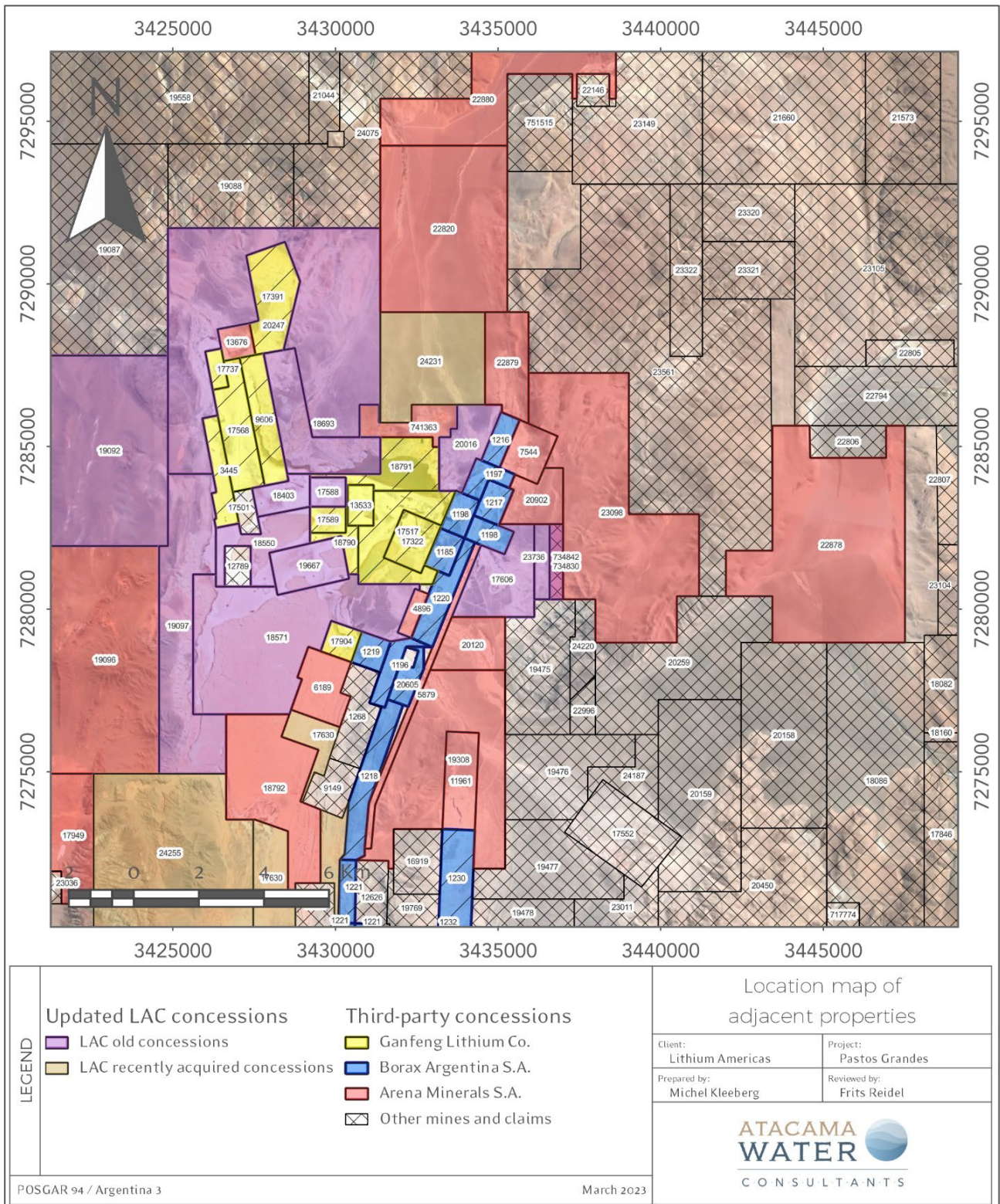
Table 23.1 Mining properties in the vicinity of the Pastos Grandes Project

Property name	File	Property name	File
Monte Blanco	1,218	Cerrito	7,544
San Pablo 6	23,322	Muñeca li	24,075
Cz 04	734,842	Avestruz	17,517
Centenario 200	20,158	La Paz lii	1,198
Doña Pancha	5,879	Quevar Quinta	19,617
Aguamarga 44	19,512	Quevar Novena	20,215
Neptali I	9,606	Aguamarga 05	19,087
Santa Rosa	1,220	Centenario 208	20,259
Elsa	1,219	Demasia San Mateo	23,036
Santa Rosa	17,568	Bicentenario	20,450
Maria Daniela	17,737	Margarita	5,569
Santa Elena	1,217	Quebracho	9,149
Ppg 05	741,363	Juan Pablito	19,769
Sol De Mañana	11,961	Industria	1,193
Aguamarga 14	19,096	La Intermedia	18,160
Tutamanta	23,583	La Gran Ruben	24,313
Monte Amarillo	1,226	Monte Azul	1,221
San Nicolas 10	23,321	Eg 04	734,837
Esperanza	1,230	La Rescatada li	17,391
Quevar Iv	19,558	La Playosa	18,791
San Cayetano I	17,322	Shiban	21,252
La Fortuna I	19,308	San Mateo	64,005
Monte Amarillo	1,226	La Paz	1,185
San Pablo 7	23,320	La Cerrana	13,676
Taron Norte	18,082	Centenario 201	20,159
Marisa 10	22,996	Casandra lii	22,797
Leoncia	13,533	Cattleya	23,149
La Pacha I	18,161	Turco	17,949
Don Felipe	17,501	Apalacheana	12,626
Centenario 8	24,187	Centenario 4	19,478
Charquito 01	22,146	Sofia 5	18,399
Cresta 2	710,411	Kratos Xv	23,133

Property name	File	Property name	File
Taron Oeste	18,086	Sijes	1,196
La Paz	1,197	Santiago Primero	12,789
Centenario 3	19,477	Yacones Viii	717,774
Aguamarga 06	19,088	San Mateo li	13,171
Cresta 1	710,405	Santa Barbara I	22,268
Casandra V	22,806	Santa Elvira	1,216
Gaston Iv	16,919	Casandra Iv	22,805
Quevar Vigesimo Cuarto	21,044	Centenario 5	19,479
Bicentenario 303	23,011	La Paz Iii	1,198
Calchin	18,790	Cumbrecita V	20,026
Centenario 1	19,475	Centenario 2	19,476
Norte Incachule	21,573	Sarita	1,208
Coronel Vidt	3,445	Ppg 04	734,830
Rio Sijes	20,605	Futuro I	12,815
Monte Azul	1,221	Cerrito	7,544
Betina	4,896	Graciela	6,189
La Buscada	17,589	Doña Pancha	5,879
Monte Azul	1,221	Cristal	5,785
El Huesito	17,552	Betina	4,896
Cita	1,232	Roberta	23,098
Quevarita li	746,319	Barreal 03	22,880
El Barreal	21,660	Barreal 02	22,879
Muñeca Iv	24,220	Barreal 01	22,878
Casandra Vi	22,807	La Relojera	22,820
Ona	1,268	Patovica I	20,902
Taron	17,846	Fortuna LI	20,120
Amapola 2	751,515	La Fortuna I	19,308
Casandra li	22,794	Almafuerte	18,792
Pozuelo	4,959	Campamento	13,886
Maria Luisa li	17,904	La Cerrana	13,676
San Mateo Iii	13,172	Sol de Mañana	11,961
Quevar Decima Tercera	20,501	Hierro Indio	1,186

Source: Mining cadastre of the Salta Province

Figure 23.1 Location map of adjacent properties



24 ADDITIONAL INFORMATION

It should be noted that the resource estimate described for the Pastos Grandes Project in Section 14 above does not include mineral resources contained in the Sal de la Puna properties that were recently obtained by LAC as part of the AMSA acquisition. A significant amount of work was completed by Centaur and AMSA on the Sal de la Puna Project as described in Sections 9, 10, and 11 above. AMSA commissioned an independent NI 43-101 Technical Report on Sal de la Puna dated September 29, 2021, with an inferred resource estimate of 106,000 t of lithium. The additional drilling and test work carried out by AMSA during 2021/2022 will result in an updated resource estimate and resource categorization that could positively affect the Pastos Grandes resources described in Section 14. A three-dimensional groundwater flow and transport model was initiated for the Sal de La Puna Project to evaluate mineral reserves during 2022; LAC is now updating this model to evaluate and estimate combined reserves for a consolidated operation in Salar de Pastos Grandes.

25 INTERPRETATION AND CONCLUSIONS

Based on the analyses and interpretation of the exploration work carried out for the Pastos Grandes Project between 2011 and 2023, the following concluding statements are prepared:

- The entire Project area has been covered by exploratory drilling between 2011 and 2023 at an approximate borehole density of one exploration borehole per-4 km²; it is the opinion of the author that such borehole density is appropriate for the mineral resource estimate described herein.
- The results of drilling 18 core holes and 30 rotary boreholes and the analysis of 501 primary brine samples (excluding QA/QC samples) identify distinct brine composition and grade at specific depth intervals, showing a relatively uniform distribution of lithium bearing brines throughout the Project to a depth of 635 m. The brine composition for the Project is summarized in Table 25.1.

Table 25.1 Summary of the average brine composition (g/L) and ratios

K	Li	Mg	Ca	SO ₄	B	Mg/Li	Ca/Li	K/Li
3,73	0,39	2,26	0,82	7,55	0,56	5,76	9,53	3,73

- The lithium bearing brine contains sufficient levels of lithium and potassium to be potentially economic for development.
- The geology in the Project consists of a relatively low permeability upper saline lacustrine unit with variable thickness. This upper unit is underlain in most parts by a lower brine aquifer hosted in unconsolidated sediments that consists of alluvial sediments, a clastic unit, and a basal gravel / breccia unit with a variable thickness of over 400 m to a drilled depth of 635 m.
- Pumping tests carried in productions wells completed in this lower brine aquifer supported brine production rates of 25 L/s over 30-day durations indicating favorable hydrogeological conditions and that brine can be commercially produced with conventional wellfield techniques.
- Geophysical surveys and brine exploration drilling carried out within the Project area indicate that the limits of the lower brine aquifer remain open laterally and at depth so that exploration potential exists to significantly increase the lithium resources documented in the report.
- It is the opinion of the author that the Salar geometry, brine chemistry composition, and the specific yield of the Salar sediments have been adequately defined to a depth 640 m to support the Mineral Resource Estimate described in Table 25.2.

Table 25.2 Mineral Resources of the Pastos Grandes Project - Dated April 30, 2023

	Measured (M)		Indicated (I)		M+I		Inferred (II)	
	Li	K	Li	K	Li	K	Li	K
Aquifer volume (km3)	13.45		8.81		22.26		6.14	
Mean specific yield (Sy)	0.11		0.11		0.11		0.08	
Brine volume (km3)	1.48		0.97		2.45		0.49	
Mean grade (g/m3)	49	495	13	134	35	352	34	350
Concentration (mg/l)	438	4419	167	1722	331	3352	403	4234
Resource (tonnes)	662,000	6,660,000	118,000	1,180,000	780,000	7,840,000	208,000	2,150,000

Notes to the resource estimate (Table 25.2):

- CIM definitions were followed for Mineral Resources.
- The Qualified Person for this Mineral Resource estimate is Frederik Reidel, CPG
- No cut-off values have been applied to the resource estimate.
- Numbers may not add due to rounding.
- The effective date is April 30, 2023

Table 25.3 shows the mineral resources of the Pastos Grandes Project expressed as lithium carbonate equivalent (LCE) and potash (KCl).

Table 25.3 Pastos Grandes Project resources expressed as LCE and KCl

	Measured and Indicated Resources	
	LCE	KCl
Tonnes	4,200,000	14,900,000

Notes to Table 25.3

- Lithium is converted to lithium carbonate (Li_2CO_3) with a conversion factor of 5.32.
- Potassium is converted to potash with a conversion factor of 1.91.
- Numbers may not add due to rounding.

26 RECOMMENDATIONS

The following technical work is recommended to further advance the Project towards construction and into production.

- Incorporate the lithium resources hosted on the AMSA properties into the resource estimate for the Project so that these resources can be properly incorporated in the numerical groundwater flow and transport modeling for final brine production wellfield design, evaluation of potential environmental constraints, and the estimation of updated reserves.
- Carry out a 30-day pumping test on AMSA production well PW-1 to characterize the southern extent of the lower brine aquifer.
- Drill three deep core holes into the lower brine aquifer to improve the confidence level of geological and drainable porosity parameters in the central clastics and basal gravel /breccia units. These holes should be completed as deep monitoring wells for additional observations point during the additional pumping tests recommended.
- Carry out 30-day pumping tests in existing brine production wells PGPW18-15 and PGPW18-17 with water level monitoring in the above-mentioned new observations points.
- Carry out 7-day pumping test on water production wells PGMW19-2 and PGPW19-3; along with additional groundwater exploration work to secure future water supply requirements from freshwater resources within the Pastos Grandes and Sijes basins.
- Numerical modelling should be resumed with the AMSA-developed 3D FEFLOW groundwater flow and transport model for the basin to carry out predictive simulations for the design and layout of the future brine production wellfield, evaluation of potential environmental effects, and the preparation of updated lithium reserves for the Project.
- Based on the results of the predictive model simulations, install three additional brine production wells in the lower brine aquifer.
- Implement systematic hydro(geo)logical monitoring programs of surface water and groundwater features to reinforce the baseline characterization of the Pastos Grandes basin. Continue with the surveys and studies to improve the quantification of the water balance components of the basin.
- Drill 7-10 deep exploration core holes aimed at increasing the lithium resource base of the Project.
- Drill four industrial water exploration wells to evaluate the resources and optimize the production strategy, including Arena Minerals' blocks to the North and East of the basin.

The estimated budget to complete and implement the above recommendations are shown in Table 26.1

Table 26.1 Estimated budget for the 2023 brine resource evaluation program

Item	Cost (USD) ¹²
Pumping tests on existing wells (3)	360,000
Infill resource drilling (3 holes)	6,300,000
Resource exploration drilling (7 holes)	16,800,000
Production drilling (8 holes)	32,800,000
Hydrogeological monitoring programs	775,000
Water supply investigation and development	1,400,000
Resource and reserve modelling and estimation	500,000
Geophysics (MT+GV+ERT)	1,100,000
Total	60,035,000

¹² Costs are estimated in US dollars Official BNA

27 REFERENCES

- Allmendinger, R.W., Jordan, T.E., Kay, S.M., and Isacks, B.L., 1997, The Evolution of the Altiplano-Puna Plateau of the Central Andes: Annual Review of Earth and Planetary Science, v. 25, p. 139-174.
- Pocitos, Provincia de Salta, República Argentina; Actas 70 Congreso Geológico Chileno, (1): 220-224, Concepción
- Alonso, R. N., Viramonte J. G. Y Gutiérrez, R., 1984. Puna Austral. Bases para el Subprovincialismo Geológico de la Puna Argentina. Actas IX Congreso Geológico Argentino. I: 25- 41.
- Alonso, R.N, 1986. Ocurrencia, posición estratigráfica y génesis de los depósitos de boratos de la Puna Argentina. Tesis doctoral. Universidad Nacional de Salta, 196 pp.
- Alonso, R.N. and Gutierrez, R., 1986. Litoestratigrafía del Neógeno Terminal. Puna sudoriental argentina. Revista del Instituto de Ciencias Geológicas, 6, pp.29-47.
- Alonso, R., Viramonte J., 1987. Geología y Metalogenia de la Puna. Estudios geológicos., 43: 393-407.
- Alonso, R.N., Jordan, T.E., Tabbutt, K.T. and Vandervoort, D.S., 1991. Giant evaporite belts of the Neogene central Andes. *Geology*, 19(4), pp.401-404.
- Alonso, R.N., 1992. Estratigrafía del Cenozoico de la cuenca de Pastos Grandes (Puna Salteña) con énfasis en la Formación. *Revista de la Asociación Geológica Argentina*, 47(2), pp.189-199.
- Ausenco, 2018. Proyecto Pastos Grandes, Línea de Base Ambiental y Social, report prepared for Millennial Lithium Corporation, July 2018
- Jordan, T.E. and Alonso, R.N., 1987. Cenozoic stratigraphy and basin tectonics of the Andes Mountains, 20-28 south latitude. *AAPG Bulletin*, 71(1), pp.49-64.
- Bianchi, A. R., Yañez, C. E., & Acuña, L. R. 2005. Base de datos mensuales de precipitaciones del Noroeste Argentino. Instituto Nacional de tecnología Agropecuaria. Proyecto Riesgo Agropecuario, Convenio Específico, (3), 41.
- Blasco, Graciela; Zappettini, Eduardo O. y Hongn, Fernando, 1996. San Antonio de los Cobres. Programa Nacional de Cartas Geológicas de la República Argentina 1:250.000. Hoja Geológica 2566-I. Provincias de Jujuy y de Salta. Boletín 217. Buenos Aires, Servicio Geológico Minero Argentino. Instituto de Geología y Recursos Minerales.
- Bradley, D.C., Munk, L., Jochens, H., Hynek, S. and Labay, K., 2013. A preliminary deposit model for lithium brines. Reston, VA, USA: US Department of the Interior, US Geological Survey.
- Cabrera, A.L., 1994. Regiones fitogeográficas argentinas. *Enciclopedia Argentina de Agricultura y Jardinería*, Tomo II, fascículo 1. Buenos Aires.
- Cassel, D.K. and Nielsen, D.R., 1986. Field capacity and available water capacity. *Methods of soil analysis: Part 1 Physical and mineralogical methods*, 5, pp.901-926.
- Cooper, H.H. and C.E. Jacob, 1946. A generalized graphical method for evaluating formation constants and summarizing well field history, *Am. Geophys. Union Trans.*, vol. 27, pp. 526-534.
- Custodio, E., & Llamas, M. 1983. Hidrología subterránea.

- Domenico, P. A., & Schwartz, F. W. 1998. Physical and chemical hydrogeology (Vol. 506). New York: Wiley.
- Dworzanowski, Marek, Mike Rosko, and Peter Ehren. 2018. Feasibility Study of the Pastos Grandes Project, Salta Province, Argentina, Technical Report No. 209020-00055-000-GE-TEN-0003 prepared to Canadian Standard NI43-101 for Millennial Lithium.
- Eaton, A.D., Clesceri, L.S., Greenberg, A.E. and Franson, M.A.H., 1995. Standard methods for the examination of water and wastewater. American Public Health Association. Inc., Washington, DC.
- Freeze, R. A. & Cherry, J. A., 1979. Groundwater. Prentice-Hall, Englewood, Cliffs, New Jersey, 604 pp.
- Gorustovich, S.A., Monaldi, C.R. and Salfity, J.A., 2011. Geology and metal ore deposits in the Argentine Puna. Cenozoic geology of the central Andes of Argentina, pp.169-187.
- Hains, D.H., Foutie, L.F. Technical Report on Pastos Grandes Project. Prepared for LSC Lithium Corporation. Dated October 25, 2018.
- Houston, J. 2006. Evaporation in the Atacama Desert: An empirical study of spatio-temporal variations and their causes. *Journal of Hydrology*, 330(3-4), 402-412.
- Houston, J. Technical Report on the Salinas Grandes-Guayatayoc Project, Jujuy-Salta Provinces, Argentina. NI 43-101 report prepared for Orocobre Ltd, April 30, 2010.
- Houston, J. et al., 2011, The Evaluation of Brine Prospects and the Requirement for Modifications to Filing Standards, *Economic Geology*, 106, 1225-1239.
- IANIGLA (Instituto Argentino de Nivología, Glaciología y Ciencias Ambientales). 2018. Inventario Nacional de Glaciares.
- Ide, F. 1978. Cubicación del Yacimiento Salar de Atacama. Memoria de Título, Universidad de Chile, Departamento de Minería, 144 p.
- Isacks, B., 1988. Uplift of the Central Andes and bending of the Bolivian orocline, *Jour. Geophys. Res.*, 284, 3211-3231.
- IUCN (International Union for Conservation of Nature), 2017. Red List of Threatened Species.
- IUCN (International Union for Conservation of Nature), 2019. Red List of Threatened Species.
- Jordan, T.E. and Alonso, R.N., 1987. Cenozoic stratigraphy and basin tectonics of the Andes Mountains, 20-28 south latitude. *AAPG Bulletin*, 71(1), pp.49-64.
- Jordan, T. E., & Gardewege, M. 1989. Tectonic evolution of the late Cenozoic central Andes (20-33 S). In *The Evolution of the Pacific Ocean Margins* (pp. 193-207).
- Ministerio de Ambiente y Desarrollo Sustentable de Argentina (MAyDS), 2017. Categorización de las Aves de la Argentina (AA). Informe del Ministerio de Ambiente y Desarrollo Sustentable de la Nación y de Aves Argentinas, edición electrónica. C. A. Buenos Aires, Argentina.
- MOSA, Methods of Soil Analysis, 2002. American Society of Agronomy, Madison, Wisconsin; Part 4.

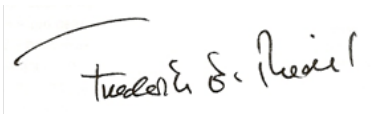
- Montgomery & Associates (M&A). 2018. Salar de Pastos Grandes Water Balance. Pastos Grandes Project, Salta, Argentina. Prepared for Millennial Lithium Corp.
- Montgomery & Associates (M&A). 2019. Phase III, Measured, Indicated, and Inferred Lithium and Potassium Resource Estimate, Pastos Grandes Project, Salta Province, Argentina. NI 43-101 report prepared for Millennial Lithium Corporation.
- Nicolli, H.B., Suriano, J.M., Kimsa, J.F., and Brodtkorb, A. 1982. Geochemical characteristics of brines in evaporitic basins, Argentinian Puna; Academia Nacional de Ciencias, Miscelanea No. 64, Cordoba, Argentina.
- Nwankwor, G.I., Cherry, J.A. and Gillham, R.W., 1984. A comparative study of specific yield determinations for a shallow sand aquifer. *Groundwater*, 22(6), pp.764-772.
- Ojeda, R.A., Chillo V. y Díaz G.B., 2015. Libro Rojo de Mamíferos Amenazados de la Argentina Mamíferos de Argentina. Sistemática y Distribución. Sociedad Argentina para el estudio de los Mamíferos (SAREM) editores. 257 p
- Ritzi Jr, R.W., Jayne, D.F., Zahradnik Jr, A.J., Field, A.A. and Fogg, G.E., 1994. Geostatistical modeling of heterogeneity in glaciofluvial, buried-valley aquifers. *Groundwater*, 32(4), pp.666-674.
- Secretaría de Ambiente y Desarrollo Sustentable (SAyDS), 2013. Resolución N°1055/2013: Clasificación del Estado de Conservación de Especies y Subespecies de Anfibios y Reptiles Nativos.
- Seggiaro, R., Hongn F., Castillo A., Pereyra F., Villegas D. y Martínez L., 2006. Hoja Geológica 2769-II, Paso San Francisco. (1:250.000). Programa Nacional de Cartas Geológicas. Instituto de Geología y Recursos Minerales, SEGEMAR. Boletín 294, 54 pp. Buenos Aires.
- Stormont, J. C., Hines, J. S., O'Dowd, D. N., Kelsey, J. A., & Eric Pease, R., 2011. A Method to Measure the Relative Brine Release Capacity of Geologic Material. *ASTM Geotechnical Testing Journal*, 34(5), 406-412.
- Theis, C.V., 1935. The relation between the lowering of the piezometric surface and the rate and duration of discharge of a well using groundwater storage, *Am. Geophys. Union Trans.*, vol. 16, pp. 519-524.
- Turner, J.M., 1960 Estratigrafía de la Sierra Santa Victoria y adyacencias. Academia Nacional de Ciencias. Boletín 41,2: 163-196.
- Turner, J.M., 1964 Descripción Geológica de la Hoja 7C- Nevado de Cachi (Provincia de Salta). Dirección Nacional de Geología y Minería. Boletín 99, 78 p. Buenos Aires.
- Turner, J.E., 1972. Puna. Geología Regional Argentina, Tomo 1: 13-56.
- Vandervoort, D.S., Jordan, T.E., Zeitler, P.K., Alonso, R.N., 1995. Chronology of internal drainage development and uplift, Southern Puna plateau, Argentine Central Andes. *Geology*, 23(2), 145-148.
- Yao, T.M., Milczarek, M., Reidel, F., Daniel Weber, P.G. and Brooker, M., A New Rapid Brine Release Extraction Method in Support of Lithium Brine Resource Estimation.

Qualified person Frederik Reidel

I, Frederik Reidel, CPG, as author of this report entitled “Lithium Resources Update Pastos Grandes Project, Salta Province, Argentina” (the “Technical Report”) with an effective date of April 30, 2023 (the “Effective Date”) and prepared for Lithium Americas Corp., do hereby certify that:

1. I am employed as Principal Hydrogeologist and General Manager by Atacama Water-Chile, residing at Badajoz 45, OF 1701, Las Condes, Santiago, Chile.
2. I am a graduate of New Mexico Institute of Mining and Technology with a Bachelors of Science Degree in Geophysics, 1986.
3. I am registered a Certified Professional Geologist (#11454) with the American Institute of Professional Geologists.
4. I am a registered Competent Person (#390) with the “Comision Calificadora de Competencias en Recursos y Reservas Mineras” (Chilean Mining Commission) under CH 20.235.
5. I have worked as a hydrogeologist for more than 30 years since my graduation. My relevant experience for the purpose of the Technical Report is:
 - Qualified Person and Member of the technical committees of Li3 Energy Ltd and Minera Salar Blanco for the development of the Maricunga Lithium Project in Chile (2011 – to date).
 - Co-author of ‘Best Practice Guidelines for the Estimation of Mineral Resource and Reserves in Brines’ prepared for the Chilean Mining Ministry and CCCRRM under Code Ch 20.235.
 - Competent Person for the Ore Reserves Statement for the Centenario Project for Eramet (2020-2021).
 - Evaluation of lithium and potash resources in Salar de Olaroz for Orocobre Ltd. in support of the project’s DFS and NI 43-101 Technical Report (2010-2011).
 - Qualified Person for the Sal de los Angeles Project, Salta Argentina for LiX Energy Corp / TSR 2016 – to date).
 - Evaluation of lithium and potash resources in Salar de Cauchari for Lithium Americas Corporation; NI 43-101 Technical Report preparation; member of the company’s Technical Advisory Panel (2009-2010).
 - Evaluation of brine resources in Salar de Hombre Muerto for FMC (1992-1993).
 - Consulting hydrogeologist in the evaluation and development of groundwater resources for international mining companies in North- and South America (1989-2012).
6. I have read the definition of “qualified person” set out in National Instrument 43-101 (“NI 43-101”) and certify that by reason of my education, affiliation with a professional association (as defined in NI 43-101) and past relevant work experience, I fulfill the requirements to be a “qualified person” for the purposes of NI 43-101.
7. I have visited and inspected Salar de Pastos Grandes on three different occasions during the AMSA 2021/2022 drilling campaign, with the most recent inspection taking place on July 18 and 19, 2022.
8. I am responsible for the entirety of the Technical Report.
9. I am independent of Lithium Americas Corp. in accordance with Section 1.5 of NI 43-101 and I have no prior involvement on the Property with LAC.
10. I have read NI 43-101, and the Technical Report has been prepared in compliance with NI 43-101 and Form 43-101F1.
11. At the Effective Date of the Technical Report, to the best of my knowledge, information, and belief, the Technical Report contains all scientific and technical information that is required to be disclosed to make the Technical Report not misleading.

Dated this 16th day of June, 2023.



Frederik Reidel, CPG